INVESTIGATION ON SWIRL IN PUMP SUMP INTAKES AND ITS CONTROL

Ph.D. THESIS

by

BHUPESH JAIN

DEPARTMENT OF CIVIL ENGINEERING
INDIAN INSTITUTE OF TECHNOLOGY ROORKEE
ROORKEE – 247667 (INDIA)
JULY, 2015

INVESTIGATION ON SWIRL IN PUMP SUMP INTAKES AND ITS CONTROL

A THESIS

Submitted in partial fulfilment of the requirements for the award of the degree

of

DOCTOR OF PHILOSOPHY

in

CIVIL ENGINEERING

by

BHUPESH JAIN

DEPARTMENT OF CIVIL ENGINEERING
INDIAN INSTITUTE OF TECHNOLOGY ROORKEE
ROORKEE – 247667 (INDIA)
JULY, 2015

INDIAN INSTITUTE OF TECHNOLOGY ROORKEE
ROORKEE

CANDIDATE'S DECLARATION

I hereby certify that the work which is being presented in the thesis entitled "**INVESTIGATION ON SWIRL IN PUMP SUMP INTAKES AND ITS CONTROL**" in partial fulfilment of the requirements for the award of the degree of Doctor of Philosophy and submitted in the Department of Civil Engineering of the Indian Institute of Technology Roorkee is an authentic record of my own work carried out during a period from Jan., 2010 to July, 2015 under the supervision of Dr. Z. Ahmad, Professor, Department of Civil Engineering, Indian Institute of Technology Roorkee, Roorkee and Dr. K. M. Singh, Associate Professor, Department of Mechanical and Industrial Engineering, Indian Institute of Technology Roorkee, Roorkee.

The matter presented in the thesis has not been submitted by me for the award of any other degree of this or any other Institute.

(BHUPESH JAIN)

This is to certify that the above statement made by the candidate is correct to the best of our knowledge.

(K. M. Singh)
Supervisor

(Z. Ahmad)
Supervisor

Date:

ABSTRACT

Water pumps used in drainage, agriculture, and industrial process often experience operational problems such as vibration, impeller damage caused by cavitations, and excessive wear of bearings. This not only results in severe deterioration of their performance but also leads to a significant increase in operational and maintenance costs. These problems probably result from non-axial flow of water in the suction pipe because of poor pump-sump design. These problems and solutions have been investigated extensively and are widely reported in the literature (Denny 1956; Gordon 1970; Tullis 1979; Melville et al. 1994). Unfortunately, the flow phenomena near the suction pipes are so complex and diverse that there is no comprehensive theoretical model to predict them. Existing design guides usually contain little more than rules of thumb for design of pump sump intakes and control of swirl.

In general, the intake structures are designed based on Hydraulic Institute Standards (HIS, 1998), British Hydromechanics Research Association (BHRA, Prosser 1977) standards, and the Japan Society of Mechanical Engineers (JSME, 1984) standards. These standards recommend construction of physical scaled models in a laboratory to design a problem free pump sump intakes. Padmanabhan and Hecker (1984) found that scaled models typically have unavoidable scale effects as swirl flow in pipe and inlet losses show scale effects**.** Moreover, the similarity laws of the model testing are not clear yet, and there are different opinions for velocity setting in the model test (Turbomachinery Society Japan 2002). Some research works recommend to perform the model study of pump sump for higher Froude number (up to three times of Froude number corresponding to Froudian conditions). However, other studies indicate that the pump sump model study is to be carried out for Froudian condition only.

The time and cost involved in sump model studies for design and optimization of sump geometry can be reduced to a large extent through CFD modelling. A number of CFD studies are reported in the literature such as Pradeep et al. (2012), Tang et al. (2011), Kang et al. (2011), Skerlavaj et al. (2009). They found that floe simulation in the pump sump intake can be accurately carried out using CFD.

Various types of anti-vortex devices (AVD) are used to control the swirling flow in pump sump intake (HIS 1998; BHRA 1977). However, the suitability of these vortex breakers in the light of flow conditions approaching the bell mouth are not discussed in literature.

Swirl produced by vortex flow decays with distance along the suction pipe due to shear at the pipe wall. As the tangential velocity increases with distance from the pipe centre, wall friction acts on the near maximum tangential velocities, producing maximum dissipation forces (Knauss 1987). Knowledge of the decay of swirl with distance is important in determining possible effects of swirl on pump and turbine performance. Limited studies are reported in literature in respect of decay of swirl. Baker and Sayre (1974) showed that the swirl decay follows an exponential function. The present study is being taken up keeping in mind the above gaps in the design and model testing of multiple pump sumps. The specific objectives of the present investigation are as follows:

1. To study swirl flow in the pump sump intake through experimentation and CFD under different approach flow to the bay.
2. To study the effect of Froude number on swirl in the pump intake through experimentation and CFD.
3. To study the effect of different types of anti-vortex devices and their dimensions on the swirl in the pump intake and to standardized the shape and size of AVDs taking into considerations the approach flow conditions.
4. To study the decay of swirl in suction pipe column of the pumps.

A 1:12 scaled model of a prototype of eight bays pump sump intake was chosen for the present study. Froude number dynamic similarity law was followed for the model study. The bell entrance Reynolds and Weber numbers were kept higher than 6×10^4 and 320 respectively for neglecting the effect of viscosity and surface tension. The model was consisted of an intake chamber, fore bay, eight bays of the pump sump and suction pipe with bell mouth. Suitable arrangements in form of perforated walls, flow straighteners, and wave suppressors were provided in the intake chamber to stabilize the flow without any disturbance in the inflow. The model was made of concrete except the floor and the front view of the bays, which were of transparent glass to visualize the flow. The bell mouth and suction pipe were also fabricated of transparent plastic.

A vortimeter was fitted in the suction pipes to measure the swirl angle of the flow. Acoustic Doppler Velocimeter was used to measure the temporal and spatial variation of velocity in bays and approach channel.

An ultrasonic flow meter was used to measure the discharge in the suction lines for calibration of bend meters fitted in the suction lines. A pointer gauge of 0.1 mm accuracy was

used to measure the water level in the sump. An OTT acoustic digital current meter (ADC) was used to measure one dimensional (1D) velocities in the bays.

The following observations were taken in each experimental run:

1. The possible existence of subsurface or Free surface vortices were explored by visualization.
2. The revolutions per minute of the vortimeter were counted, and the swirl angle was calculated for each suction line.
3. Velocity distributions in the bays were measured for selected runs.

The experimental runs were conducted for maximum discharge (13.69 L/s) and minimum water level (666 mm) for all combinations of pump operation. Experiments were also run for higher discharges at minimum water level for studying effect of Froude number on swirl. Different combinations of the pumps were chosen considering the symmetry of flow in the system and the time required running the model.

Swirl and velocity in bays for design discharge, maximum and two times of design discharge were also observed to validate the CFD model results.

Cross type anti-vortex device (AVD) of three heights i.e, 25mm, 50 mm and 75 mm have been tested for control of swirl in suction pipes under minimum water level and maximum discharge conditions in the pump sump model. It was found that as height increases, the effectiveness of the breaker increases with respect to swirl in combination A. Three different sizes of cross type anti-vortex devices are used in the physical model below the bell mouth intake for the control of swirling flow in the suction lines. Out of the three sizes of AVD, the middle size is found more effective in controlling the swirling flow. To find the most optimum AVD, a suitability index is developed and used in present study. From this AVD of 50 mm height is found most suitable in all the combinations of pumps and flow conditions. Nevertheless the higher size of the AVD breaks the swirling nature of the incoming flow, however, due to blockage effect it induces additional swirl which results in higher swirl compared to medium size of the AVD.

A CFD model was developed for the pump sump intake model. A 3 m length of approach channel, forebay and eight bays configuration were modelled. The walls of suction pipes were

considered as thin walls. A multi-block structured mesh with about 5.7 million hexahedral cells was generated using ANSYS ICEMCFD Hexa mesher. The sump model dimensions were same as in the physical model. The orthogonal quality of the mesh is of 0.37 on scale from 0 to 1 and the maximum aspect ratio was 13. O-Grid technique was used to create smooth mesh near the intakes. Two O grids were used - one inside the suction line and one outside the suction lines.

The finite-volume method (FVM) was used to discretize the governing equations. QUICK scheme was used for convective term of the momentum equations. Second order discretization was employed for pressure equation. Pressure and velocity coupling were enforced using SIMPLEC algorithm. Steady state solutions were obtained by iterative method in pseudo time using Fluent solver. Accuracy of the results obtained from the FVM increases as the grid spacing decreased. To find the optimum spacing, grid dependency tests for three sizes of grid (coarse, fine and finer) have been performed. Standard k-ε turbulence model has been used in this study.

At the inlet, a uniform velocity was taken as upstream boundary condition. At the outlets of suction pipes, outflow boundary condition was specified in which the gradients of all the variables were assumed to be zero. No-slip and no-penetration conditions were employed at the solid walls (bed, suction-line walls, side and back-walls). Standard wall function approach (Launder and Spalding 1974) was used to model the flow near solid walls. For the free surface, not considering shear stresses caused by the wind and heat transfer from the atmosphere, a rigid lid assumption was employed (i.e. symmetrical conditions).

CFD model is verified by conducting mesh dependency test and the mesh dependence of the solution was estimated by running simulation for three hex meshes. To validate the CFD model, the swirl angle in suction lines and velocity distribution in bays are compared to the experimental results however results for one combination are discussed in detail. Results show good agreement with the experimental results.

CFD modelling has been carried out to investigate the effectiveness of three shapes of the AVD i.e. vertical backwall splitter, L shape splitter and cross type. For each shape, three sizes of the AVD have been investigated. For each AVD, swirl angle in the suction line, flow pattern near the bell mouth, subsurface vortices have been investigated. It is found that L shape AVD of medium size is more effective in having favourable flow conditions in the suction lines.

Swirl angle for different Froudian conditions by changing flow rate in suction line were observed. It was found that as the Froude number (based on suction line diameter and axial velocity) increases, the swirl angle first increases then become constant. Therefore, it can be concluded that there is no need to perform model test at higher than Froude number conditions.

Swirl angles produced by vortex flow decay with distance along the suction pipe due to shear at the pipe wall. The decay of swirl has been also found in CFD results. The decay of swirl was exponential in the present study which is same as reported by Baker and Sayre (1974). A new relationship between decay of swirl along the pipe and Froude number is proposed from the CFD results.

The present study shall contribute immensely for the design of pump sump intakes, Flow simulation in the sump, and suction line, understanding of swirling flow and their control.

ACKNOWLEDGEMENT

The author wishes to express his heart-felt gratitude to Dr. Z. Ahmad, *Professor,* Department of Civil Engineering and Dr. K. M Singh, *Associate Professor*, Department of Mechanical and Industrial Engineering, Indian Institute of Technology Roorkee, Roorkee (India) for their valuable guidance and inspiring encouragement in pursuance of this work. He remains indebted to them for giving their precious time freely at all stages of this study.

The author would like to put on record his sincere thanks to Dr. C. S. P. Ojha, *Professor and Head*, and all faculty members of Department of Civil Engineering, Indian Institute of Technology Roorkee, Roorkee (India), for their timely advice and kind help.

The author is very much thankful to Shri Yashvant Singh Pundir, Shri Vinod Sharma, Shri Pramod Kumar, Shri Mohd. Aslam, Shri Rati Ram, Shri Ashok Kumar, Shri Chhotelal Yadav, Shri Mohd. Anees, Mohd. Nadeem, Shri Ajay, and other supporting staff of the Hydraulic laboratory of Indian Institute of Technology Roorkee, Roorkee (India), for the facilities extended to him in the laboratory.

The author wises to express his thanks to the Dr. Navneet Gupta, Coordinator and Head Computer Center, IIT Roorkee and supporting staff for computational facilities extended to him in Computer Center.

The author wishes to express his thanks to the seniors at IIT Roorkee Mr. Amrit Roy, Mr. Alok, Mr. Nikhil Agarwal, Mr. Manish Goyal, Mr. Kunal Jain, Mr. Sanjeev, Mr. B. Ramesh, Mr. Ajmal, Mr. Himanshu, Mr. Seraj Ahmad, Mr. Ajay Lodhi, Mr. Ajay kumar, Mr. Ankit Chakravarti, Mr. Umesh, Mohd. Aamir, Mohd. Hashid, Mr. Pryadarshi, Mr. Lokpriya Shrivastava, Mr. Kapil Rohila Mr. Medalson Ronghhang, Mrs. Soma kumara, Mr. Rakesh Pratap Singh, Mr. Vijit Rathore and Mr. Chetan Sharma for cooperation and moral encouragement.

The author wishes to express his thanks to Mr. Chandan kumar, Mr. Nalin Negi, Mr. Virendra kumar, Mr. Gaurav Kabra, Mr. Chirag Trivedi, Mr. Ankur, Mr. Nitesh Dutt, Mr. Ajay Bohra, Mr. Sandeep Chouhan and Mr. Nitesh Ahir for the moral support during my stay at IIT Roorkee.

The author has a lifelong regards towards his parents. It was the power of their blessings, which gave him courage and confidence to materialize this dream.

Lastly, the author wishes to record his gratitude and warm sentiments towards his wife **Nikita** for her understanding, moral support and also patiently bearing his inattentiveness towards her during his research work.

BHUPESH JAIN

Date:

Place:

TABLE OF CONTENTS

LIST OF FIGURES

LIST OF TABLES

LIST OF SYMBOLS

ROMAN SYMBOLS

A	Area
B	Backwall clearance
C	Floor clearance
$C\mu$	Constant = 0.09
$C_{1\varepsilon}$, and $C_{2\varepsilon}$,	Turbulence model constants
C_w	Sidewall clearance
D	Suction pipe diameter
D_b	Bell diameter
Fr	Froude Number
g	Gravitational acceleration =9.81 m/s^2
h	Height of AVD
k	Turbulent kinetic energy
L_b	length of bay
n	Angular velocity of vortimeter in RPM
N_Γ	Circulation number
Q	Discharge
r	Radius
S	Submergence
T	Surface tension (N/m)
u	Velocity in x- direction
v	Velocity in y- direction
V	Average axial velocity in the suction pipe
V_θ	Tangential velocity at the tip of the vortimeter
w	Velocity in z- direction
W	Width of bay
We	Weber Number
W_i	Width of inlet
x, y, z	Rectangular Cartesian coordinates

GREEK SYMBOLS

ε	Rate of dissipation of turbulent kinetic energy
θ	Swirl Angle
θ_{max}	Maximum swirl
ω	Vorticity
ω_x	x component of vorticity vector
ω_y	y component of vorticity vector
ω_z	z component of vorticity vector
σ	Standard deviation
μ	Dynamic viscosity
μ_t	Turbulent viscosity
σ_ε	Turbulent Prandtl number for dissipation rate
σ_k	Turbulent Prandtl number for turbulent kinetic energy
v	Kinematic viscosity
π	pi=3.14159
ρ	Density of water
Γ	Circulation inside the vortex

SUBSCRIPTS

d	Design
max	Maximum
m	Model
p	Prototype
r	Ratio
in	Inlet

ABBREVIATIONS

ADC	Acoustic Digital Current-meter
ADV	Acoustic Doppler Velocimeter
ANSI/HIS	American National Standard Institute / Hydraulic Institute Standards
AVD	Anti Vortex Device
BHRA	British Hydrodynamic Research Association
CFD	Computational Fluid Dynamics
IS	Indian Standard
NPSH	Net Positive Suction Head
RANS	Reynolds Average Navier Stokes Equations
RMS	Root Mean Square
SIMPLEC	Semi-Implicit Method for Pressure Linked Equations-Consistent
RSD	Relative standard deviations

CHAPTER 1 **INTRODUCTION**

1.1 BACKGROUND

Pump sump intakes are necessary to transport large amount of water for various applications such as irrigation, water supply, thermal power plants, nuclear power plants and industrial processes. These can be single or multiple pump type intakes depending upon the requirements and the availability of space. The present study deals with the investigation of swirl in a multiple pump sump intake model and its control.

Swirl in flow is quantified with swirl angle that is equal to $\tan^{-1}$ of the ratio of tangential and axial velocities of flow entering in to the pump intake. It is, therefore, present in axial flow if non-zero tangential velocity components exist. Swirl angle is commonly used to estimate indirectly flow circulation and it can be measured by means of a swirl meter (vortimeter) installed in a pipe downstream of the flow. The measurement of swirl in the suction pipe has widely been practiced, as this swirl and entrance losses have some correlation (Padmanabhan and Hecker 1982). Swirl present at the inlet to the suction bell will be transmitted to the impeller and this could induce impeller vibrations and cavitation, and could also lower the pump efficiency.

Unfortunately, the swirl phenomenon associated with pump sump intakes is so complex and diverse that there is no comprehensive theoretical model to predict swirl in the pump sump intakes. Existing design guides (American National Standards Institute (ANSI) 1998; Bureau of Indian Standards (BIS) 2003; Prosser 1977) usually contain little more than rules of thumb for pump performance. Although little is known about the effect of swirl on pump performance, it is generally accepted that the swirl angle just upstream of the pump should be less than about 5^o (Sweeney et al. 1982). Large swirl angle produces unfavourable angles of attack of the flow onto impeller blades, producing excessive separation and loss of efficiency. In comparison to this criterion, the tangential velocity distribution just downstream from a standard, short radius, pipe bend indicate an integrated swirl angle of about 8^o (Knauss 1987). An additional concern in some applications is the effect of swirl on the accuracy of flow meters. Padmanabhan and Janek (1980) show that flow with a swirl of 20^o produces 2% error in flow measurement using a standard American society for mechanical engineering (ASME) orifice meter with a diameter ratio of 0.6.

Several studies have been reported in the literature in respect of investigation of flow phenomenon associated with the pump sump intakes (Anwar and Amphlett 1980; Anwar 1965, 1966, 1967, 1968; Anwar et al. 1978; Arboleda and El-Fadel 1996; Bauer and Nakato 1997; Chang 1977; Daggett and Keulegan 1974; Denny and Young 1957; Denny 1956; Dhillon 1980; Durgin and Hecker 1978; Farell 1976; Fletcher 1979; Frizell 1994; Gordon 1970; Haindl 1959; Haradasa and Cox 1980; Jain et al. 1978; Knauss 1987; Lewellen 1962; Melville et al. 1994; Nathan 1981; Odgaard and Dlubac 1983; Padmanabhan and Hecker 1982, 1984; Padmanabhan 1984; Prosser 1977; Rahiman et al. 2003; Swainston 1977; Sweeney et al. 1982; Tullis 1979).

Physical model testing has widely been used to identify the swirl and other hydraulic problems (such as air entrainment, entry loss, cavitation damage etc.) associated with existing or proposed design of pump sump intakes. Also, the design guides recommend for physical model testing for satisfactory design of large pumping stations. Several physical model studies have been reported in the literature (Ahmad et al. 2011; Choi et al. 2010; Dimas and Vouros 2012; Eldho 2010; Kang et al. 2011, 2014; Kim et al. 2012; Nakato and Jong 1999; Nakato and Kennedy 1977; Patel et al. 2013; Pradeep et al. 2012; Rozainy et al. 2008; Samir A S Ibrahim 2011; Shabayek 2010; Tang et al. 2011).

Since last two decades, due to advancement in computational facility CFD (computational fluid dynamics) models are in quite a demand to model the pump sump flow. Several researchers (Bayeul-Laine et al. 2010a; b; Chen and Guo 2007; Choi et al. 2010; Chuang et al. 2014; Constantinescu and Patel 2000; Desmukh and Gahlot 2010, 2011; Issa and Bois 2009; Issa et al. 2008; Jermy and Ho 2008; Kim et al. 2012, 2015; Li et al. 2006; Long et al. 2012; Lucino and Duro 2010; Meena et al. 2013; Okamura et al. 2007; Park et al. 2011a; b; Patel et al. 2013; Patel 2012, 2013, 2014; Peijian et al. 2013; Pradeep et al. 2012; Pratap and Chavan 2013; Rajendran and Patel 2000; Rozainy et al. 2008; Shibata et al. 2000; Shukla and Kshirsagar 2008a; b; Skerlavaj et al. 2011; Tang et al. 2011, 2010; Thomas and Williams 1992, 1994, 1995; Thomas et al. 1995; Tokyay and Constantinescu 2006; Wicklein et al. 2006; Zhao et al. 2013; Zhou et al. 2009) used CFD modelling as an alternative method to the physical modelling in designing and analysing pump sump intakes. Therefore, in the present study, a CFD model has been developed and used to study the swirling flow in the multiple pump sump intake model and its control.

In this chapter, the hydraulic problems associated with pump intakes, factors affecting the pump sump approach flow, various sources of swirl, basic concepts of controlling swirl, brief

literature review, identified gaps, need for study, objectives and adopted methodology are described. At end, the organization of the thesis has been presented.

1.2 PUMP SUMP INTAKES

To define the terminology related to the multiple pump intakes, a definition sketch of a three pump sump intake model is shown in Figure 1.1. In the present study, a rectangular eight bay vertical (upward) pump intake has been used to study the flow phenomenon. Commonly used arrangements such as bay/divide wall, fore-bay, suction pipes, backwall, floor, sidewall, approach channel, bell mouths, stop log gates, trash racks are shown in Figure 1.1.

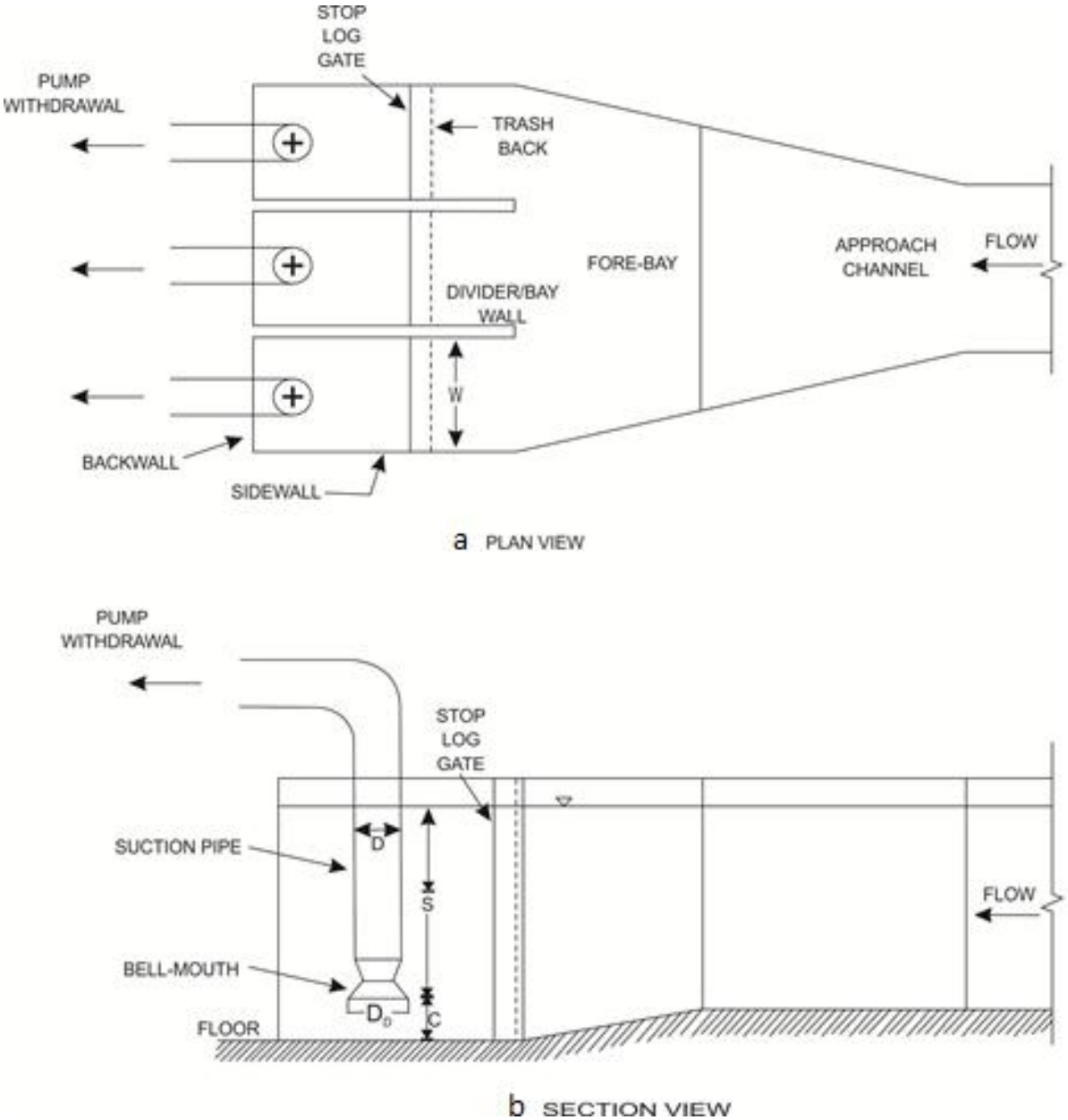

Figure 1.1 General features of a multiple pump sump intake (a) plan view and (b) sectional view

Several researchers (Melville et al. 1994; Sweeney et al. 1982; Tullis 1979) investigated the pump sump flow and summarized the possible hydraulic problems and detrimental effects on the pump operation. Brief discussions on major hydraulic problems of concern are as follows:

(A) Air drawing surface vortices could reduce the pump capacity and increase the required net positive suction head (NPSH) depending upon the amount of air drawn. For centrifugal pumps, small quantities of air such as, 3 to 6 % by volume at the pump location, decreases the efficiency of the pump, and when the volumetric concentration rises to 7 to 20% substantial performance degradation would result (Murakami et al. 1969). Denny and Young (1957) reported that presence of 1% air entrained in water flow reduces the efficiency of a centrifugal pump by 15%.

(B) Non-air drawing vortices, with a strong coherent core visible with dye injection or strong enough to pull debris, are also considered objectionable since they may cause vibrations due to impellers intercepting non-symmetrical pressure fields.

(C) Surface and subsurface vortices are known to contribute to swirl in the flow into the suction bell. Swirl present at the entrance to the suction bell will be transmitted to the impeller and this could induce impeller vibrations and cavitation, and also could lower the pump efficiency. Magnitude of allowable swirl depends on the type of pump and no definite answers are available. As a general rule, swirl angles above 5^{o} should be considered unacceptable (Sweeney et al. 1982).

(D) Uneven flow distribution to the impeller would give rise to unbalanced loading on the impeller. Uniform velocities at the impeller location in magnitude within ±5% of the mean velocity may be considered permissible (Tullis 1979).

Vortices formed in pump sump intakes can be classified by several means such as location of vortex formation (surface or sub surface vortices), time (steady/stable or unsteady/unstable), strength etc. Therefore, to evaluate the strength of vortices at pump intakes systematically the vortex scale varying from a surface swirl to full air core vortex is shown in Figure 1.2 (a) as recommended by (ANSI/HIS 1998). Vortex types are identified by visual observation with the help of dye and artificial debris. Sub surface vortices usually terminate at the sump walls and floor, and may be visible only when the dye is injected near the vortex core. The classification of subsurface vortices as per American National Standards Institute (ANSI) (1998) is shown in Figure 1.2 (b).

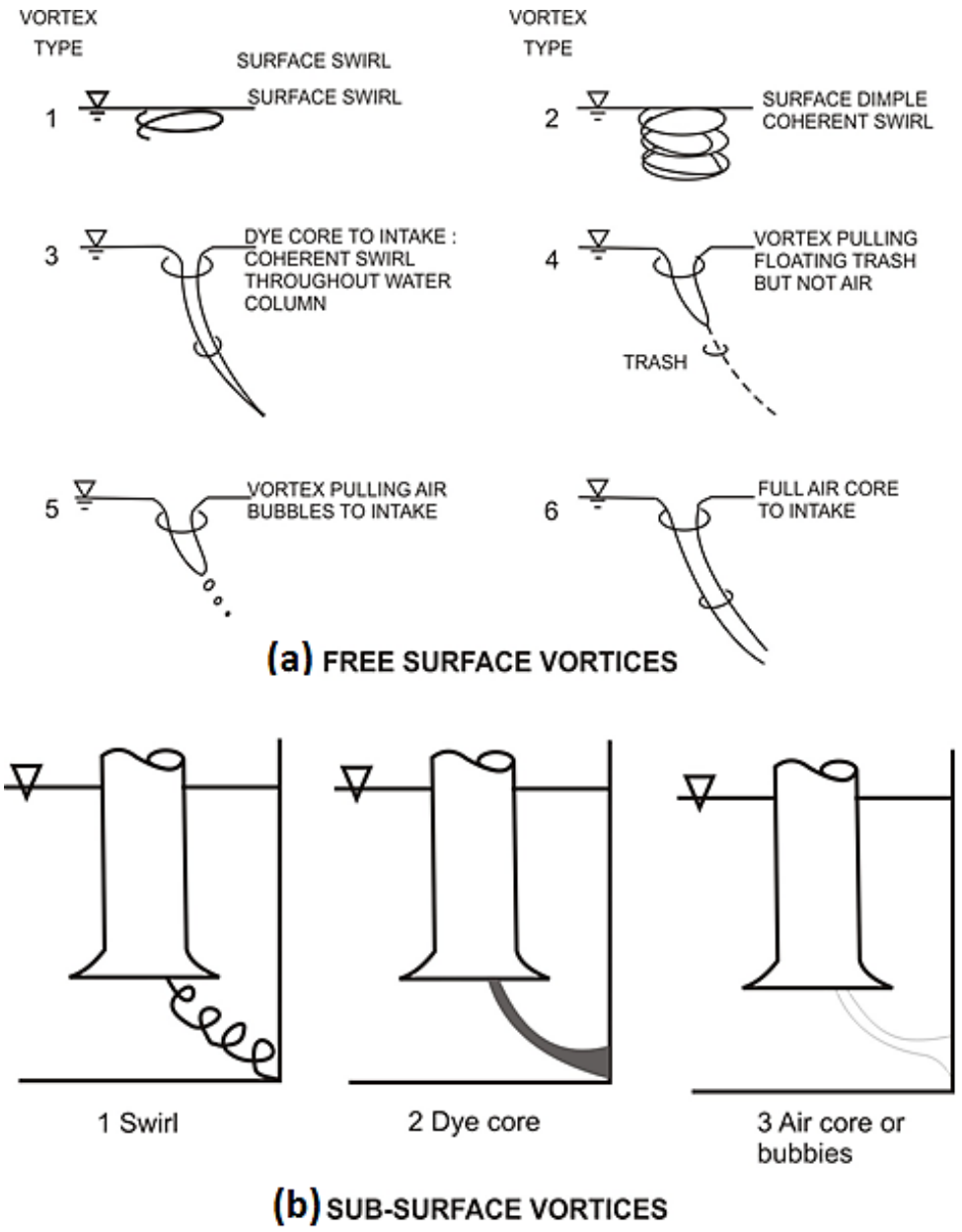

Figure 1.2 Classification of (a) free surface vortices and (b) subsurface vortices (ANSI/HIS 1998)

Typical impacts of adverse approach flow patterns are (Knauss 1987).

1. Increase of head losses due to the hindered intake process.

2. Reduction of maximum intake rate by the vortex flow itself or by means of adjusted operational conditions aimed at minimizing swirling flow problems.
3. Reduction of efficiency of the hydraulic machines due to the decreased discharge and by operating the machines within an unfavourable region of efficiency occurring at lower flow rates.

4. Deterioration of the running conditions of the hydraulic machines by entrained air associated with fluctuations of flow rate and pressure distribution, at least resulting in considerable drops of efficiency, rough operation conditions and environmental impact by increased noise.
5. Stimulation of vibrations and cavitation inception lead-in to wear and damage of construction elements (impeller blades, bearings or other important parts of the installation).
6. Production of an unbalanced loading of pump impellers or turbine runners by swirl and uneven flow distribution.
7. Appearance of slug flow conditions within the conduit due to accumulation of entrapped air (sudden release of large air pockets, flow pulsations).
8. Increase in operational problems by the suction of debris possibly pulled down by surfaces vortices (e.g. asymmetric blockage of screens, dislocation of bulk head and damage to grating).

1.3 FACTORS AFFECTING THE PUMP APPROACH FLOW

Various parameters such as approach channel geometry, minimum desirable or critical submergence at the pump suction bell (S_c), and sump geometrical features including floor clearance (C), bay width (W) and backwall clearance (B) that affect the performance of a pump as a result of their effect on hydraulic problems.

1.3.1 Approach channel

The geometry and orientation of the approach channel with respect to the pump bay (or bays) and the velocity of the flow in the channel are very important since they all affect the circulation inside the sump and thereby contribute to circulation or swirl. Side wall expansions or floor slope changes in the approach channel near the pump bay usually cause flow separations and formation of eddies contributing to circulation. Side wall expansions, if unavoidable, should have expansion angles preferably less than 20^o (Knauss 1987). Floor slope changes should be less than 10^o (Knauss 1987). Similarly, an off-set or bend in the approach channel near the pump bay entrance would be undesirable since it would generate a non-uniform flow into the bay. Non-streamlined obstructions such as screen supports located at the sump entrance could also to a lesser extent contribute to flow separation and eddying. Intuitively, the lower the velocities of approach flow, the lower would be any circulation inside the sump due to approach flow non-uniformities. Generally an approach flow velocity of less than 0.3m/s is considered acceptable (Knauss 1987).

1.3.2 Minimum desirable submergence at pump suction bell

The minimum desirable submergence at the pump suction bell should not be less than a critical value below which objectionable surface vortices would occur. Unfortunately, objectionable vortices and hence the critical submergence are defined differently by individual researchers. The most common definition of an objectionable vortex is one that is on the verge of drawing air into the suction pipe. The critical submergence is depended on the approach flow patterns and other sources of vorticity existing in the sump and hence a universal value of critical submergence cannot be fixed.

1.3.3 Floor clearance

Floor clearance affects the available submergence since the higher the floor clearance the lower will be the available submergence on the suction bell entrance for a given water level. Hence, provision of more than necessary floor clearances may enhance formation of submerged vortices. Commonly, recommended values of the floor clearance lie between 0.4 to 0.75 of bell diameter (Chang 1977; Prosser 1977) and often the pump manufacturers input is required to select a suitable value in this range.

1.3.4 Back wall clearance and bay width

The width of the pump bay governs the approach velocity while in the case of wet well pump sumps, the back and side wall clearances from the outer periphery of the bell would affect the frequency and strength of any vortices. Very small back wall clearance gives rise to submerged vortices. A bay width of not less than 2 times of bell diameter and a back wall clearance of not less than 0.25 times of bell diameter are commonly recommended (Chang 1977; Prosser 1977). The pump column is usually located in the mid-width of the bay which fix the side wall clearances and it is advantageous to have the back wall clearance small. An upper limit of 0.5 of bell diameter is often recommended (Prosser 1977).

1.4 SOURCES OF SWIRL

Among the many sources of swirl, the most common encountered one is an eccentricity of the approach flow relative to the intake and the connected conduit. In most of the cases, asymmetry in the approach flow field due to geometrical conditions causes vortex formation. There are also special hydraulic processes responsible for swirl production in geometrically symmetric installations, even with an ideal velocity distribution in the approach flow. Durgin and Hecker (1978) categorized vorticity sources into the following three fundamental types:

a) Non-uniform approach flow to the sump due to geometric orientation of the sump or approach channel or due to streaming flow patterns generated by obstructions such as intake piers (Figure 1.3 a).
b) The existence of shear layers of high velocity gradients, including separated boundary layers which are inherently rotational (Figure 1.3 b), and
c) Rotational wakes generated by objects or obstructions in the way of the approach flow to the sump (Figure 1.3 c).

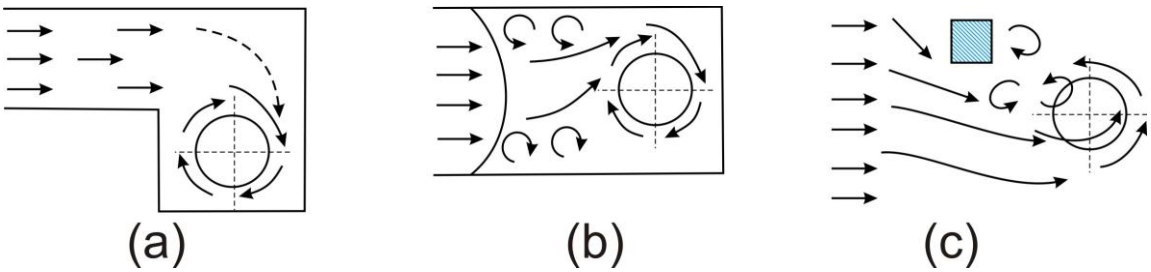

Figure 1.3 Sources of vorticity (a) offset introduction (b) velocity gradients, and (c) obstruction (Durgin and Hecker 1978)

Item (a) is a major source of vorticity in surface vortices while item (b) is a major source of vorticity in subsurface vortices. A good design of the pump sump essentially involves reducing the contribution from these vorticity sources as far as practicable and thereby reducing the strength of the vortices generated by them to the acceptable limits. An analytical determination of the strength of these vorticity sources and their combined effect on vortex formation is impossible due to the complexity of the system, and hydraulic model studies are often used in verifying or arriving at an acceptable sump design.

In literature one can find a lot of schematic illustrations showing various examples of intake prone to vortex formation as shown in Figure 1.4 (Denny and Young 1957) and Figure 1.5 (Anwar 1968). Vortices mainly stimulated by: eccentric orientation of the intake relative to a symmetric approach flow area, asymmetric approach flow conditions due to irregularities in boundary lining, unfavourable effects of obstructions such as an offset, piers or dividing walls. Non-uniform velocity distribution is caused by boundary layer separation, wind action, wakes, counter currents and other reasons.

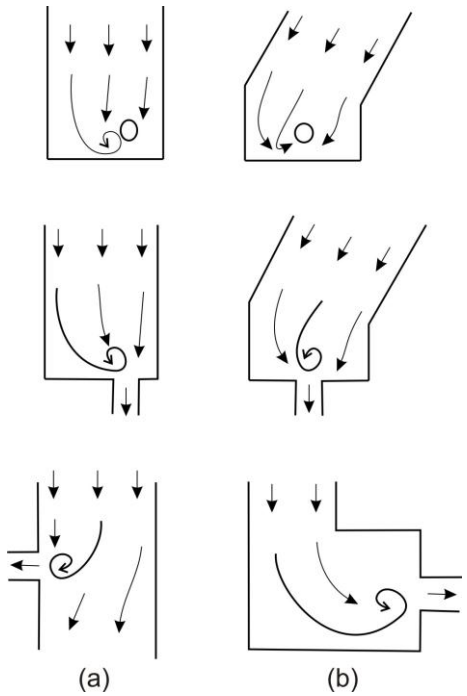

Figure 1.4 Rotational flow arising from (a) asymmetry and (b) change in direction of boundaries (Denny and Young 1957)

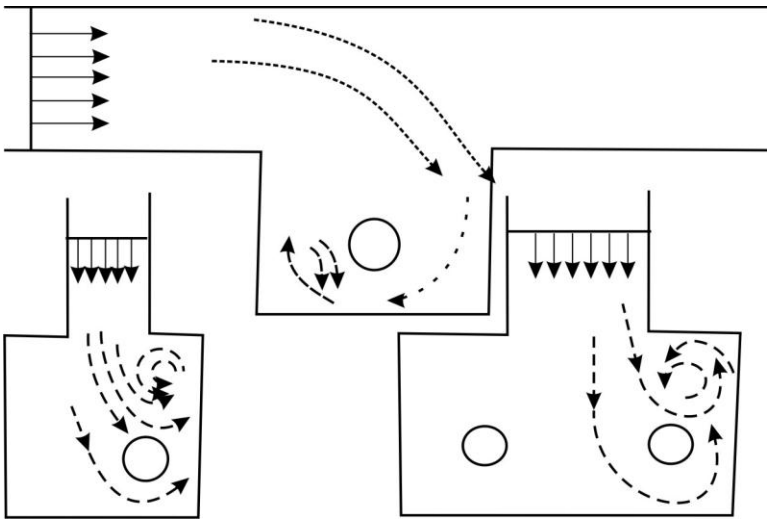

Figure 1.5 Intake prone to vortex formation (Anwar 1968)

1.5 CONCEPTS OF CONTROLING SWIRL/AIR ENTRAINMENT

The pump operational problems can be addressed under two headings first air entrainment and second swirl entrainment. Air entrainment in general results from the surface vortices and this depends very much on the water depth above the intake. Critical submergence of the intake can be related to the given circulation strength as shown in Figure 1.6. The critical submergence increases with increasing circulation strength. One important design parameter concerning avoidance of air entrainment by intake vortices is to choose submergence requirements above the critical stage. On the other hand the entrained swirl, with otherwise

equal conditions the indicated swirl angle is independent of the flow rate and also independent of the occurrence of air ingestion. The amount of entrained swirl is predetermined by the given submergence of the intake. Related to overall symmetrical conditions, the entrained swirl decreases with increasing water depth as shown in Figure 1.6 (Knauss 1987). If it is necessary to raise the water level in order to avoid air entrainment, then simultaneously swirl intrusion will be reduced. However, critical submergence conditions cannot be directly related to critical swirl entrainment.

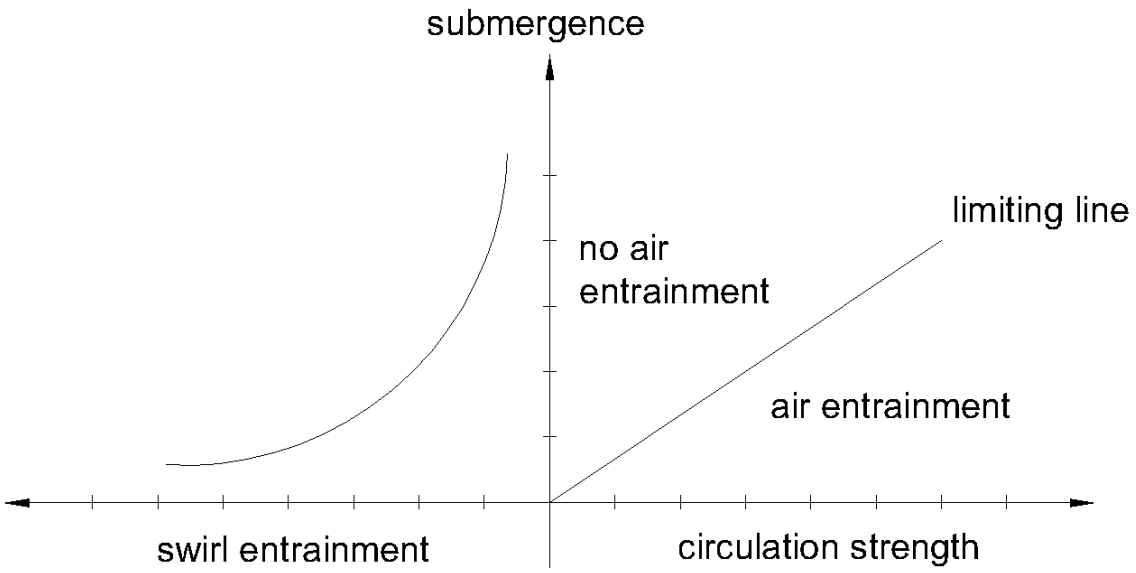

Figure 1.6 Basic relationship between circulation strength, submergence, air and swirl entrainment (Knauss 1987)

The air drawing surface vortices can be controlled mainly by three methods: (a) increasing the submergence of the pump entrance from the water surface to values above critical limits that cause objectionable vortexing; (b) eliminating the approach flow non-uniformities, thereby reducing the contribution from this vorticity source to surface vortexing; and (c) providing vortex suppression devices. As regards to the first method, the submergence can be increased by lowering the sump floor and/or pump bell suction entrance or by increasing the minimum water level at which the pump is operated. Both of these options may be restrictive due to practical considerations. As regards, the second method could be attempted by a combination of several means; namely; modification of sump geometry and location with respect to approach channel and/or use of flow distributors or velocity modification devices (head loss devices) such as screens, gratings, and perforated walls. In the third method, the rotational energy contributing to vortices is dissipated significantly with suppressing devices such as horizontal gratings, cages, and rafts. This method is especially suitable if both approaches (a) and (b) above is restricted by practical considerations.

Controlling of subsurface vortices mainly involves elimination of large velocity gradients in the flow and avoiding flow separation inside the sump. To achieve this, the sump geometry should avoid sudden flow transitions and should provide sufficient wall and floor clearances from the bell entrance to avoid flow separations with large velocity gradients. Artificial devices such as floor cones, splitters, and fillets, are installed to prevent flow separation and to guide the flow into the suction bell. A good arrangement generally is derived by trial using a hydraulic model so that the intensity of induced swirl in suction pipe would be negligible.

1.6 BRIEF REVIEW OF LITERATURE

A vast amount of literature exists on the topic of air entrainment in pump sump intakes and its solutions; however, less attention has been focused on the swirl entrainment and its control. In general, swirl is not a big problem unless it is contributing to increased entrance losses and/or swirling pipe flow downstream from the entrance of suction pipe.

Of interest, how this swirl is affected by vortices at the inlet. A clear dependency between these two factors may at first thought appear obvious, but extensive measurements by Padmanabhan and Hecker (1982) indicates no statistically significant dependency between the vortex types and swirl. Still, this must be noted that in the vortex classification the initial occurrence of an air core to the inlet and larger air cores occupying significant portions of the inlet area are not delineated. Relatively large air core vortices would have an effect on the inlet loss coefficient, as shown by Anwar (1966) and Daggett and Keulegan (1974). In support to this hypothesis Arboleda and El-Fadel (1996) found that approach flow condition creates an excessive swirl (up to 25^{o}) even in the absence of surface and subsurface vortices. It is already mentioned the severity of such a larger swirl angles. So it appears, however, that vortices with incipient air cores, or lesser types, do not sufficiently increases the swirl to warrant concern.

There is no theoretical model available in the literature to estimate the swirl therefore, physical model studies are recommended by the British hydromechanics research association (BHRA) (Prosser 1977), hydraulic institute standards (HIS) (American National Standards Institute (ANSI) 1998), Indian standards (IS): 15310 (Bureau of Indian Standards (BIS), 2003), Turbomachinery Society Japan (TSJ), (Knauss 1987), Japan Society of Mechanical Engineers (JSME) (1984). Thus, several scaled model studies are reported in literature were reviewed critically for the present research work and are discussed in detail in Chapter 2 (Arboleda and El-Fadel 1996). Most of the literature on pump intake flow deals with air

entrainment, with swirl receiving only cursory attention and most of the reported studies are carried out to solve the site specific problems.

Moreover, the similarity laws of the model testing are not yet clear, and there are different opinions for velocity setting in the model test (Kawakita et al. 2012). Some research work indicates that performing the model study of the pump sump for higher Froude number (up to three times of Froude number corresponding to Froudian conditions). However, other studies indicate that the pump sump model study is to be carried out for Froudian condition only. Therefore, it is necessary to investigate the effect of different Froudian conditions on swirl.

Insufficient experimental and numerical literature exists on the effectiveness of anti-vortex devices to control the swirl. None of the reported studies give definite criteria to control swirl.

Baker and Sayre (1974) investigated the decay of swirl in smooth pipes with Reynolds numbers between 12,500 and 200,000. Their results showed that the angular momentum flux decreased exponentially along the pipe. This decay rate was found to be a function of Reynolds number and initial conditions. The decay of swirl is necessary to estimate the effect of swirl on pump and turbines.

1.7 NEED FOR THE STUDY

Following points are derived from the review of literature:

1. The generated swirl in the pump sump intake due to asymmetric in the approach flow conditions and dimensions of the pump sump has not been studied extensively in the literature.
2. Literature review reveals that some literature indicates performing the model study of the pump sump for higher Froude number even up to three times of Froude number corresponding to Froudian conditions. However, other literatures indicate that the pump sump model study is to be carried out for Froudian condition only. Therefore, there is a need to study the effect of Froude number on the swirl in the pump intake.
3. Various types of vortex breakers have been suggested in the literature to minimize the spiral motion in pump intake. However, the suitability of these vortex breakers in the light of flow conditions approaching the bell mouth is not discussed in literature.
4. A very few studies are reported with respect to the decay of swirl in suction pipe.

The present study was undertaken to investigate the flow process in pump bays by conducting experimentation on a scaled physical model and developing a computational fluid dynamics (CFD) model for the same model.

1.8 OBJECTIVES

The specific objectives of the present investigation are as follows:

1. To study swirl flow in the pump sump intake through experimentation and CFD under different approach flow to the bay.
2. To study the effect of Froude number on swirl in the pump intake through experimentation and CFD.
3. To study the effect of different types of vortex breakers and their dimensions on the swirl in the pump intake and to standardize the shape and size of vortex breakers taking into considerations the approach flow conditions.
4. To study the decay of swirl in suction pipe column of the pumps.

1.9 METHODOLOGY

To achieve the above objectives, numerical and experimental studies were carried out for an eight pump intake model (scale 1:12). First, swirl in different flow conditions was observed in the pump sump intake model for different pump combinations. Then the stringent combination was finalized. Velocity and swirl were recorded for different pump combinations to validate the CFD model. The effect of Froude number on swirl has been observed through experimental results. For the stringent conditions of flow that induce maximum swirl, different sizes of cross type breaker have been tested for swirl control.

A CFD model has been developed for simulation of flow in the pump sump. The CFD model results were compared with the experimentally observed values to validate the CFD model. For the simulation, CFD solver ANSYS Fluent has been used. After verification and validation of the CFD model, decay of the swirl and the effect of the Froude number on swirl have been studied. Full descriptions of methodology are described in relevant chapters.

1.10 LIMITATIONS

The limitations of the present study are as follows:

1. The present study has been carried out using clear water; therefore, the findings need consideration for water containing sediments.

2. The study has been carried out in non-silted pump sump under arid zone conditions. Therefore, in silted conditions, the findings of this study shall need examination.
3. The experiments have been carried out for pump running conditions, the pump start-up and shutdown conditions are not considered in the present study.

1.11 STRUCTURE OF THE THESIS

For the purpose of lucid presentation, this thesis is divided into eight Chapters. Chapter 1 provides the basics of pump sump intake problems, objectives, and methodology of the present study. Chapter 2 describes the state-of-the art theory and literature review related to the pump sump intakes. Chapter 3 describes the experimental setup and procedure adopted for the experimental investigations in the present study. Chapter 4 describes the CFD model development procedure. Chapter 5 describes the verification and validation of the CFD models used in present study. Chapter 6 describes the flow characteristics of the flow in pump sump, while Chapter 7 details the effect of various shapes and sizes of AVDs on pump approach flow. Chapter 8 presents a summary of the conclusions drawn from the present study along with the recommendations for future study.

CHAPTER 2 THEORY AND LITERATURE REVIEW

2.1 INTRODUCTION

Problems associated with pump intakes cannot be solved completely with analytical approach, therefore, alternative methods to identify the flow problems and their remedial measures are required. Physical modelling and computational fluid dynamics (CFD) modelling were used as alternative methods. This chapter deals with the theory related to physical and CFD modelling of the pump sump model. The dimensionless parameters, similarity laws and the model acceptance criteria are described in the physical modelling whereas in CFD modelling the procedure of CFD modelling has been described. Further, a detailed review of the relevant physical and CFD model studies related to the pump sump intakes are described in this chapter.

2.2 PHYSICAL MODELING

To solve the hydraulic problems at pump sump intakes, physical modelling is recommended for the following conditions as recommended by (American National Standards Institute (ANSI) 1998):

1. Pump sump with non-symmetric approach flow (such as due to an offset or bend in the approach channel upstream near the sump) if the submergence Froude number is greater than 0.25.
2. Multiple pumps with a common approach channel and a multitude of pump operating sequences.
3. Pump sumps of large capacities greater than about 9000 m^3/hr per pump (considering the cost of such large installations, a model study is warranted).
4. Pump sumps with possibilities of obstructions to approach flow close to the pump location, such as debris, blockage of trash racks or screens.
5. Pump sumps with minimum water levels below the recommended values but practical limitations do not allow a higher water level.

2.2.1 Dimensionless parameters

Physical modelling of hydraulic structures is theoretically founded on the principle that all the forces acting on water can be represented using a number of dimensionless parameters and that equality of these parameters between model and prototype will produce a similar flow condition. Typical dimensionless numbers are Froude number, Fr, Reynolds number, Re, and

Weber number, We, which account for gravitational, viscous and surface tension forces, respectively.

Froude number

The Froude number, Fr, is defined as the ratio between the inertial and gravitational forces acting on the flow and is defined as

$$\mathrm{Fr} = \frac{V}{\sqrt{gD}} \tag{2.1}$$

where D = characteristics length (intake diameter herein), V = characteristic velocity (average velocity through the suction pipe) and g = gravitational acceleration (9.81 m/s^2).

Practically, all studies to date, indicate that investigation of the hydraulic problems in pump sump intakes through model studies should be performed according to Froude-scaling. Therefore, most models are first scaled to this parameter. In a Froude-scaled model, the inertial and gravitational forces are similarly reduced such that the Froude number is unchanged. Unfortunately, at the same time, viscous and surface tension forces cannot be adequately reduced, thus simultaneous equality of all parameters is not possible. The extra influence that the viscous and surface tension forces have on the modelling of swirling flows is called a scale effect (Hecker 1981).

Reynolds number

The Reynolds number, Re, provides a relation between the inertial and viscous forces and is defined as

$$\mathrm{Re} = \frac{VD}{\nu} \tag{2.2}$$

where ν = kinematic viscosity.

There are conflicting opinions on the influence that the Reynolds number has on the formation of air entraining vortices. Haindl (1959) found that the formation of a free surface vortex is primarily a function of the Reynolds number. Although he argued that Reynolds equality is essential for similitude in vortex formation, the most subsequent investigators found that Froude dependence is dominant and Reynolds equality is of a secondary concern.

The influence of viscosity may also be dependent on the manner in which the circulation in the flow is produced. As already discussed, the primary sources of vorticity are eccentricity in the approaching flow, velocity gradients at boundaries and rotational wakes behind obstructions. The latter two sources are influenced by viscosity and, therefore, may be more Reynolds number dependent than the first source (Durgin and Hecker 1978).

Daggett and Keulegan (1974) showed that the discharge through an intake is influenced by viscous effects when $\mathrm{Re} < 2.5\times10^{4}$ and that beyond this value, viscous effects are unimportant. The concept of a limiting Reynolds number beyond which viscous influence on vortex formation is negligible has also been endorsed by Anwar et al. (1978) and Anwar and Amphlett (1980) and also by Jain et al. (1978) who argued that the limiting Reynolds number is Froude number dependent.

Weber number

The Weber number, We, relates the inertial forces to the surface tension forces acting on a fluid element. It is defined as

$$\mathrm{We} = V\sqrt{\frac{\rho D}{T}} \tag{2.3}$$

where ρ = density of water and T = surface tension.

The influence of surface tension on vortex formation is not well understood and in previous studies, for the most part, has been neglected. There is also an inherent difficulty in evaluating the influence of the Weber number alone. Hecker (1981) pointed out that isolation of the effect of the Weber number would require the plotting of a vortex-related parameter against the Weber number for constant values of circulation and Reynolds number. However, due to the inter-relationship between the Weber and Reynolds number, such a plot would be difficult to generate. Jain et al. (1978) performed experiments with liquids of different surface tensions and determined that vortex formation is independent of Weber number as long as $\mathrm{We} > 11$. Additionally, Daggett and Keulegan (1974) found that surface tension does not influence vortex intensity. Thus, if a model is sufficiently large, it can be safely inferred that surface tension does not significantly influence vortex flow and its consideration can, therefore, be omitted in the modelling process (Dhillon 1980).

2.2.2 Similarity laws

It is apparent that swirling flow is dependent both on the Froude and Reynolds numbers. However, this dependence is not well defined, and constancy of both Froude and Reynolds numbers cannot be attained simultaneously in hydraulic modelling, appropriate modelling criteria should be followed in order to minimize scale effects created by this inherent problem. In this section, some notable attempts by past investigators to develop such criterion are examined.

Reynolds scaling

Although, for the most part, it is believed that Reynolds number has only a secondary influence on vortex formation, Haindl (1959) found that the formation of vortices in a slowly draining reservoir is primarily dependent on the Reynolds number. Therefore, Haindl (1959) argued that the geometrical similarity and Reynolds constancy are required to ensure correct model prototype similarity. However, numerous subsequent studies have shown that Froude similarity is the dominant criteria (Anwar 1968; Durgin and Hecker 1978; Jain et al. 1978; Anwar and Amphlett 1980).

Anwar's criterion

Anwar (1968) and Anwar and Amphlett (1980) showed that for $(Q/\nu S) > 3\times10^4$, viscous forces do not influence vortex formation and that, if this condition is met, vortex behaviour is dependent only on circulation and the Froude number. Anwar (1968) suggests that a geometrically similar model, based on Froude constancy with a sufficiently high Reynolds number, will adequately reproduce prototype circulation and vortex behaviour if its scale is not less than 1:20.

Padmanabhan and Hecker (1984) found that no significant scale effects occurred in 1:2 and 1:4 models operated under Froude similarity, thus confirming that intake vortices can be adequately modelled by Froude-scaling at scales larger than that prescribed by Anwar (1968).

Jain *et al.* Criterion

Jain et al. (1978) found that the limiting Reynolds number at which viscous forces no longer influence the critical submergence is dependent on the Froude number and that Froude number similarity can be used at any scale to simulate prototype performance if an appropriate correction factor is used to adjust the results. This correction factor is defined by Jain et al. (1978) and has a value of unity when the value of the Reynolds numbers is high in comparison to the Froude number, or when

$$\frac{g^{1/2}d^{3/2}}{\mu} > 5\times10^{4} \tag{2.4}$$

Therefore, according to Jain et al. (1978), a Froude-scaled model will reproduce prototype conditions with acceptable accuracy provided that the intake diameter is of sufficient size to ensure a high enough Reynolds number such that viscous forces can be neglected.

Equal velocity criterion

Some investigators have suggested the use of larger intake velocities than those required by Froude scaling. Based on their experimental results, Denny and Young (1957) suggested that prototype performance can be adequately simulated under similar submergence conditions if equal model-prototype velocities are used. However, a larger than Froudian intake velocity is likely to exaggerate vortex formation through amplification of the axial stretching mechanism and thus, subsequent investigators have found that this approach leads to a conservative design (Dhillon 1980). Additionally, as noted by Hecker (1981), for some scale ratios, the use of the equal model prototype velocity approach can seriously undermine the primary Froude-scaling criterion and thus, the approach flow conditions and resulting circulation will not be properly reproduced.

2.2.3 Model acceptance criteria

The acceptance criteria for the model test given in ANSI/HIS (1998) are as follows:

1. Free surface and sub-surface vortices entering the pump must be less severe than vortices with coherent cores, i.e. surface vortices of type 3 and sub-surface vortices of type 2 (Figure 1.2).
2. Velocities at points in the throat must be within 10% of the cross-sectional area average velocity. Time-varying fluctuations in velocity at a point shall produce a standard deviation from the time-averaged signal of less than 10%.
3. Air entrainment into pump inlets should be nil.
4. Swirl angles entering the pump must be less than 5 degrees.

In recent years, most of the model tests for pump stations have been completed using scale-model tests. Scale-model tests are currently considered the most reliable way to assess pump intake designs in relation to these criteria. Disadvantages of these kinds of tests are high costs, long time to build test facilities and limited access to experienced testing specialists. CFD

analysis has the potential of giving much more detailed information of the flow field at a fraction of the cost and time needed for scale-model tests.

2.3 CFD MODELLING

Computational Fluid Dynamics (CFD) is the use of computer-based simulation to analyse systems involving fluid flow (Versteeg and Malalasekera 2007). CFD modelling is quite popular with the advancement of computational facilities. Several CFD model studies have been reported in the literature. This section describes the general procedure for CFD modelling. Detailed step-by-step procedure has been described in Chapter 4. The complete CFD modelling procedure can be divided into the following three stages (Figure 2.1):

1. Pre-processing
2. Solver run
3. Post processing

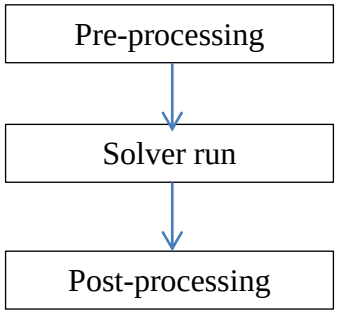

Figure 2.1 Flow chart of the CFD analysis process

2.3.1 Pre-processing

Pre-processing consists of geometry creation and mesh/grid generation. For geometry creation and mesh generation, many 3D modelling tools are available such as ICEMCFD, Design Modeler, Gambit, SolidWorks, AutoCAD, CATIA etc. Some of these are for both geometry and mesh generation such as ICEMCFD, Gambit etc. The detailed procedure has been described in Chapter 4.

2.3.2 Solver run

After creating the geometry and mesh, the mesh is transported to the solver. Again, there are many commercial solvers are available to solve the flow problem. In present study, fluent solver has been used for CFD simulations. The details of the solver specification have been described in Chapter 4.

2.3.3 Post processing

After the solver run, the generated data from the solver is processed for the analysis purposes. For post processing of the data, many tools are available such as TechPlot, Excel, and CFD-Post etc. In present study, CFD-Post has been utilised for streamlines, contour plots, charts etc. For quantitative analysis, Excel and Sigma Plot have been used to plot various graphs.

2.4 FLUENT

Fluent is a commercial software to solve fluid flow problems and used in the present study to simulate the flow in multiple pump sump intake. The numerical method in Fluent is based on a cell center finite volume method (FVM) capable of using both structured and unstructured meshes, and thus, provides complete mesh flexibility in complex topologies.

2.5 PREVIOUS NUMERICAL AND EXPERIMENTAL STUDIES

Several experimental and numerical studies were reported in the literature to investigate the flow phenomenon associated to the pump sump intakes. The detailed discussion of the relevant numerical and experimental studies has been presented herein.

Haradasa and Cox (1980) tried to improve the approach flow in a one bay vertical pump intake by the use of anti-vortex devices (AVDs). They tried four different shapes and sizes of AVDs as shown in Figure 2.2. They tested the model for different water levels and different discharges. They used vortimeter for swirl measurement and also computed inlet loss coefficient.

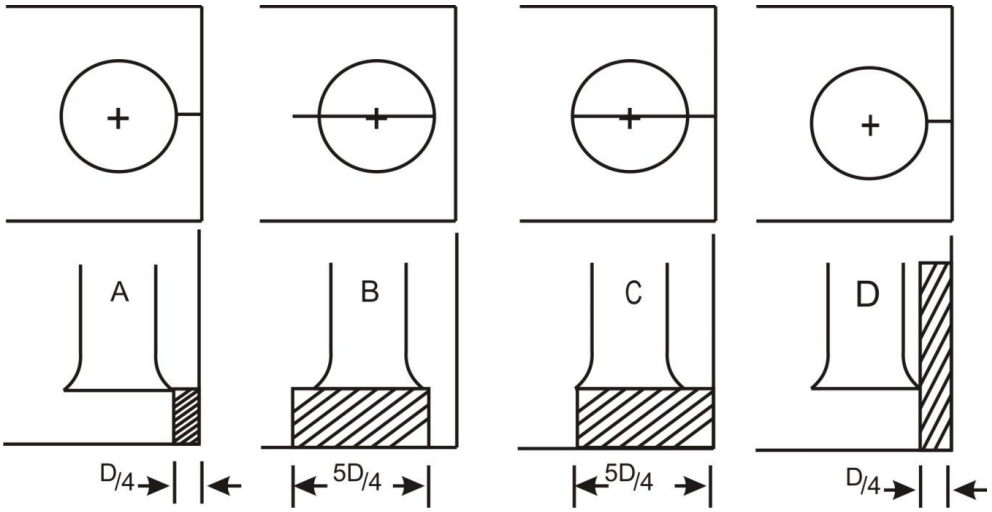

Figure 2.2 Anti vortex devices (Hardasa and Cox 1980) (D = 135 mm)

Hardasa and Cox (1980) found that all the tested AVDs produced significant reduction in swirl, entry loss and pressure head fluctuations at the intake. In general the AVD type C gave the least swirl whilst AVD of type D gave the lowest entry loss. However, from the qualitative results they observed AVD of type D shows severe air entrainment due to its influence on surface and near surface flow between the intake and the backwall where the most of the vortices were propagated. Hence, they recommended that the any AVD downstream of the intake should be placed well below the expected minimum sump water level. AVD B produced the steadiest swirl and the least air entrainment and submerged vortices. They concluded that the AVD B is best suitable among the four even though the swirl as indicated by vortimeter was marginally higher than compared to AVDs C and D. Further, they said that the main difference between the AVD B and other AVDs was that it allows free stream movement of flow between the intake and the backwall. AVD C, which shows least swirl, is identical to the AVD B except for its position relative to the rear wall. In conclusion, the best results can be achieved by using an AVD similar to B, placed further downstream of the bell mouth lip but allowing sufficient clearance to permit the flow between intake pipe and rear wall. From the swirl at different water levels they found that the swirl decreases as the water level increases.

Odgaard and Dlubac (1983) reported an experimental model (scale 1:10) study a four pumps intake sump. In model tests, they found that the pump sump model does not meet the model acceptance criterion. They observed, Type 4 vortices (ANSI/HIS 1998) (pulling trash but not air) forming on the surface of water around the pump column, and Type 5 vortices (ANSI/HIS 1998) (pulling intermittent air bubbles), emanating from the floor and back wall of the sumps, to enter the pump bells, and the swirl of the flow entering the pumps was more than 10°. Also, the transverse distribution of velocity in the pump sumps was not uniform, which caused unacceptable large-scale turbulence in the approach flow. They ameliorated the flow situation by design modifications, which consisted of the installation of (1) Two straight vertical vanes in downstream of columns (2) one vertical vane parallel with, the outer wall of the approach channel; and (3) one vertical guide vane in continuation of the side wall of the approach channel. The aforementioned modifications greatly reduced the turbulence in the approach flow. They suggested a AVD which consists of a floor and backwall splitters in the bays as shown in Figure 2.3. They proposed this to reduce the swil and to prevent the two persistent floor and backwall vortices from forming.

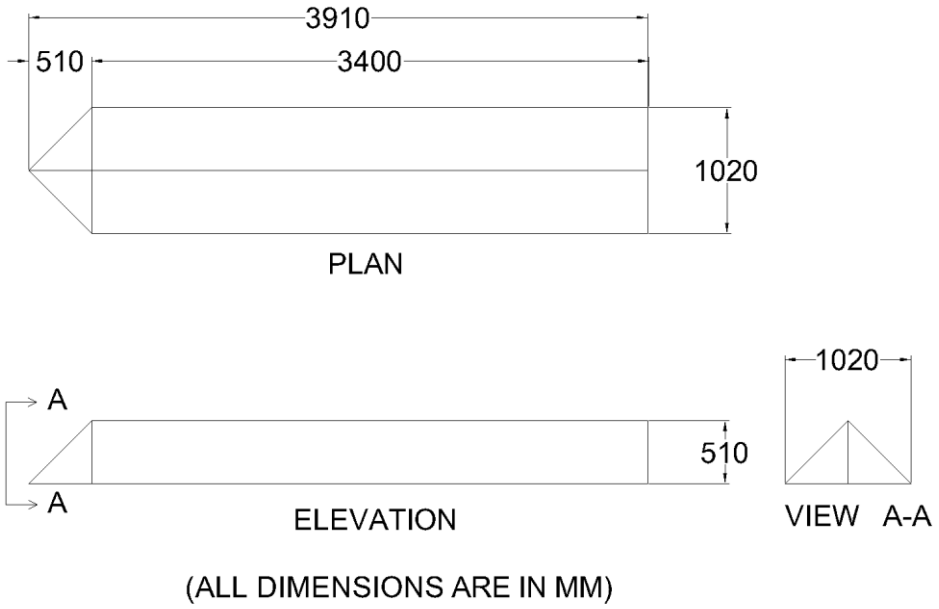

Figure 2.3 Details of anti-vortex device (Odgaard and Dlubac 1983)

Arboleda and El-Fadel (1996) reported a pump sump model study (scale 1:18) of a sump design, which was highly dependent on the approach flow conditions. They found several hydraulic deficiencies during model testing. The flow distribution within pump cells was uneven, with flow velocities skewed in both the horizontal and vertical planes. They found that significant deviations from existing design guidelines will be required to attain a generalized sump design. They found adverse effects of approach flow conditions on hydraulic performance that can be mitigated with flow distribution and guidance structures. A combination of baffles, horizontal beams, ramps and flow splitters will provide satisfactory flow conditions. The modifications suggested by them are shown in Figure 2.4.

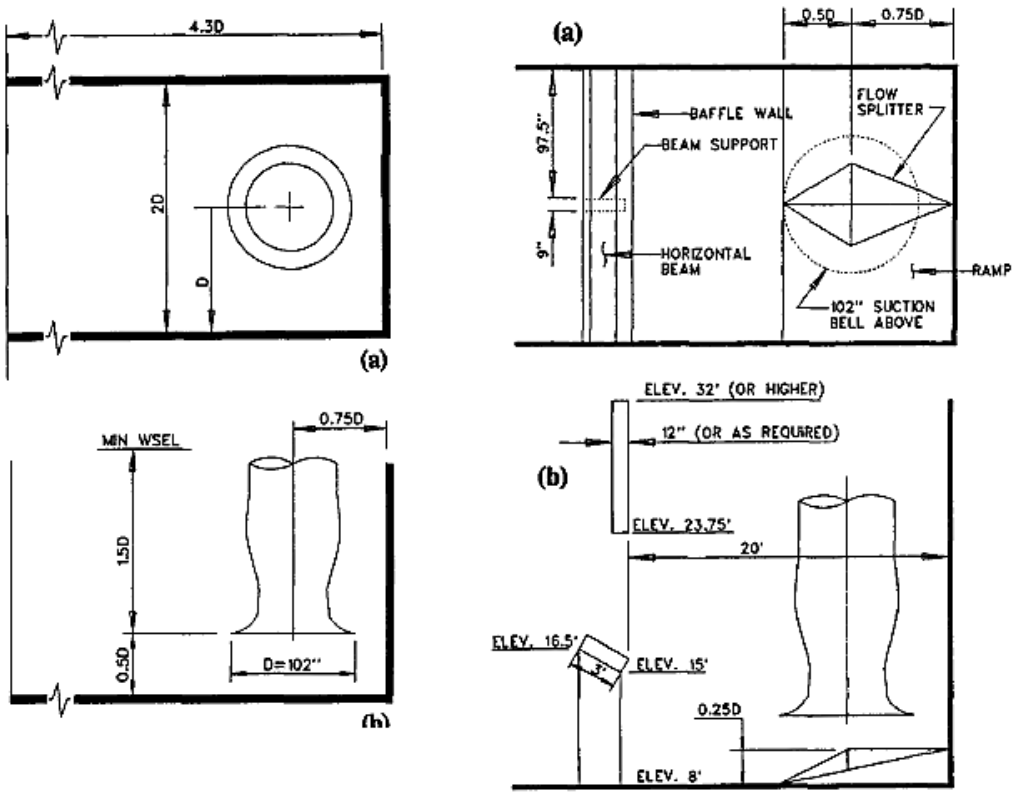

Figure 2.4 Layout of AVD (a) without and (b) with modifications (Arboleda and El-Fadel 1996)

Constantinescu and Patel (1998) proposed a Reynolds average Navier Stokes (RANS) based CFD model with near-wall modelling capabilities that can be used to improve design methods to avoid the formation of strong free surface and subsurface vortices in pump intakes. Their study concentrated on simplified pump intake geometry as shown in Figure 2.5, which did not contain the usual vortex suppressing devices found in realistic intakes but in which the flow retained the main complexities encountered in more complex geometries. Their CFD model solved the RANS equations with the two layer k-ε turbulence closure of (Chen and Patel 1988) for the simulations. The details are given in Constantinescu and Patel (1998). They assumed free surface as flat and they neglected the surface tension during the simulations. They used no slip conditions on all solid surfaces, including all channel walls and the inside and wetted outside of the pipe. In preliminary tests, they found satisfactory results from the CFD model with respect to the numerical performance, i.e., convergence and grid dependency of solution, as well as agreement of results with previous calculations.

Constantinescu and Patel (2000) further investigated the effect of the turbulence model and the effect of wall roughness on the flow. They discussed their observations with respect to the prediction of critical flow features, such as subsurface and free surface vortices and the level

of swirl inside the pump column. Main conclusion of their study was that a near wall turbulence model is essential to predict the important flow features in pump intakes. This is because large adverse pressure gradients and massive separation are present in the pump column region. They concluded that the two layer k-ε model and the low Reynolds number k-ω model predict similar results on smooth surfaces. They found that the high Reynolds number k-ω model, which takes roughness into account, predicted weaker vortices. Their result showed that the effect of roughness was simulated correctly, at least qualitatively. Based on the observation, they suggested that the wall roughness can be used as a vortex suppressing device.

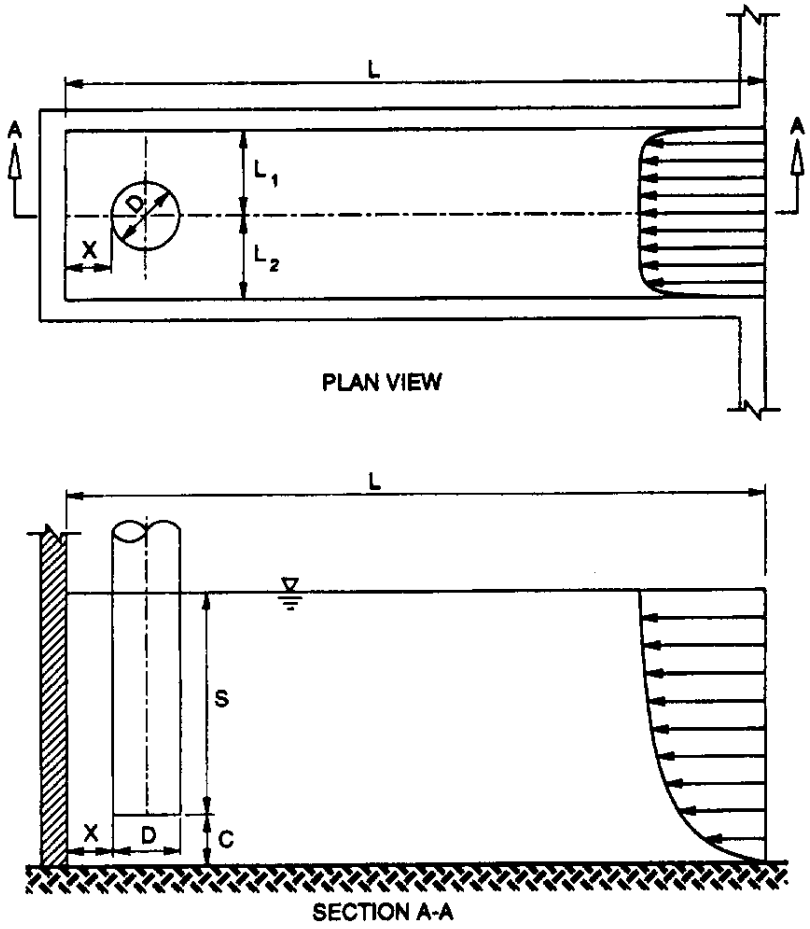

Figure 2.5 Pump sump model of Constantinescu and Patel (1998)

Rajendran and Patel (2000), and Rajendran et al. (1999) collected data to validate the CFD model proposed by Constantinescu and Patel (1998). They used experimental data which include mean velocity and vorticity distributions in relevant sections measured using PIV techniques of identical geometry and for same flow conditions used for the validation. Figure 2.6 shows relative sizes of the regions where they compared the experimental and numerical results, and the direction from which the flow was viewed. They found that the number and

the type of the vortices observed in the experiments were predicted correctly by the CFD model. The distribution of the vorticity inside the cores of these vortices was also predicted reasonably well by the model, especially for the vortices that were found to be relatively stable in the experiment. Figure 2.7 shows experimental results obtained by Rajendran et al. (1999) for various vortices.

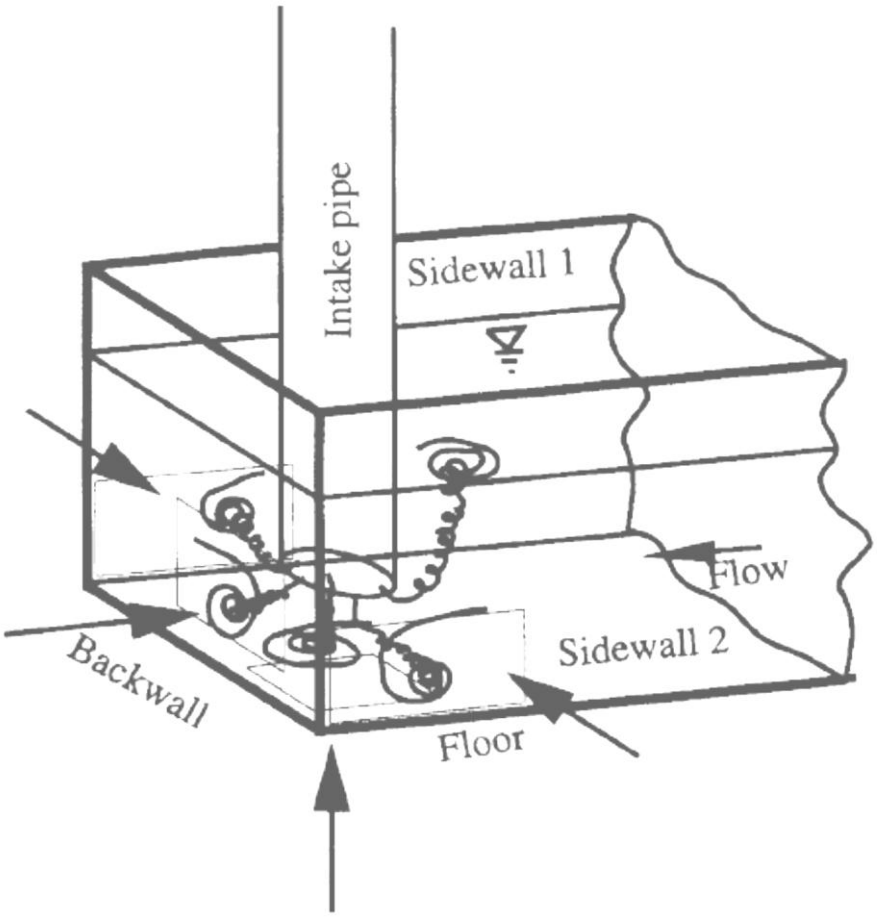

Figure 2.6 Vortices and main regions of comparison between experimental and numerical results (Rajendran and Patel 1999)

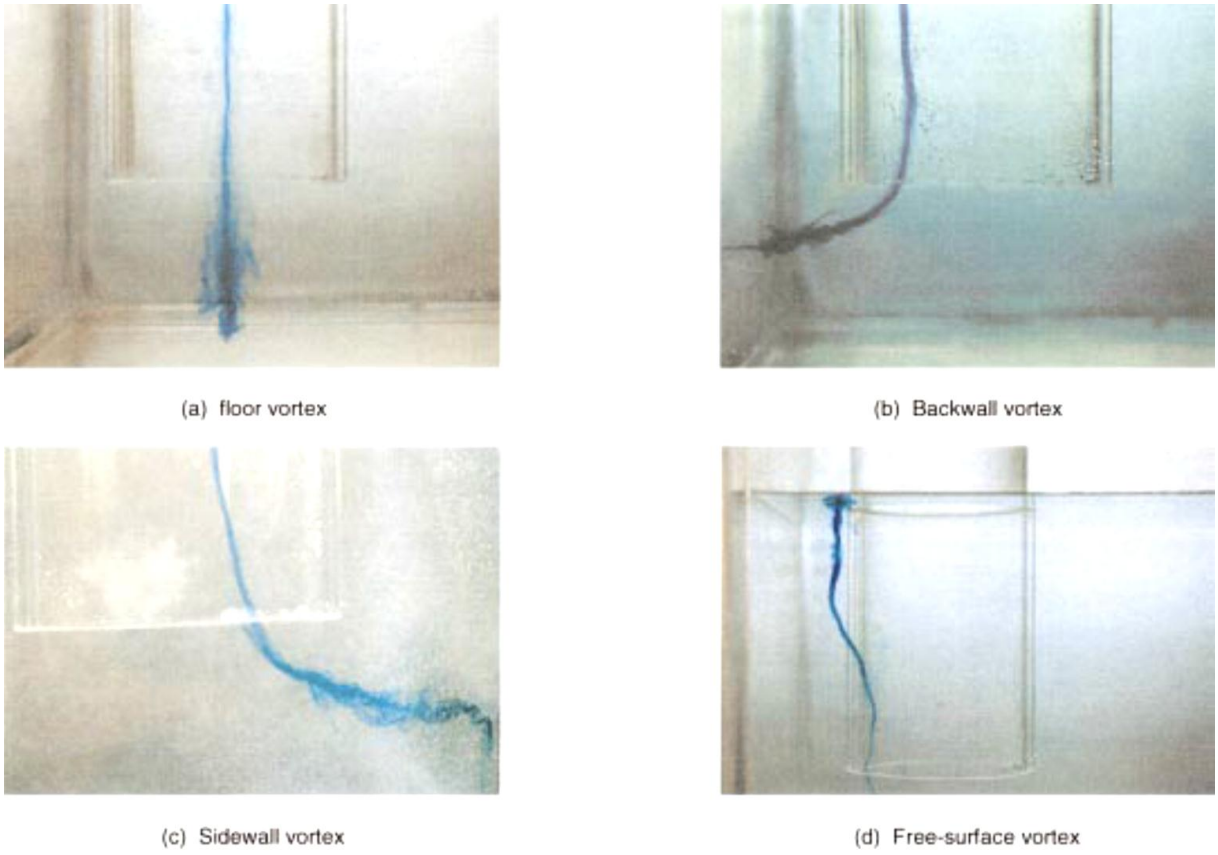

Figure 2.7 Visualization of vortices (Rajendran and Patel 1999)

Ansar and Nakato (2001) carried out detailed measurements of three-dimensional flows within a rectangular single-pump bay area of a right angle water intake model. They investigated the swirling flow characteristics within the pump sump in with and without cross-flow conditions using an acoustic Doppler velocimeter (ADV). They observed nearly uniform streamwise velocities in the pump bay and weak free-surface vortices near the pump column in without cross flow conditions as shown in Figure 2.8 (a). With cross flow, they found the existence of a large recirculation zone upstream of the pump column such that strong streamwise velocities were present at higher depths and near the left sidewall, while the reverse current concentrated at lower depths along the sidewall as shown in Figure 2.8 (b). Flow patterns in the latter case were also characterized by strong free-surface vortices in the vicinity of the pump column and a strong floor-attached subsurface vortex underneath the pump bell. Deep flow-turning vanes could be incorporated into the trash racks design to cope with strong cross-flow conditions.

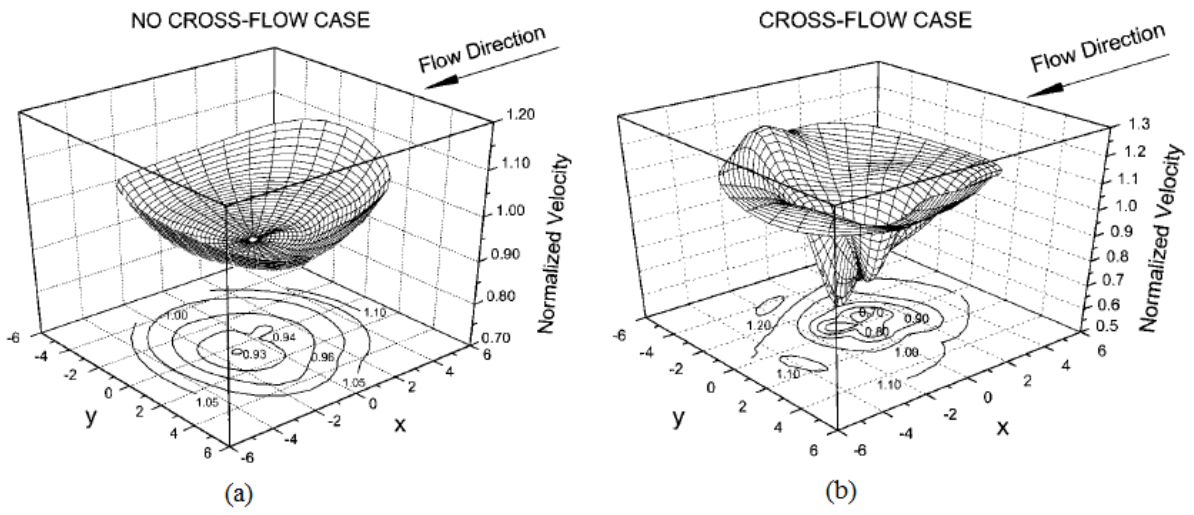

Figure 2.8 Velocity distributions at pump throat for (a) no cross flow conditions (b) cross flow condition (Ansar et al. 2001)

Ansar et al. (2002) further performed CFD simulations on relatively coarse meshes (approximately 150,000 cells) of the flow in single and dual pump intakes using a simplified version of the model of Constantinescu and Patel (1998). They used an inviscid model (the solid surfaces were treated as slip walls) under the assumption that the main cause of vortex formation is due to inviscid rotational effects in the intake. They found that the inviscid model was able to predict reasonably well the velocity profiles inside the approach channel away from the solid boundaries for the cases (without and with cross flow) studied experimentally by same authors. However, they found the model failed partially in the prediction of the location of the free surface vortices.

Li et al. (2004) used a CFD model proposed by Lai et al. (2003), U^{2}RANS, with capability to use arbitrarily shaped cells, to simulate the flow in a pump sump intake. They performed simulations on the same pump sump model as used by Constantinescu and Patel (1998). The standard *k*-ε turbulence model with wall functions was used. For the simple intake case, all the mean vortices observed in the experiments were accurately simulated, in the sense that the shape, location and direction of rotation of the main eddies were predicted correctly. Overall the results obtained with U^{2}RANS showed the same level of agreement with the experimental data as the previous simulation of Constantinescu and Patel (1998). Two U^{2}RANS solutions were obtained by considering with and without thickness of pipe wall. With the exception of the free surface vortices, the pipe wall thickness was found to have insignificant effect on the vortex patterns inside the pump bay. The principal advantage of this new numerical model was its robustness, derived from its capability to use unstructured, multi-block grids, providing quick and steady convergence, as well as requiring simple initial conditions. These

capabilities are further evaluated by Li et al. (2001) through applications of the numerical model to simulate flow in pump intakes with practical geometries.

Tokyay and Constantinescu (2006) reported large-eddy simulation (LES) in conjunction with an accurate non-dissipative non-hydrostatic Navier-Stokes massively parallel solver to predict the flow and vortical structures in a pressurized pump intake of complex geometry. The design of the pressurized pump bay consists of one pump column with two approaching channels of identical section and several flow training devices. Tokyay and Constantinescu (2006) validated the LES model using particle image velocimetry data collected by Yulin et al. (2000) on the same laboratory model. Also, to demonstrate the performance of the LES model, they compared the results from steady simulations employing the SST (shear stress transport) Reynolds-averaged-Navier-Stokes with LES. They found that even if SST can fairly successfully capture the mean velocity distribution and mean vortical structures in some regions, overall LES can more accurately predict the mean flow and turbulence statistics compared to the steady SST model.

Desmukh and Gahlot (2010, 2011) evaluated the feasibility of commercial CFD software CFX to design the pump sump intakes. They tested a physical model (scale 1:11) of three bays pump intake. In the part of the study (2011), they studied the effect of expansion angle in the forebay using CFD modelling. They concluded that the reducing the angle of expansion improves the flow conditions considerably. Further, they stated that this is to be confirmed by model study.

Pratap and Chavan (2013) did a physical and CFD model study (scale 1:10) of a four bay pump sump. They used k-ε turbulence model to model the turbulence. They specified the zero pressure inlet boundary conditions at the inlet and average velocity at the outlet. They treated the free surface as free slip wall boundary conditions. For all remaining walls (pipe wall, floor and sidewalls) they specified no-slip boundary conditions. For physical modelling, they used Froude number similitude conditions and concluded that the CFD modelling can be used to model the pump sump flow conditions.

Pradeep et al. (2012) did an experimental and CFD model study (scale 1:12) of a horizontal pump intake system with six pumps. For the same model, they did CFD simulations using Fluent solver. They compared the CFD simulation and physical model test results for the flow conditions as given in Table 2.1. They used Fluent solver to solve the RANS equations along with k-ε turbulence model. They used Pitot tube and the vortimeter for the velocity and swirl

angle measurements, respectively. They suggested need of PIV to measure the complete flow field for the validation purposes. They compared the velocity distribution at the cross section of draft tube inlet, swirl angle in the pump suction pipe and streamline patterns in the sump chamber.

Table 2.1 Flow conditions (Pradeep et al. 2012)

S. No	Case	Pump No in operation	Flow conditions
1	Case 1	#1#2#3#6	2Fr
2	Case 2	#1#6	Equal velocity
3	Case 3	#1#2#3#$#5#6	Fr
4	Case 4	#1#2#3#$#5#6	2Fr

Meena et al. (2013) used six bays pump intake model (scale 1:12) to investigate the flow by CFD modelling. They used finite volume based Fluent solver to solve the RANS equation along with SST (shear stress transport) *k-w* model to model the turbulence. They specified the inlet section at the entrance as inlet boundary and pipe outlets as pressure outlet with relative average static pressure of zero atmospheric. No slip shear condition for all the walls. The free surface they treated as wall with specified shear equal to zero. They analysed the CFD results by comparing the measurement of velocity at various locations in the physical model study. The velocity measurements were performed on the grids at the entrance of forebay and in the forebay. They used P-EMS (programmable electro-magnetic systems velocity meter) to measure the velocity at any point in the flow. They also analysed the vorticity and pattern of the streamlines. They compared the experimental and computed velocities at various grid locations and found that the velocities are in good agreement to each other.

Kang et al. (2014) did an experimental investigation on a four bays pump sump intake model based on Froude number similitude ($D = 0.6D_b$). They performed the tests under subcritical flow conditions (Fr = 0.36 to 0.46) and different pump combinations. They used swirl meter/vortimeter to measure swirl angles. In preliminary tests they found that the swirl angles are very strong and beyond the acceptance limits. Therefore, they tried to find the solution of the problem. They performed the tests to find the effective shape of floor splitter as an AVD. For this they used three types of quadrilateral submerged bar with different shape and dimension in sectional area as shown in Figure 2.9. They confirmed that the installation of the AVD is very effective to reduce abnormal vortices including sub-surface vortices, pre-swirls and other undesirable hydraulic phenomena. They found splitters with square sections (AVD

a and b) showed partly large swirl angles beyond the acceptable criteria of (American National Standards Institute (ANSI) 1998) though a large square was more effective than a small one. Meanwhile, the splitter with trapezoidal section showed swirl angle values of less than 5 degrees in all cases of pump operation. Among the three types of AVD, the trapezoidal splitter is the most effective one to suppress the vortices as shown in Figure 2.10. It is very useful to reduce the occurrence of submerged vortices and to obtain stable inflow condition for designing a high performance pump sump. They also mentioned that the swirl angle showed relatively large value at the large Froude number.

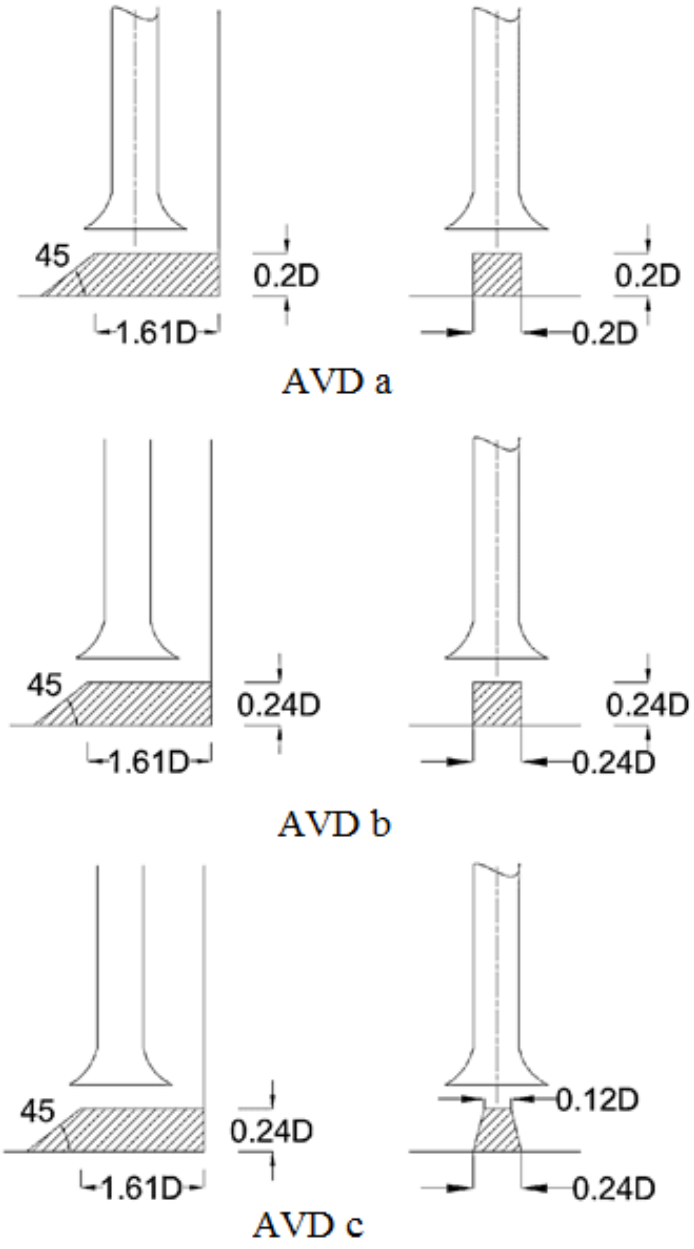

Figure 2.9 Schematic views of AVDs (Kang et al. 2014)

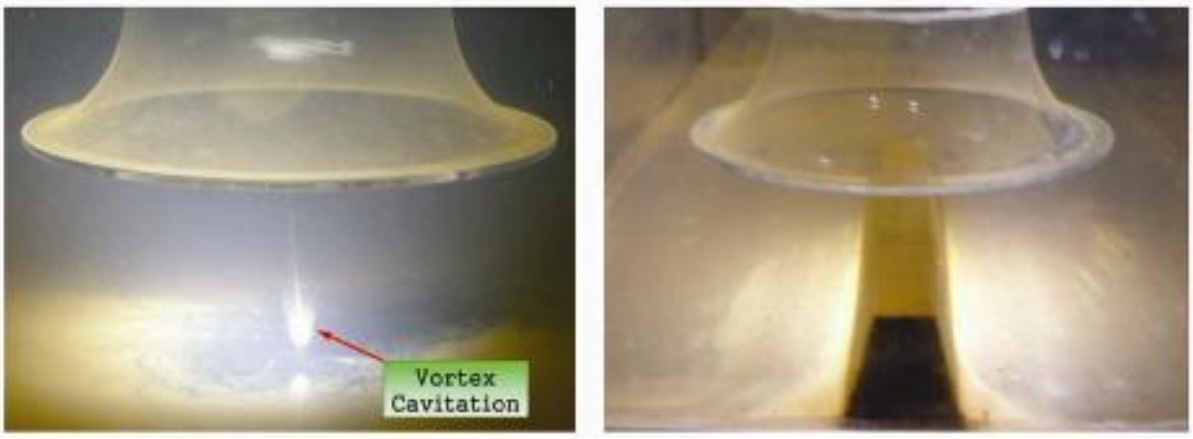

Figure 2.10 Observed flow under the bell mouth with and without AVD (Kang et al. 2014)

Kim et al. (2015) investigated a three bays pump sump model (scale 1:10) designed as per (American National Standards Institute (ANSI) 1998) standards using physical and CFD modelling as shown in Figure 2.11 and Figure 2.12. It consists of two drum screens, two inlets, three pumps and one dummy channel. They checked the flow uniformity and causes of vortex occurrence in the model and further they suggested the modifications to control the excessive swirl and vortices. They proposed the modifications as shown in Figure 2.13. They used vortimeter to evaluate the swirl in physical model tests. They used a wire mesh inside the sump with drum screen has same porosity as the real case.

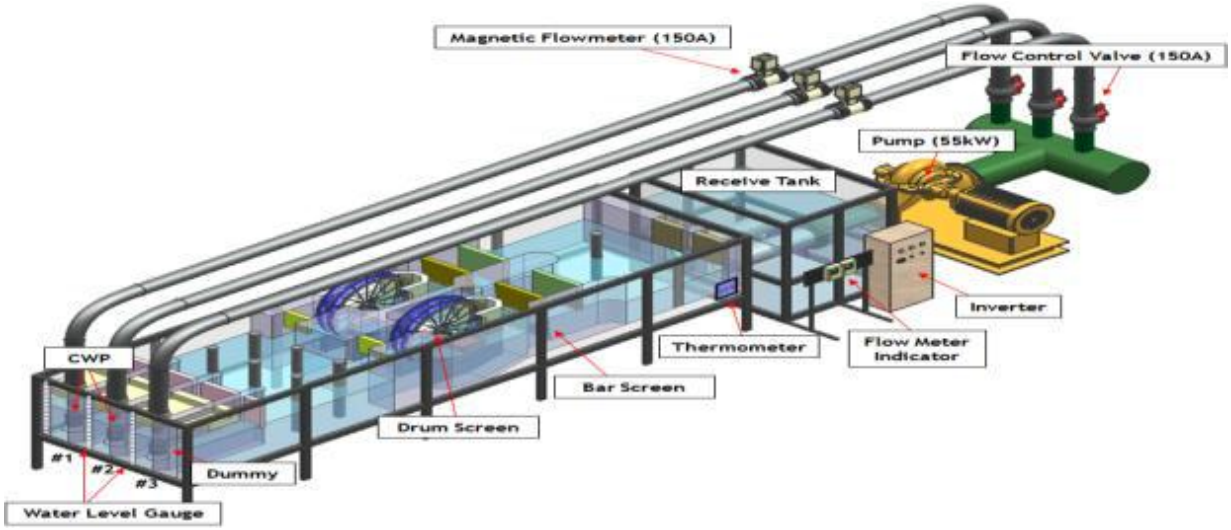

Figure 2.11 Experimental set up of Kim et al. (2015)

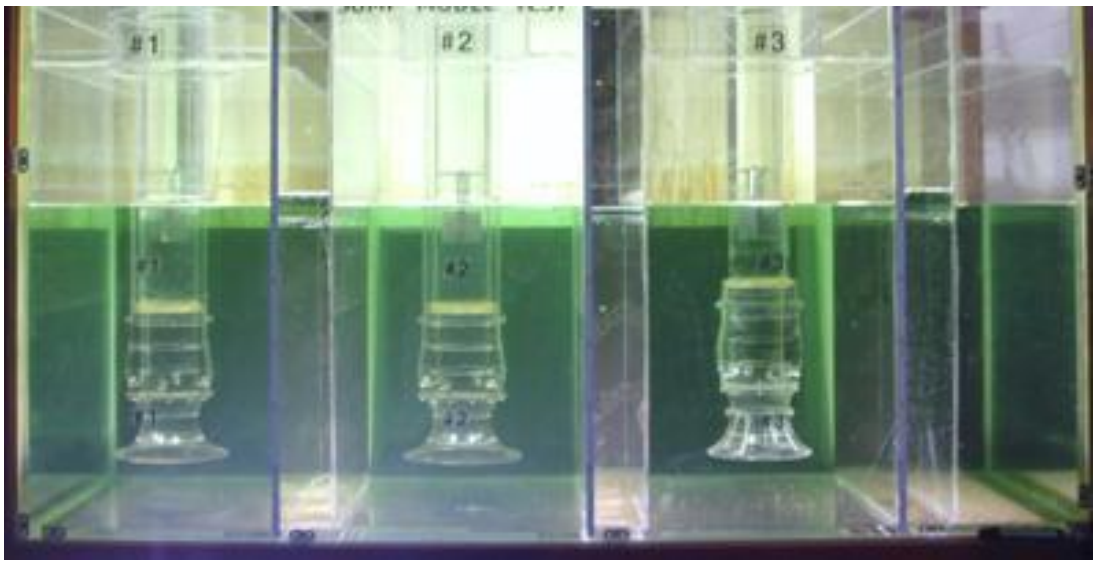

Figure 2.12 Close up view of the bays and bell mouths (Kim et al. 2015)

In CFD modelling, Kim et al. (2015) observed the difference between single phase and two phase CFD analysis. In single phase CFD analysis, there is no noticeable effect in pressure at the region behind the distributor when it is inserted as shown in Figure 2.13b. But in two phase analysis, there is a pressure drop behind distributor and its effect has to be considered. Therefore, they did two phase steady state calculations using a finite volume solver ANSYS CFX. They used shear stress transport (SST) turbulence model to model the turbulence.

They found quite comparable results from the CFD modelling and mentioned that the differences in their results are due to unavoidable errors in experiments, such as the water flow causing the swirl meter to fluctuate and not completely turn, and the innate problem that CFD cannot exactly replicate experimental conditions.

(a) bottom AVD (b) distributor at the front side of common bay

Figure 2.13 AVD design proposed by Kim et al. (2015)

Figure 2.16-2.16 depict the velocity contours and vortex core region. Figure 2.16 shows the velocity contours at the plane 1m above the bottom without an AVD and Figure 2.15 shows the same with an AVD. While comparing the two figures, it is observed that there is a strong jet flow in the common bay in Figure 2.16, and hence, high swirl angles develop. But in Figure 2.15, distributors help to make the flow uniform, reduce the axial flow, and hence result in a very small swirl angle. Figure 2.16 shows the vortex core region obtained by submerged bottom vortex method. The side walls (left and right), back wall and bottom vortex are shown in the figure with red circles.

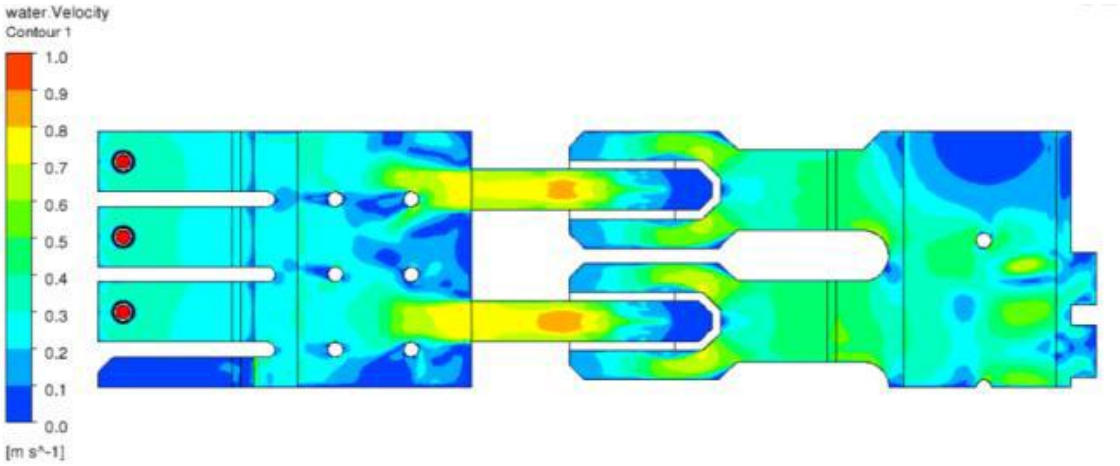

Figure 2.14 Velocity contours in a horizontal plane without AVDs (Kim et al. 2015)

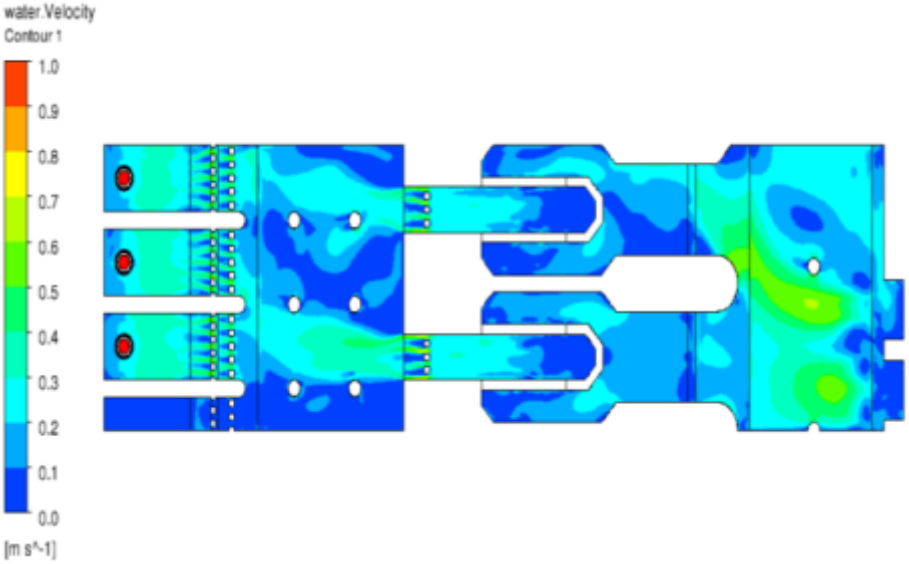

Figure 2.15 Velocity contours in a horizontal plane with AVDs (Kim et al. 2015)

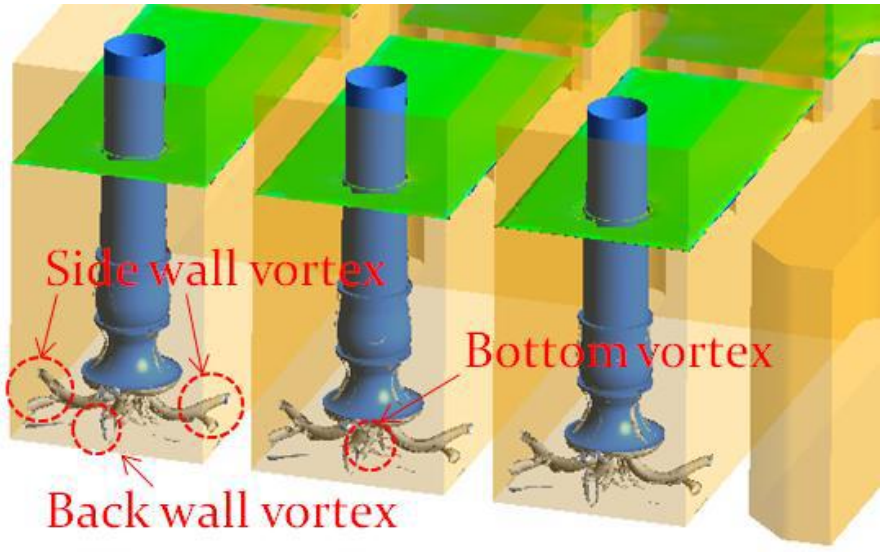

Figure 2.16 Vortex core region without AVDs (vorticity 5 s^{-1}) (Kim et al. 2015)

2.6 CONCLUDING REMARKS

The following points were noted after discussing the theory related to pump sump modeling and review of the relevant studies:

- The generated swirl in the multiple pump sump intakes has not been studied extensively.
- Effect of Froude number on swirl and decay of swirl in suction pipes has not been studied extensively.
- Literature review reveals that there is a need to investigate the swirl and its causes.
- A very few studies were reported that discusses the effect of AVDs on swirl.

CHAPTER 3 **EXPERIMENTAL PROGRAMME**

3.1 INTRODUCTION

This chapter deals with the experimental program of the present study. Experimental setup, equipments, calibration of bendmeters for discharge measurements and procedure for conducting the experimental runs to investigate the flow characteristics of multiple pump sump intakes under different flow conditions and configurations are presented herein. Experimental setup was constructed and fabricated in the Hydraulics Laboratory of the Department of Civil Engineering, I.I.T. Roorkee, India.

3.2 EXPERIMENTAL SETUP

In present study, a multiple (8 bays) pump sump intake model (scale 1:12) has been used based on the Froude number (Fr) similitude. The prototype pump-sump was consisted of an approach channel, forebay and eight bays for eight cooling water pumps. The approach channel was 14m wide and 6.8m deep. The width of the forebay at inlet was 14.0m and both the side walls of the forebay were flared by 20^0 and the bottom floor had 10^0 downward slope. The bed level of the channel and floor of the sump were -7.0 m and -9.7 m, respectively. The maximum and minimum water levels in the sump were -1.7 m and -0.5 m, respectively. Eight bays, each of length 16.0 m and width 4.4 m with 1 m pier thickness are provided for eight pumps. Vertical screen consisting of 20 mm circular diameter bars with clear spacing between them as 50 mm is provided at the entrance of each bay. A stop gate of height 3 m was provided behind the screen at distance 1.5 m from the screen. Details of pumps and prototype flow conditions are as given in Table 3.1.

Table 3.1 Details of pumps in the prototype

S. No.	Description	pumps
1	No. of working pumps	6
2	No. of pumps standby	2
3	Total number of pumps	8
4	Design flow per pump	20,500 m^3/hr
5	Maximum flow per pump	24,600 m^3/hr

Flow in the pump sumps is mainly governed by gravitational and inertial forces. Therefore, it is necessary to preserve the ratio of these forces both in model and prototype by adopting Froude similarity law. The undistorted model, which requires geometrical similarity of all the

dimensions of model and prototype is commonly used for sump model study. The ratio of all corresponding dimensions in model and prototype be equal, i.e.,

$$L_r = \frac{L_m}{L_p} \tag{3.1}$$

where L_r = length scale, L_m = length of model, and L_p = length of prototype. Froude similarity law requires equal Froude number F in model and prototype.

$$\text{Fr} = \frac{V}{\sqrt{gD}} \tag{3.2}$$

where V = axial velocity in suction pipe; g = the gravitational constant; and D = suction pipe diameter (here the suction pipe diameter).

The scale ratios for velocity V, discharge Q, and time T resulting from Eq. (3.1) and (3.2) for the scale ratio L_r = 1/12 in the present case are

$$V_r = \frac{V_m}{V_p} = \sqrt{L_r} = \frac{1}{3.46} \tag{3.3}$$

$$Q_r = L_r^2 \times V_r = L_r^{2.5} = \frac{1}{498.83} \tag{3.4}$$

$$T_r = \frac{L_r}{V_r} = \sqrt{L_r} = \frac{1}{3.46} \tag{3.5}$$

All the dimensions of the model are fixed on scale 1/12 and discharges are calculated using Eq. (3.4). Thus, in the model

Design discharge of each pump (Q_d)	= 0.011416 m^3/s;
Maximum discharge of each pump (Q_{max})	= 0.013699 m^3/s;
Total design discharge of six working pumps (Q)	= 0.068494 m^3/s

Figure 3.1 shows the plan and L-section of the experimental set-up. In this figure, the Arabic figures represent an assigned number of the bell mouth given from right to left as #1, #2, #3, #4, #5, #6, #7 and #8. Dimensions of pump sump model are given in Table 3.2.

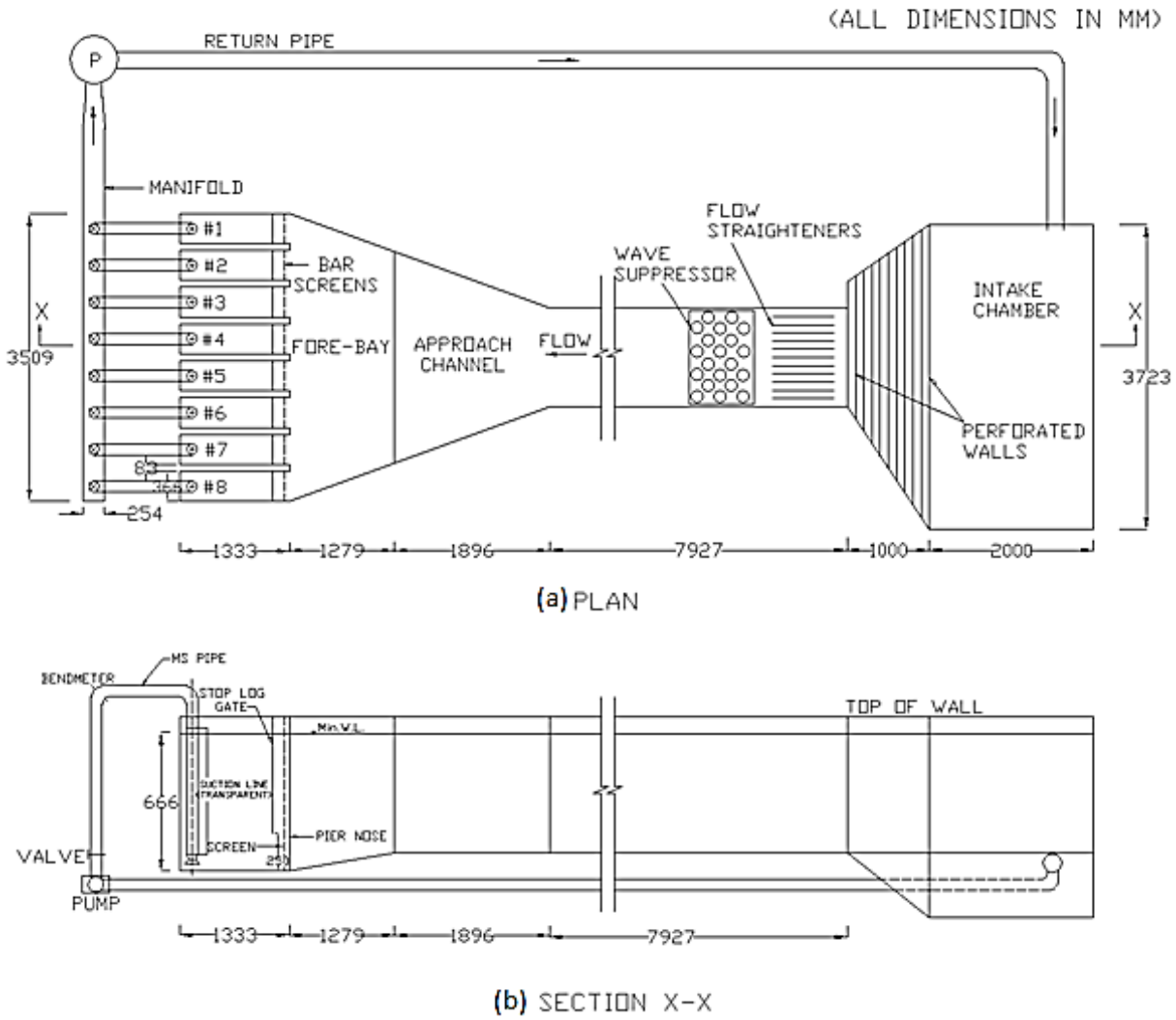

Figure 3.1 Plan and sectional view of the model pump sump

The setup was consisted of an intake chamber, approach channel, fore-bay, trash racks, stop-log gates, bays, suction columns each with bell-mouth entry, a manifold, pump and return pipe. Photographs showing the different components of the setup are given in Figure 3.2 to Figure 3.5. Suitable arrangement of perforated walls, flow straighteners and wave/flow suppressors were provided in the intake chamber and channel section to stabilize the flow without any inflow disturbance as shown in Figures 3.2 and 3.3. Flow straighteners were provided for ensuring equal distribution of discharge across the width of the channel. Figure 3.4 shows trash racks, pier noses and stop log gates. Figure 3.5 shows the close up view of the gates and trash racks.

Table 3.2 Dimensions of the pump sump model

S. No.	Description	Size in mm
1	Suction line diameter (D)	134
2	Bell mouth diameter (D_b)	179
3	Submergence (S)	666
4	Width of Inlet	1198
5	Height of inlet	441
6	Floor clearance	92
7	Sidewall clearance	116
8	Backwall clearance	78
9	Length of sloped portion	1279
10	Length of bay	1333
11	Width of bay	366
12	Bay wall thickness	83
13	Opening height of stop-log gate	250
14	Manifold diameter	254
15	Diameter of return pipe	203
16	Width of approach channel	1197

A Centrifugal pump of 45 hp was used to circulate the water in the model. The model was constructed of concrete except the floor and the backwall of the bays, which were of transparent glass to enable visualization of the flow. The bell-mouth at inlet of intakes and suction pipe up to length 600 mm were of transparent plastic. A vortimeter was fitted in the suction columns to measure the swirl of the flow approaching to the pump. Clear water enters in each suction line through a transparent bell-mouth, transparent acrylic pipe, 90^0 elbows, and a straight pipe of length 1200 mm, a 90^o bend and a valve. The bends were used to measure the discharge while the valve was used to regulate the flow in the suction lines. All suction line were connected to a manifold pipe, which was connected to a centrifugal pump that pump the water and feed to the intake chamber.

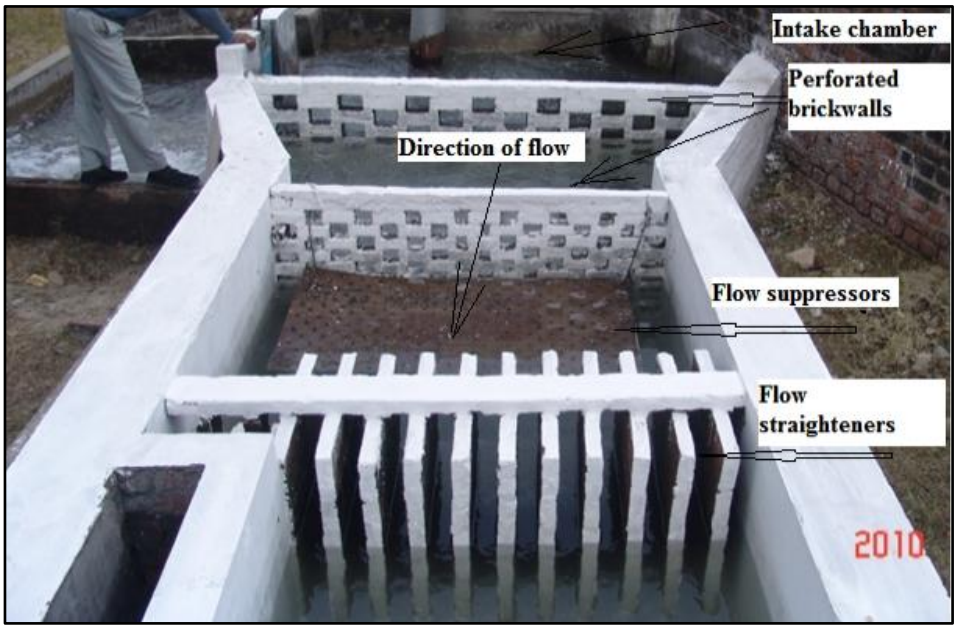

Figure 3.2 Intake chamber, perforated brick walls and flow suppressors of the model

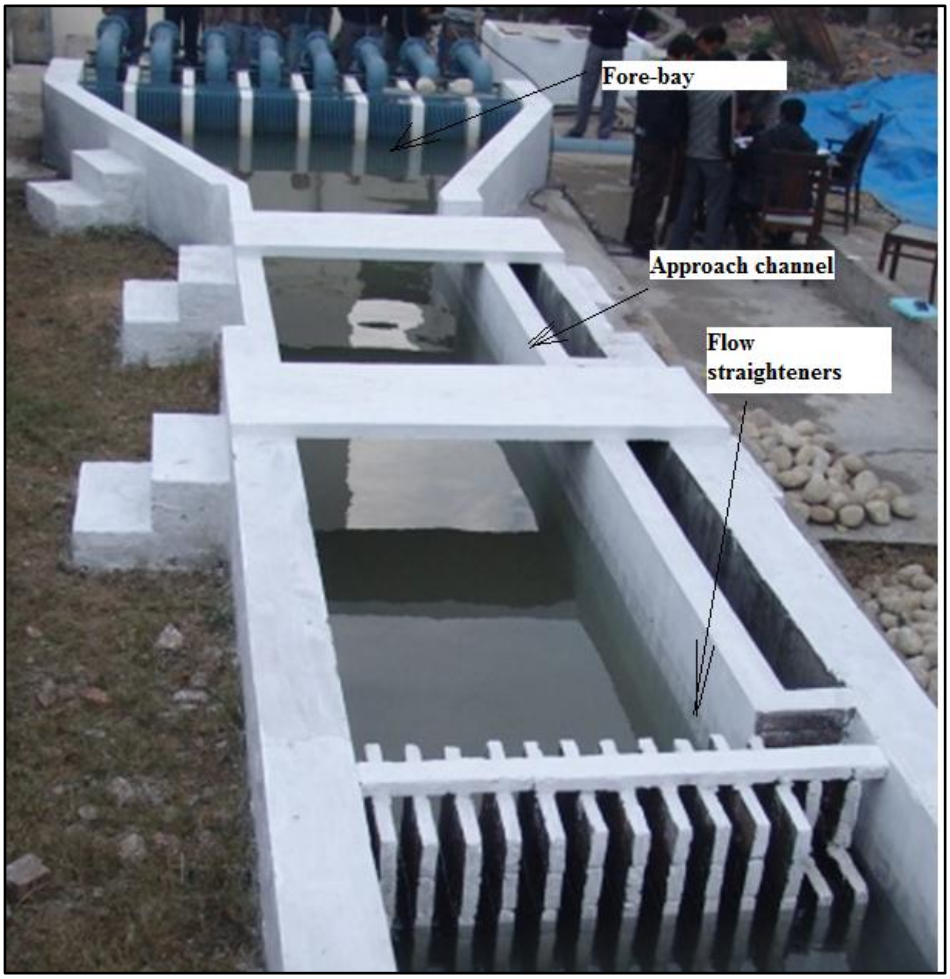

Figure 3.3 Approach channel, flow straighteners, fore-bay area and bays of the model

Figure 3.4 Divergent portion, pier noses, trash racks and stop log gates of the model

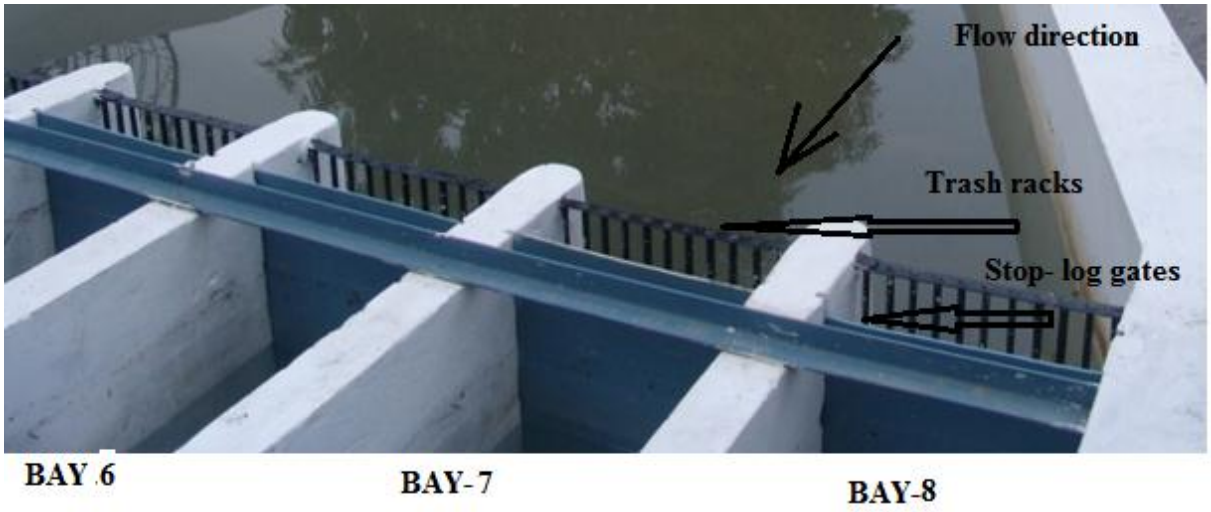

Figure 3.5 Close-up view of trash racks and stop log gates of the model

A smooth transition at the beginning of the approach channel was provided to ensure equal velocity distribution across the width. A valve was fitted in the delivery pipe to regulate the total discharge in the sump. The pump was placed at a level lower than the minimum water level in the sump to avoid the priming problem.

3.3 EQUIPMENTS USED

Velocity at a point was measured using acoustic Doppler Velocimeter (ADV) and/ or acoustic digital current meter (ADC). Ultrasonic flow meter (UFM) was used to calibrate the bend-meter. Point gauges of accuracy $\pm$0.1mm were used to measure water surface levels. To

measure the swirl in suction columns vortimeter were used. Description of the main instruments used and the procedure of measurement are described below.

3.3.1 Acoustic Doppler velocimeter (ADV)

The acoustic Doppler velocimeter (ADV) is a multi-purpose measuring instrument which is highly precise in measuring the velocity components in all three dimensions. The instrument is highly advanced as compared to other velocity measurement devices such as propeller or mechanical gauge, electromagnetic current meter, hydrogen bubble technique, Pitot tube and hot films anemometer. It measures the velocity for various applications independent of the quality of water in which it is used. ADV is used in wave basins, laboratories, rivers and oceanographic researches. In the recent times, various investigations on open channel flow have been conducted by using the ADV.

The acoustic sensor includes a single transmit transducer and three receiver transducers as shown in Figure 3.6. Probes were consisted of sensor with almost any combination of 3D or 2D on the basis of sampling volume location, sensor mounting and sensor location (Figure 3.7). Scattering of signals from the small particles forms the Doppler velocity. The particles which are naturally present in the water bodies are sufficient for the proper operations. Micro bubbles in the vertical water column in the sump and dust particles in flowing water (closed pipe, open channels etc.) act as the natural seeding. Seeding must be added to the crystal clear water (tow tanks, some wave flumes and ship models) with an approximate concentration of 10 mg/L, (Sontek 1997).

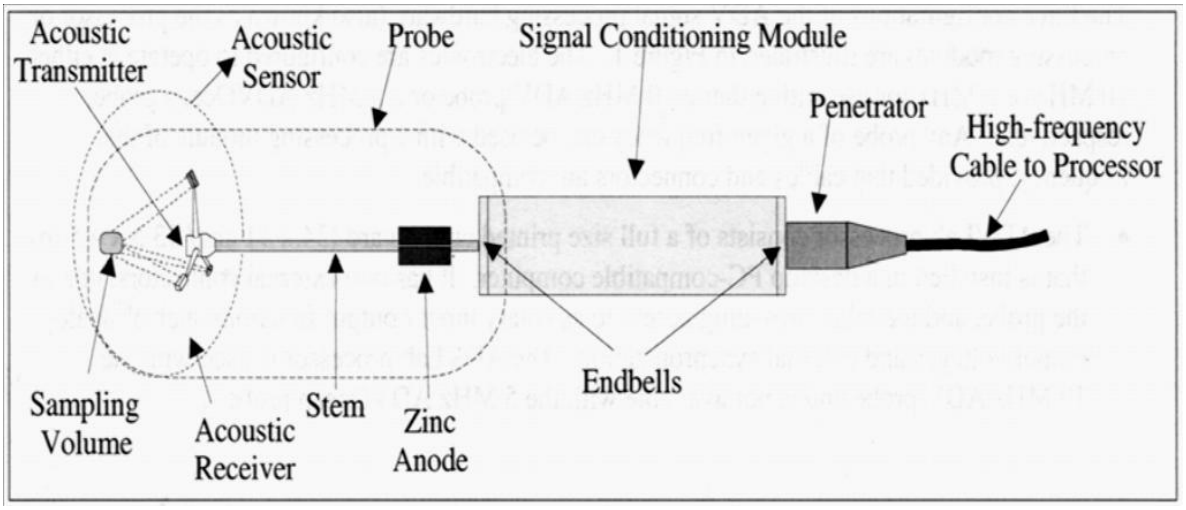

Figure 3.6 Acoustic Doppler velocimeter (Sontek, 1997)

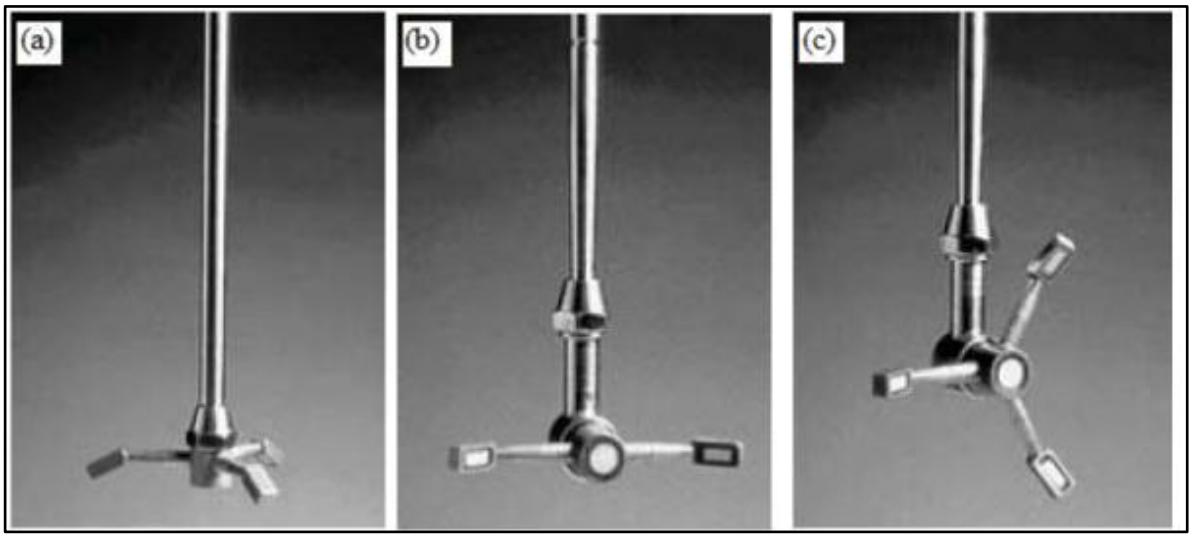

Figure 3.7 Different types of probes (a) down looking 3D, (b) side looking 2D and (c) side looking 3D

ADV has become a useful instrument in measuring 3D velocity fields in laboratory and field environments. ADV records the Doppler shift created by acoustic targets in the flow. The sampling volume of a MicroADV is located about 5 cm away from the probe. According to SonTek, the sampling volume is cylindrical with a diameter of 4.5 mm and length of 5.6 mm. It can measure flow velocities from about 1 mm/s to 2.5 m/s. Data can be acquired at sampling rates up to 50Hz. The leading edge of the sampling volume can be placed as close as 0.5 mm to a boundary.

3.3.2 Ultrasonic flow-meter (UFM)

An ultrasonic flow meter measures the velocity of any liquid or gas through a pipe using ultrasonic transducers. In the present study, an ultrasonic flow meter of make Polysonics DCT7088 was used. This ultrasonic flow meter can be operated on pipe diameters ranges from 13 mm to 6 m; fluid temperatures from –4.44°C to 200°C; and velocities from of 0.30 m/s to 32 m/s. Measurement accuracy can be in the range of ±1% of the measured velocities, and speed of response can be as fast as 1s. The handheld microprocessor-based converter provides a local graphical display and has a keypad for calling up page menus for flow data, trend displays, setting up site parameters, and other requirements. The converter can log data for as many as 20 sites and 40,000 data points. It can also provide a PC interface via RS-232 serial communication, and an output of 4–20MA DC for operating a digital controller, DCS, PLC, or recorder. The flow meter has a built-in, rechargeable battery and can operate continuously for five hours. Advanced digital signal processing improves its performance where the flowing fluid contains air or gas bubbles. Photograph of ultrasonic flow meter

while measuring discharge in the pipe is shown in Figure 3.8. The bend meters were calibrated with UFM to measure flow rate in different suction columns.

Figure 3.8 Ultrasonic flow-meter

3.3.3 Acoustic digital current-meter (ADC)

Propeller-type current meters have been used for more than 200 years and are one of the first hydrometric measuring devices for velocity. In open channels, flow velocity is still measured predominantly with vertical axis or horizontal axis current meters. The use of mechanical current meters, such as the propeller type, is restricted by initial speed requirements and the inability to measure backflow. The latest acoustic velocity meters overcome these restrictions. The OTT ADC (acoustic digital current-meter) measures flowing water velocities. The OTT ADC, equipped with a built-in pressure sensor, measures point velocity and depth from the free surface and both measurements are presented on a graphical handheld display.

The OTT ADC consists of two components, the sensor and the display unit, connected by a sensor cable. The sensor as shown in Figure 3.9 (a) is the basic element of the instrument. The OTT ADC sensor is comprised of two transducers that operate independently of each other. Each transducer measures the velocity of small particles, also known as scatters, in the measurement volume located 10 to 15 cm in front of the sensor, as shown in Figure 3.10. For velocity measurements, ADC has been used in the present study. Figure 3.11 shows the photographic view of one instant location of the ADC.

Figure 3.9 a) Photographic view of sensor b) schematic and c) display unit.

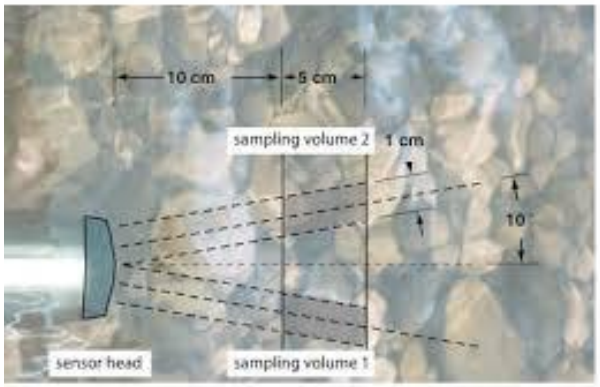

Figure 3.10 Measurement locations of ADC sensor

(a) (b)

Figure 3.11 Acoustic digital current meter probe and handheld unit respectively

3.3.4 Vortimeter

The intensity of flow rotation was measured using vortimeter, which consisted of a straight-vane propeller with four vanes mounted on a shaft with low friction bearings. This meter measured tangential velocity in the pump columns, assuming solid body rotation (Lee and Durgin, 1980). The revolutions per unit time of the vortimeter tip were used to calculate tangential velocity (V_θ). Further swirl angle, θ, which is indicative of the intensity of flow circulation, is defined by

$$\theta = \tan^{-1}\left(\frac{V_\theta}{V}\right) \tag{3.6}$$

where $V_\theta = \pi DN/60$, is the tangential velocity at the tip of the vortimeter blade; N = angular velocity of vortimeter in RPM; and V = average axial velocity in the suction pipe.

The diameter and height of vortimeter were taken equal to 0.75D and 0.60D, respectively, and located at impeller level, i.e., 213.75 mm above the plane of the bell mouth entrance. The location, details and the photographic view of vortimeter are shown in Figure 3.12. These vortimeters were fitted in all eight suction pipes of the model. Swirl in suction columns at impeller level (as per the prototype condition) were measured by vortimeter. The rotations in different vortimeters were counted for two minutes to measure the RPM of the vortimeter blades. As the swirl is unsteady in nature the three conjunctive readings were made to count the rotations and average of that rotations were taken to compute the swirl from Eq. (3.6).

As the swirl decays along the distance of suction pipe, American National Standards Institute (ANSI) (1998) recommends that vortimeter should be placed at 4D distance from the entrance of the suction pipes. However, in present study the vortimeter is located at impeller level.

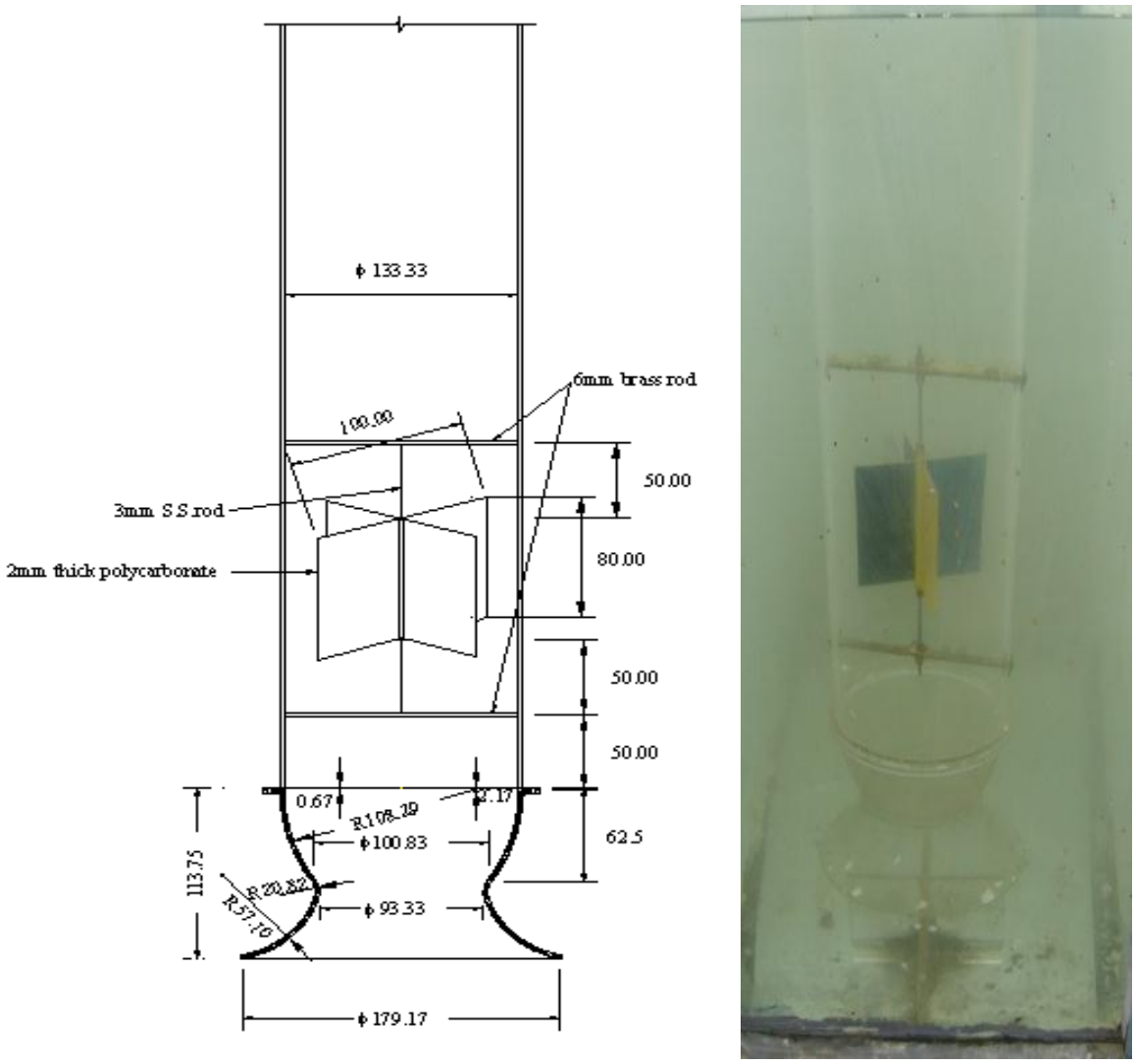

(a) (b)

Figure 3.12 (a) Position of vortimeter (b) photographic view of vortimeter

3.4 EXPERIMENTAL PROCEDURE

First water level up to the marked level i.e. LWL was maintained and the pump was started to start flow of water in the model. Flow through all suction columns was ensured. We waited till the flow got stabilised in the model. After getting the steady state conditions, the valves were operated slowly to control the discharges in different pumps. As and when required, the main valve at the outlet of the pumps was also adjusted to get the desired flow conditions. After stabilisation of flow in the model, the relevant observations were taken.

The flow in the sump was visualized using food dye to identify the separation of flow and dead zones. Surface vortices were inspected visually, and types of vortices were identified

with the help of dye injection. The possible existence of subsurface vortices was explored by dye injection at selected locations on the wall and floor near the bell mouth, where a vortex may form.

The revolutions of vortimeter were counted for two minute durations in each pump bays for various combinations of bell mouth operations. The combination of bell mouths in operations giving high swirl angle was considered as a ***stringent combination***. For this stringent condition, at a distance of 900 mm upstream of the pump centre line, the cross-sectional velocity profile of the approach flow was measured at three verticals. For each vertical, the velocity was measured at three points for the stringent combinations of bell mouth in operations. The axial velocity at the throat of the bell mouth was measured at two perpendicular axes for one of the stringent combinations of pumps in operations. Sufficient time interval between the two successive runs was ensured. Experimental runs carried out in present study are listed in Table 3.3.

Table 3.3 Test conditions

S. No.	Description	Number of runs	Q (L/s)
1	Data collection for validation purposes	12	11.44, 13.69, 22.88
2	Initial tests for different bell mouth operation	17	13.69
3	Effect of Froude number	14	8.0 to 38.0
4	Effect of cross type AVD on swirl	12	13.69

3.5 CALIBRATION OF BENDMETERS

The bends fitted in upstream of the valves were used to measure the discharges in different suction pipes as shown in Figure 3.13 and Figure 3.14. All bends were calibrated separately by measuring discharges in suction lines using ultrasonic flow meter. The pressure difference in bend was measured using manometer as shown in Figure 3.15. Discharges in suction lines were measured using Ultrasonic flow meter. Calibration charts are shown in Figure 3.16 to Figure 3.23. The fitted equations for different bend-meters are given in Table 3.4. In these equations Q is in L/s and Δh is in cm.

Figure 3.13 Bend meters, valves and manifold of the model

Figure 3.14 Close-up view of bend meters used to measure discharge of the model

Figure 3.15 Manometer board used to measure pressure difference

Table 3.4 Fitted discharge equations for the bend-meters

S. No.	Bendmete	Discharge equation	S. No.	Bend-meter	Discharge equation
1.	Bend 1	$Q = 4.457\Delta h^{0.403}$	5.	Bend 5	$Q = 5.120\Delta h^{0.37}$
2.	Bend 2	$Q = 4.457\Delta h^{0.429}$	6.	Bend 6	$Q = 2.900\Delta h^{0.528}$
3.	Bend 3	$Q = 2.722\Delta h^{0.549}$	7.	Bend 7	$Q = 3.625\Delta h^{0.464}$
4.	Bend 4	$Q = 3.000\Delta h^{0.528}$	8.	Bend 8	$Q = 2.928\Delta h^{0.526}$

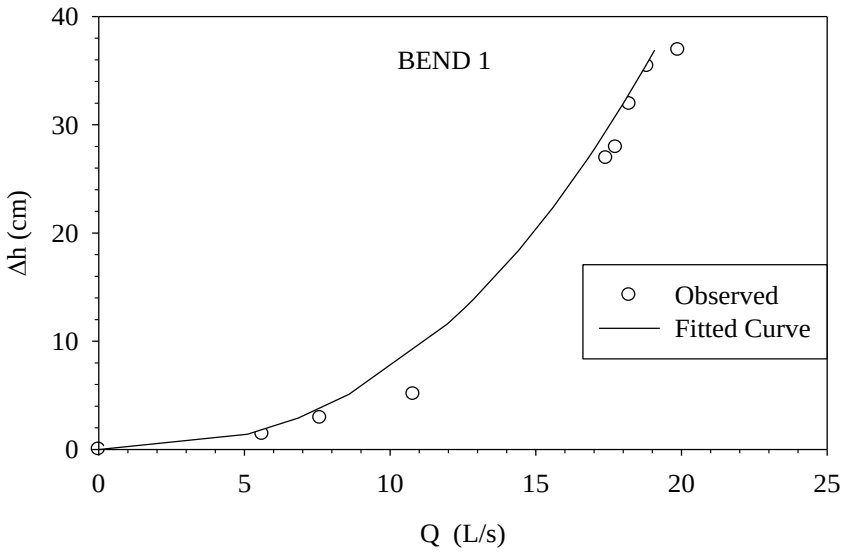

Figure 3.16 Calibration chart for bend-meter 1

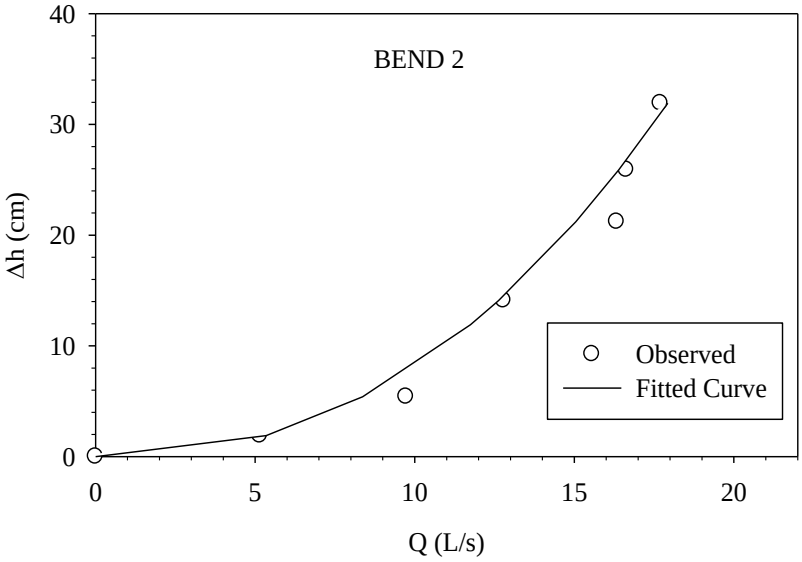

Figure 3.17 Calibration chart for bend-meter 2

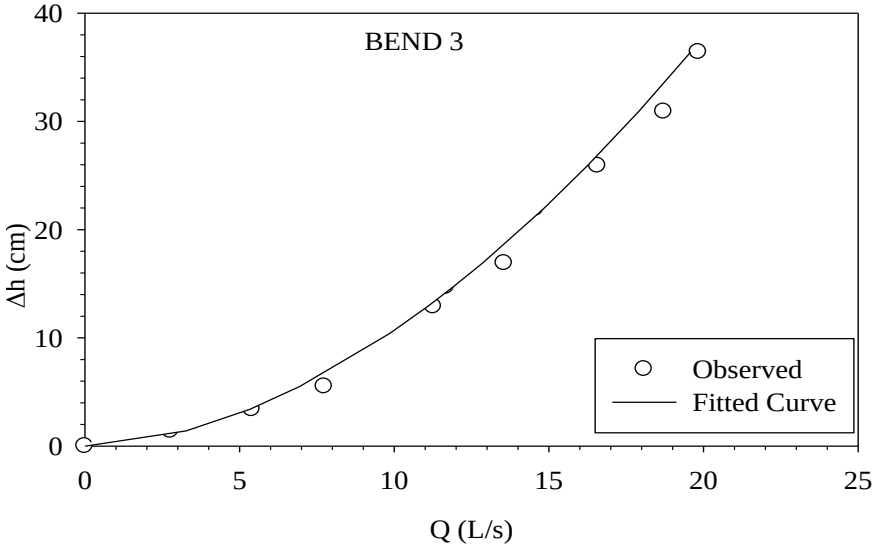

Figure 3.18 Calibration chart for bend-meter 3

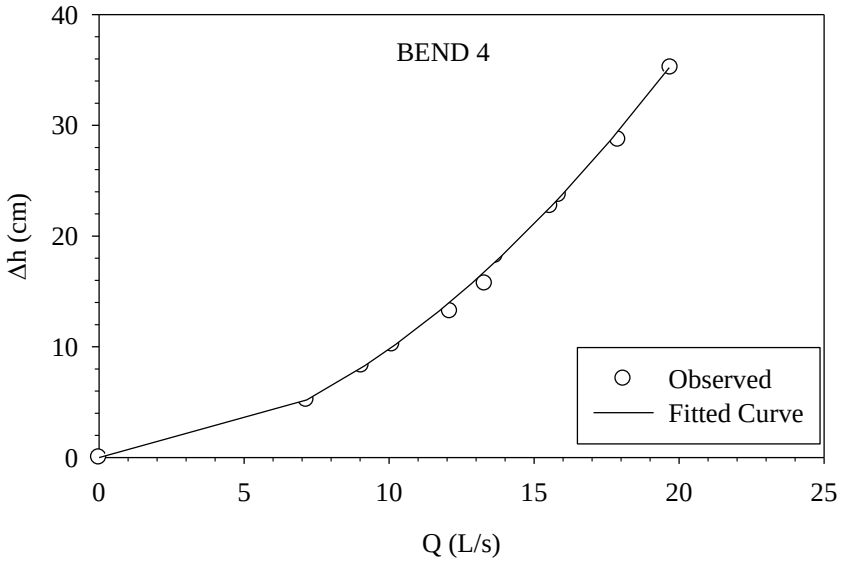

Figure 3.19 Calibration chart for bend-meter 4

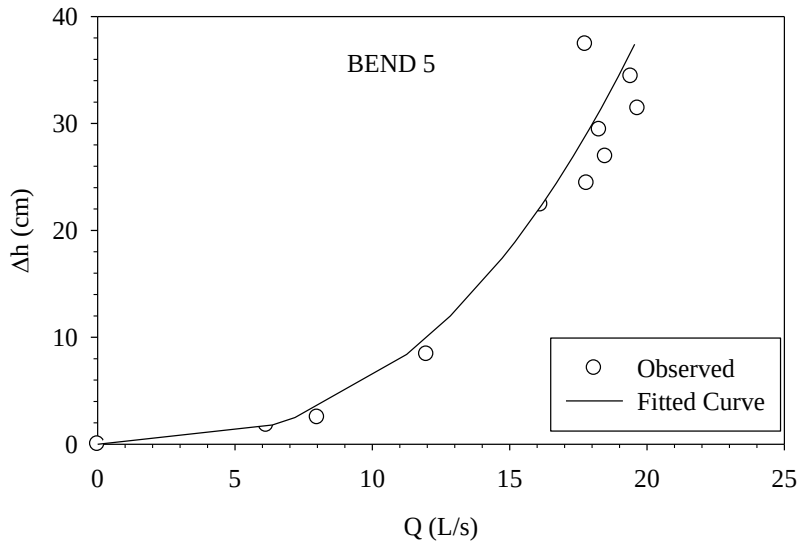

Figure 3.20 Calibration chart for bend-meter 5

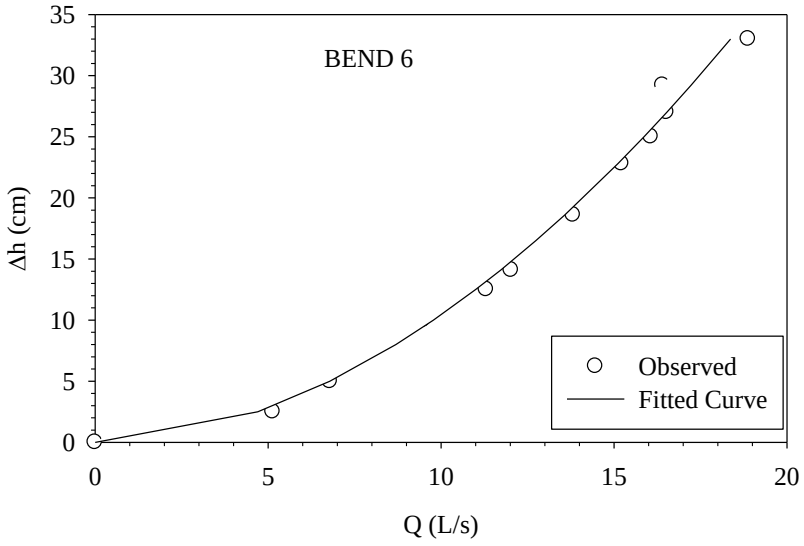

Figure 3.21 Calibration chart for bend-meter 6

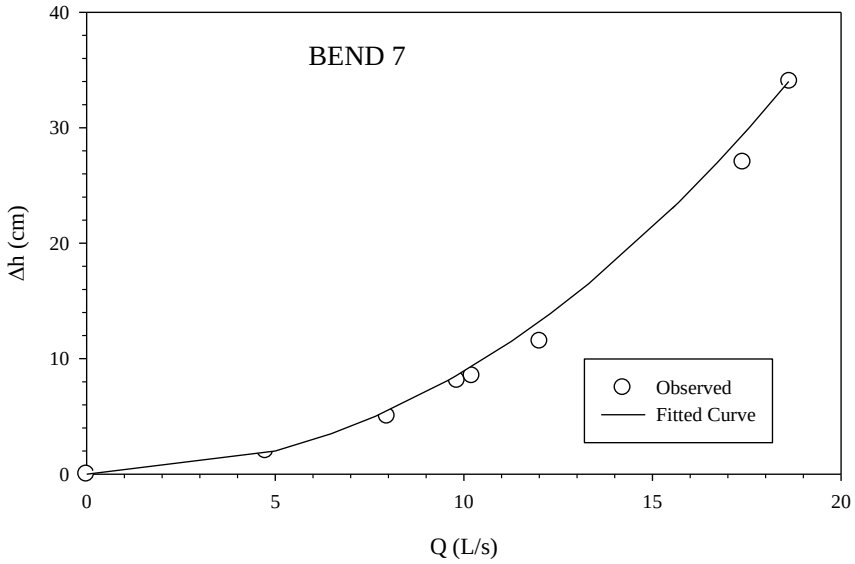

Figure 3.22 Calibration chart for bend-meter 7

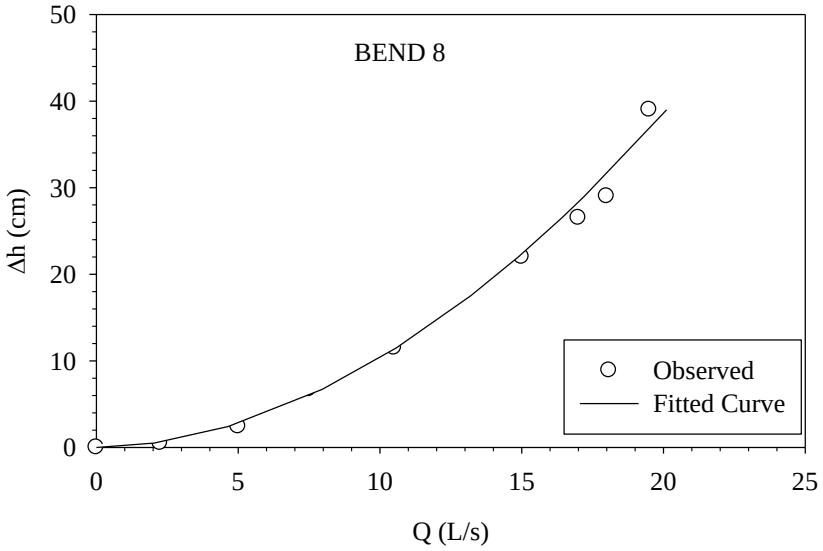

Figure 3.23 Calibration chart for bend-meter 8

3.6 RANGE OF COLLECTED DATA

The ranges of data collected in the present study are given in Table 3.5.

Table 3.5 Range of collected data in present study

S.no.	Parameters	Unit	Range of data
1	Q_s	L/s	11.41-22.82
2	θ	degrees	0-8
3	V_a	m/s	0.8-1.61
4	u_{in}	m/s	0.12-0.25
5	Fr	dimensionless	0.6-2.39
6	Re	dimensionless	123387 -246645

3.7 CONCLUDING REMARKS

The experimental data for different flow conditions by changing discharge and combination of operational bell mouths were collected for the validation of the CFD model results. The collected data will be analysed in the Chapter 5. The experimental data to investigate the effect of Froude number on swirl were also collected and that shall be discussed in Chapter 6. The experimental data for the flow characteristics for different bell mouth conditions were also collected to find the stringent combinations. Also the effect of AVD on swirl has been investigated experimentally and shall be discussed in Chapter 7. The validity of findings of the present study is limited to range of data given in Table 3.5.

CHAPTER 4 **CFD MODELLING**

4.1 INTRODUCTION

This chapter deals with the procedure adopted for the development of the CFD model to investigate the flow phenomenon in the pump sump model for different approach flow conditions. The CFD modelling has also been carried out in present study to investigate the effect of Froude number on swirl and to find the suitability of anti-vortex devices (AVD) for controlling the swirl. The complete procedure of CFD modelling has been described in this chapter that includes geometry/fluid domain creation, mesh generation, governing equations and solver settings.

4.2 GEOMETRY CREATION

The fluid domain considered herein is replica of the laboratory model of the multiple pump sump intakes described in Chapter 3. Geometric model for CFD analysis is shown in Figures 4.1 and 4.2. This can be pictured by filling the model with water and subtracting all structures, i.e. walls, floor, gates and suction pipes as shown in the isometric view in Figure 4.3. The geometry of the CFD model was prepared using the ANSYS CAD module, ICEMCFD. To assign different boundary conditions (i.e. walls, free surface, outlet, inlet, interior etc.), various parts were created during the geometry creation as shown in Figure 4.3. Following approximations in the CFD model have been adopted to make the geometry simple so that the computational efforts can be reduced:

1. The thickness of suction pipes, gates and anti-vortex devices were treated as a thin wall, as shown in Figure 4.3.
2. Instead of the bends, valves and manifold assembly in the downstream part of the suction columns in the physical model, straight suction columns of length 12D were created starting from the bell entrance to reduce the effect of outlet boundary condition on the swirl at impeller level and flow patterns in the fluid domains.
3. In the CFD model, instead of a water circulatory system as provided in the physical model, the inlet boundary has been placed 22.5D upstream from the forebay entrance to get the fully developed flow in the forebay area.
4. The trash racks and the pier noses were not modelled.

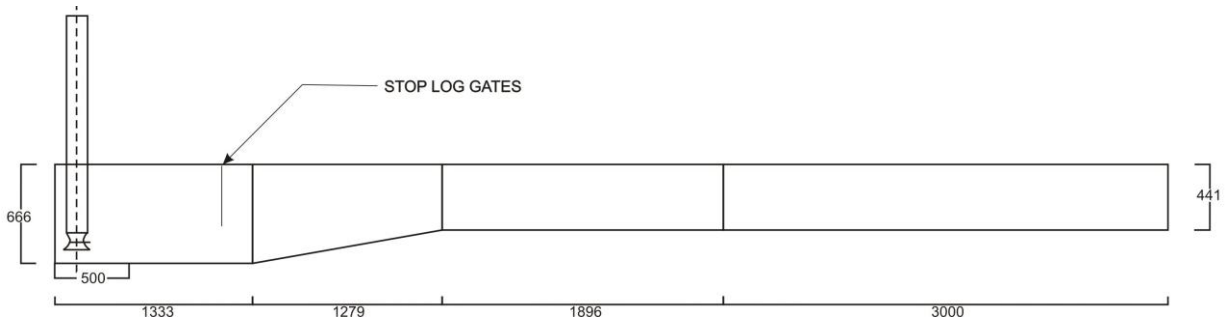

Figure 4.1 Sectional view of the pump intakes-CFD model (all dimensions in mm)

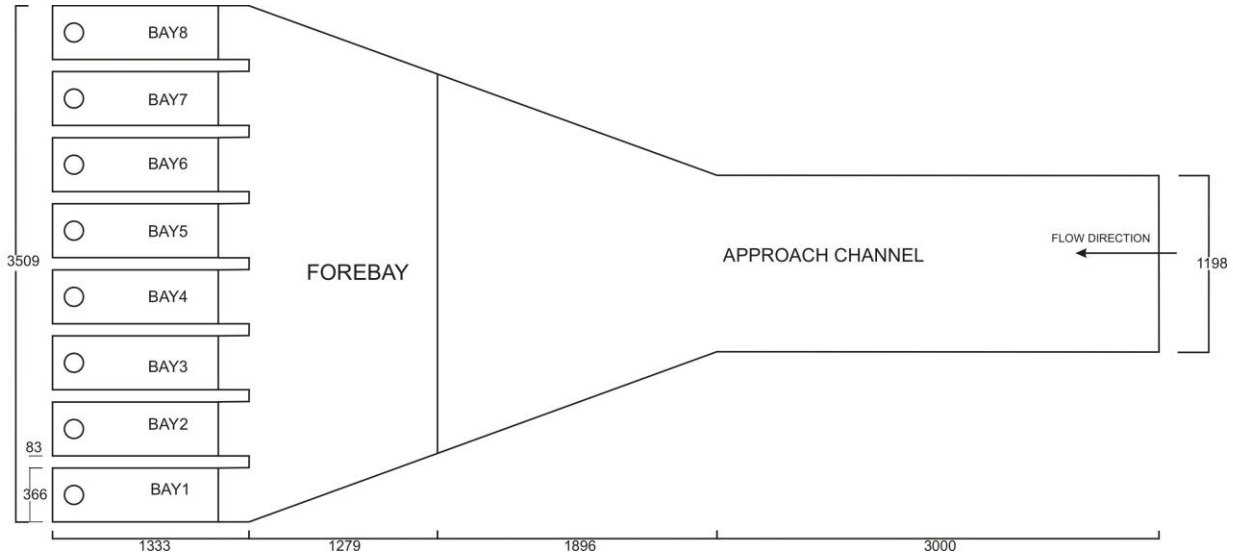

Figure 4.2 Plan view of the pump intakes-CFD model (all dimensions in mm)

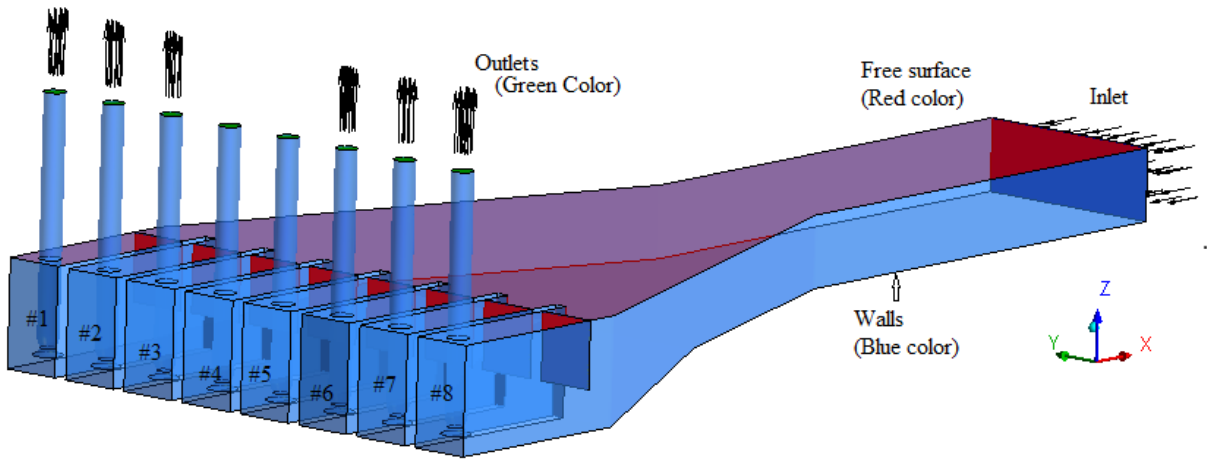

Figure 4.3 Isometric view and different boundaries of the pump intakes-CFD model

Ten different fluid domains were created for different configurations. The names and description of the domains are given in Table 4.1. The names of the fluid domains were

assigned such that the last two letters represent the type of AVD installed in that domain. The details of the AVDs are described later in chapter 7.

Table 4.1 Details of fluid domains created

S. No.	Name of domain	Description of domain
1	FDWB	Without AVD
2	FDA1	With type A1 AVD in all pump bays
3	FDA2	With type A2 AVD in all pump bays
4	FDA3	With type A3 AVD in all pump bays
5	FDB1	With type B1 AVD in all pump bays
6	FDB2	With type B2 AVD in all pump bays
7	FDB3	With type B3 AVD in all pump bays
8	FDC1	With type C1 AVD in all pump bays
9	FDC2	With type C2 AVD in all pump bays
10	FDC3	With type C3 AVD in all pump bays

4.3 MESH GENERATIOIN

After the geometry creation and assignment of the boundary conditions, the computational domain was divided into cells which form a mesh or a grid. For grid generation, ICEMCFD module of ANSYS has been used. Several parts of the grid are grouped into regions also known as parts such as walls, inlet, outlet, top, fluid etc. where the boundary conditions were applied. ICEM offers generation of various types of grids e.g. tetrahedral, hexahedral, hybrid etc. In the present study, a hexahedral conformal mesh with global mesh size 16 mm was created for fluid domains described in previous section.

For mesh generation the complete domain has been divided in 355 blocks as shown in Figure 4.4. The grid near suction pipes was created using O grid technique to get good quality mesh near intakes as shown in Figure 4.5.

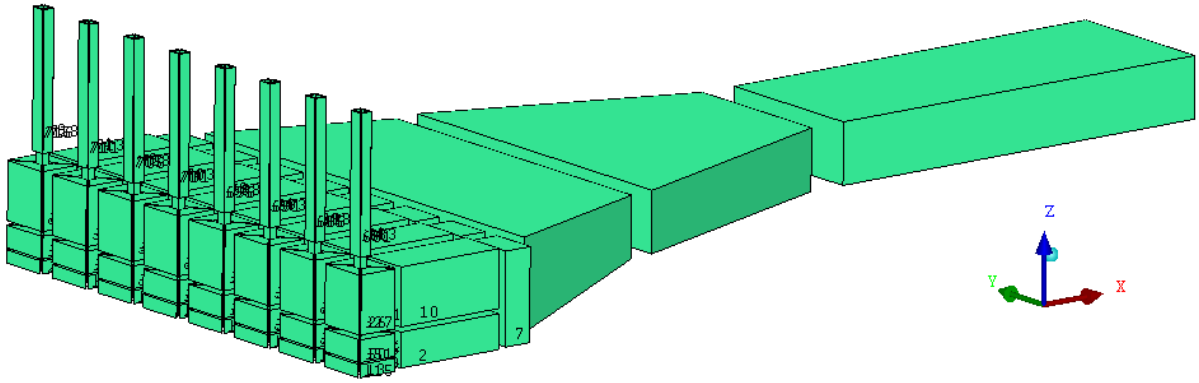

Figure 4.4 Blocking view of the pump sump CFD model

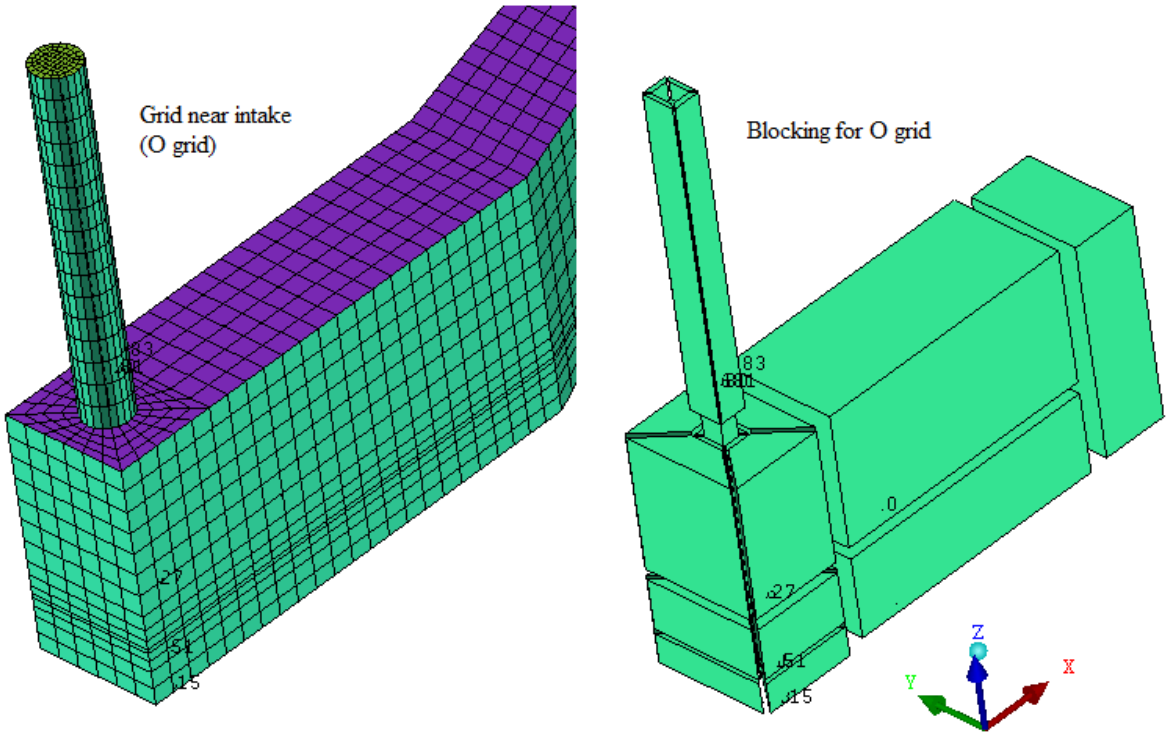

Figure 4.5 Mesh and blocking view of O-Grid near intake

The mesh for FDWB model has 57,69,374 nodes and 5,57,11,036 cells. Figure 4.6 shows the sectional view of the mesh passing through all suction pipes. Figure 4.7 shows the close-up views of mesh in different parts of the domain. Mesh figures shown are schematic representation of the actual grids for sake of clarity.

Figures 4.8 and 4.9 show the plan and sectional view of the mesh, respectively. Total twelve different meshes were created and the number of nodes and elements are given in Table 4.2. In this table, M1, M2 and M3 grids were created for grid sensitivity tests that are discussed later in Chapter 5.

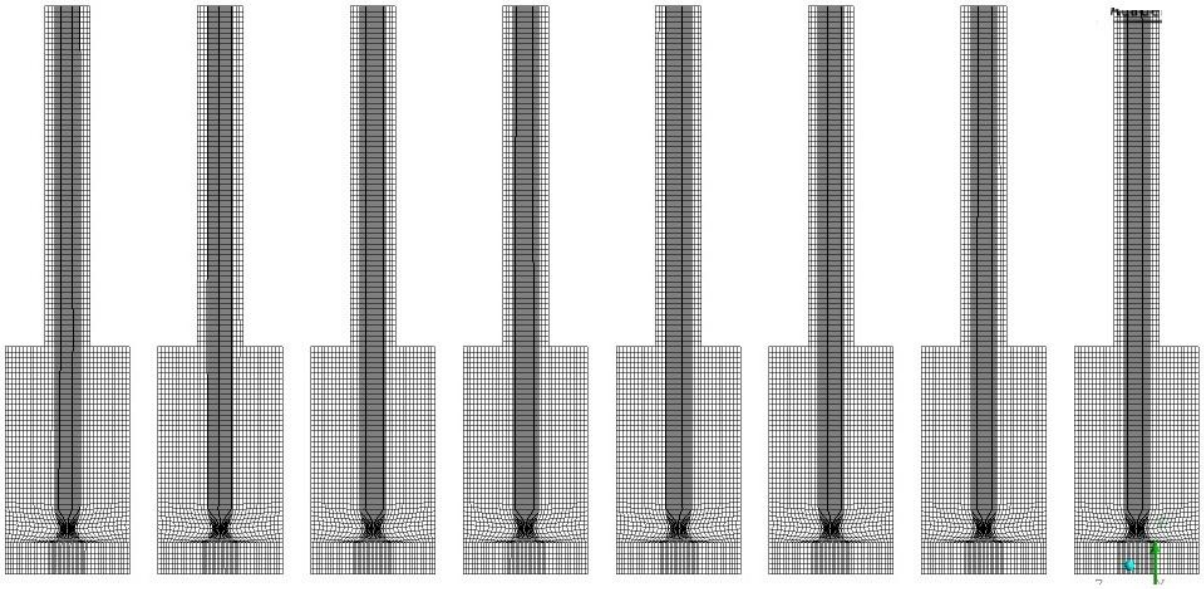

Figure 4.6 Sectional view of grid passing from the centre lines of all suction pipes

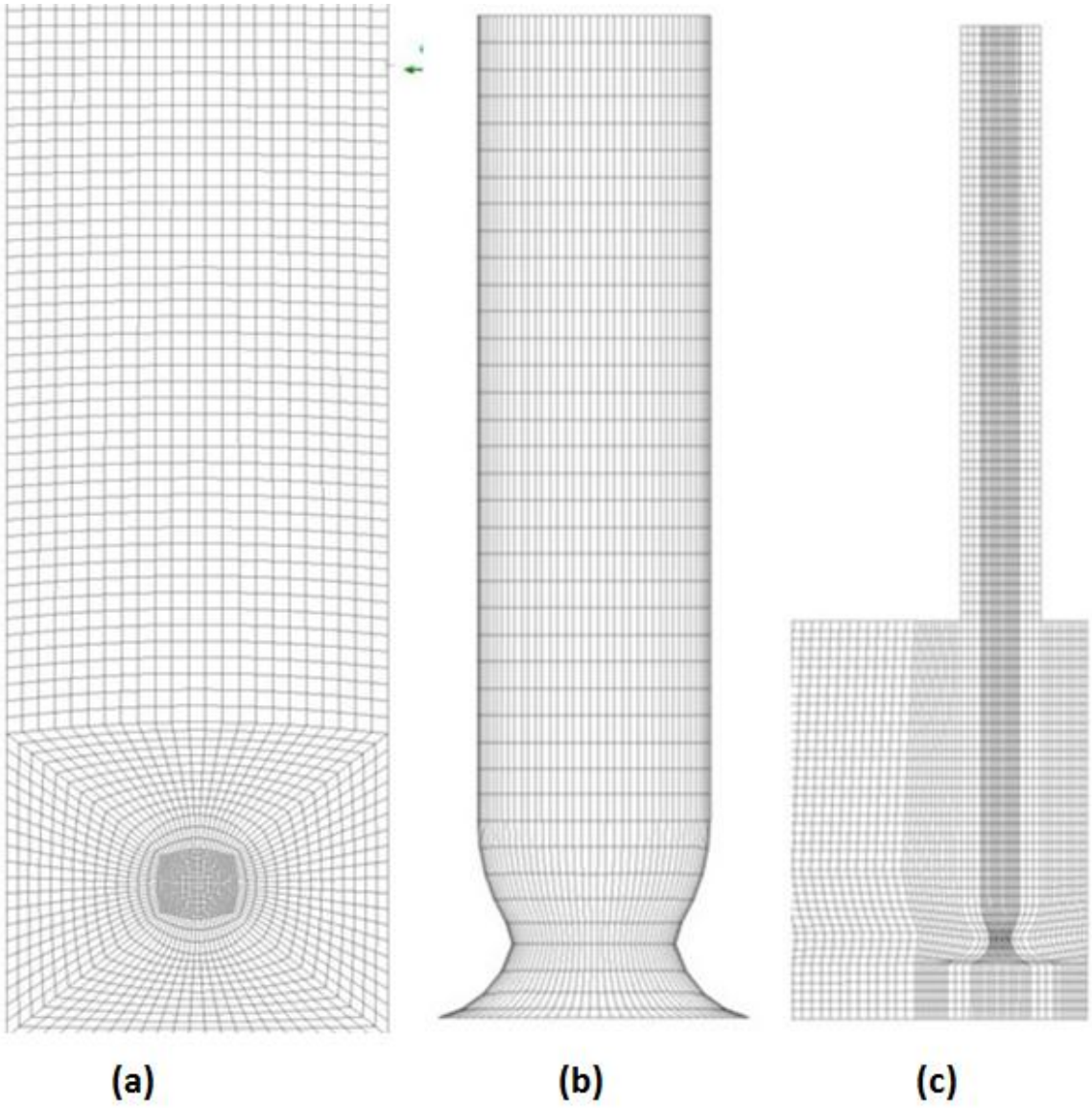

Figure 4.7 (a) Plan view of grid near intake, (b) view of surface mesh on suction pipe and (c) sectional view passing from center line of suction pipe

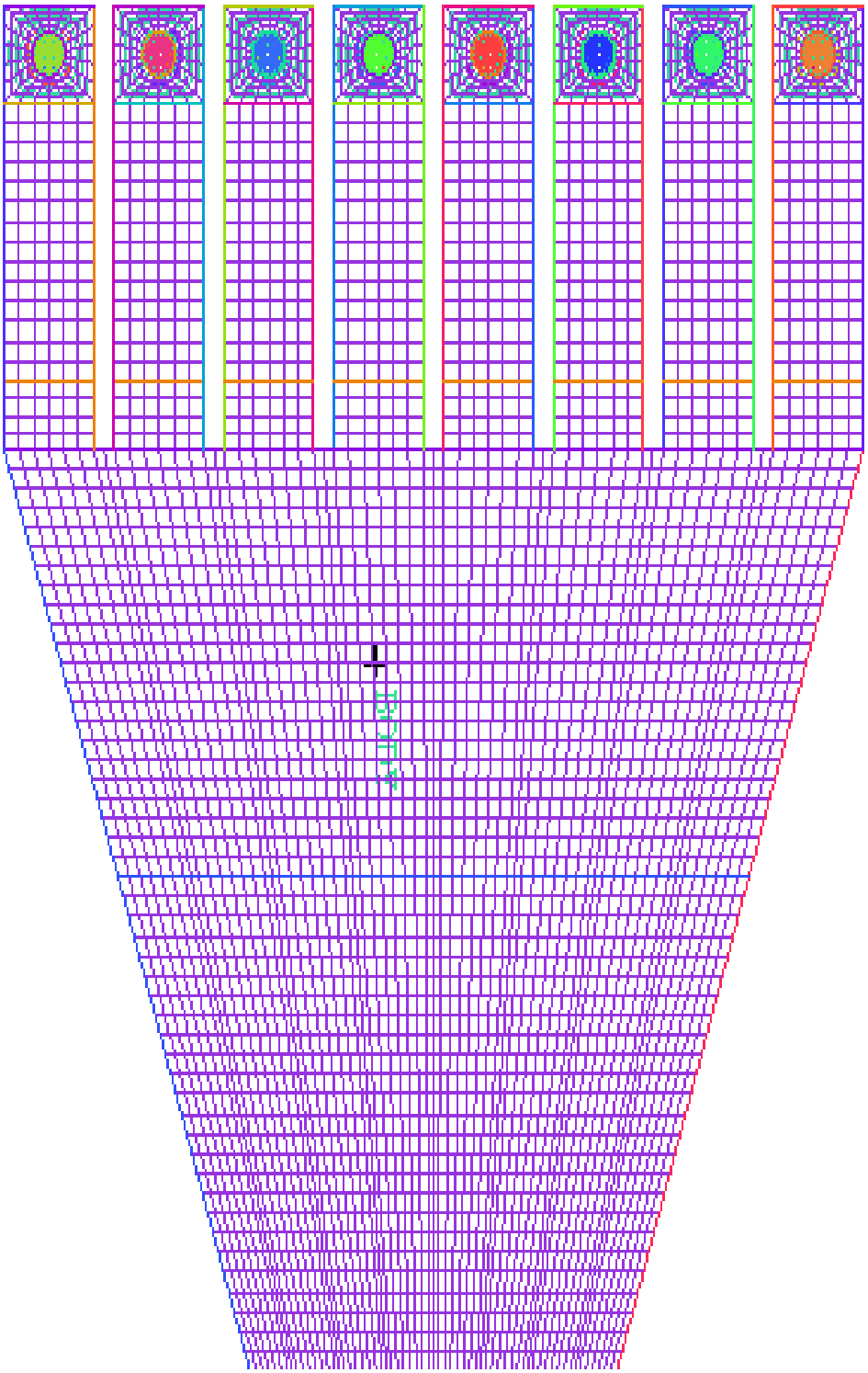

Figure 4.8 Schematic plan of grid

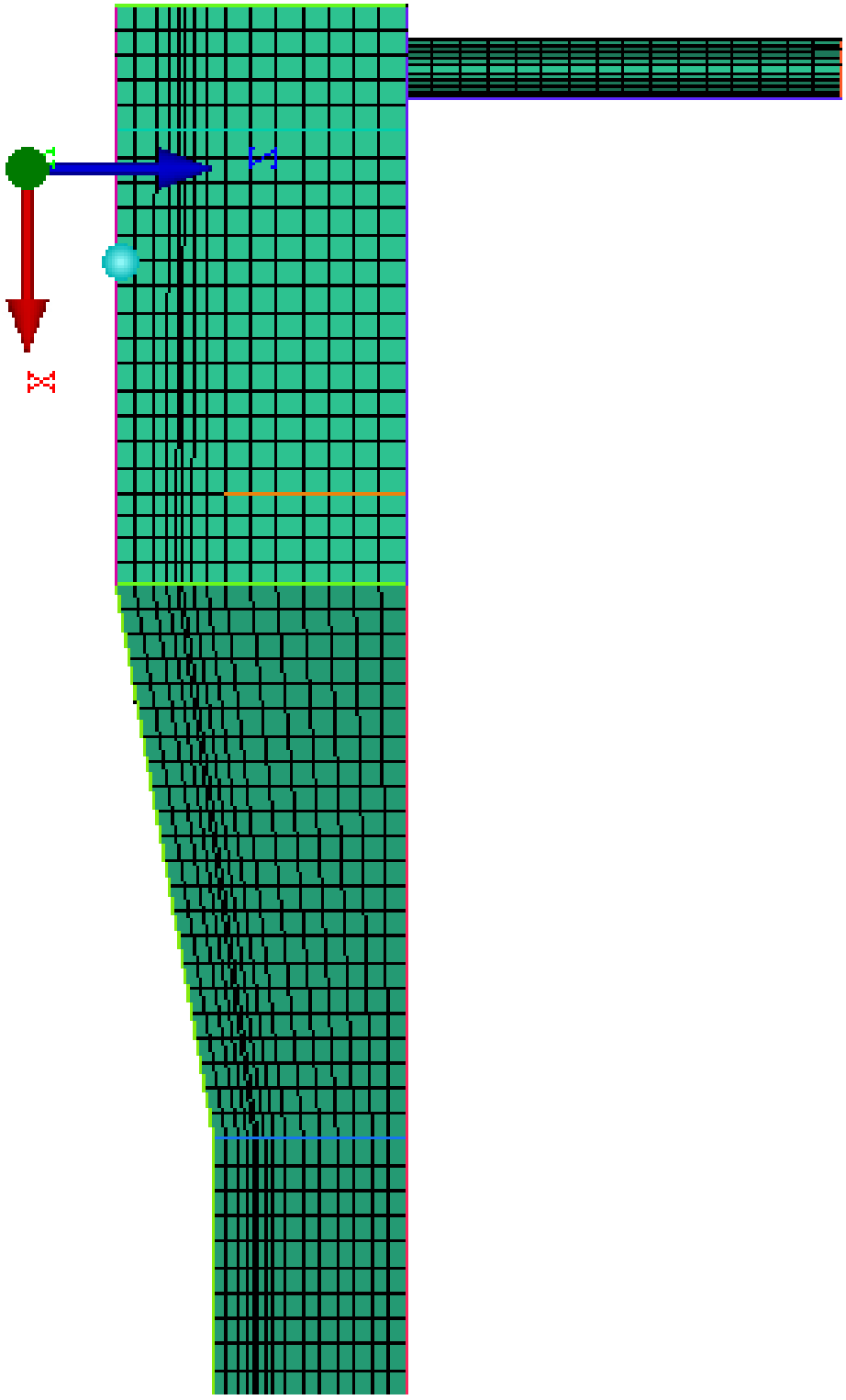

Figure 4.9 Schematic X-sectional view passing from centre line of #4 bay

Table 4.2 Different mesh parameters for all the meshes created

S. No.	Object	Nodes	Elements	Fluid Domain	Remarks
		$\times 10^6$	$\times 10^6$		
1	M1	0.15	0.13	FDWB	Coarser Grid
2	M2	0.90	0.85	FDWB	Coarse Grid
3	M3	5.79	5.57	FDWB	Fine Grid
4	MC3	6.39	6.14	FDC3	Type C3 AVD
5	MC2	6.3	6.06	FDC2	Type C2 AVD
6	MC1	6.51	6.26	FDC1	Type C1 AVD
7	MB3	6.49	6.25	FDB3	Type B3 AVD
8	MB2	6.62	6.37	FDB2	Type B2 AVD
9	MB1	6.69	6.45	FDB1	Type B1 AVD
10	MA3	6.4	6.15	FDA3	Type A3 AVD
11	MA2	6.49	6.25	FDA2	Type A2 AVD
12	MA1	6.36	6.12	FDA1	Type A1 AVD

4.4 MESH QUALITY

Poor quality of the mesh causes oscillating nature of the solution variables which increases numerical uncertainty resulting in diverged solutions. Hence, mesh quality is important for controlling the discretization errors. Therefore, good quality of mesh in the entire domain was maintained. Several quality check parameters are available in ICEMCFD. Among these, a few parameters of major importance from the literature are discussed. The statistics for different mesh quality parameters are given in Table 4.3 for grid M3, which was selected after the grid dependency test.

The nodes were distributed bi-geometrically on the edges to get large number of elements near the junctions of two different edges of blocks. The minimum angle and orthogonality of the elements were about 19.3^o and 40.9^o, respectively. The value of 0^o indicates a worst elements and 90^o indicates a perfect element in the domain.

In ICEMCFD, the term ‘quality’ is a weighted diagnostic between determinant, max *orthogls* and max *warpgls*. The minimum of the three normalized diagnostics is used as quality of the

mesh in ICEMCFD. A value of one represents perfect hexahedral element, while a value of zero is a totally inverted cube with a negative volume or an inverted element. If a degenerated and/or negative element is present in the discretised domain, the mesh file will not be run by the Fluent. Therefore, the quality must be at least positive to run the solver. In the present work, quality of the mesh was maintained above the 0.3 for all 12 grids. From the quality statistics, it is observed that less than 3% of total elements were in range of 0.3 to 0.8 and remaining 97% is in range of 0.8 to 1.0.

Another parameter, equiangle skewness, of the element is presented in Table 4.3 which may be estimated by

$$\text{Equiangle skewness} = 1.0 - \max\left(\frac{(\phi_{\max} - \phi_e)}{(180 - \phi_e)}, \frac{(\phi_e - \phi_{\min})}{\phi_e}\right) \qquad (4.1)$$

where, ϕ_{max} = largest angle in the face or element, ϕ_{min} = smallest angle in the face or element, ϕ_e = angle of an equiangular face or element (e. g. 90^o for a hexahedral). The skewness value greater than 0.15 is generally considered for the numerical simulations.

Table 4.3 Quality of the optimum mesh selected for simulations

S. No.	**Quality**			**Equiangle skewness**		
	Range	**% of Nodes**	**No of elements**	**Range**	**% of Nodes**	**No of elements**
1	0-0.3	0	0	0-0.2	0	0
2	0.3-0.4	0.05	2764	0.2-0.3	0.065	3653
3	0.4-0.5	0.04	2219	0.3-0.4	0.049	2756
4	0.5-0.6	0.34	19221	0.4-0.5	0.428	23824
5	0.6-0.7	0.62	34777	0.5-0.6	0.890	49593
6	0.7-0.8	2.05	114273	0.6-0.7	1.68	93544
7	0.8-0.9	6.12	340909	0.7-0.8	6.26	348626
8	0.9-1.0	90.77	5056873	0.8-1.0	90.63	5049058

4.5 FLUID PROPERTIES

The following fluid properties were used for all the CFD simulations:

- Newtonian Fluid (Water)

- Gravitational acceleration acting in the negative z-direction at a rate of 9.81 m/s^2
- Density of Water = 998.2 kg/m^3
- Viscosity of Water = 1.003 x 10^{-3} kg/m-s

4.6 TRANSPORT EQUATIONS

Four transport equations along with the additional equations for turbulence models were used to obtain the solution. They included a continuity equation and three momentum equations. Two equations of eddy viscosity models were used herein to model the turbulence. The equations are presented using vector and tensor notations. Water is considered a Newtonian incompressible fluid for the simulation. Based on the Reynolds averaging of the instantaneous Navier Stokes equations, the Reynolds-Averaged Navier-Stokes (RANS) equations can be written in the following form:

- Conservation of mass

$$\frac{\partial u_i}{\partial x_i} = 0 \tag{4.2}$$

- Conservation of momentum

$$\frac{\partial}{\partial x_j}(\rho u_i u_j) = -\frac{\partial p}{\partial x_i} + \frac{\partial}{\partial x_j}\left[\mu\left(\frac{\partial u_i}{\partial x_j} + \frac{\partial u_j}{\partial x_i}\right)\right] + \frac{\partial}{\partial x_j}(-\rho\overline{u_i' u_j'}) \tag{4.3}$$

where ρ = density of water; μ= kinematic viscosity; u_i = Reynolds averaged velocity field; u_i' are independent random fluctuations.

4.6.1 Turbulence modelling

Standard *k*-ε model has been used in the present study. The standard *k*-ε (Launder and Spalding 1972) model is based on transport equations for the turbulence kinetic energy (*k*) and its dissipation rate (ε). The values of *k* and ε are determined directly from the differential transport equations for the turbulence kinetic energy and turbulence dissipation rate which are as follows:

$$\frac{\partial(\rho k)}{\partial t} + \frac{\partial}{\partial x_i}(\rho v_i k) = \frac{\partial}{\partial x_j}\left[\left(\mu + \frac{\mu_t}{\sigma_k}\right)\frac{\partial k}{\partial x_j}\right] + G_k - \rho\varepsilon + S_k \tag{4.4}$$

$$\frac{\partial}{\partial t}(\rho\varepsilon)+\frac{\partial}{\partial x_i}(\rho v_i\varepsilon)=\frac{\partial}{\partial x_j}\left[\left(\mu+\frac{\mu_i}{\mu_\varepsilon}\right)\frac{\partial\varepsilon}{\partial x_j}\right]+C_{1\varepsilon}\frac{\varepsilon}{k}G_k-C_{2\varepsilon}\rho\frac{\varepsilon^2}{k}+S_\varepsilon \tag{4.5}$$

where μ_t represents turbulent viscosity, and G_k represents the generation of turbulence kinetic energy due to the mean velocity gradients, $C_{1\varepsilon}$, and $C_{2\varepsilon}$ are model constants, σ_k and σ_ε are the turbulent Prandtl numbers for k and ε, respectively, and S_k and S_ε are source terms.

4.6.2 Modelling turbulent production

From the equation for the transport of k, the term G_k, representing the production of turbulence kinetic energy, may be defined as

$$G_k=-\rho\overline{u_i u}_j\frac{\partial u_j}{\partial x_i} \tag{4.6}$$

To evaluate G_k, in a manner consistent with the Boussinesq hypothesis,

$$G_k=\mu_t S^2 \tag{4.7}$$

where S is the modulus of the mean rate of strain tensor defined as

$$S^2=\sqrt{2S_{ij}S_{ij}} \tag{4.8}$$

4.6.3 Modelling the turbulent viscosity

The turbulent or eddy viscosity is computed by combining k and ε as follows:

$$\mu_t=-\rho C_\mu\frac{k^2}{\varepsilon} \tag{4.9}$$

where C_μ is constant.

4.6.4 Model constants

The model constants $C_{1\varepsilon}$, $C_{2\varepsilon}$, C_μ, σ_k, and σ_ε have the following values:

$C_{1\varepsilon}$=1.44, $C_{\varepsilon 2}$=1.92, C_μ=0.09, σ_k =1.0, σ_ε=1.3

These default values have been determined from experiments for fundamental turbulent flows including frequently encountered shear flows like boundary layer, mixing layers and jets as well as for decaying isotropic grid turbulence.

4.7 BOUNDARY CONDITIONS

4.7.1 Inlet

The complete fluid domain has one inlet of size ($9D \times 3.31D$). At the inlet the mean velocity normal to the boundary and turbulence parameters, k and ε were assigned. The k and ε are computed from the following equations:

$$k = 0.03u_{in}^2 \tag{4.11}$$

$$\varepsilon = \frac{k^{1.5}}{0.005W_i} \tag{4.12}$$

where u_{in} = average velocity at inlet and W_i= width of inlet at approach channel

4.7.2 Outlets

At the other end of the solution domain, namely, the pipe outlets, the condition of zero second derivatives is applied to the velocity components (Outflow). This implies that there is no feedback from the pipe system and pump located beyond that section. A pressure condition may be applied here in in lieu of the velocity gradient. This, however, would require knowledge of the downstream system components. To ensure global mass conservation, an out-flow ratio 0.1666 is defined at outlet of running pumps (for 6 pumps in operation), and 0 at closed pumps.

4.7.3 Free surface

The present CFD models assume that the free surface is flat and treats it as a stress free plane of symmetry. This implies that surface tension effects are neglected. The stress free plane tends to suppress the vertical movement of turbulent eddies by flattening them and redistributing the energy of the vertical velocity fluctuations near the free surface to fluctuations parallel to it. No attempt is made to model the turbulence near the free surface, i.e., the variations in the turbulence length and velocity scales near the free surface are not explicitly accounted for in the turbulence models.

4.7.4 Walls

All solid surfaces of the domain, including all channel walls, stop log gates and the inside and wetted outside of the pipe were treated as wall boundary, on which the no slip condition was

applied to all velocity components. The walls were assumed to be smooth (roughness height = 0, roughness constant = 0.5), thus boundary roughness was not taken into considerations.

4.7.5 Initial condition

To start the numerical solution and advance it in pseudo time to converged steady state, it is necessary to prescribe the initial values of all the velocity components, pressure, and turbulence parameters throughout the solution domain.

4.8 SOLVER SETTINGS

The following solver settings were used in all the simulations carried out in the present study:

- Double precision, segregated steady solver
- Second order upwind discretization for momentum, and Turbulence
- Under-relaxation factors for pressure, momentum, turbulent kinetic energy, and turbulent dissipation rate are equal to 0.3, 0 7, 0.8 and 0.8 respectively
- SIMPLEC algorithm for pressure-velocity coupling
- Convergence criteria (RMS< 10^{-6})

4.9 SWIRL ANGLE COMPUTATIONS

Swirl angle was computed by creating a function in Fluent. Area weighted average of swirl is calculated on a pseudo circular surface located at the same position as that of the vortimeter as in physical model, which is a surface of 0.75*D* diameter circular plane at impeller level). Therefore swirl angle is defined first using UDF in Fluent and area weighted average over a circular plane of diameter 0.75*D* has taken as swirl angle. Figure 4.10 shows the pseudo planes in CFD model used to compute the swirl angles.

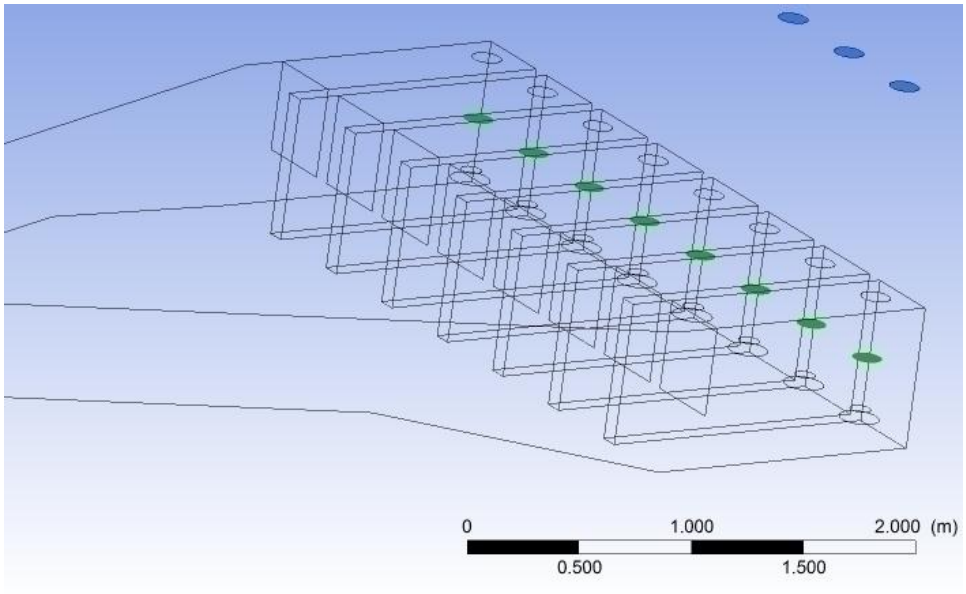

Figure 4.10 Planes used to compute swirl angles

4.10 MONITORING SOLUTION CONVERGENCE

Convergence is very important part for any CFD model and judging convergence is not an easy task as there are no universal metrics for judging convergence. In Fluent the convergence can be monitored dynamically by checking several parameters.

In present study, two methods for the convergence monitoring have been adopted first method was monitoring scaled residuals (u, v, w, continuity, k and ε) for conserved variables and second were swirl angles in all operating pumps. The convergence history plots are discussed in Chapter 5.

Double precision residuals as adopted in present study can go up to twelve orders of magnitude. Residual definitions that are useful for one class of problem are sometimes misleading for other classes of problems. Therefore, it is necessary to judge convergence not only by examining residual levels, but also by monitoring relevant integrated quantities such as swirl angle in the present study. Also, the level of residuals depends upon the initial guess. Therefore, low residuals do not signify the accuracy of the solution. In present study, the inlet parameters were used to initialize the solver runs.

The scaled residual for pressure based solver in Fluent is defined as the imbalance of some quantity (mass, energy or momentum) between the neighbouring cells, given by a ratio of the residual at M^{th} iteration to the largest absolute value of the residual in the first few iterations. For an example, the scaled residual for the continuity equation can be defined as

$$\frac{R^{c}_{iterationM}}{R^{c}_{iterationm}} \qquad (4.11)$$

where the numerator is the continuity residual (i.e. the mass imbalance between the neighbouring cells) at M^{th} iteration and the denominator is the largest continuity residual in the first *m* iterations.

4.11 GRID SENSITIVITY

A comprehensive grid sensitivity study necessitates obtaining solutions for the same flow with successively finer grids, until an optimal grid is obtained. This grid is defined as one with the minimum number of cells such that any solution obtained on a finer grid does not differ significantly from the solution obtained from the optimal grid. To rigorously study grid dependence of the solution, all grid parameters which affect the solution (grid type, number of nodes, clustering near the walls, aspect ratios, etc.) should be independently studied. For three dimensional flows, seven grids, generated using doubling (or halving) the grid spacing separately in each direction, have to be used to determine the grid dependence of the solution (Stern et al. 1999). As a minimum requirement, three solutions on grids which have been refined simultaneously in all directions may be used. A non-integer refinement of the grid may also be used in this case. Because of the very high requirements in terms of grid nodes to obtain numerical solutions with a near wall turbulence model at high Reynolds number for pump intake flows, the latter method was used.

4.12 TEST CONDITIONS

Total CFD simulation runs carried out to achieve different objectives of the present study are given in Table 4.4. The details of the runs are described in later chapter.

Table 4.4 Total CFD simulation runs

S. No.	Description	Number of runs	*Q* (L/s)
1	CFD simulations for verification	3	13.69
2	CFD simulations for validation	12	11.44, 13.69, 22.88
3	Effect of Froude number	5	8.0 to 49
4	Effect of cross type AVD on swirl	40	13.69

4.13 CONCLUDING REMARKS

A CFD model has been developed to investigate the flow in the pump sump intake. Further the CFD model has been used to investigate the flow phenomenon. Total 60 number of runs were carried out to achieve the objectives. The CFD model was first validated by comparing the experimental data and described in Chapter 5. After that the effect of Froude number on swirl has been investigated and discussed in Chapter 6. The CFD model has been further used to optimize the size of AVDs and described in Chapter 7.

CHAPTER 5 VERIFICATION AND VALIDATION OF CFD MODEL

5.1 INTRODUCTION

This chapter deals with verification and validation of the CFD models used in present study to simulate the flow in multiple pump sump intake models. This is required to gain confidence in the CFD model results.

Uncertainty in the results of the CFD models is both due to numerical errors in the solution of the governing equations and modelling errors in the mathematical representation of the physics involved. Numerical errors are due to discretization, velocity-pressure coupling, artificial dissipation, iterative and grid convergence, geometrical approximations and computer round-off. Two other issues related to numerical uncertainty are convergence of the solutions and the effect of grid refinement. Assessment of numerical uncertainty is known as verification of the CFD model and described in Section 5.2.

Modelling errors are due to turbulence models, free surface treatment, etc. The effect of approximate treatment of the free surface is clarified later by comparison with the experimental results in Section 5.3.

5.2 VERIFICATION OF THE CFD MODEL

5.2.1 Convergence

Steady state simulation results, at Q_p = 13.69 L/s, (Re = 1,47,965; Fr = 0.84 and operational bell mouth numbers #1, #2, #3, #6, #7 and #8) were obtained to evaluate the convergence properties of the CFD model. Average velocity at inlet (u = 15.56 cm/s) of approach channel with turbulence specifications (i.e. k and ε) was prescribed at the inlet. The outlets, free surface and walls were assigned as outflow, symmetry and no slip wall conditions. The two equation k-ε model along with scalable wall functions to model the turbulence and the near wall flow respectively, for the base pump sump model fluid domain i.e. FDWB and M3 hexahedral mesh (5.79 Million nodes) as described in Chapter 4, were used.

The residuals for the governing equations i.e. continuity, momentum and turbulence equations are presented in Figure 5.1 with the scaled residual on Y-axis and iteration number on X-axis. It can be easily observed in this figure that the residual of the continuity equation at convergence was smaller than 10^{-6}. As recommended in the Fluent, this result is satisfactory

for the grid used in the simulations for which the global mesh size was 16 mm. Similarly for the remaining equations, i.e. momentum equation and turbulence model equations the residuals reduced up to 10^{-7}. The turbulence quantities show better residual reduction properties compared to those of the velocity and continuity in present solver settings.

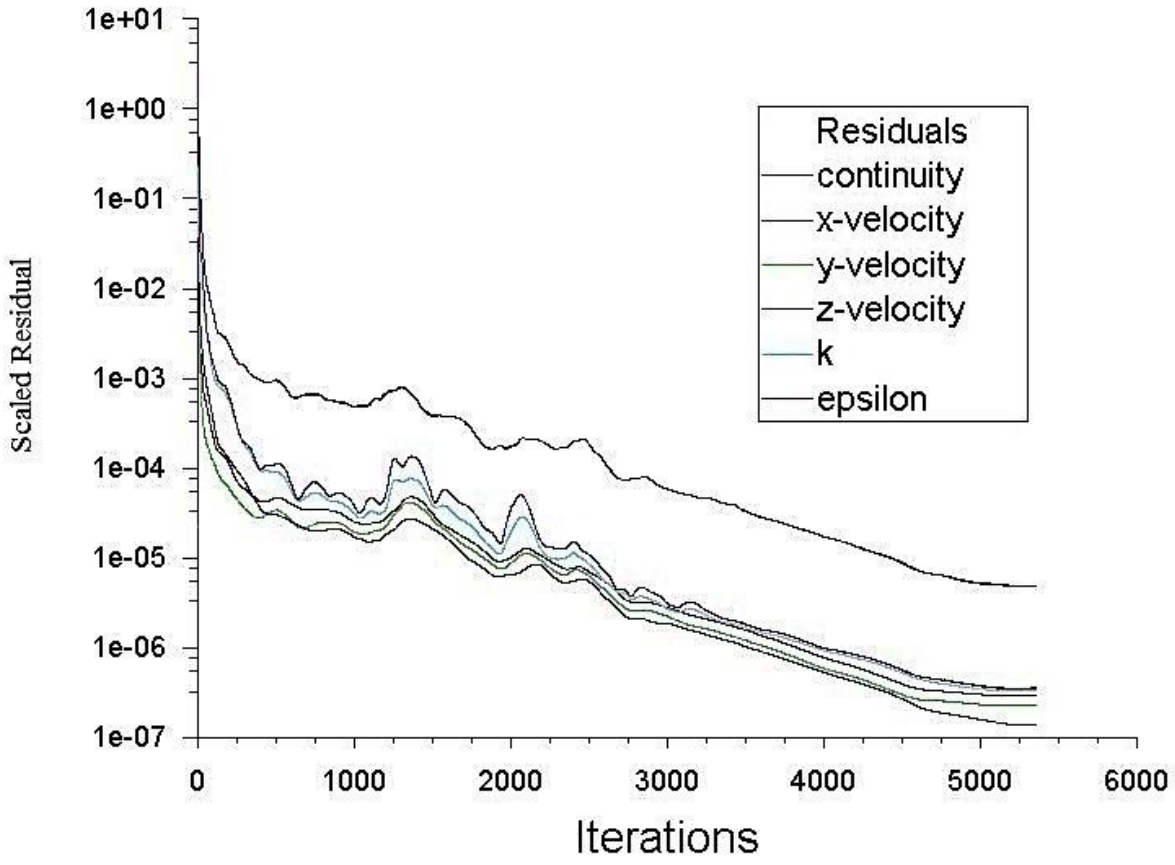

Figure 5.1 Convergence/residual history of the governing equations for run A.

Figure 5.2 shows the swirl angle history obtained from solver. The procedure for computing the swirl angle already described in previous chapter has been used in the whole thesis. It can be easily observed in both graphs that after 3,000 iterations there is no significant variation in the computed swirl angles up to 5,400. Therefore, the obtained solution can be considered as stable solution.

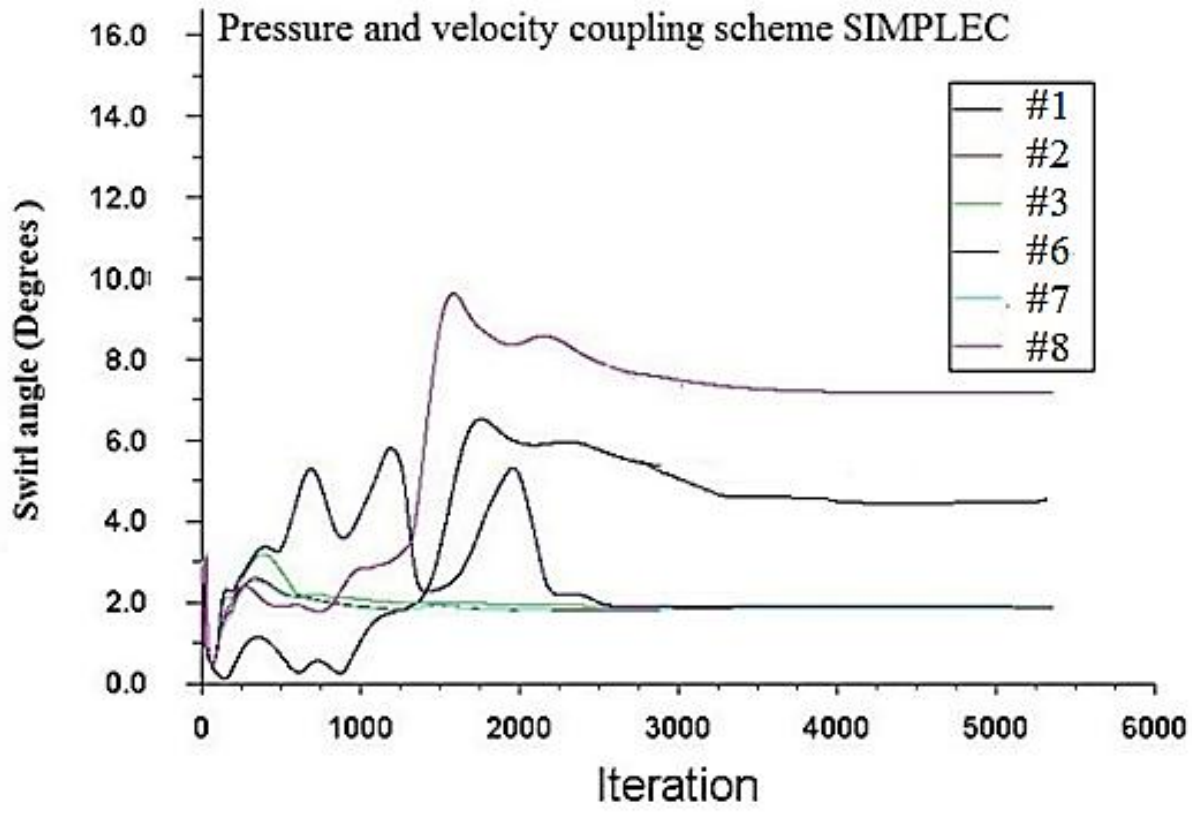

Figure 5.2 Swirl angle history in all working pump bays for run A

5.2.2 Grid sensitivity

The grid dependence of the solution was estimated by three solver runs on three grids (namely M1, M2 and M3) for the base pump sump model as given in Table 5.1. Numerical simulations were carried out for (Re =1, 47, 965; Fr =0.84) Q_p = 13.6 L/s (Table 5.1) with three different grids for the base fluid domain (FDWB) and keeping all other solution parameters constant.

A quantitative comparison among the results obtained with the three grids is shown in Figure 5.3 for swirl angles in suction pipes, and also tabulated in Table 5.1. It is clear from the Figure 5.3 that the grid M3 and M2 have relatively low variation as compared to the grid M2 and M1 therefore it can be assumed that the results of grid M3 are independent for the further refinement.

Table 5.1 Swirl angles (Degrees) for different grids for Q_s = 13.69 L/s

Run No.	Run name	Mesh	Swirl angles					
			Operational bellmouth no.					
			#1	#2	#3	#6	#7	#8
1	AM1	M1	4.1	3.73	3.76	3.72	3.68	5.64
2	AM2	M2	4.75	1.99	2.1	2.08	1.99	6.63
3	AM3	M3	4.5	2.5	2.75	2.75	3.3	4.5

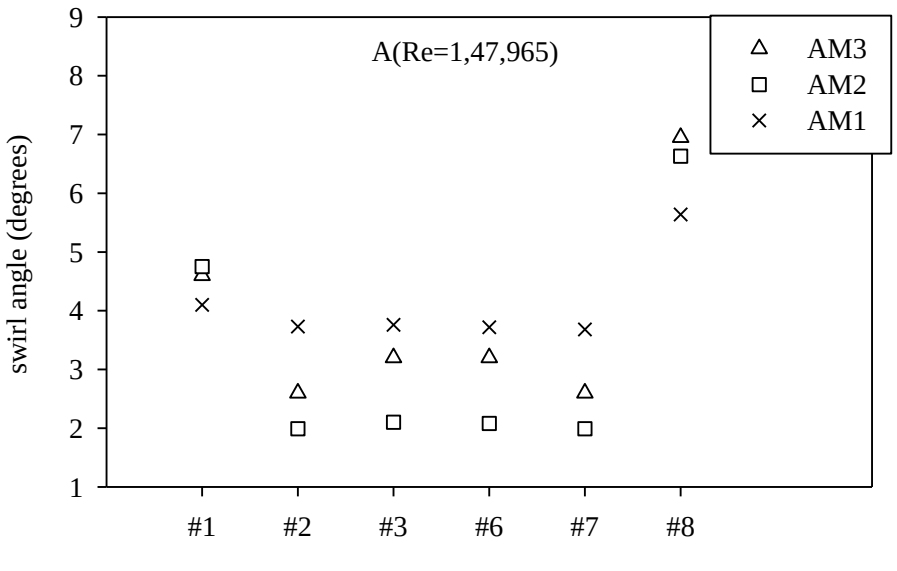

Figure 5.3 Swirl angles for run AM1, AM2 and AM3

Figures 5.4 to 5.6 show the flow patterns at the free surface (z= 5D) calculated with grids M1, M2 and M3, respectively. The streamlines and contours of vorticity component ω_z were constructed from the calculated in-plane velocity field (the normal component of velocity is zero under the plane of symmetry assumption). When plotted in this way, the solution reveals vortices and swirling motions. It is observed that the flow topology does not change with grid refinement. In these figures, the out plane vorticity has been non-dimensionalized with the $D = 134$ mm and $V = 0.97$m/s. Depending on the maximum out plane vorticity, the position of free surface vortices namely V1 and V2 in bay #1 and #8 respectively has been located.

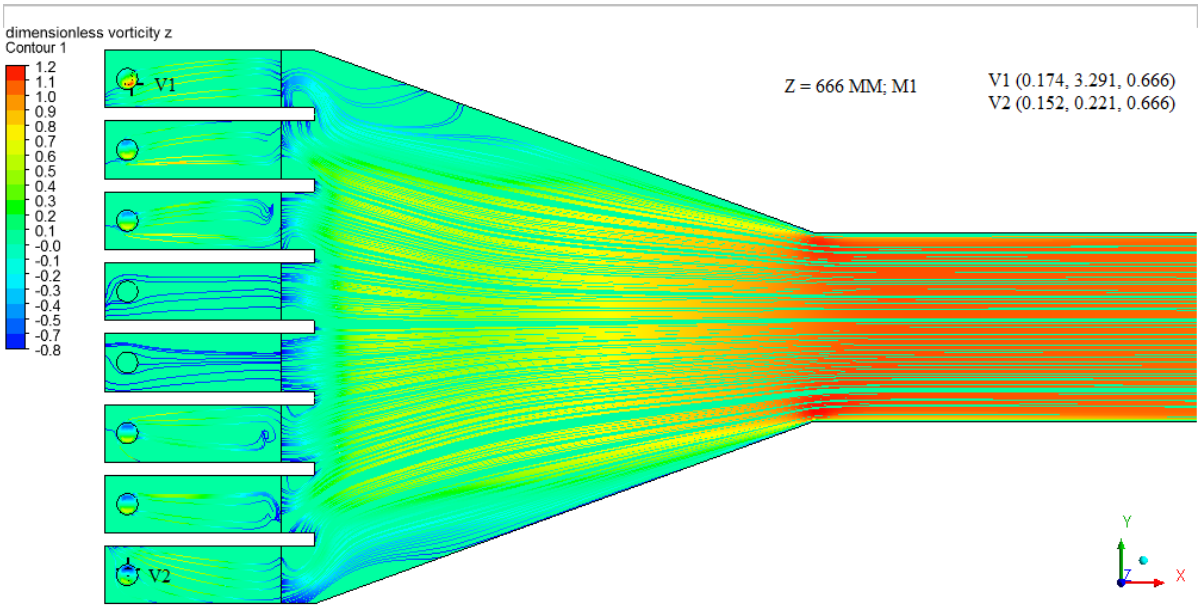

Figure 5.4 Streamline and out-plane vorticity contours at $z = 5D$ for run AM1

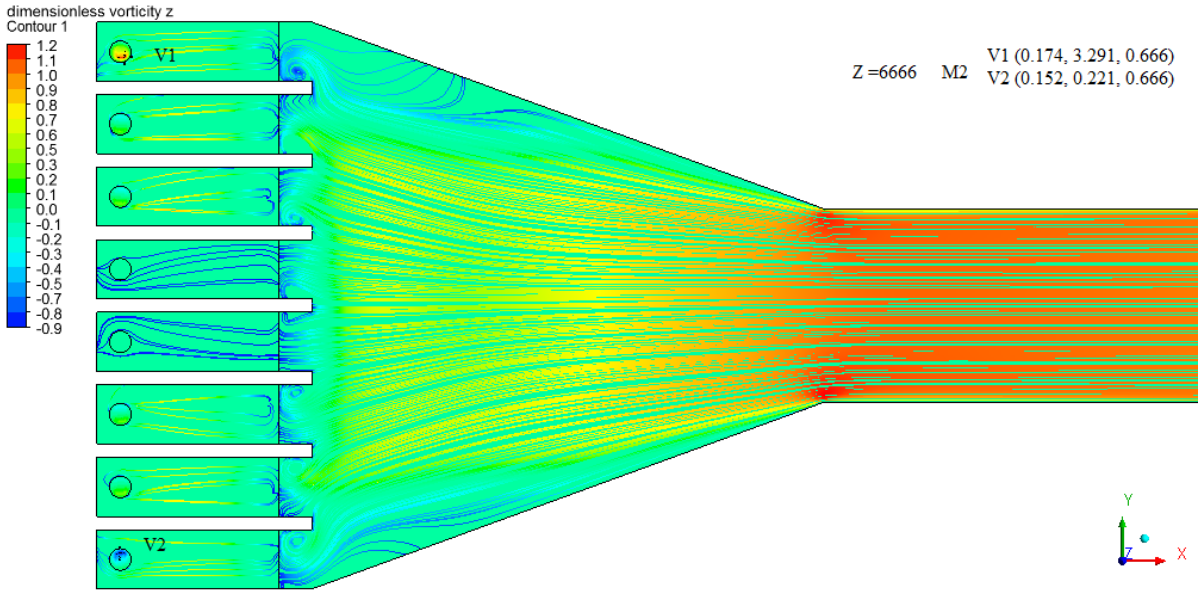

Figure 5.5 Streamline and out-plane vorticity contours at $z = 5D$ for run AM2

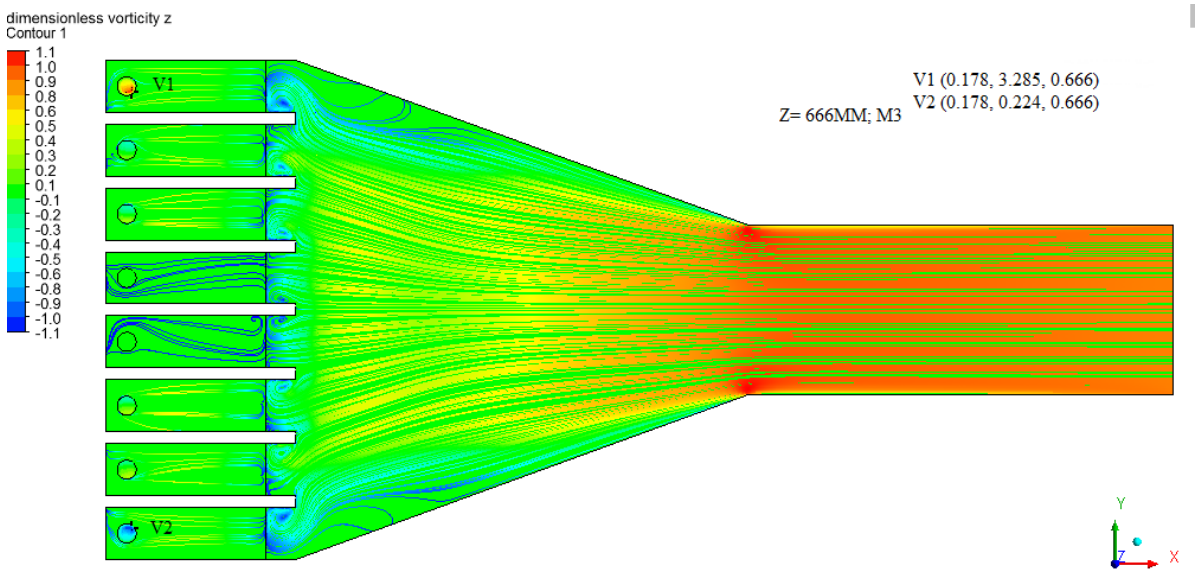

Figure 5.6 Streamline and out-plane vorticity contours at $z = 5D$ for run AM3

Figures 5.7 to 5.9 show the flow in planes parallel to the floor. In each case, the "streamlines" and the component of vorticity normal to that plane were calculated from the in plane velocity components. For clarity the figures show only a few streamlines overlaid on contours of the vorticity component. Once again these reveal the underlying vortical structures and indicate that grid refinement has no effect on the overall flow topology. Analysis of these figures gives information on the location, shape, size and intensity of predicted vortices. There is good agreement between predictions with the M2 and M3 grids at the free surface.

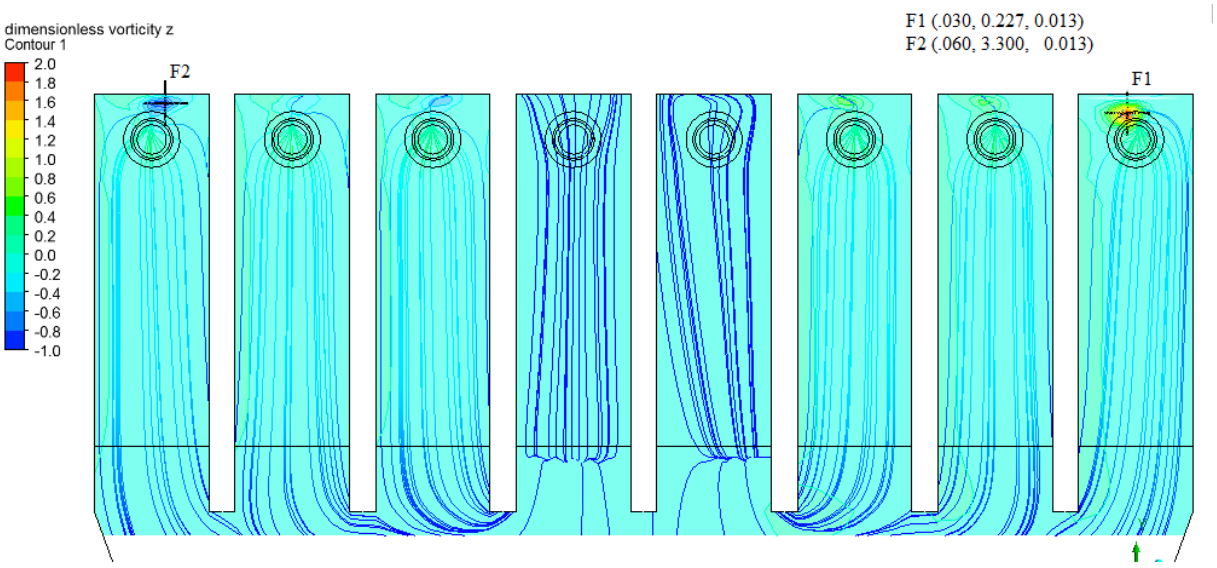

Figure 5.7 Streamlines and out-plane vorticity contours at $z = 0.01D$ for run AM1

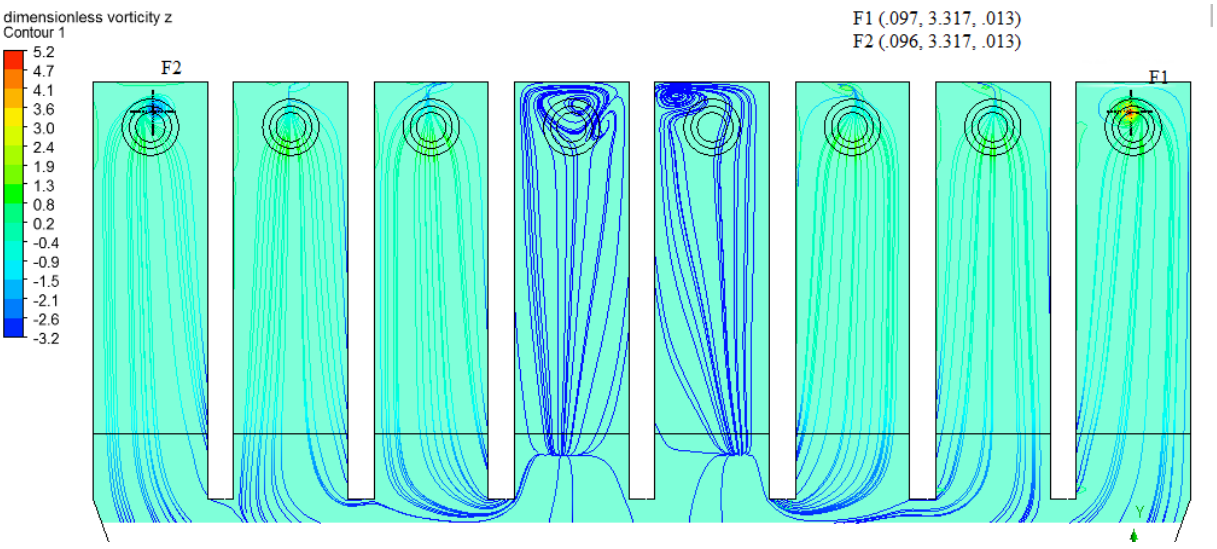

Figure 5.8 Streamline and out-plane vorticity contours at $z = 0.01D$ for run AM2

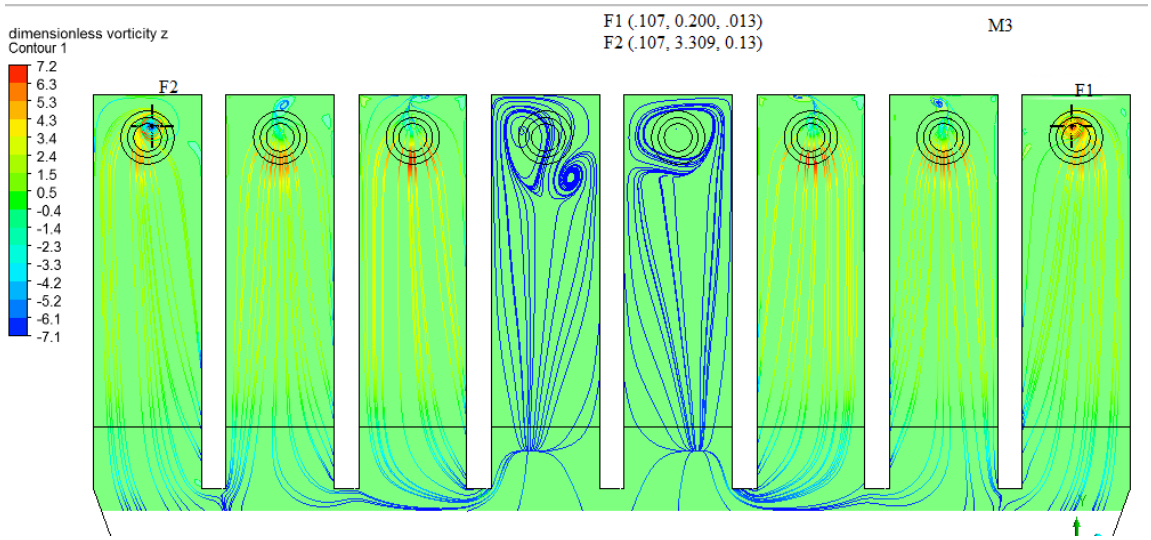

Figure 5.9 Streamline and out-plane vorticity contours at z = 0.01D for run AM3

Figures 5.10 to 5.12 show the streamline and out-plane vorticity contours in plane x=0.01D. From these figures, it is observed that there are some differences in the strength of the backwall attached vortices. Therefore, a more quantitative measure of grid sensitivity is needed.

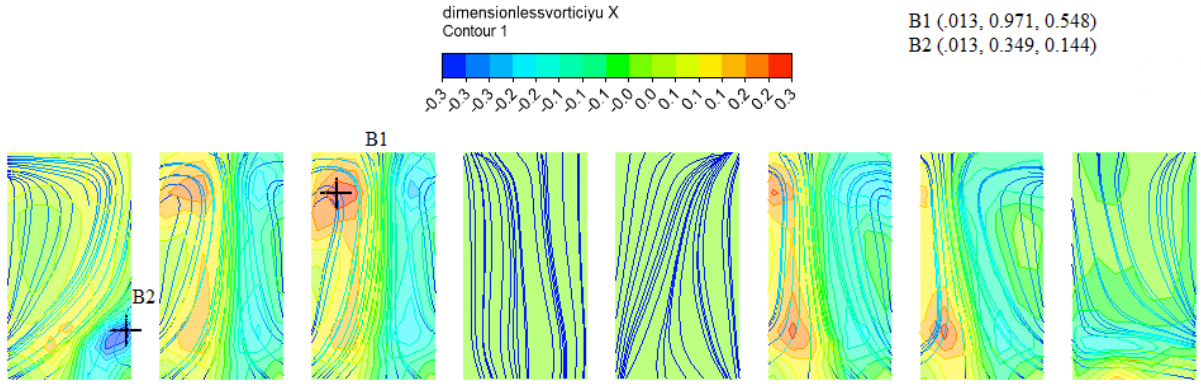

Figure 5.10 Streamline and out-plane vorticity contours at x = 0.01D for run AM1

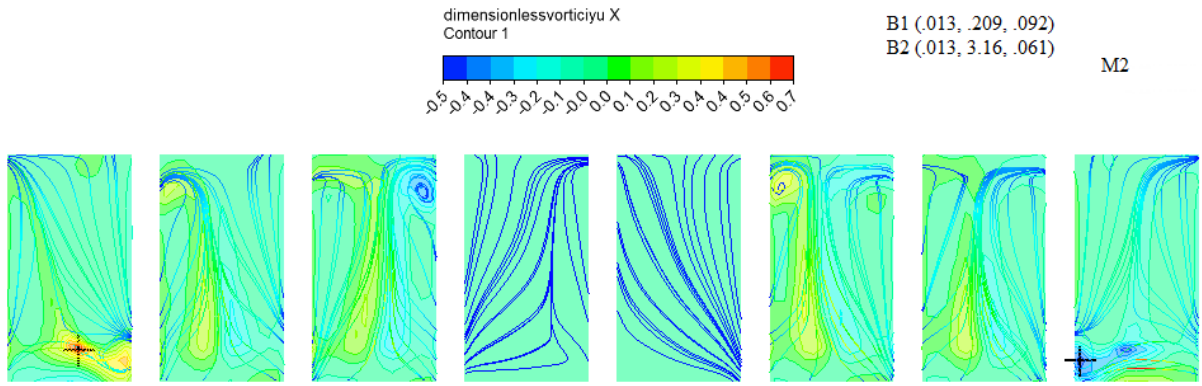

Figure 5.11 Streamline and out-plane vorticity contours at x = 0.01D for run AM2

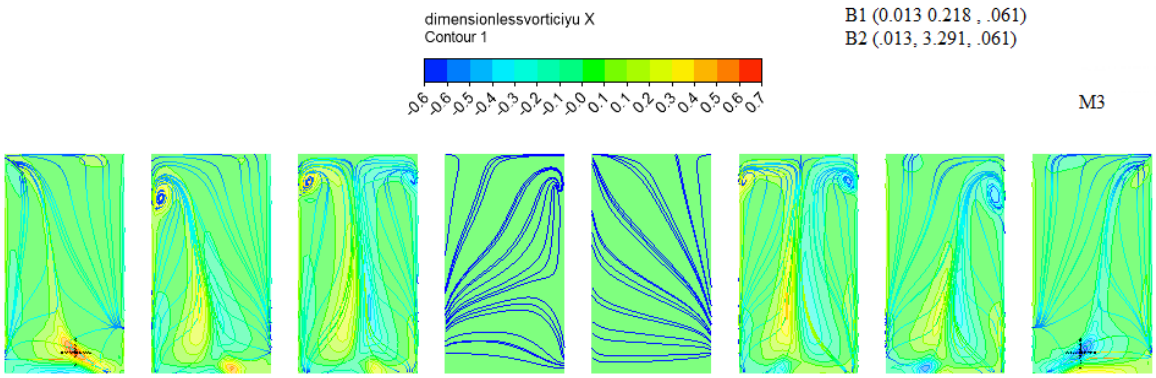

Figure 5.12 Streamline and out-plane vorticity contours at $x = 0.01D$ for run AM3

A quantitative comparison among the results obtained with the three grids is made in for selected vortices V1, V2, F1 and F2. Due to symmetry, only one of a pair of symmetric counter rotating vortices was analysed in each case. In planes containing more than one vortex pair, the pair closest to the pipe was chosen. For each vortex, the circulation (Γ) around a constant vorticity contour

$$\Gamma(\omega_{Z0}) = \int_{\omega_z > \omega_{z0}} \omega_Z dA \tag{5.1}$$

and the area A within that contour

$$A(\omega_{Z0}) = \int_{\omega_z > \omega_{z0}} dA \tag{5.2}$$

were calculated, and converted to an average or effective tangential velocity and radius as follows:

$$V_\theta = \Gamma / 2\pi r \tag{5.3}$$

$$r = \sqrt{A/\pi} \tag{5.4}$$

The radial distribution of the nondimensionalized tangential velocity, V_θ / V, and circulation Γ/VD, provide measures of the vortex strength and size. These are shown in Figures 5.13 to 5.16 for the three grids. It is observed that the solutions are remarkably grid independent except in the case of the backwall vortex, where a difference of about 25% in intensity is found between the coarse (M1) and medium grids (M2) but it is only 4% between the medium and fine (M3) grids.

The position of the vortices considered above may be described in terms of the location of the point of maximum vorticity relative to the bay walls, or the pipe centre. These positions are summarized in Table 5.2. The maximum variation in position is found to be within 4%, except for the vertical coordinate of the backwall vertex, in which a difference between the medium and coarse grid solution is less than 3% in the coordinates of all vortices.

Table 5.2 Effect of grid on vortex location

S. No.	Case	Bay No	Vortex name	*x*	*y*	*z*
1	AM1	#1	V1	0.174	3.291	0.666
2		#8	V2	0.152	0.221	0.666
3	AM2	#1	V1	0.174	3.290	0.666
4		#8	V2	0.141	0.221	0.666
5	AM3	#1	V1	0.178	3.285	0.666
6		#8	V2	0.178	0.224	0.666
1	AM1	#1	B1	0.013	0.971	0.548
2		#3	B2	0.013	0.349	0.144
3	AM2	#1	B1	0.013	0.209	0.092
4		#3	B2	0.013	3.160	0.061
5	AM3	#1	B1	0.013	0.218	0.061
6		#3	B2	0.013	3.291	0.061
7	AM1	#1	F1	0.030	0.227	0.013
8		#8	F2	0.060	3.300	0.013
9	AM2	#1	F1	0.097	0.193	0.013
10		#8	F2	0.096	3.317	0.013
11	AM3	#1	F1	0.107	0.200	0.013
12		#8	F2	0.107	3.309	0.013

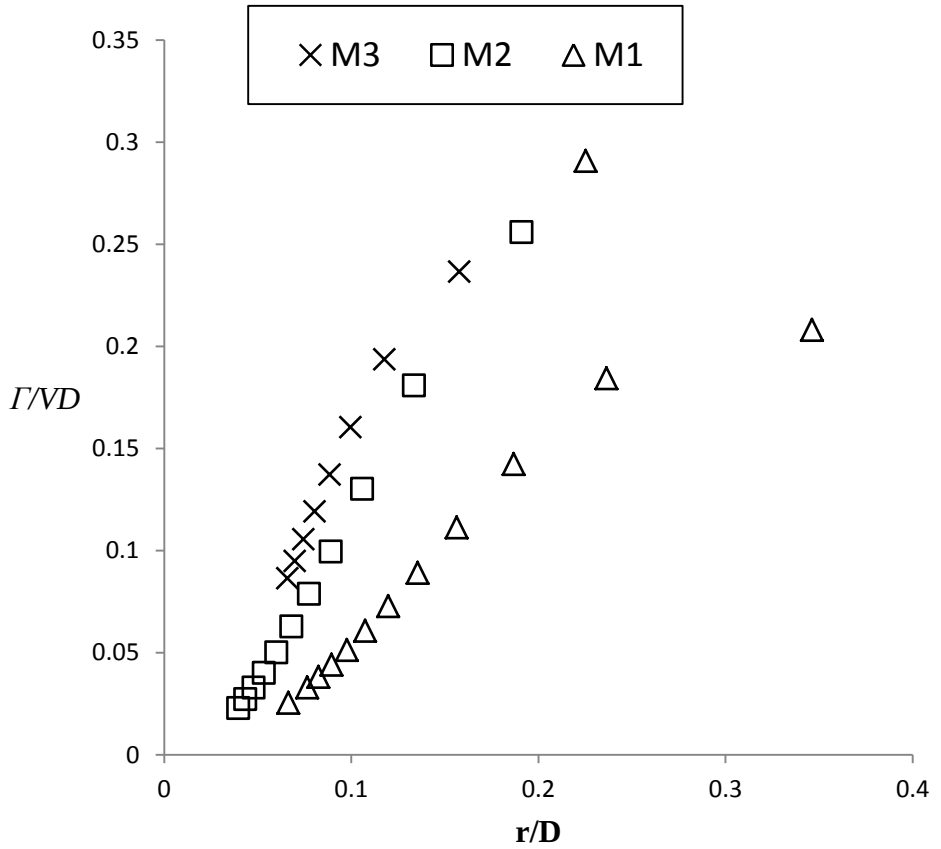

Figure 5.13 Grid dependency study of the floor attached subsurface vortex F1: Circulation

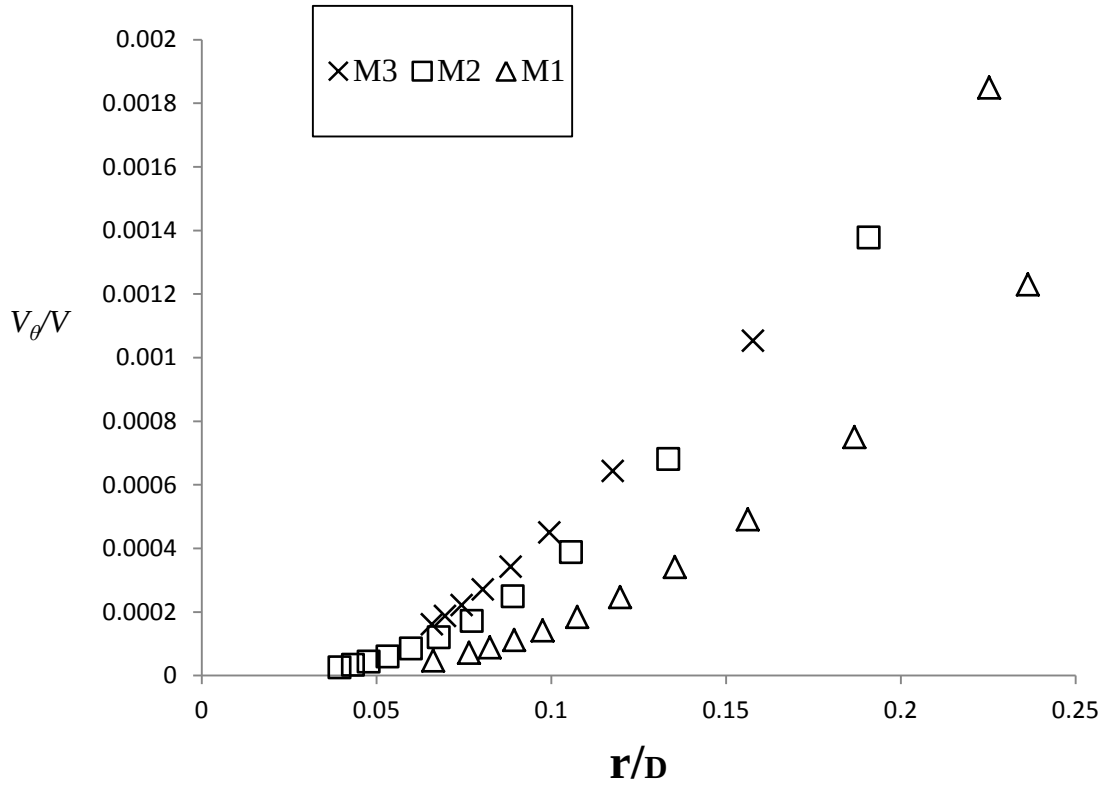

Figure 5.14 Grid dependency study of the floor attached subsurface vortex F1: Dimensionless tangential velocity

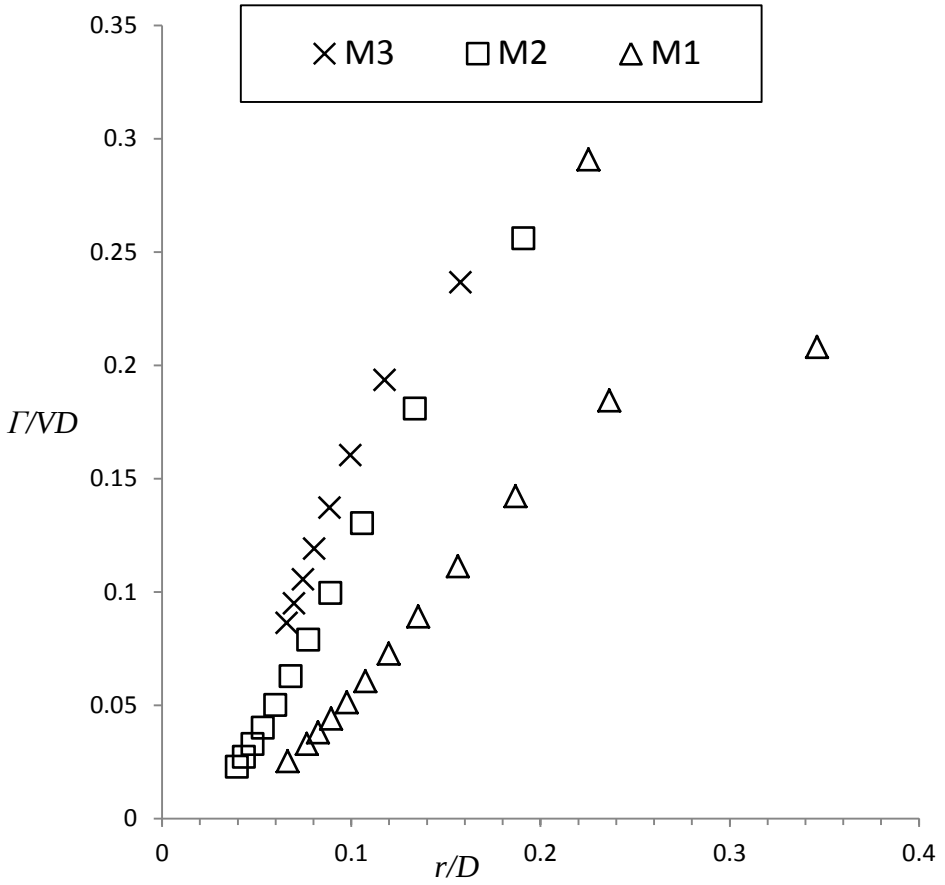

Figure 5.15 Grid dependency study of free surface vortex V1: Circulation

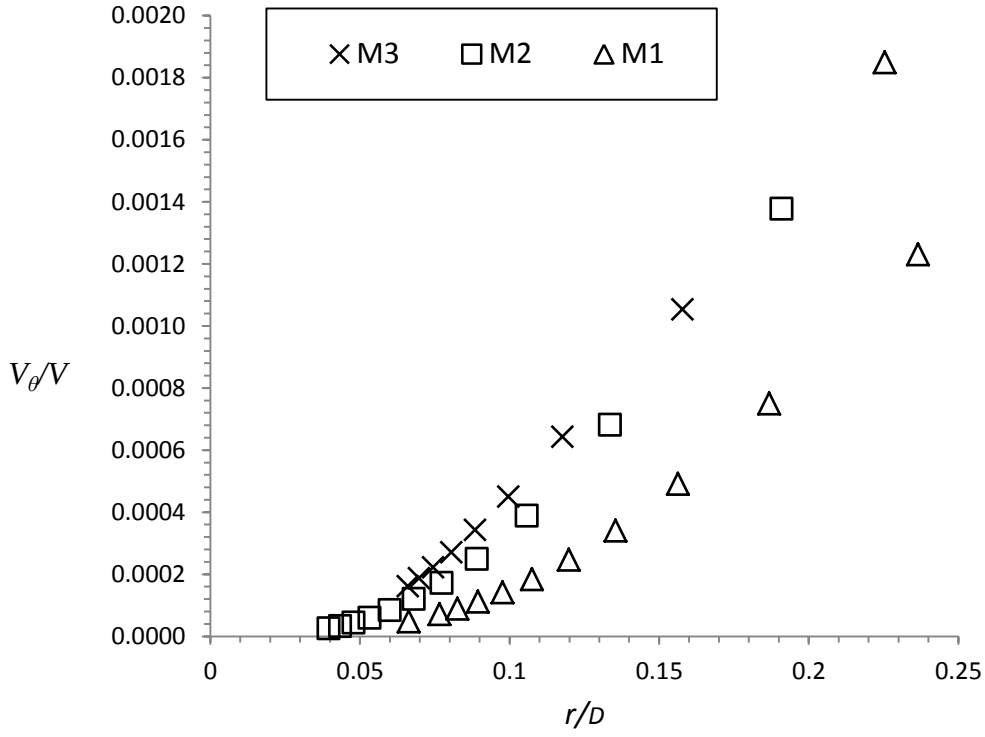

Figure 5.16 Grid dependency study of free surface vortex V1: Dimensionless tangential velocity

Finally, the decay of swirl in the pipe, a quantity of considerable interest in pump intake design, is considered to test the grid sensitivity. Figure 5.17 shows the distribution of swirl along the distance from the inlet of the pipe for the three grids. The *z* is considered as distance from the bell mouth and is nondimensionalized with the pipe diameter (*D*), swirl after the bell end is considered as maximum swirl (θ_{max}) used to nondimensionalize the swirl at any distance.

The results presented in this section lead to the conclusion that the solution becomes practically grid independent starting with the medium grid, M2, with the solutions on the medium and fine grids being practically indistinguishable in most respects, and differing by at most 3% in others. Therefore, almost all subsequent calculations in this study were performed on a grid with the same number of nodes as the fine grid, M3, to insure grid independent solutions.

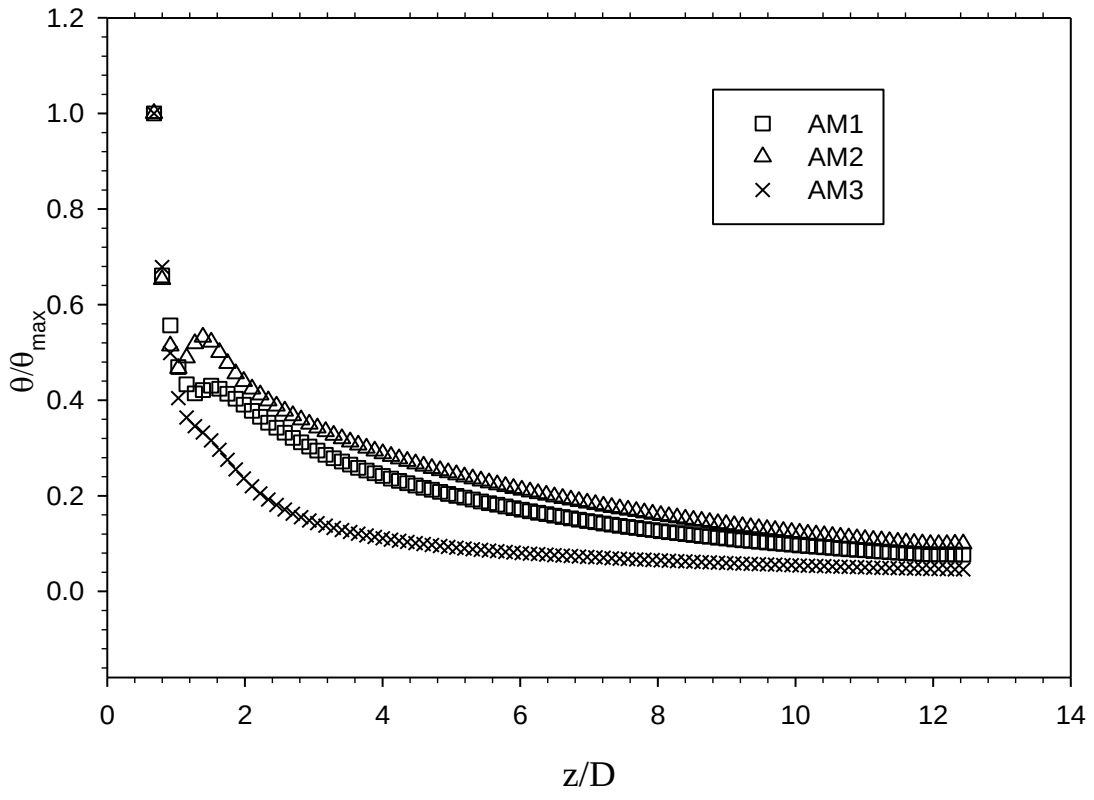

Figure 5.17 Grid dependence of decay of swirl along distance in suction pipe

5.3 VALIDATION OF THE CFD MODEL

In spite of the many published studies, until very recently there was no experimental data that was complete and comprehensive enough to allow a detailed quantitative validation of the CFD models in multiple pump sump intakes as the present case is.

The experimental data used to validate the CFD model of the laboratory model are given in Table 5.3, and are briefly described below. The laboratory experiments (Table 5.3) were performed under flow conditions, namely with Reynolds, Froude and weber numbers, for which surface tension and free surface elevation effects could be neglected. Swirl in the pump sump columns were measured by vortimeter readings for 2 minute duration. The velocity used for the validation purposes was measured using ADC. The total experimental runs carried out are given in Table 5.3.

Table 5.3 Experimental and CFD model runs for validation of the CFD model.

Run No.	Run Name	Q	Q_p (L /s)	Fr	Re	Bell mouth operation
1	DA	68.46	11.41	0.70	123387	#1, #2, #3, #6, #7, #8
2	DB					#1, #2, #5, #6, #7, #8
3	DC					#3, #4, #5, #6, #7, #8
4	DD					#1, #3, #4, #5, #6, #8
5	MA	82.14	13.69	0.84	147965	#1, #2, #3, #6, #7, #8
6	MB					#1, #2, #5, #6, #7, #8
7	MC					#3, #4, #5, #6, #7, #8
8	MD					#1, #3, #4, #5, #6, #8
9	2FA	136.92	22.87	1.41	246645	#1, #2, #3, #6, #7, #8
10	2FB					#1, #2, #5, #6, #7, #8
11	2FC					#3, #4, #5, #6, #7, #8
12	2FD					#1, #3, #4, #5, #6, #8

5.3.1 Description of simulations

The CFD simulations were conducted for the same geometric and flow conditions as in the experiments. Swirl angles were computed and compared with the experimentally observed values of swirl angles. The k- ε turbulence model with scalable wall function approach has

been used to model the turbulence. The free surface is treated as symmetry boundary conditions.

5.3.2 Results and discussions

Swirl angle comparison

Table 5.4 to 5.7 give the computed swirl angle from experimental and CFD model runs given in Table 5.3. Figures 5.18 to 5.29 show the comparison of swirl angles simulated using CFD and experimentally observed in working pumps for different flow conditions and pump combinations. It is observed that the CFD model results are slightly lower than the physical model values that may be due to Reynolds averaging of the quantities or assumptions involved in modelling turbulence. Apart from this under prediction, in totality CFD results are in good agreement with the experimental values. One to one matching of swirl angle is partially in order however, the trends of experimental and numerical results are same.

Table 5.4 Comparison of swirl angles computed from experimental and CFD model runs at Q_s=11.44 L/s

S. No.	Operational bell mouth No..	Swirl angles							
		DA		DB		DC		DD	
		Exp.	CFD	Exp.	CFD	Exp.	CFD	Exp.	CFD
1	#1	5	4.5	5.85	4	-	-	5.9	5
2	#2	2.8	2.5	6	4.5	-	-	-	-
3	#3	3	2.75	-	-	5	5	4.23	3
4	#4	-	-	-	-	3	2.35	3.05	2.45
5	#5	-	-	3.87	2.8	3.5	2.45	2.8	2.45
6	#6	3	2.75	2.45	2.25	2.4	2.1	4.23	3.25
7	#7	4.6	3.3	3	2.18	2.5	1.9	-	-
8	#8	5.2	4.5	7	5.84	4.7	4	7	5

Table 5.5 Comparison of swirl angles computed from Experimental and CFD model runs at Q_s = 13.69 L/s

S. No.	Operational bell mouth no.	Swirl angles							
		MA		MB		MC		MD	
		Exp.	CFD	Exp.	CFD	Exp.	CFD	Exp.	CFD
1	#1	7.5	4.5	6	5	-	-	7	6.5
2	#2	3.5	2.6	7.5	6	-	-	-	-
3	#3	4	3.2	-	-	6.6	5.7	4.8	3
4	#4	-	-	-	-	4	2.9	3.5	2.7
5	#5	-	-	4	3.5	3.0	2.6	2.8	2.7
6	#6	4.2	3.2	3.2	3	2.9	2.2	3	2.8
7	#7	3	2.6	3.5	3.1	2.5	2.3	-	-
8	#8	7.21	6.9	7.5	5.6	5.5	3.3	7.4	5.0

Table 5.6 Comparison of swirl angles computed from Experimental and CFD model runs at Q_s = 22.88 L/s

S. No.	Operational bell mouth no.	Swirl angles							
		2FA		2FB		2FC		2FD	
		Exp.	CFD	Exp.	CFD	Exp.	CFD	Exp.	CFD
1	#1	7.7	5	7.6	7.2	-	-	7.5	6
2	#2	4.6	3.9	7.7	6.5	-	-	-	-
3	#3	4.1	3.5	-	-	7.6	5	5.2	3.1
4	#4	-	-	-	-	3.2	2.8	3.8	3.3
5	#5	-	-	4.1	2.9	3.5	2.8	4.1	3.3
6	#6	4.6	3.5	3.3	2.9	2.5	2.2	3.5	3.1
7	#7	5	3.9	4.1	3.6	3.2	2.6	-	-
8	#8	7.6	6	7.7	6.7	7.6	5.1	7	6

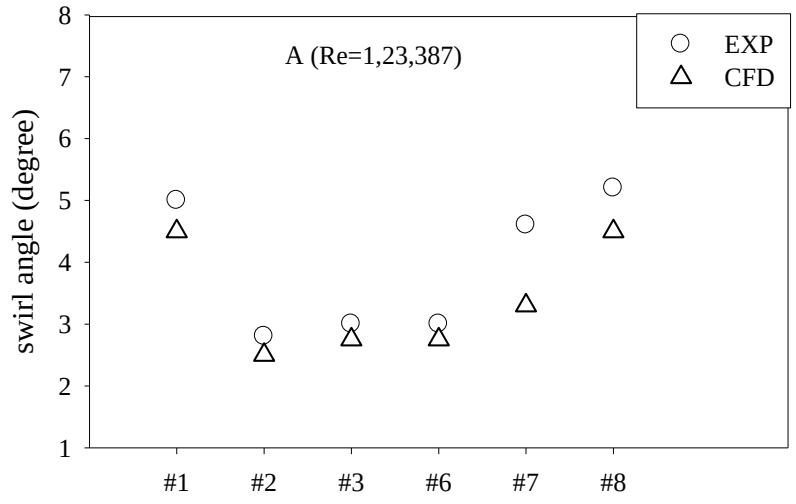

Figure 5.18 Swirl angle comparison for run DA

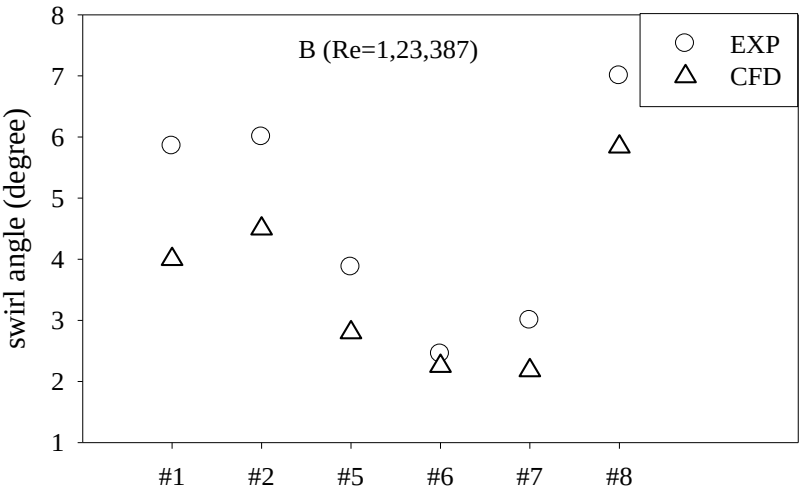

Figure 5.19 Swirl angle comparison for run DB

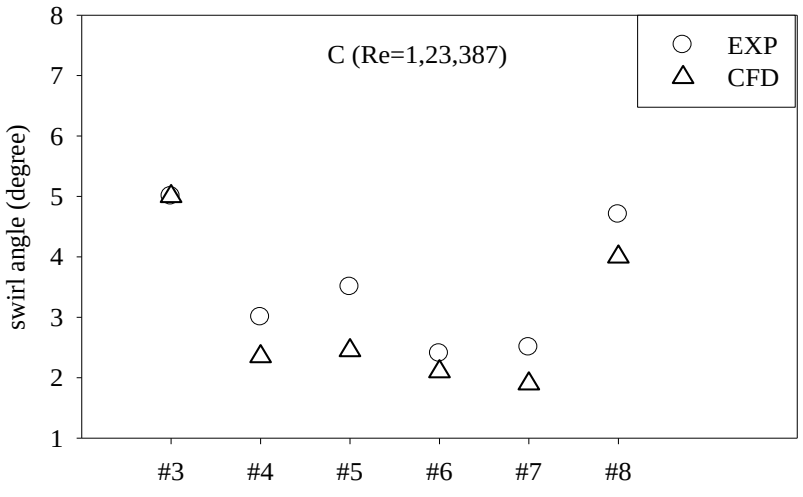

Figure 5.20 Swirl angle comparison for run DC

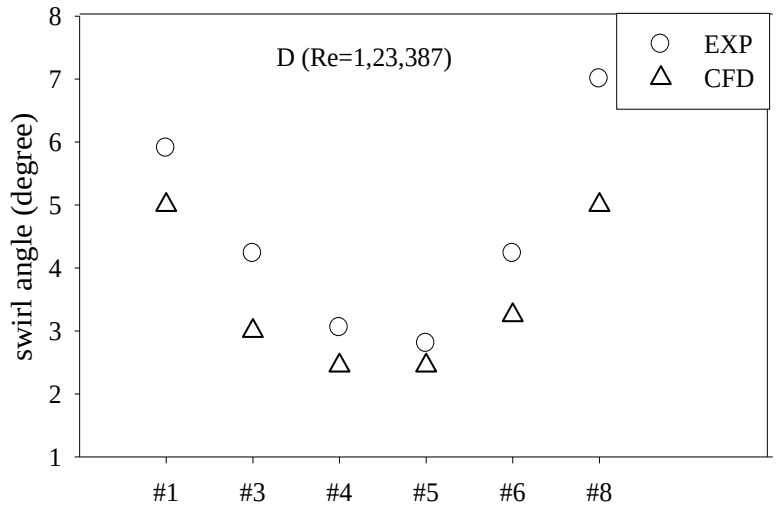

Figure 5.21 Swirl angle comparison for run DD

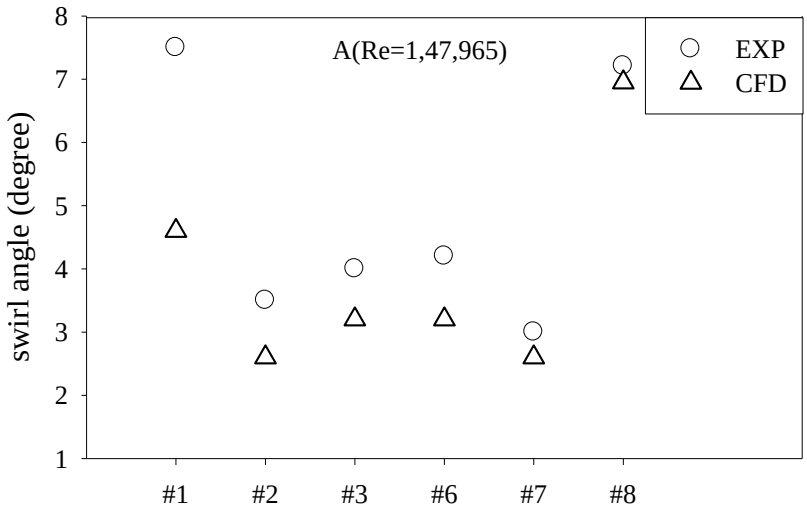

Figure 5.22 Swirl angle comparison for run MA

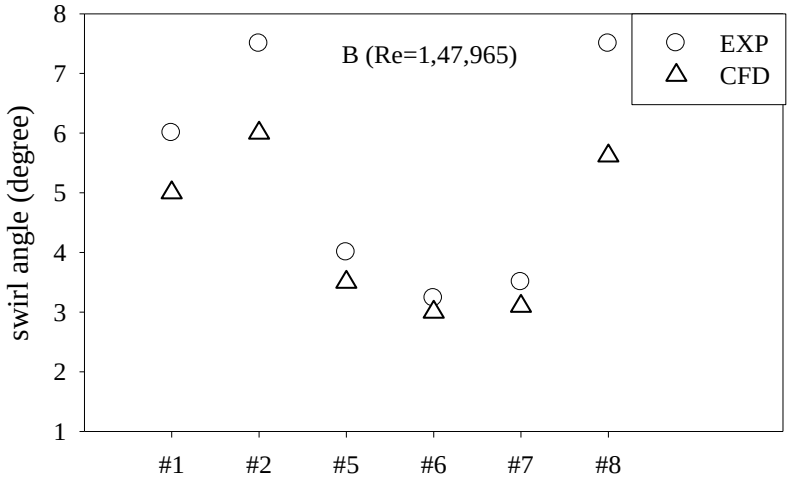

Figure 5.23 Swirl angle comparison for run MB

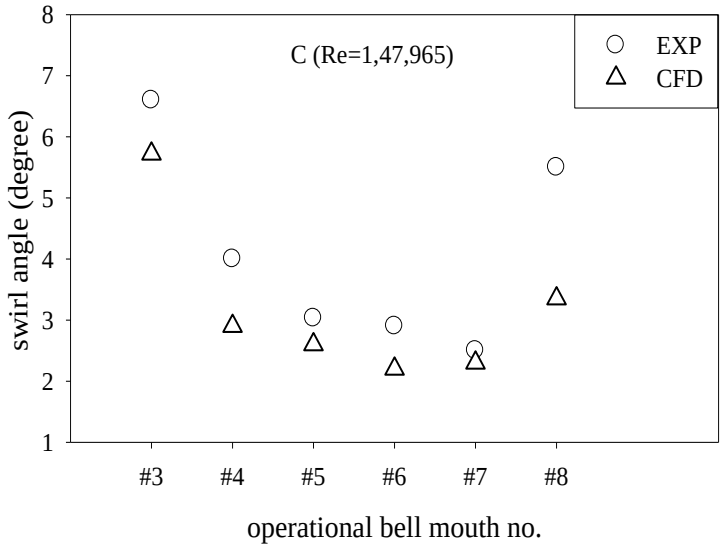

Figure 5.24 Swirl angle comparison for run MC

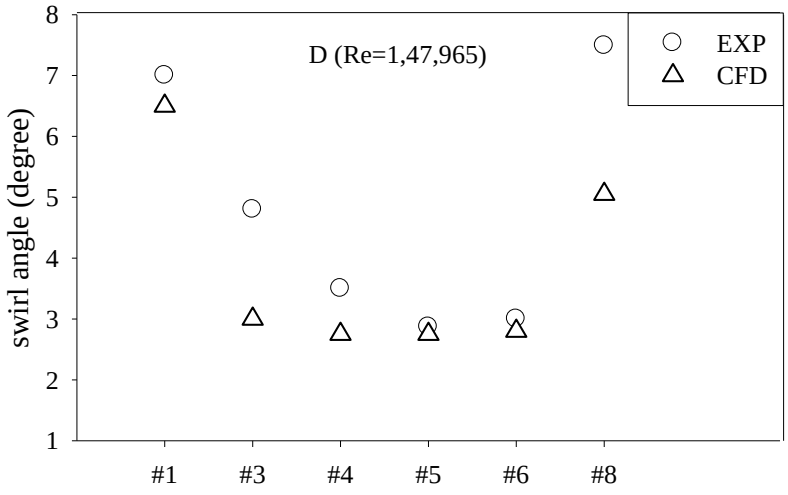

Figure 5.25 Swirl angle comparison for run MD

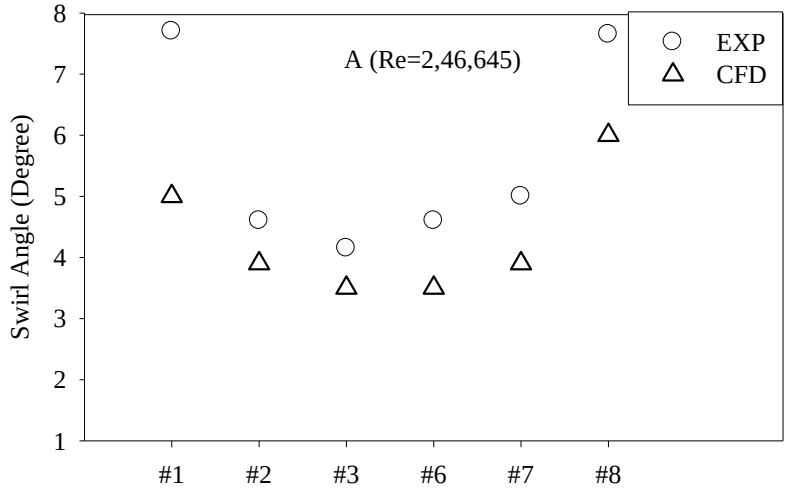

Figure 5.26 Swirl angle comparison for run 2FA

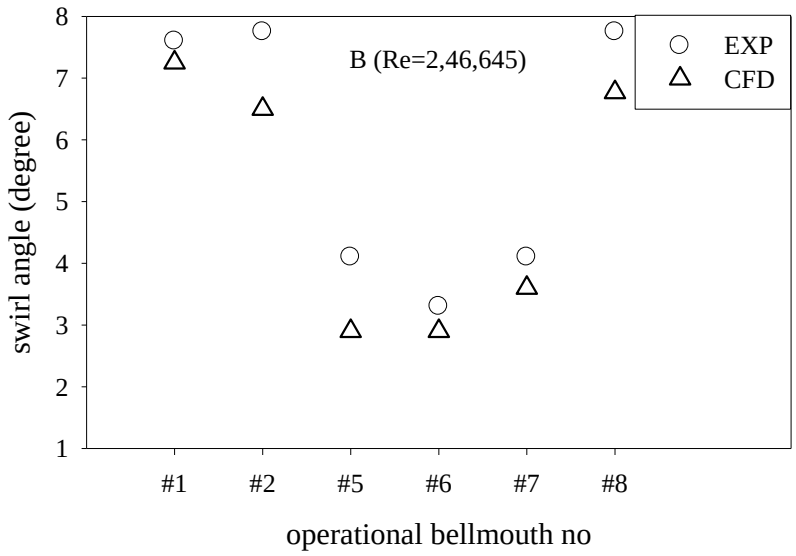

Figure 5.27 Swirl angle comparison for run 2FB

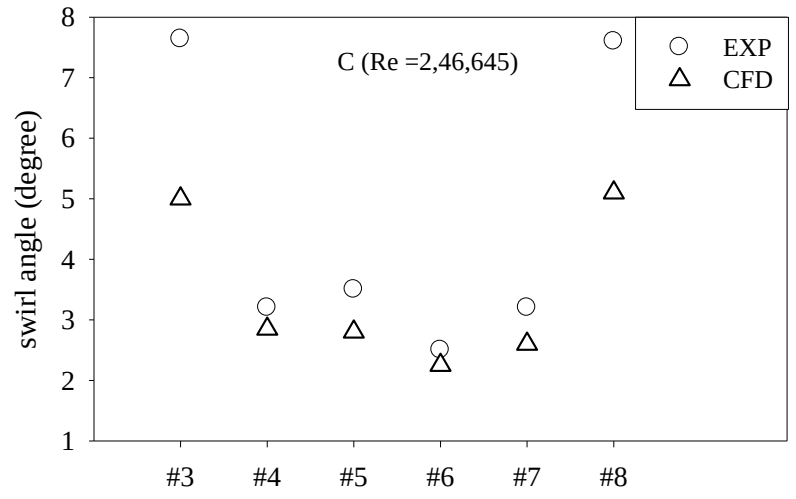

Figure 5.28 Swirl angle comparison for run 2FC

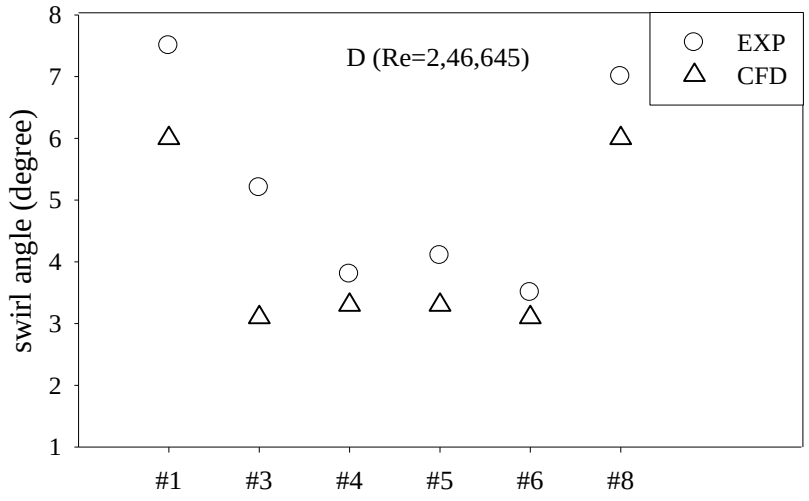

Figure 5.29 Swirl angle comparison for run 2FD

Velocity data comparison

Further, the computed velocity has been compared with the velocities measured by ADC. Figure 5.30 shows the locations where the measurements were carried out for case A and maximum discharge conditions (Re =1,47,965; Fr =0.84). Good agreements between computed and observed results validate the developed CFD model as shown in Figure 5.31.

For one flow condition, the velocity data comparison has been presented here (even though for all combinations the velocity data has been collected and compared). The computed velocity profile in all the bays is compared with experimental results for this combination. Velocity distribution at verticals has been compared with CFD simulation results in a plane parallel to backwall i.e., x = 50 cm. It is clearly observed that the CFD model results match with the experimental data. Slight variation can be seen that can be due to unsteady nature of the flow or may be due to some experimental errors.

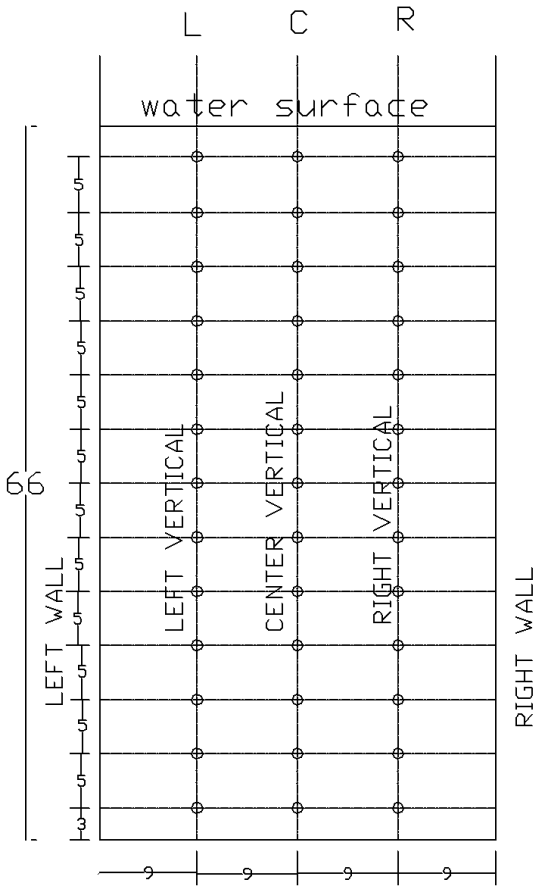

Figure 5.30 Locations of verticals and points where velocities were measured in the bays (all dimensions are in cm)

The relative standard deviations (RSDs) of the velocity data obtained from the experiments and that of the CFD for four bays with running pumps are given by the following

$$\sigma = \sqrt{\frac{\sum_{i=1}^{i=n}\left(u_i - u_{avg}\right)^2}{n}} \tag{5.6}$$

$$u_{RSD} = \frac{\sigma}{u_{avg}} \tag{5.7}$$

where σ = standard deviation, n = number of velocity measurements, u_i= velocity (measured or computed) at a particular location in m/s, u_{avg}=measured or computed average velocity in m/s and u_{RSD} = relative standard deviation (percentage). Values of u_{RSD} are tabulated in Table 5.7 for all the cases and both the procedures. RSD is an estimate of fluctuations of velocity data from its mean value. Although in most of the cases the values are comparable, in few cases the deviations of the experimental and computational values of u_{RSD} are precisely due to the limited number of points used in order to calculate the velocity distribution at the verticals in bays.

Table 5.7 Relative standard deviation (RSD) of velocity distribution at the bays for run A.

Bay No.	Vertical	Experimental. u_{RSD}	CFD u_{RSD}
Bay 1	Left	1.86	1.71
	Center	2.17	2.00
	Right	2.00	2.40
Bay 2	Left	1.88	2.00
	Center	2.13	2.17
	Right	1.78	1.86
Bay 3	Left	2.50	2.60
	Center	2.00	2.17
	Right	1.83	1.86
Bay 6	Left	1.83	2.17
	Center	2.17	2.17
	Right	1.83	2.17
Bay 7	Left	2.50	2.60
	Center	2.50	2.17
	Right	2.00	2.00
Bay 8	Left	2.17	2.20
	Center	2.33	2.00
	Right	2.17	1.71

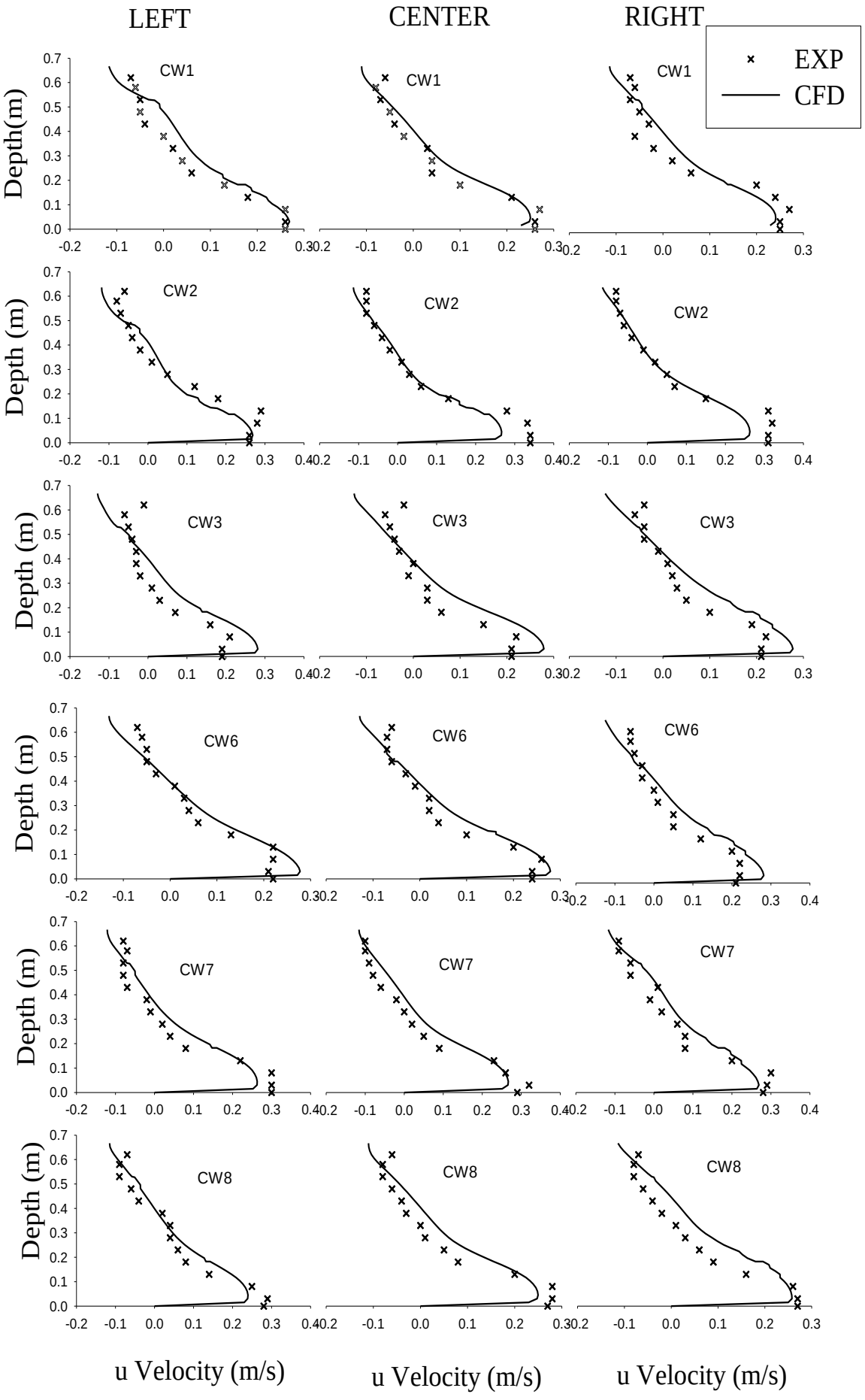

Figure 5.31 Velocity distribution in all bays at for CAWB combination.

5.4 CONCLUDING REMARKS

The developed CFD model has been verified by investigating its convergence properties and grid dependency tests. The swirl angles, decay of swirl, location and characteristics of different vortices were used to check the grid dependency of the CFD model results. Also the swirl angles and velocity distribution in different bays computed from CFD model runs were compared with experimental values for the validation of the CFD model results. It can be concluded from the above discussions that the CFD model can be used as an alternate tool for simulation of flow in the pump sump. From the results of swirl at different discharges, it is concluded that the swirl increases as the discharge increases. Therefore, to ensure the swirl free intake it is necessary to test the model for at least maximum discharge conditions.

CHAPTER 6 CHARACTERISTICS OF SWIRLING FLOW

6.1 INTRODUCTION

This chapter deals with the results obtained from the experimental and CFD model runs carried out to investigate the characteristics of swirling flow in the multiple pump sump intake under different approach flow conditions. The effect of Froude number (Fr) on the swirl has also been investigated using experimental as well as CFD model runs. In addition the decay of swirl obtained from CFD model runs, with the distance from the bell entrance has been analysed and discussed herein. A relationship between decay of swirl and Froude number (Fr) has been proposed. The experimental results are discussed first followed by CFD model results.

6.2 EXPERIMENTAL RESULTS

To investigate the swirl in different approach flow conditions, the swirl angle has been computed by vortimeter readings for two minute duration. Also, the free surface and subsurface vortices have been visualised during experimental runs. The velocity distribution in pump bays has been measured using acoustic Doppler velocimeter (ADV) to investigate the spatial and temporal variation of velocity in bays and intake channel.

6.2.1 Swirl in different bell mouth operations

To investigate the swirl in different bell mouth operating conditions, swirl in seventeen runs were computed using Eq.(3.6) and are given in Table 6.1 and also shown graphically in Figure 6.1. The low water level $S = 666$ mm and discharge $Q = 13.69$L/s through each operating suction line ($\mathrm{Re} = 1,47,965$; $\mathrm{Fr} = 0.84$) was maintained. The computed swirl angles were computed from the measured revolutions per minute of the vortimeter and average axial velocity in the suction pipes. The vortimeter readings were obtained by counting the revolutions of vortimeter blade for two-minute duration. In most of the tests, high swirl angles, i.e., >5 degrees were observed. Out of the 17 conducted tests, the following runs had high (>5°) swirl angles and these combinations were treated as stringent cases:

- A 6 pumps operations (#1#2#3#6#7#8)
- B 6 pumps operations (#1#2#5#6#7#8)
- C 6 pumps operations (#3#4#5#6#7#8)
- D 6 pumps operations (#1#3#4#5#6#8)

Table 6.1 Swirl for different bell mouth operations for Q_s = 13.69L/s

Run no	Run name	Swirl angles								operational bellmouth number
		#1	#2	#3	#4	#5	#6	#7	#8	
1	A	7.5	3.5	4	-	-	4.2	3	7.2	1+2+3+6+7+8
2	B	6	7.5	-	-	4	3.2	3.5	7.5	1+2+5+6+7+8
3	C	-	-	6.6	4	3	2.9	2.5	5.5	3+4+5+6+7+8
4	D	7	-	4.8	3.5	2.9	3	-	7.5	1+3+4+5+6+8
5	E	-	-	-	2.5	0.7	2.6	1.5	1.6	4+5+6+7+8
6	F	2.8	-	-	2	0	1.5	1.3	-	1+4+5+6+7
7	G	2.8	5.6	-	-	-	5.5	6.6	3.4	1+2+6+7+8
8	H	5.8	-	-	2.6	0.8	0.6	-	2.5	1+4+5+6+8
9	I	-	-	-	-	1.3	1.5	1.3	0.2	5+6+7+8
10	J	3.6	4.5	-	-	-	-	6.3	4.5	1+2+7+8
11	K	4.5	-	-	-	-	2.8	4.5	2.3	1+6+7+8
12	L	-	-	-	-	-	1.7	5	3.6	6+7+8
13	M	1.5	-	-	0.4	-	-	-	2.7	1+4+8
14	N	1.5	-	-	-	-	-	4	0.8	1+7+8
15	O	-	-	-	-	-	-	2.2	0	7+8
16	P	-	-	-	1.5	-	-	-	0.3	4+8
17	R	-	-	-	-	-	-	-	2.1	8

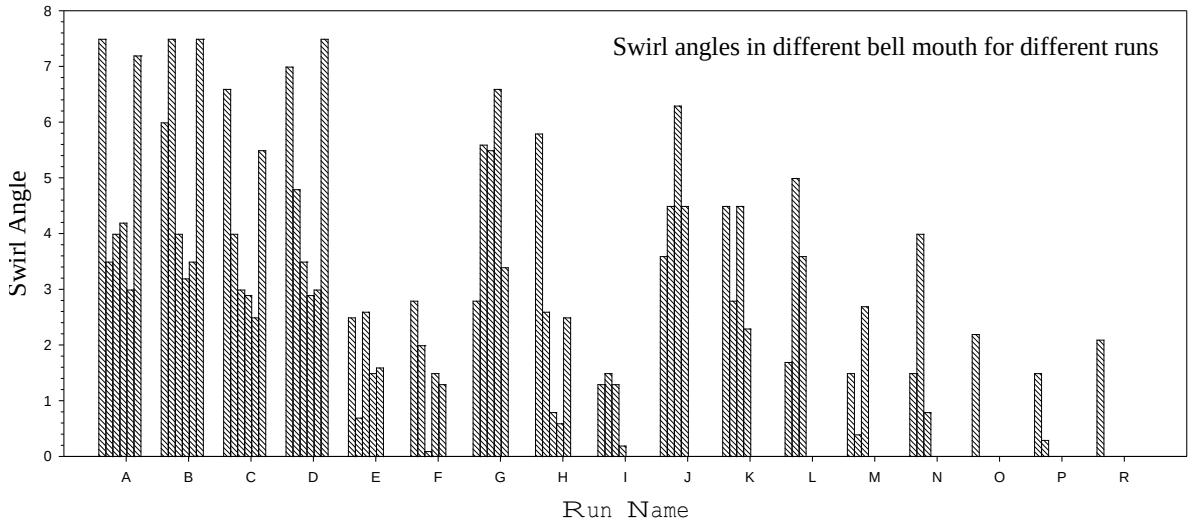

Figure 6.1 Swirl angle for different pump operation condition

6.2.2 Flow visualization

Flow in the model was visualized in the forebay to identify flow separation and dead zones. No separation of flow and dead zones were noticed in any of the test runs. Furthermore, no separation of flow was observed when the dye was injected on the bed of the forebay as shown in Figure 6.2. This confirms that a 20° diversion of side wall and 9° downward slopes are sufficient for negligible flow separation in the forebay. The flow approaching the bay was straight.

Figure 6.2 Dye injected at bed of the forebay

Subsurface vortices

Type-2 (dye core) subsurface vortices were noticed in most of the tests. For one of the stringent combination, i.e., A, the flow near the bell mouth number #1 was visualized by injecting the dye from the right and left sides as shown in Figure 6.3 (a) and (b), respectively. It was noticed that the flow has a spiral motion.

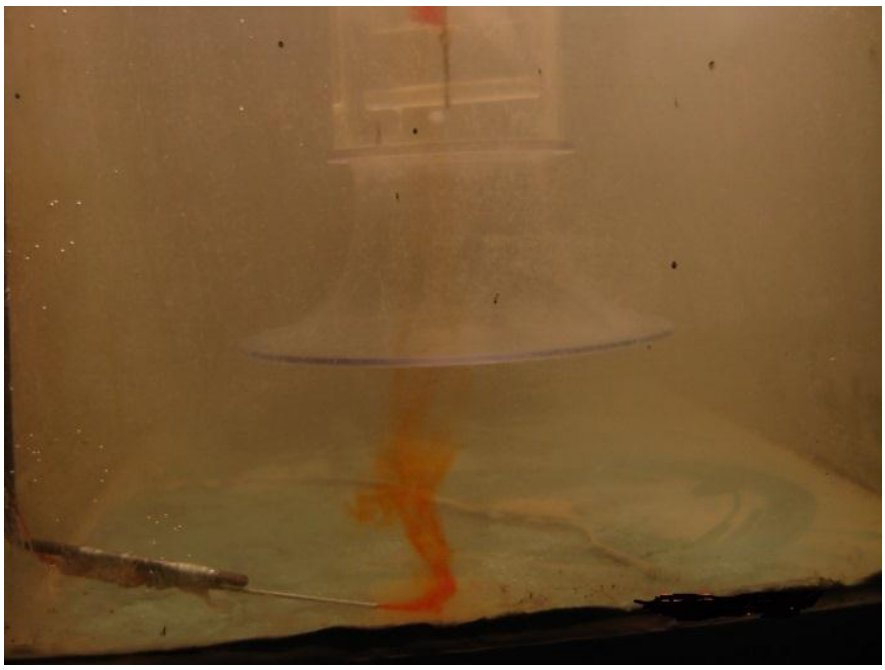

(a) Right hand side

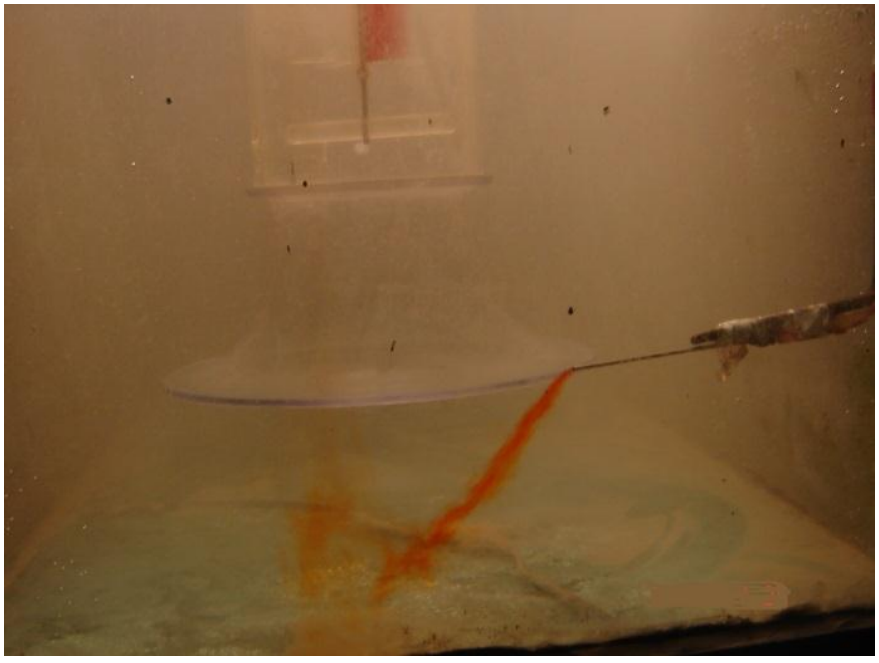

(b) Left hand side

Figure 6.3 Dye injected near the bell mouth of bay 1

Free surface vortices

Also no free surface vortices severe than Type 2 were observed in the model during run as shown in Figure 6.4.

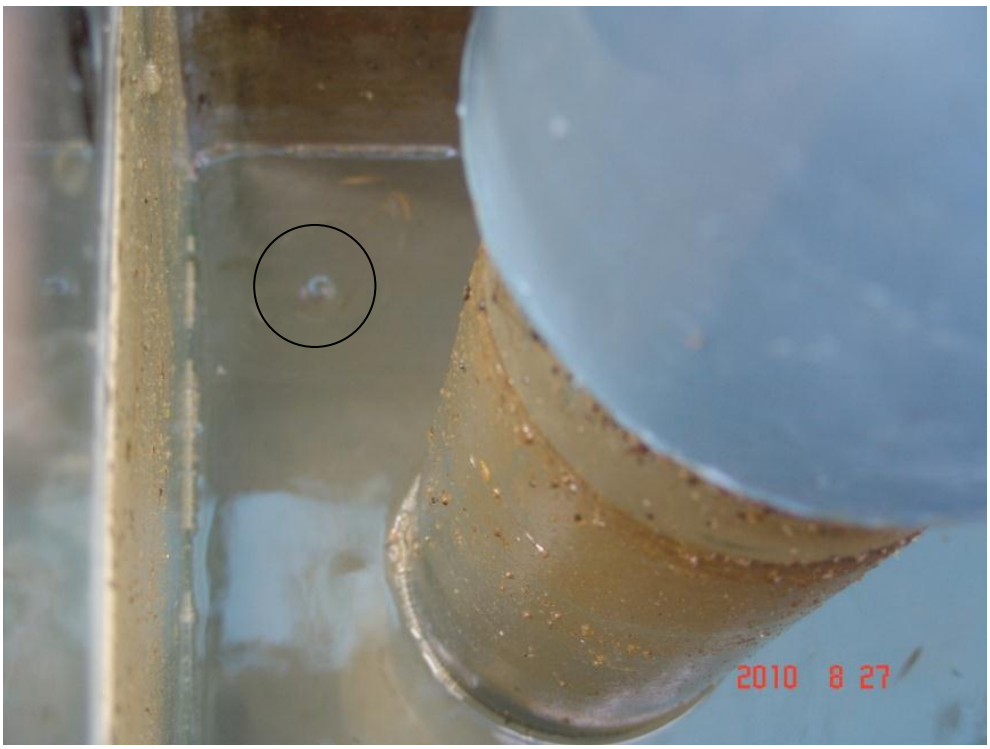

Figure 6.4 Type 2 surface vortex

6.2.3 Velocity distribution in the bays

Three-dimensional velocities were measured in the bays for operational bell mouth number #1, #2, #3, #6, #7 and #8 at maximum discharge and minimum/low water level. Velocity in the direction of flow x is *u*, upward vertical direction z is *w* and transverse direction y is v. Coordinates y and z follow right-handed coordinate system. These velocities were measured at three points at height 20 cm from the bed of the bay; 733.33 mm upstream of the centre line of the suction line; and y = 70 mm , 183 mm, 253 mm from the left pier (as per ANSI/HIS 1998). At each point, 3D velocities were measured for 20 s. The temporal variations of measured velocities in the bays are shown in Figures 6.5 and Figures 6.6. Due to low velocities of the order of 5 mm/s in the bays, the use of miniature type propeller current meter and conventional Pitot tube were not practically feasible. Thus, Nortek 10 MHz acoustic Doppler velocimeter (ADV) meter was used for this purpose. Measurement velocity distribution in bays of #1, #2, #3, #6, #7, and #8 were fairly uniform across the width of the bays. However, large fluctuations in the velocities from the time-averaged were observed in all the bays due to locations of points being downstream of the stop gates.

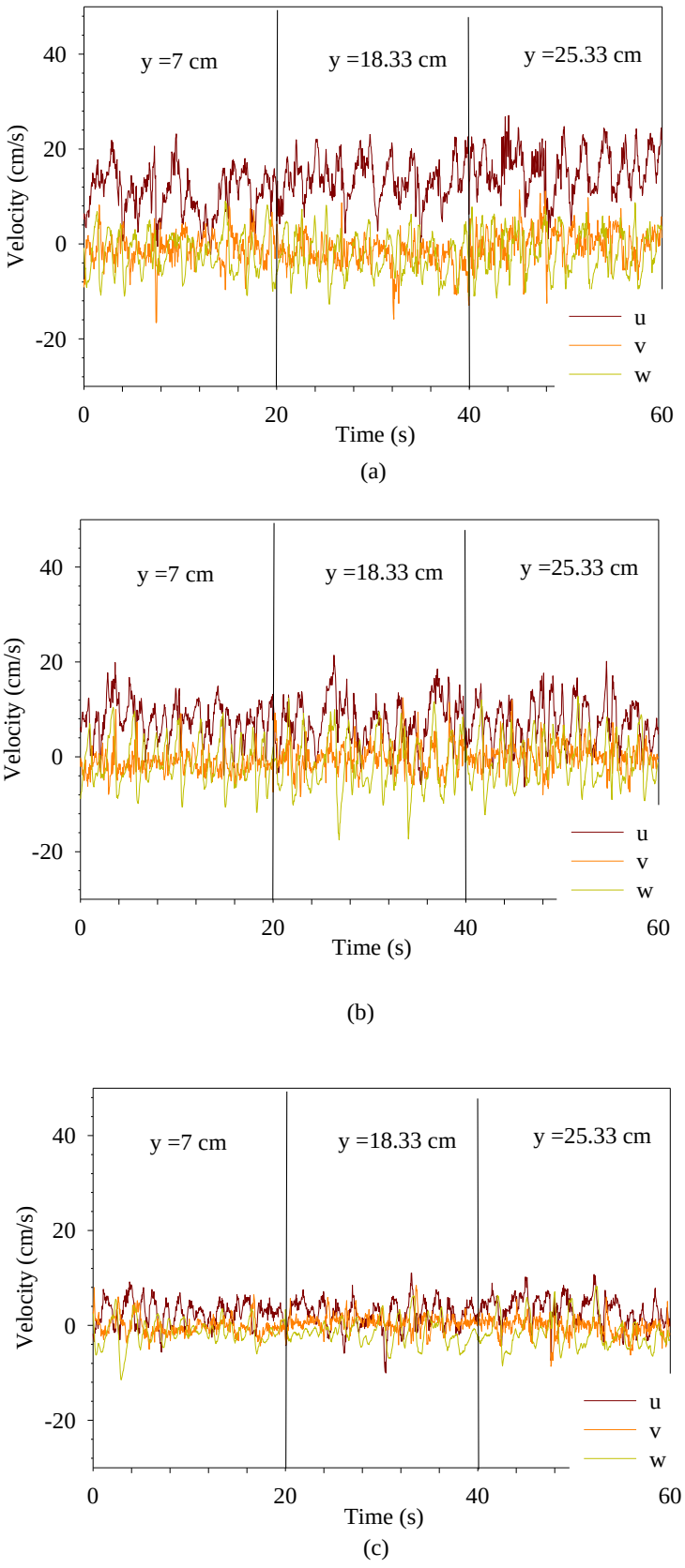

Figure 6.5 Temporal and spatial variation of velocity: (a) bay #1, (b) bay #2 and (c) bay #3

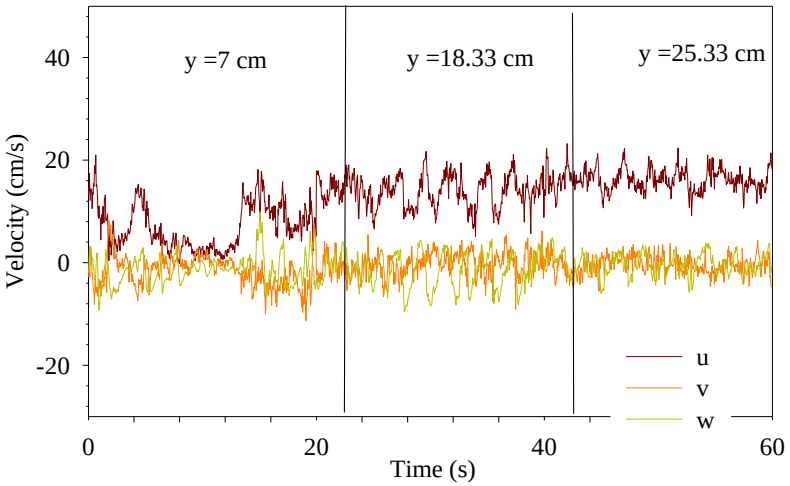

(a)

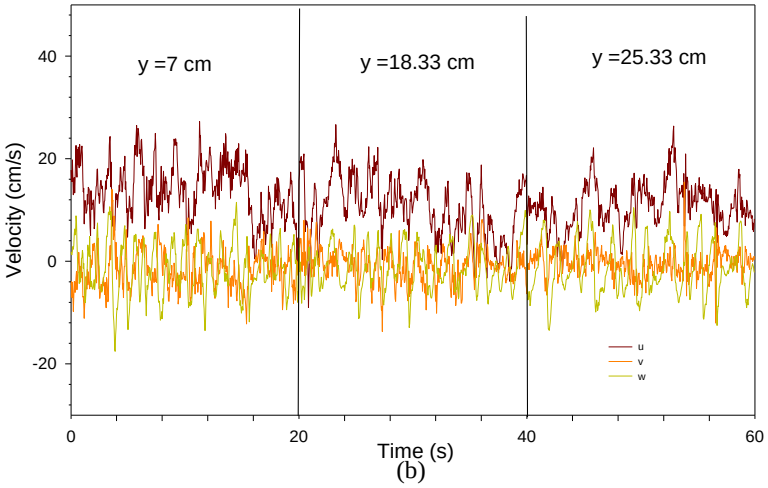

(b)

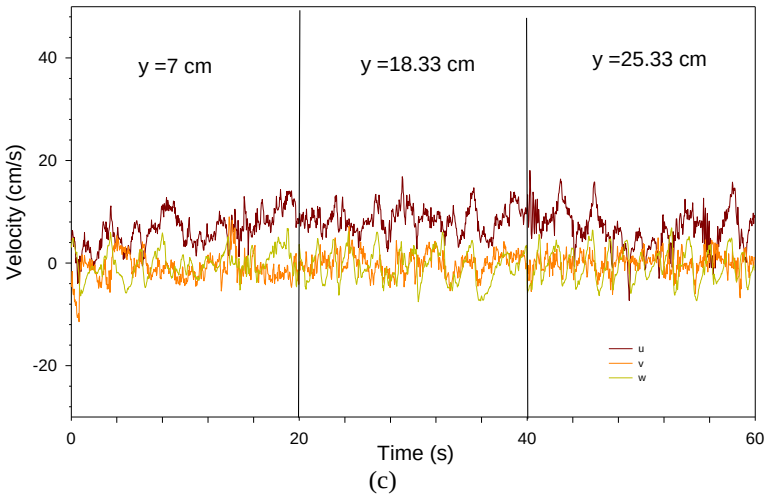

(c)

Figure 6.6 Temporal and spatial variation of velocity: (a) bay #6, (b) bay #7 and (c) bay #8

6.2.4 Velocity distribution in the intake channel

For one of the stringent conditions of pump operations, the velocity in the approach channel at the head of the forebay and at mid depth and y = 10 cm, 30 cm, 50 cm, 70 cm, 90 cm and 110 cm from the left wall of the approach channel was measured. The 3D velocities were measured using ADV for 20 s at a single point for maximum discharge and at minimum water level. Temporal variation of 3D velocities in the intake channel is shown in Figure 6.7, which indicates that the longitudinal velocity is of the order of 0.15 m/s, however, other velocities are negligible. The fluctuations in velocity from their time-averaged value are also low. The longitudinal velocity distribution across the intake channel is uniform.

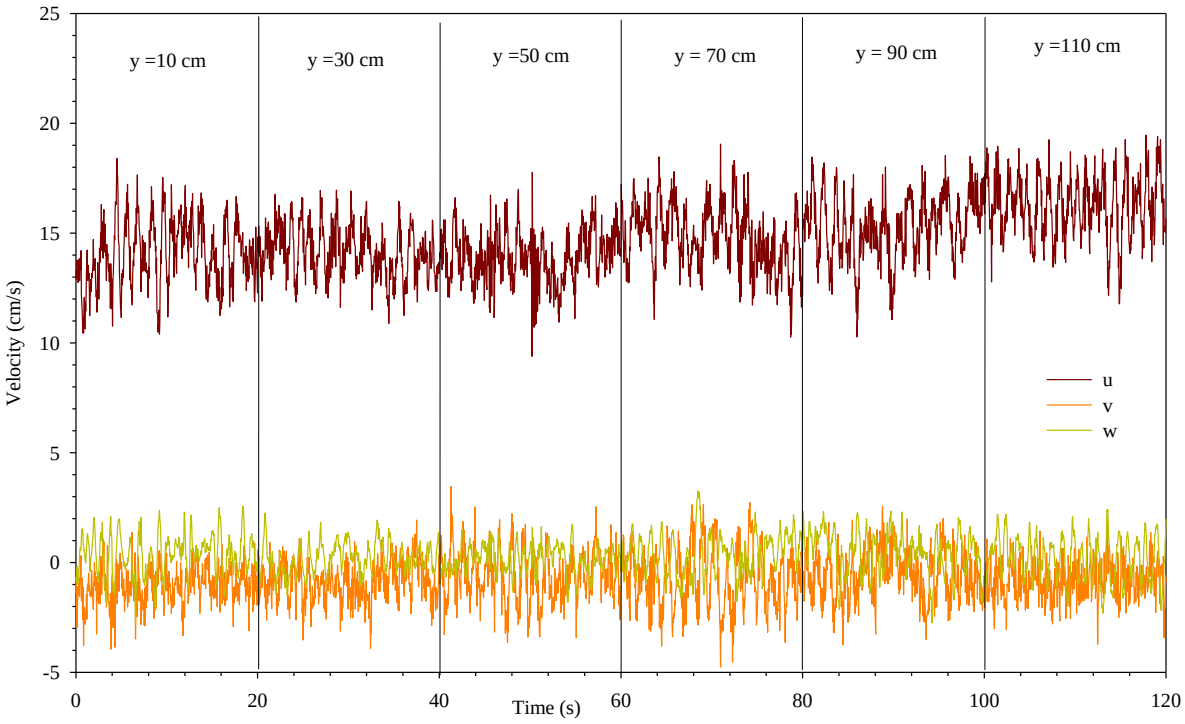

Figure 6.7 Temporal variation of velocity in intake channel at different lateral distances

Figure 6.8 show the flow in forebay under dye injection. Figure 6.8 (a) shows the flow pattern in forebay near left side of the approach channel while Figure 6.8 (b) shows the flow pattern near right side wall of the approach channel.

(a)

(b)

Figure 6.8 Visualization of flow in a) forebay b) in forebay towards right wall

Figure 6.9 shows the velocity distribution in the forebay area visualized with the help of thread. The approach flow profile also show the symmetric flow conditions in the approach flow.

Figure 6.9 Shape of a thread placed on water surface

6.3 EFFECT OF FROUDE NUMBER

Effect of Froude number, Fr, on swirl has been investigated using both physical and CFD modelling. To study the effect of Froude number experimentally the two operational bell mouths (#1 and #2) at minimum water level conditions were to attain maximum Froude number condition. Fourteen experimental runs were carried out at different discharges as listed in Table 6.2 and the vortimeter readings were observed for two minutes duration to compute the swirl angles. A sufficient time interval has been made between two successive runs to ensure the steady state condition during successive test runs.

Table 6.2 Swirl at different Froudian Conditions in one pump bay i.e. #1

s.no.	Fr	Re	Q (L/s)	swirl angle (degree)
1	0.67	100104.04	11	4.45
2	0.93	140007.12	15	4.50
3	1.13	170364.18	18	5.84
4	1.3	195816.21	21	6.15
5	1.45	218148.92	23	6.30
6	1.58	238274.08	25	6.37
7	1.71	256731.43	27	6.45
8	1.82	273871.69	29	6.59
9	1.93	289937.89	31	7.39
10	2.03	305106.59	32	7.37
11	2.12	319510.88	34	7.61
12	2.21	333253.96	35	7.61
13	2.3	346417.78	37	7.62
14	2.39	359068.71	38	7.42

To study the effect of Froude number on swirl, CFD simulations for different Froude numbers (Fr = 0.5 to 3.0) were carried out. Simulations to study the effect of Froude number on the swirl and decay of swirl along the distance from the bell inlet, for six different flow conditions (Fr = 0.5, 1.0, 1.5, 2.0, 2.5, and 3.0) as given in Table 6.3 were carried out for base pump combination A and $S = 666$ mm. In each case, average inlet velocity (u_{in}) with turbulence specifications (i.e. k and ε) was prescribed at the inlet situated at 22.5D upstream of the forebay area to get the fully developed flow at forebay and the pump bays. Also the length of modelled suction columns was approximately 12D in all bays to get the flow unaffected from the downstream outlet boundary conditions. The free surface was specified as symmetry boundary conditions and the outlets were treated as outflow condition in each case. The two equation k-ε turbulence model and scalable wall functions were used to model the

turbulence and near wall flow respectively in the solver i.e. Fluent in each simulation. The FDWB fluid domain and M3 hexahedral mesh (57.9 Million nodes) of good quality (Minimum Orthogonal Quality>0.3; Aspect Ratio 1-20) were used as described in Chapter 4, in all simulations.

Table 6.3 Simulations to study Froude number effect on swirl

S.No.	Run Name	Q (L/s)	Fr	Re	u_{in} (m/sec)	Swirl angle (degree)
1.	F05	8.08	0.5	96022.21	0.09189	6.37
2.	F10	16.17	1.0	192044.43	0.18378	7.45
3.	F15	24.25	1.5	288066.64	0.27567	7.77
4.	F20	32.34	2.0	384088.86	0.36757	8.05
5.	F25	40.42	2.5	480111.07	0.45946	8.3
6.	F30	48.51	3.0	576133.29	0.55135	8.56

From Figure 6.10, it is clear that swirl increases up to certain level of increase in Froude number thereafter the swirl becomes constant may be due to higher turbulence near the vortimeters. This can be due to unsteady nature of the flow as the RANS computes average swirl. The subsurface vortices increase with discharge because of high-velocity shear near the bottom floor and the side walls near the bell mouth, which results in a higher swirl angle. However, the rate of increase of the swirl angle at discharges more than the Froudian discharge is not significant. The minor increase in the swirl angle at higher discharges, i.e. at higher Froude number and velocity, is mainly attributed to high turbulence rather than the presence of swirl in the flow. Thus, the results in Figure 6.10 show that the study of the pump sump model should be conducted at Froudian similarity and not at higher Froude numbers. This finding resolved the issue of not conducting the pump-sump study model at higher Froude numbers.

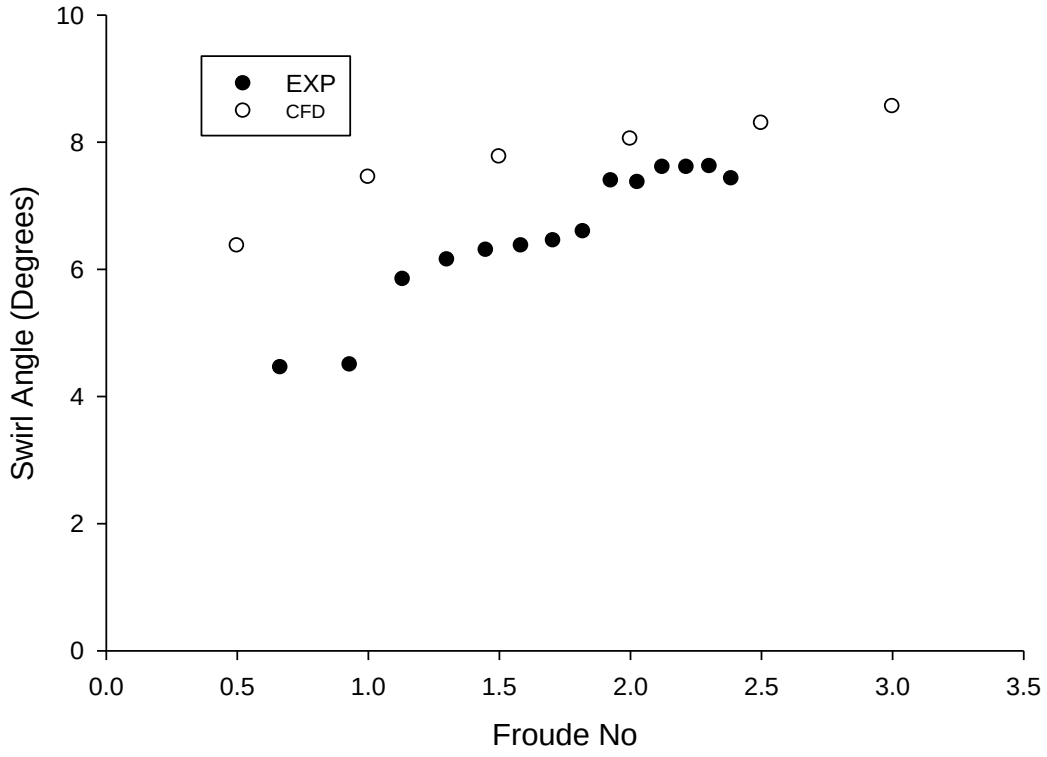

Figure 6.10 Swirl variation with different Froude Number in #1

6.4 DECAY OF SWIRL

To improve the performance of the pumps, it is desirable to achieve low swirl flow conditions inside the pump column at impeller level/pump level. The level of swirl inside the pump column is dependent on the overall strength of the circulatory motions inside the pump bay, the intensity of the various subsurface vortices and the separation eddies shed around the pump bell. In the case studied in the present work, the most important factor is the intensity of the floor attached vortex that enters inside the pump column. Knauss (1987) reported swirl angle produced by the vortex flow decay with distance along the suction pipe due to shear at the pipe wall. Therefore, the swirl angle is computed at different distances from the bell entrance for different Froudian conditions. The swirl angle variations along the suction pipes were analysed and found that the swirl angle decays exponentially along the distance from bell entrance. It is also reported in the literature Baker and Sayre (1974) that swirl decays exponentially along the distance.

As shown in Figure 6.11, (θ/θ_{max}) was calculated for different values of *z/d* and is found to decay by 60% between the pump bell and a level located at 1.7*D* from it, mainly due to turbulent dissipation effect. Then, the decay is much milder and appears to have a constant value. The CFD model can be used to estimate what would be the minimum length of the

pump column upstream of the pumps needed such that the level of swirl at the pump will not be detrimental to its efficiency.

From the analysis of swirl decay along suction line, the following relationship between the decay of swirl, distance from bell entrance and Froude number has been proposed.

$$\left(\theta / \theta_{max}\right) = 1 - 0.366\left(z / D\right)^{0.216} \mathrm{Fr}^{-0.058} \qquad (6.1)$$

where θ = swirl angle at z; θ_{max} = swirl angle at suction pipe entrance; Fr = Froude number; *z/D* = non dimensionalized distance from the inlet suction pipe.

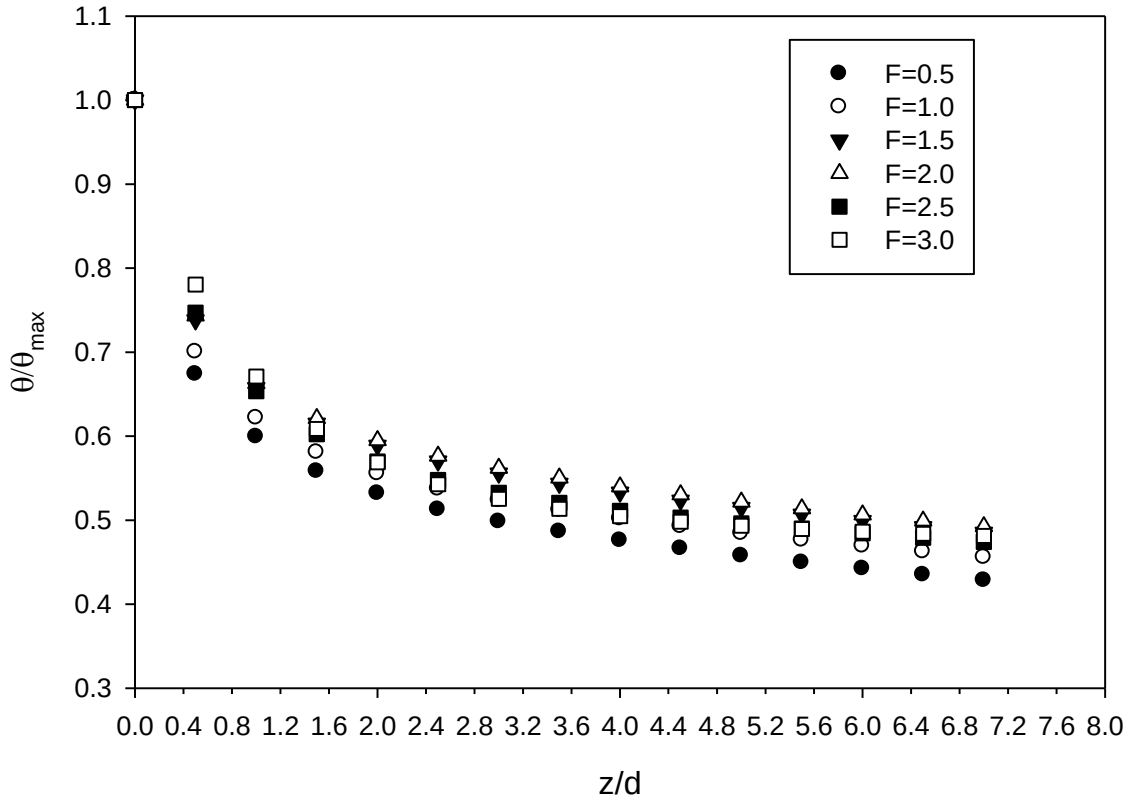

Figure 6.11 Decay of swirl along the distance in suction pipe for different Froudian conditions

The computed swirl angle using Eq. (6.1) along the length of suction pipe for one flow condition (for Fr = 0.5) and also computed using CFD is shown in Figure 6.12, which indicates that computed swirl angle using Eq. (6.1) matches well with the computed swirl by CFD model.

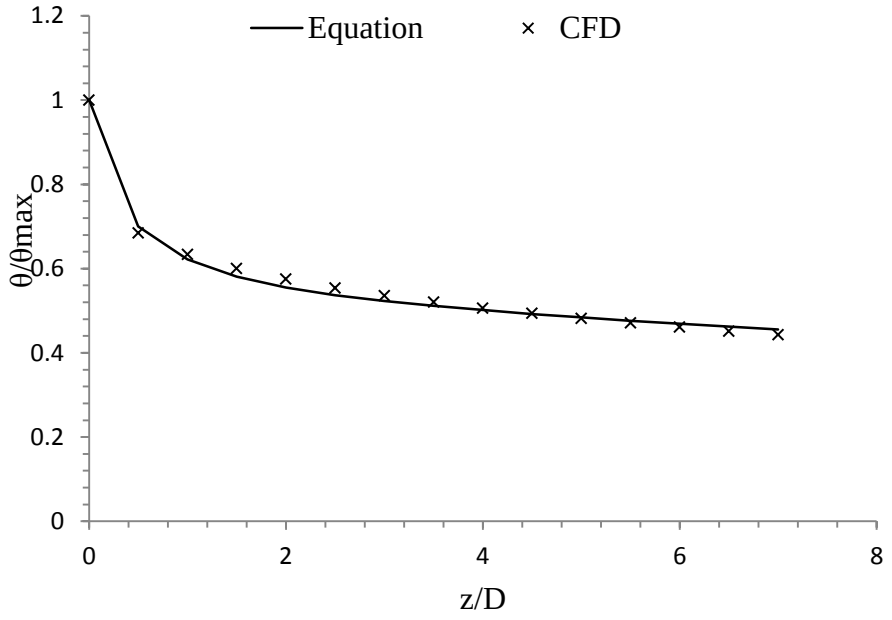

Figure 6.12 Comparison of swirl computed from proposed equation and CFD model

6.5 CONCLUDING REMARKS

From the swirl in different pump combinations, it is clear that the swirl increases as the number of pumps in operation increases. Therefore, it can be concluded that the testing of model shall be done for maximum number of pump combinations preferably. Also it is observed that the pumps near the corner of the sump show higher swirl.

From the Froude number effect on swirl, it can be concluded that the model tests shall be carried out at 2F conditions only, beyond this is not necessary to ensure the swirl free intakes designs.

Swirl in the model for maximum discharge and minimum water levels were beyond the acceptance limit so it is necessary to provide some modifications to the design. Thus, some additional arrangements are needed to arrest the swirl angle for all the tests that is described in Chapter 7.

CHAPTER 7 OPTIMIZATION OF SHAPE AND SIZE OF ANTI-VORTEX DEVICE

7.1 INTRODUCTION

In this chapter, analysis of collected data is discussed, to investigate the performance of different anti-vortex devices (AVDs) for suppressing the submerged vortices, which occurs around the pump intakes and causes excessive swirl at pump impeller level. It is well known from the previous studies e.g., (Kim et al. 2015; Kang et al. 2014; Zhao et al. 2013; Kim et al. 2012; Tang et al. 2011; Ahmad et al. 2011; Shabayek 2010; Choi et al. 2010; Arboleda and El-Fadel 1996; Knauss 1987; Sweeney et al. 1982; Nathan 1981; Odgaard and Dlubac 1983) that the swirl flows in pump approach flow can be controlled by means of anti-vortex devices (AVD) such as splitters, vertical walls, floor cones etc.

However, there is lack of definite criteria to design such devices in existing literature (American National Standards Institute (ANSI) 1998; Bureau of Indian Standards (BIS) 2003; Knauss 1987; Prosser 1977). Therefore, in present study a detailed investigation using laboratory and CFD modelling has been carried out for optimizing the shape and size of AVDs to contribute in the available knowledge of designing such devices.

In present work, AVDs of three different shapes (namely A, B and C) and three sizes comprising nine different AVDs were considered as shown in Figure 7.1. In this figure AVDs (A1, A2, A3, B1, B2, B3, C1, C2 and C3) were shown and among these three AVDs (C1, C2 and C3) were evaluated using both physical as well as CFD modelling, rest were evaluated using CFD modelling only.

The evaluation of the AVDs was made primarily by the measurement of swirl angles indicating strength of vortices and pre-swirls. Also the dye study has been carried out to visualize the presence of sub surface vortices near the intakes. Out plane vorticity, velocity vectors, contours and streamline patterns were used for the analysis of the CFD model results. Also the decay of swirl in suction columns was analysed and used to evaluate the performance of the AVDs. From the analysis, guidelines were suggested to design such devices. Results of experimental investigations were discussed first followed by the CFD.

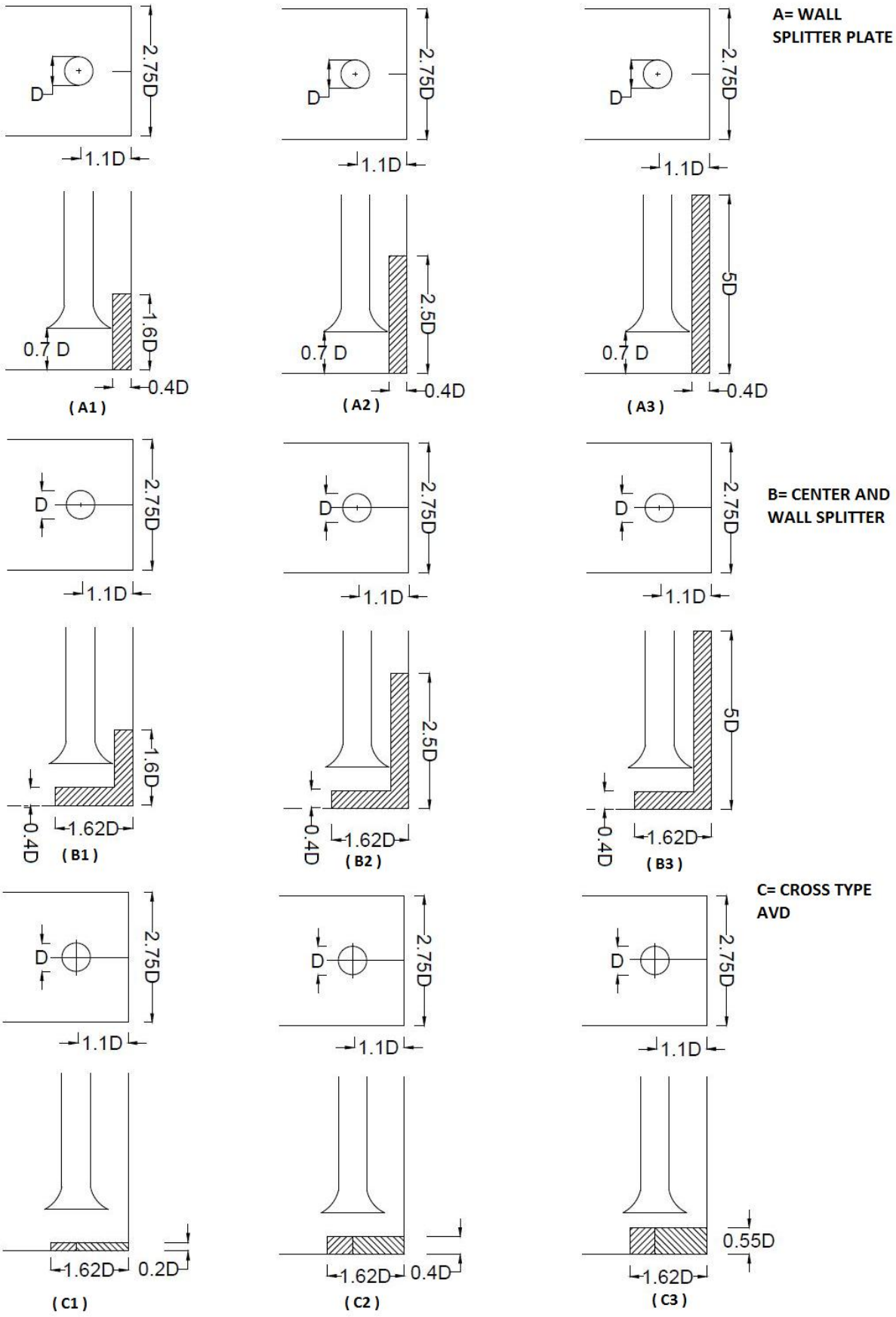

Figure 7.1 Various dimensions of AVDs and their positions in the bays

7.2 PHYSICAL MODEL TESTS

The main geometrical parameters for the pump sump model were backwall distance, $B = 78$ mm; submergence, $S = 666$ mm; floor clearance, $C = 92$ mm; bay width, $W = 366$ mm; bay length, $L_b = 1333$ mm; bell diameter, $D_b = 179$ mm. These values are in the recommended range of American National Standards Institute (ANSI) (1998) and other design standards (Bureau of Indian Standards (BIS) 2003; Prosser 1977). Flow in the pump sump model for base pump sump model and with AVDs (namely C1, C2, and C3 type) is shown in Figure 7.2. Total sixteen experimental runs were carried out.

Experimental runs were carried out at $Q = 13.69$L/s; Froude number, $\mathrm{Fr} = 0.84$; Reynolds number, $\mathrm{Re} = 1,47,765$ Weber number We = 1750 in the pump sump model for different bell mouth operation conditions as given in Table 7.1. The Reynolds number and the Weber number are such that the viscous and surface tension affects are negligible to extrapolate the model results to the prototype. The run names are such that first indices represents the operational bell mouth combination (i.e., A, B, C and D) and last two indices represent the AVD name (i.e., C1, C2 and C3).

Figure 7.2 Photographic view of the C type devices (C1, C2 and C3)

Six bell mouth operational conditions were used to study the effect of cross type AVDs of three different sizes i.e., h = 0.20D, 0.40D and 0.55D. The AVDs were made from 6mm thick acrylic sheets and pasted at centre, below the bell mouth on the floor in all eight bays of the model. Four runs were performed without AVDs (run number 1 to 4) and twelve runs (run number 5 to 16) with AVDs.

Table 7.1 Swirl angles (in degrees) for without AVD and with AVD (C type) conditions

Run no.	Run name	Swirl angles						Col. [1]	Col. [2]	Col. [3]	Col. [4]	Col. [5]	Col. [6]
		Operational bell mouth number											
		#1	#2	#3	#6	#7	#8						
1	A	7.5	3.5	4	4.2	3	7.2	7.5	3.0	4.5	0	0	0
2	AC1	8.8	3.2	1.6	1.2	5.6	9.2	9.2	1.2	8.0	-1.7	1.8	0.1
3	AC2	2.8	0.8	1	2	2.8	2.8	2.8	0.8	2.0	4.7	2.2	6.9
4	AC3	2.8	0.6	1.8	2.8	0.6	1.8	2.8	0.6	2.2	4.7	2.4	7.1
		#1	#2	#5	#6	#7	#8						
5	B	6	7.5	4	3.2	3.5	7.5	7.5	3.2	4.3	0	0	0
6	BC1	1.2	1	1.2	3.2	9.0	1.0	9.0	1.0	8.0	-1.5	2.2	0.7
7	BC2	2.4	1.4	1.6	2.8	3.2	2.6	3.2	1.4	1.8	4.3	1.8	6.1
8	BC3	3.2	1.2	3	5.8	0.4	4.2	5.8	0.4	5.4	1.7	2.8	4.5
		#3	#4	#5	#6	#7	#8						
9	C	6.6	4	3	2.9	2.5	5.5	6.6	2.5	4.1	0	0	0
10	CC1	0.4	3.0	1.2	1.0	3.0	1.0	3.0	0.4	2.6	3.6	2.1	5.7
11	CC2	2.4	0.8	0.6	2	2.6	2.6	2.6	0.6	2	4	1.9	5.9
12	CC3	1.8	0.4	3.0	6.0	0.2	4.4	6.0	0.2	5.8	0.6	2.3	2.9
		#1	#3	#4	#5	#6	#8						
13	D	7	4.8	3.5	2.9	3.0	7.5	7.5	2.9	4.6	0	0	0
14	DC1	2.4	3.0	1.2	1.0	3.0	1.0	3.0	1.0	2.0	4.5	1.9	6.4
15	DC2	3.0	0.8	0.8	1.4	2.8	1.8	3.0	0.8	2.2	4.5	2.1	6.6
16	DC3	0.4	2.4	1.6	2.4	7.0	5.4	7.0	0.4	6.6	0.5	2.5	3.0

The stabilised flow at the channel inlet was provided by the use of flow straighteners, wave suppressors and the perforated walls in the upstream of the channel. For each case, the six vortimeter readings in stable flow conditions for two minute duration were recorded to compute the swirl in the suction columns. Figures 7.3 and 7.4 show vortimeter and the AVD fitted in the one pump bay respectively. In addition to the swirl, flow in the model was

observed for the presence of vortices and as and when required dye study was carried out to confirm the presence of vortices.

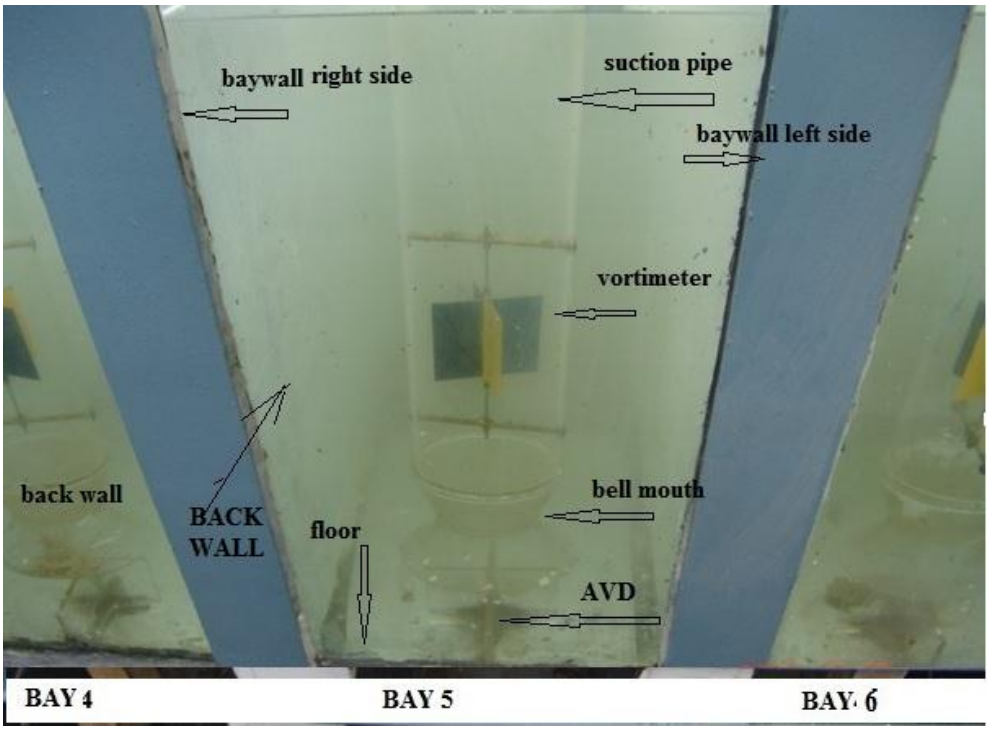

Figure 7.3 View of bell mouth, vortimeter and transparent suction pipe

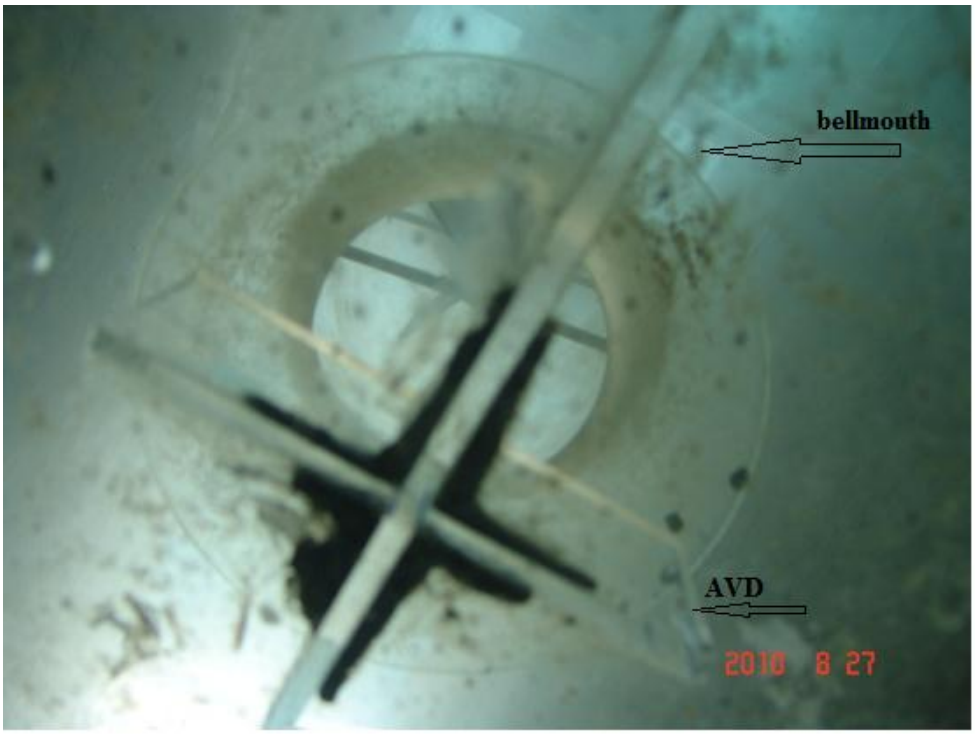

Figure 7.4 Up-looking view of the bell mouth and C type AVD in a bay

7.2.1 Experimental results

Swirl for the runs were observed and the computed swirl angle results are tabulated in Table 7.1 and analysed critically. The aim of the analysis was to find the most suitable AVD size for the present conditions. Therefore, it is clear that the swirl angle should be minimum for each run and bay. However, it is very difficult to decide from the swirl angles that which AVD is most suitable, because sometimes the AVD adequate for one run or bay may not be sufficient for the other. This necessitates the formulation of a criterion to select the most optimum AVD. To do this a suitability index (S.I.) for each AVD has been calculated by the following criterion. The analysis is listed in Table 7.1.

a) AVD should control the swirl under a limit ($<3^{\circ}$) as per the American national standards institute (ANSI) (1998) standard acceptance criteria in all the pump bays. To ensure this a maximum swirl (only magnitude of the swirl angles used) observed were sorted and checked for the condition i.e., swirl angle $<3^{o}$ (column 1 of Table 7.1 lists the maximum swirl in each run). If the condition is satisfied, the corresponding AVD for that run will be assigned suitability index (SI) 4 (= no of possible conditions). SI will be zero if any violation of this condition occurs.
b) The variation in maximum and minimum swirls for a given bell mouth operation should be less for an optimum AVD. To ensure this the difference between the maximum swirl (i.e. column 1 of Table 7.1) and minimum swirl (i.e. column 2 of Table 7.1) observed in that particular bell mouth operation has been computed in column 3 (i.e. column 3 of Table 7.1 = column 1 of Table 7.1 - column 2 of Table 7.1) for each run and indexed from 1 to 4 depending upon the difference, largest difference is given index 1 and the smallest as 4. If any ambiguity occurs the preference will be given to the smaller AVD.
c) The difference of maximum/minimum swirl from the reference condition i.e. without AVD condition (max/min. swirl without AVD – max/min swirl with AVD) should be optimum for both maximum and minimum swirl (+ ive and largest; + ive sign shows reduction in swirl and largest ensures index for limit). To avoid the conflict the sum of the two values has been used to index the AVDs.

From the above mentioned criteria's, the analysis of the computed swirl angles in all runs has been carried out and the indices were tabulated in Table 7.2. In Table 7.2, the cumulative suitability index of the run/AVD was calculated by summation of all the indices for each case, i.e.

Cumulative SI= SI using criterion a + SI using criterion b + SI using criterion c

Finally, the suitability of each AVD has been computed by summing all cumulative SIs for each case, and is given in Table 7.2.

In Table 7.1 the columns 1 to 6 represents the following values:

- **Col. 1** Maximum swirl
- **Col. 2** Minimum swirl
- **Col. 3** Col.1- Col.2
- **Col. 4** Variation of max. swirl with respect to without AVD
- **Col. 5** Variation of min. swirl with respect to without AVD
- **Col. 6** Col. 4+ Col. 5

Table 7.2 Suitability indices according to adopted criteria

S. no.	**AVD**	**Suitability index of AVDs for different criteria (a), (b) and (c) for each run**												**Cumulative suitability indices of AVD for each run**				**Cumulative suitability of each AVD**
		case A			**case B**			**case C**			**case D**							
		a	**b**	**c**	**a**	**b**	**c**	**a**	**b**	**c**	**a**	**b**	**c**	**A**	**B**	**C**	**D**	**SI**
		[2]	[3]	[4]	[5]	[6]	[7]	[8]	[9]	[10]	[11]	[12]	[13]	[14]	[15]	[16]	[17]	[18]
1.	-	0	1	1	0	3	1	0	2	1	0	2	1	2	4	3	3	12
2.	C1	0	2	2	0	1	2	4	3	3	4	4	3	4	3	10	11	28
3.	C2	4	4	3	0	4	4	4	4	4	4	3	4	11	8	12	11	42
4.	C3	4	3	4	0	2	3	0	1	2	0	1	2	11	5	3	3	22

The swirl angles as given in Table 7.1 for different bell mouth operations with AVD and without AVD have been compared and were also shown in Figures 7.5 to 7.8 for lucid presentation of the phenomenon. From these figures, it is clear that the AVD C3 and C2 lead to less than 5^o swirl in all test runs. Furthermore, the AVD C3 and C2 provide almost similar reductions in swirl angles. In run A, the AVD C2 gives lower swirl angles than the AVD C3. It is noted that for corner bays, AVD C3 gives lower swirls and for interior bays sometimes C2 is better and for others C3 is better. Thus, the above quantitative analysis provides an approach to decide the optimum AVD.

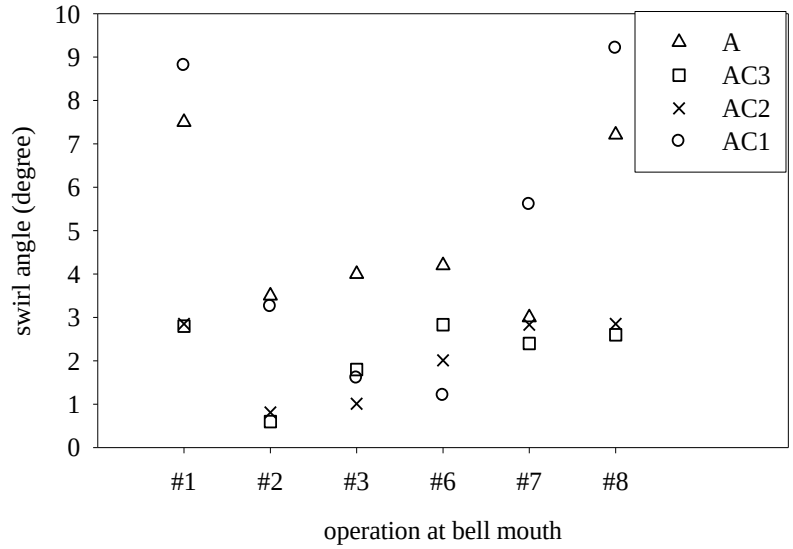

Figure 7.5 Swirl for combination A for different AVDs

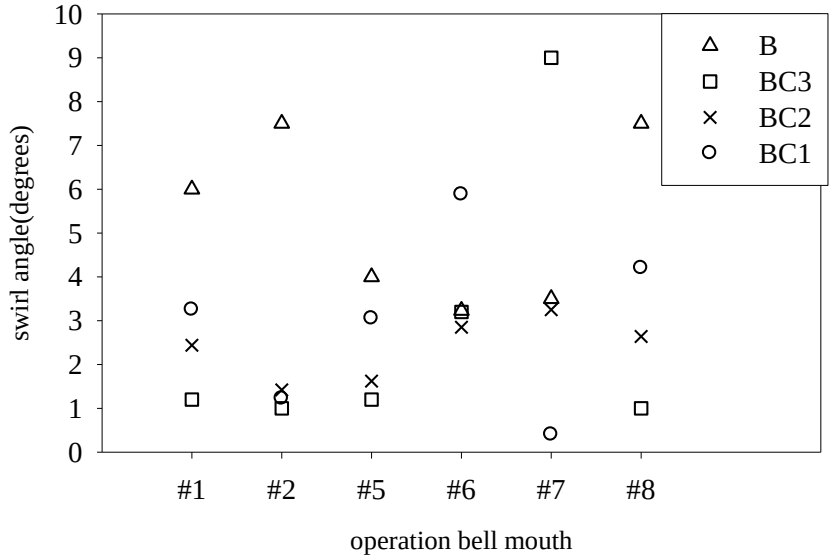

Figure 7.6 Swirl for combination B for different AVDs

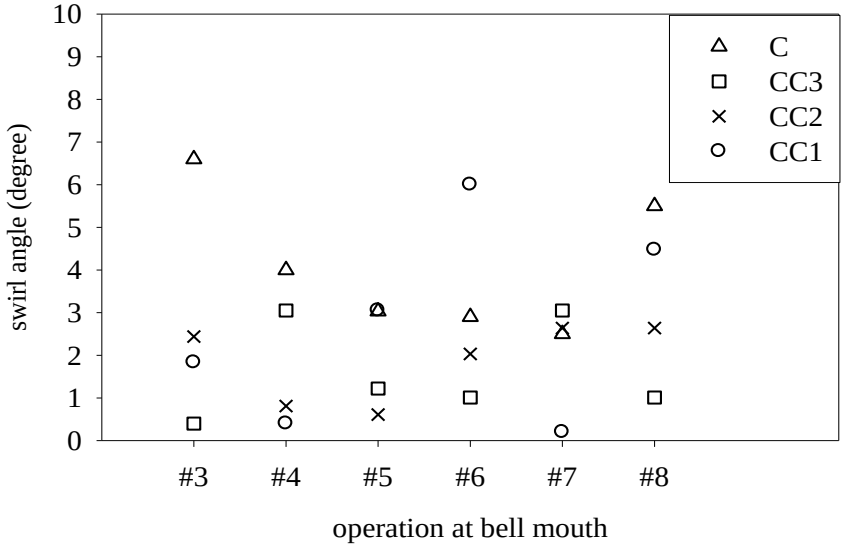

Figure 7.7 Swirl for combination C for different AVDs

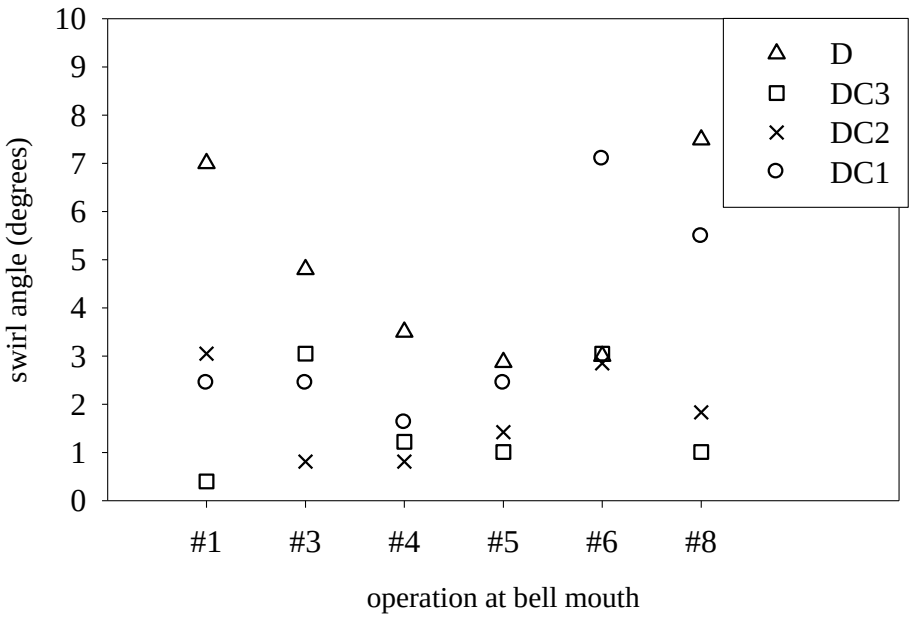

Figure 7.8 Swirl for combination D for different AVDs

7.2.2 Flow visualization

The flow in the model was primarily visualised by simple eye visualization for the presence of surface vortices and for subsurface vortices. The subsurface vortices were visualized by injecting an inert dye using hypodermic needle as shown in Figure 7.9. Swirling flow can be easily seen due to dispersion of dyes from both the sides. This indicates the presence of subsurface vortex attached to the floor. With AVDs, the dye visualization results of run AC2 are shown in Figure 7.10.

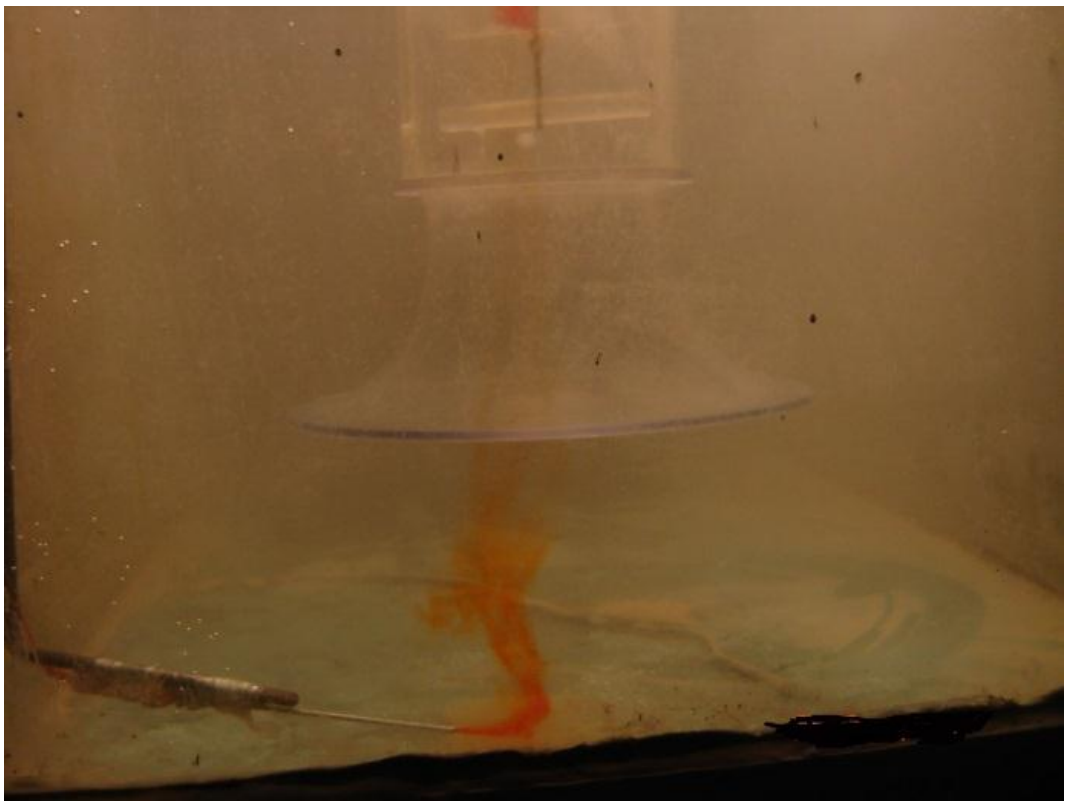

(a)

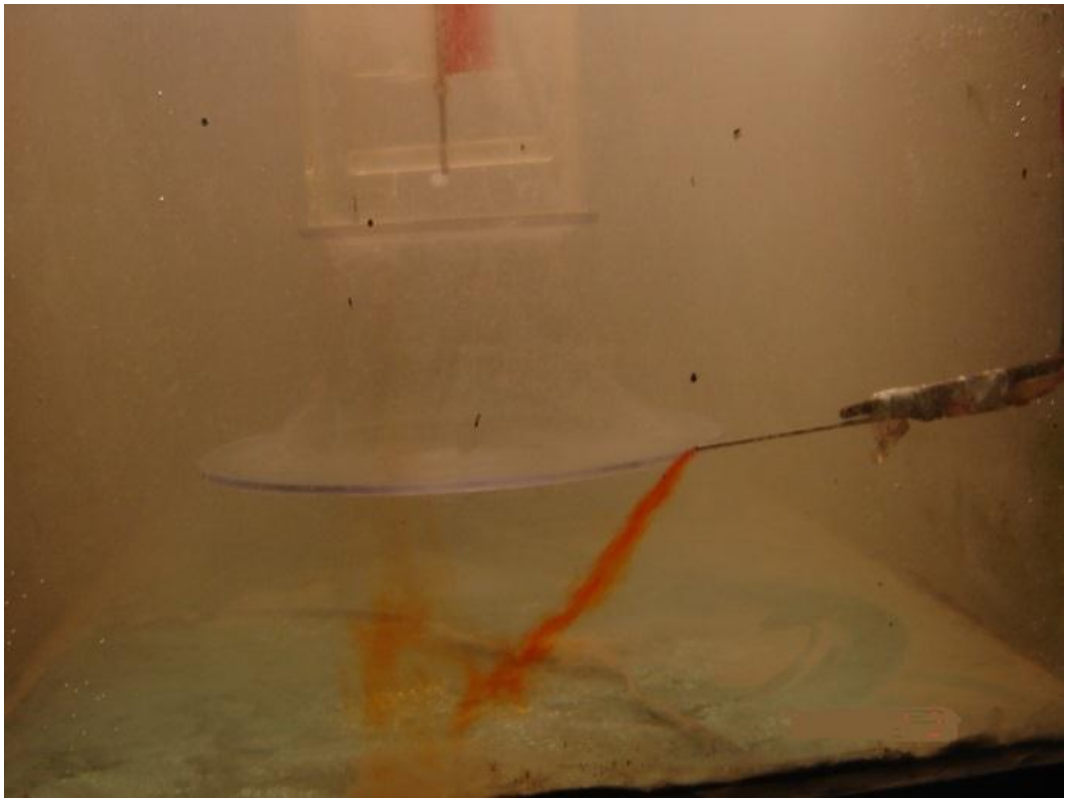

(b)

Figure 7.9 Dye injected near the bell mouth in bay #1 from (a) right side and (b) left sides

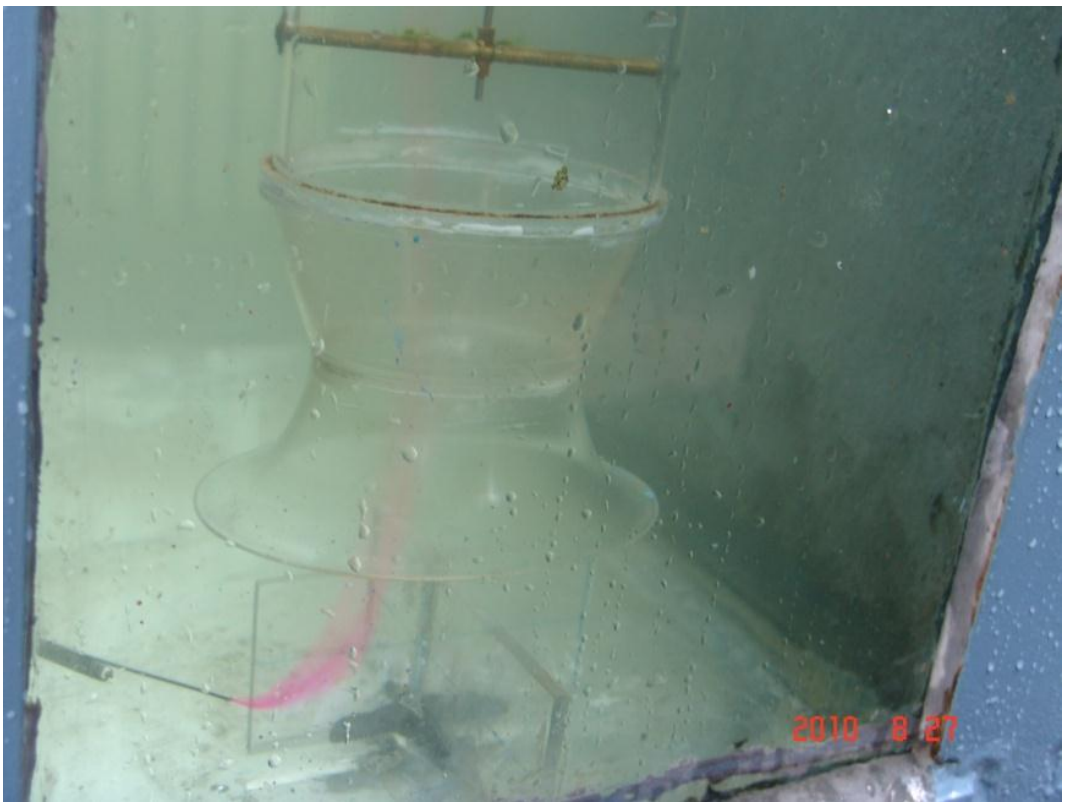

(a)

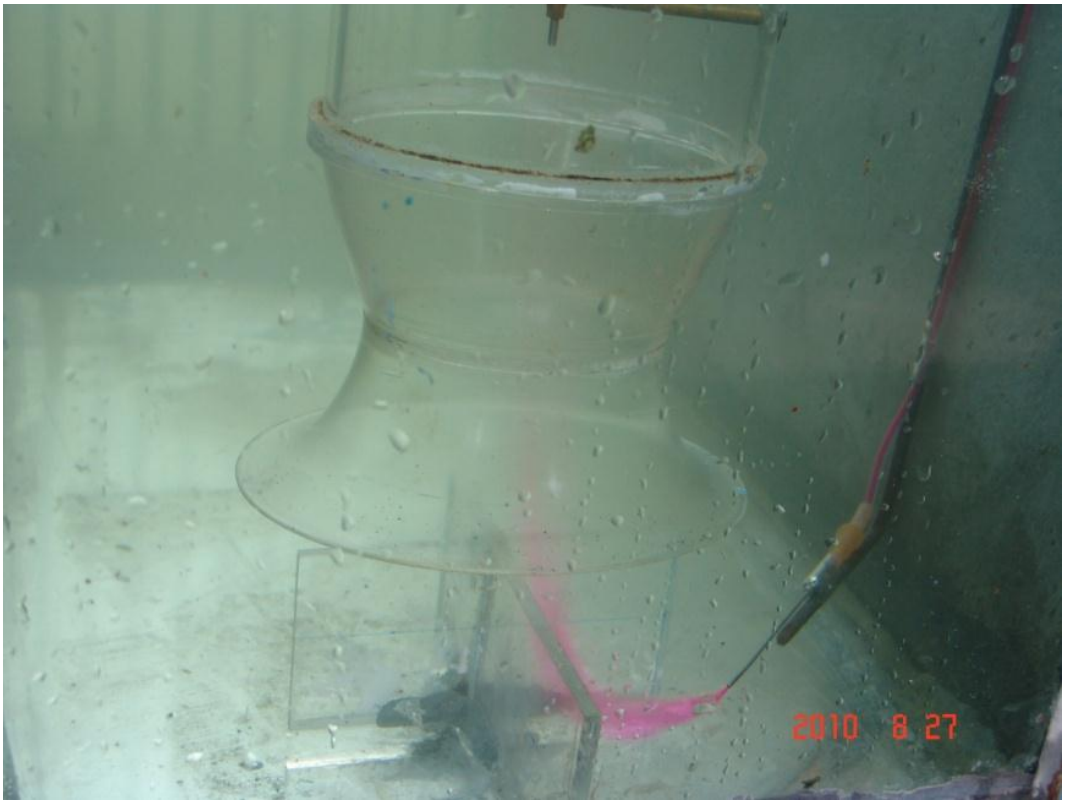

(b)

Figure 7.10 Dye injected near bell mouth in bay #1 from (a) right hand side (b) left side for run AC2

7.3 CFD MODEL RUNS

Experimental works are time taking and costly exercises. To save the time and cost involved in the design processes, CFD modelling is preferred. To standardize the shape and size of AVDs, forty CFD model simulation runs were carried out and the results are presented herein. The details of the CFD models are described in chapter 4. The details of the nine different AVDs of different shapes and sizes are shown in Figure 7.1.

The boundary conditions and the solver settings were same as used in the base pump sump CFD model. Table 7.3 lists total forty CFD simulation runs on Fluent solver for ten different CFD models and four different bell mouth operational conditions (namely A, B, C and D). A brief description of all the simulations was described first followed by the analysis of the simulated data.

Two different scenarios were considered first with base CFD model and second with the AVDs. Each simulation was carried out for ($\mathrm{Re} = 147965$; Fr = 0.84; S = 666 mm) for six bell mouth operational conditions. Constant velocity with turbulence specifications (i.e. k and ε) was prescribed at the inlet situated at 22.5D upstream of the forebay area to get the fully developed flow at forebay area (D = 134 mm). Also, the length of modelled suction columns was approximately 12D in all the pump bays to get the fully developed flow at impeller level and independent from the downstream outlet boundary conditions. The free-surface was specified as symmetry boundary conditions and the outlets were treated as outflow condition.

The run name, AVD type, fluid domain name, mesh name are listed in Table 7.3. The k-ε turbulence model and scalable wall functions were used to model the turbulence and near wall flow respectively in the solver i.e. Fluent. To ensure the pressure and velocity coupling in the segregated solver SIMPLEC algorithm was used. For each case, the swirl angle is computed and the flow patterns in different planes are analysed and presented herein.

Results computed from all CFD simulation runs listed in Table 7.3, are analysed and presented herein. First swirl angles are compared for different AVDs for four pump combinations (i.e., Combination A, B, C and D) after this qualitative analysis using streamlines and out-plane vorticity contour plots has been drawn. The qualitative results are presented here for Case A only.

Table 7.3 CFD simulation runs for $Q_s = 13.69 L/s$

S. No	Run name	AVD	Fluid domain	Mesh name	Bell mouth operation
1	A		FDWB	M3	#1, #2, #3, #6, #7, #8
2	B				#1, #2, #5, #6, #7, #8
3	C				#3, #4, #5, #6, #7, #8
4	D				#1, #3, #4, #5, #6, #8
5	AC1	C1	FDC1	MC1	#1, #2, #3, #6, #7, #8
6	BC1				#1, #2, #5, #6, #7, #8
7	CC1				#3, #4, #5, #6, #7, #8
8	DC1				#1, #3, #4, #5, #6, #8
9	AC2	C2	FDC2	MC2	#1, #2, #3, #6, #7, #8
10	BC2				#1, #2, #5, #6, #7, #8
11	CC2				#3, #4, #5, #6, #7, #8
12	DC2				#1, #3, #4, #5, #6, #8
13	AC3	C3	FDC3	MC3	#1, #2, #3, #6, #7, #8
14	BC3				#1, #2, #5, #6, #7, #8
15	CC3				#3, #4, #5, #6, #7, #8
16	DC3				#1, #3, #4, #5, #6, #8
17	AA1	A1	FDA1	MA1	#1, #2, #3, #6, #7, #8
18	BA1				#1, #2, #5, #6, #7, #8
19	CA1				#3, #4, #5, #6, #7, #8
20	DA1				#1, #3, #4, #5, #6, #8
21	AA2	A2	FDA2	MA2	#1, #2, #3, #6, #7, #8
22	BA2				#1, #2, #5, #6, #7, #8
23	CA2				#3, #4, #5, #6, #7, #8
24	DA2				#1, #3, #4, #5, #6, #8
25	AA3	A3	FDA3	MA3	#1, #2, #3, #6, #7, #8
26	BA3				#1, #2, #5, #6, #7, #8
27	CA3				#3, #4, #5, #6, #7, #8
28	DA3				#1, #3, #4, #5, #6, #8
29	AB1	B1	FDB1	MB1	#1, #2, #3, #6, #7, #8
30	BB1				#1, #2, #5, #6, #7, #8
31	CB1				#3, #4, #5, #6, #7, #8
32	DB1				#1, #3, #4, #5, #6, #8
33	AB2	B2	FDB2	MB2	#1, #2, #3, #6, #7, #8
34	BB2				#1, #2, #5, #6, #7, #8
35	CB2				#3, #4, #5, #6, #7, #8
36	DB2				#1, #3, #4, #5, #6, #8
37	AB3	B3	FDB3	MB3	#1, #2, #5, #6, #7, #8
38	BB3				#3, #4, #5, #6, #7, #8
39	CB3				#1, #3, #4, #5, #6, #8
40	DB3				#1, #2, #5, #6, #7, #8

7.3.1 Effect of AVDs on swirl

The swirl angles computed for four cases (i.e. A, B, C, and D) for $S = 666\,\text{mm}$ and $Q_s = 13.69\,\text{L/s}$ were tabulated for different AVDs and without AVD in Table 7.4 to 7.7, for different operational bell mouth combinations namely A, B, C and D respectively and also presented graphically in Figures 7.11 to 7.22.

It is observed that swirl in without AVDs were showing swirl greater than 5 degrees. Therefore, it is required to control the swirl in the pump sump model. Among the nine AVDs it is very difficult to decide which AVD is most suitable for all bell mouth combinations as what may be adequate for one combination or bay may not be sufficient for another. The same procedure adopted for the results of experimental runs was used for the CFD simulations and accordingly the suitability of different AVDs are given in Table 7.8. Rank of the AVD for criteria (a) is defined as one if the constraints were satisfied else it is zero. The AVD having swirl angle values ($<5^{\circ}$) fulfils the criteria (a) and ranked as 1 and even a single violation of the condition were ranked 0 for that AVD as given in Columns 2, 5, 8, and 11 of Table 7.8.Rank of AVDs for criteria (b) for that AVD, varying from 1 to 10 has been fixed as given in Column 3, 6, 9, 12 of Table 7.8. Similarly for the Rank of AVD for (c) criteria for that AVD, varying from 1 to 10 has been fixed and given in column 4, 7, 10, 13 of Table 7.8.

Table 7.4 Swirl angles in different pumps with different AVD for combination A.

S. No	AVD	Bell mouth number						Col [1]	Col [2]	Col. [3]	Col. [4]	Col. [5]	Col [6]
		#1	#2	#3	#6	#7	#8						
1	A	4.5	2.6	2.8	2.8	3.3	4.5	4.5	2.6	1.9	0.0	0.0	0.0
2	AA1	2.0	2.0	2.0	2.0	2.0	2.0	2.2	2.0	0.2	2.3	0.6	2.9
3	AA2	2.2	1.8	2.1	2.0	1.9	2.2	4.1	1.8	2.3	0.4	0.8	1.2
4	AA3	3.9	4.1	4.0	4.0	4.1	4.1	4.1	3.9	0.2	0.4	-1.3	-0.9
5	AB1	2.9	2.4	2.8	2.8	2.7	2.6	2.9	2.4	0.5	1.6	0.2	1.8
6	AB2	2.1	1.8	2.1	2.1	2.0	2.2	2.2	1.8	0.3	2.4	0.8	3.1
7	AB3	2.1	1.8	2.1	2.1	1.9	2.1	2.4	1.8	0.6	2.1	0.8	2.9
8	AC1	2.3	2.3	2.3	2.4	2.3	2.3	2.4	2.3	0.1	2.1	0.3	2.5
9	AC2	2.1	1.9	1.9	1.9	1.9	2.1	4.5	1.9	2.7	0.0	0.8	0.7
10	AC3	4.5	3.3	3.7	3.7	3.3	4.5	4.5	3.3	1.3	0.0	-0.7	-0.7

Table 7.5 Swirl angles in different pumps with different AVD for combination B

S. No	AVD	Bell mouth number						Col [1]	Col [2]	Col. [3]	Col. [4]	Col. [5]	Col [6]
		#1	#2	#5	#6	#7	#8						
1	B	4.0	4.5	2.8	2.3	2.2	5.8	5.8	2.2	3.7	0.0	0.0	0.0
2	BA1	3.6	3.7	2.3	2.2	1.9	3.6	3.8	1.9	1.9	2.0	0.3	2.3
3	BA2	2.0	1.9	3.8	3.5	3.8	2.0	4.0	1.9	2.2	1.8	0.3	2.1
4	BA3	3.6	3.7	4.0	4.0	3.8	3.6	4.0	3.6	0.5	1.8	-1.4	0.4
5	BB1	2.8	2.4	3.1	2.9	2.8	2.4	3.1	2.4	0.6	2.8	-0.3	2.5
6	BB2	2.2	2.3	2.4	2.3	2.2	2.0	2.4	2.0	0.4	3.5	0.1	3.6
7	BB3	1.8	2.1	2.4	2.3	2.1	2.0	7.1	1.8	5.3	-1.3	0.4	-0.8
8	BC1	7.1	6.0	3.6	3.8	4.3	4.4	7.1	3.6	3.5	-1.3	-1.5	-2.7
9	BC2	5.1	4.1	2.0	1.9	2.2	2.0	5.1	1.9	3.2	0.8	0.3	1.1
10	BC3	3.5	3.3	2.9	2.8	2.5	2.7	3.5	2.5	1.0	2.4	-0.3	2.1

Table 7.6 Swirl angles in different pumps with different AVD for combination C

S.No	AVD	Bell mouth number						Col [1]	Col [2]	Col. [3]	Col. [4]	Col. [5]	Col [6]
		#3	#4	#5	#6	#7	#8						
1	WB	5.0	2.4	2.5	2.1	1.9	4.0	5.0	1.9	3.1	0.0	0.0	0.0
2	CA1	1.9	2.1	2.3	2.2	1.9	1.8	2.5	1.8	0.7	2.5	0.1	2.6
3	CA2	2.0	2.0	2.5	2.3	2.0	1.9	4.3	1.9	2.4	0.8	0.0	0.8
4	CA3	4.1	4.0	4.3	4.2	4.1	4.0	4.3	4.0	0.3	0.8	-2.1	-1.3
5	CB1	2.9	2.8	3.0	3.0	3.0	2.6	3.0	2.6	0.4	2.0	-0.7	1.2
6	CB2	2.0	2.2	2.4	2.4	2.2	1.9	2.4	1.9	0.5	2.6	0.0	2.6
7	CB3	1.9	2.1	2.4	2.3	2.3	1.9	4.7	1.9	2.9	0.3	0.0	0.3
8	CC1	4.7	3.9	3.5	4.0	4.3	4.3	4.7	3.5	1.2	0.3	-1.6	-1.3
9	CC2	2.6	2.1	1.8	2.0	2.3	1.9	2.6	1.8	0.8	2.4	0.1	2.5
10	CC3	2.6	2.6	2.5	2.6	2.6	2.4	5.0	2.4	2.6	0.0	-0.5	-0.5

Table 7.7 Swirl angles in different pumps with different AVD for combination D

S. No	Run name	Bell mouth number						Col. [1]	Col. [2]	Col. [3]	Col. [4]	Col. [5]	Col. [6]
		#1	#3	#4	#5	#6	#8						
1	D	5.0	2.4	2.5	2.1	1.9	4.0	5.0	1.9	3.1	0.0	0.0	0.0
2	DA1	1.9	1.9	2.4	2.4	1.9	1.9	2.4	1.9	0.5	2.6	0.0	2.6
3	DA2	1.9	1.9	2.4	2.4	1.9	1.9	4.0	1.9	2.1	1.0	0.0	1.0
4	DA3	3.5	3.8	4.0	4.0	3.8	3.5	4.0	3.5	0.6	1.0	-1.6	-0.6
5	DB1	2.7	3.0	3.0	3.1	2.7	2.5	3.1	2.5	0.6	1.9	-0.6	1.3
6	DB2	2.2	2.1	2.4	2.4	2.1	2.2	2.4	2.1	0.3	2.6	-0.2	2.5
7	DB3	1.9	2.0	2.4	2.4	2.1	1.9	3.1	1.9	1.2	1.9	0.0	1.9
8	DC1	3.1	2.4	2.6	2.6	2.4	3.1	4.0	2.4	1.6	1.0	-0.5	0.6
9	DC2	3.9	1.7	1.9	1.9	1.8	4.0	6.6	1.7	4.8	-1.6	0.2	-1.4
10	DC3	6.6	4.3	4.8	4.8	4.3	6.6	6.6	4.3	2.3	-1.6	-2.4	-4.0

Table 7.8 Suitability indices for all AVDs

S.No.	AVD	Suitability index of AVDs for different criteria (a), (b) and (c) for each run												Cumulative suitability indices of AVD for each run				Cumulative SI
		A			B			C			D			A	B	C	D	
		a	b	c	a	b	c	a	b	c	a	b	c					
	[1]	**[2]**	**[3]**	**[4]**	**[5]**	**[6]**	**[7]**	**[8]**	**[9]**	**[10]**	**[11]**	**[12]**	**[13]**	**[14]**	**[15]**	**[16]**	**[17]**	**[18]**
1	-	0	3	3	0	2	3	0	1	4	0	2	4	6	5	5	6	22
2	A1	10	9	9	0	6	8	10	7	10	10	9	10	28	14	27	29	98
3	A2	10	2	5	0	5	7	10	4	6	10	4	6	17	12	20	20	69
4	A3	0	8	1	0	9	4	0	10	2	0	8	3	9	13	12	11	45
5	B1	10	6	6	0	8	9	0	9	7	0	7	7	22	17	16	14	69
6	B2	10	7	10	10	10	10	10	8	9	10	10	9	27	30	27	29	113
7	B3	10	5	8	10	1	2	10	2	5	10	6	8	23	13	17	24	77
8	C1	10	10	7	0	3	1	0	5	1	0	5	5	27	4	6	10	47
9	C2	10	1	4	0	4	5	10	6	8	0	1	2	15	9	24	3	51
10	C3	0	4	2	0	7	6	10	3	3	0	3	1	6	13	16	4	39

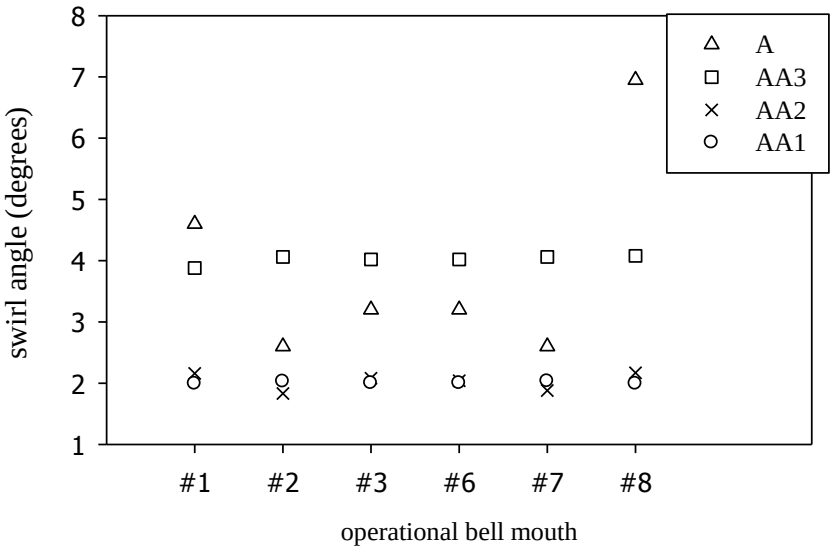

Figure 7.11 Swirl angles in working bays for run A, AA3, AA2 and AA1

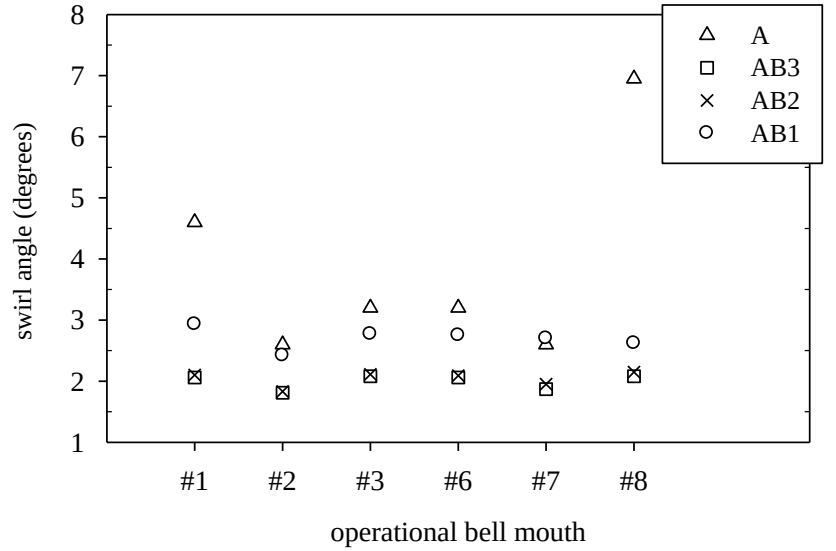

Figure 7.12 Swirl angles in working bays for run A, AB3, AB2 and AB1

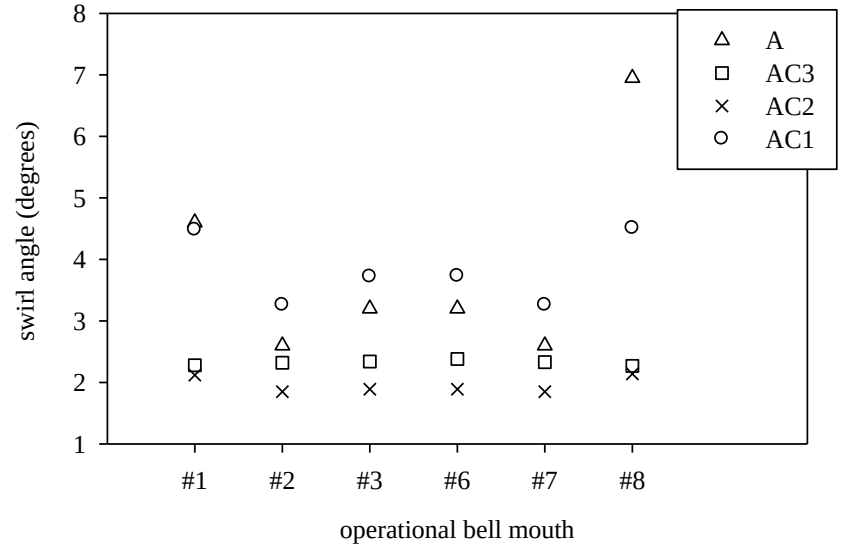

Figure 7.13 Swirl angles in working bays for run A, AC3, AC2 and AC1

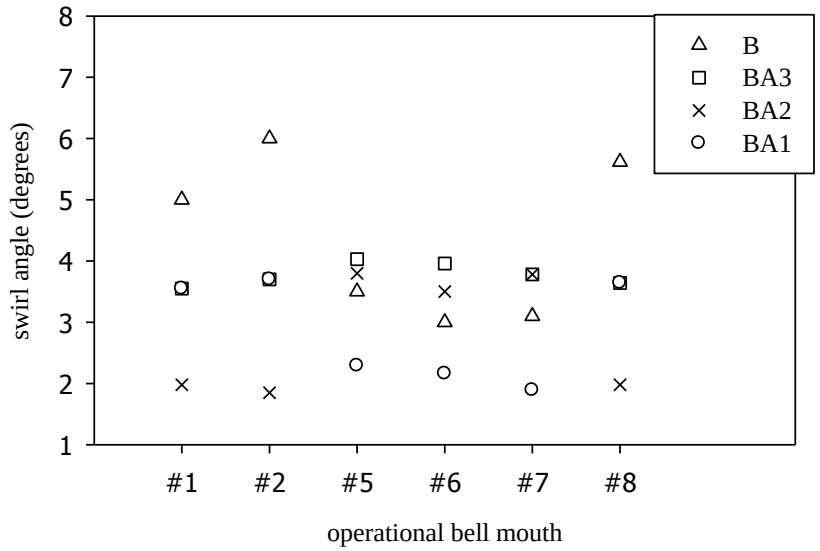

Figure 7.14 Swirl angles in working bays for run B, BA3, BA2 and BA1

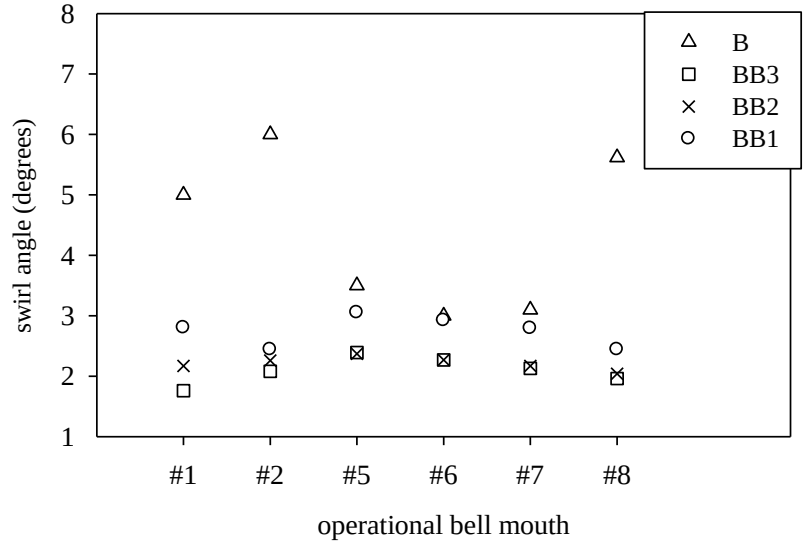

Figure 7.15 Swirl angles in working bays for run B, BB3, BB2 and BB1.

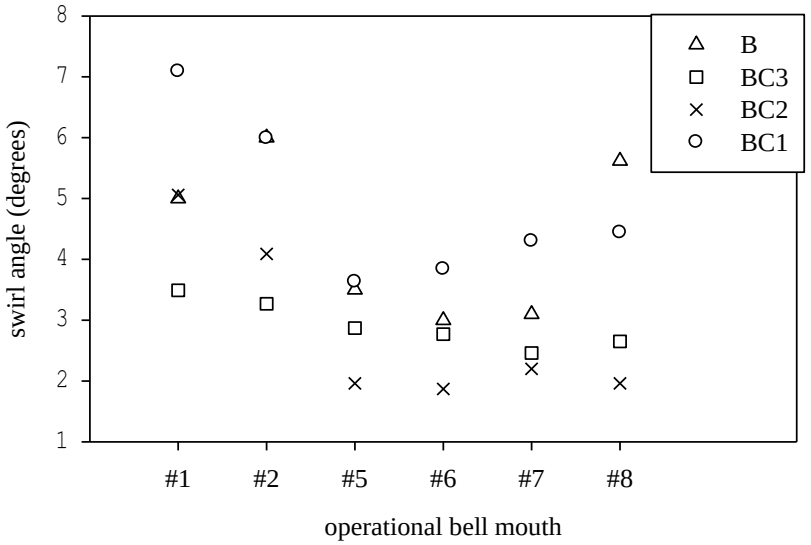

Figure 7.16 Swirl angles in working bays for run B, BC3, BC2 and BC1

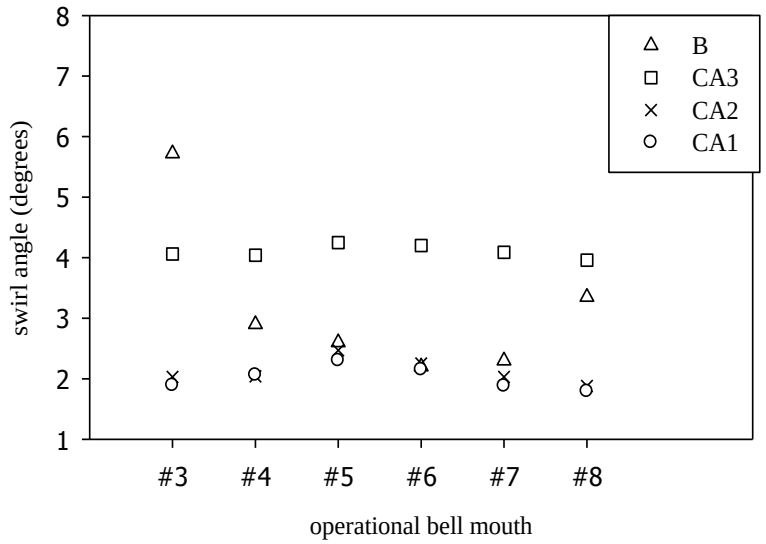

Figure 7.17 Swirl angles in working bays for run C, CA3, CA2 and CA1

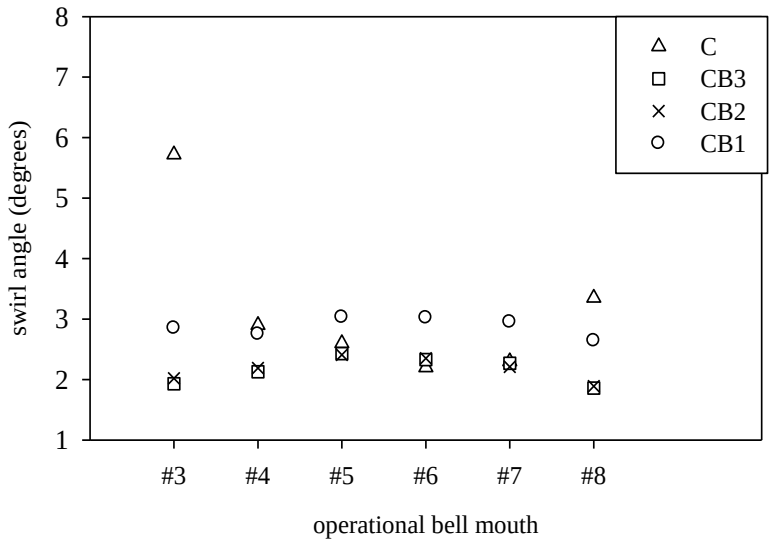

Figure 7.18 Swirl angles in working bays for run C, CB3, CB2 and CB1

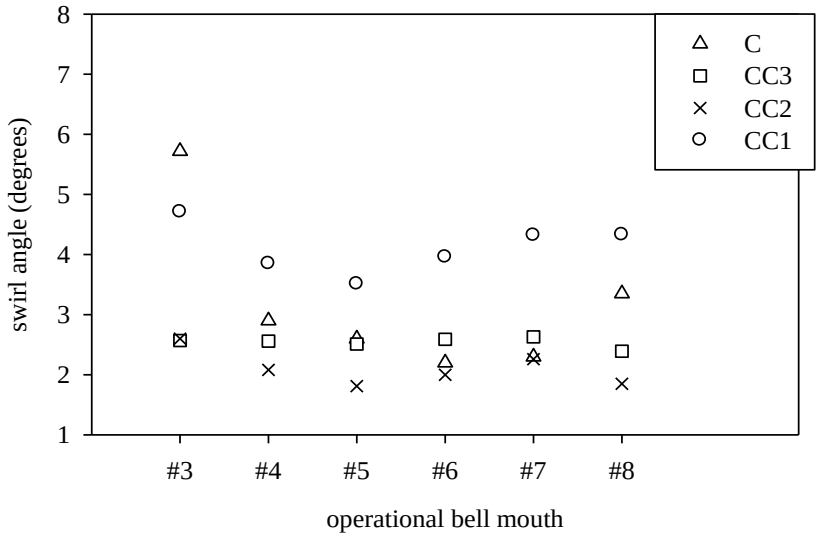

Figure 7.19 Swirl angles in working bays for run C, CC3, CC2 and CC1

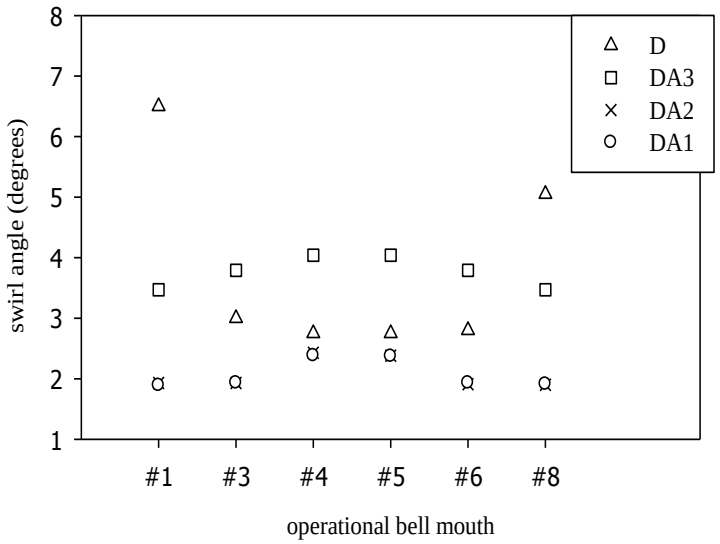

Figure 7.20 Swirl angles in working bays for run D, DA3, DA2 and DA1

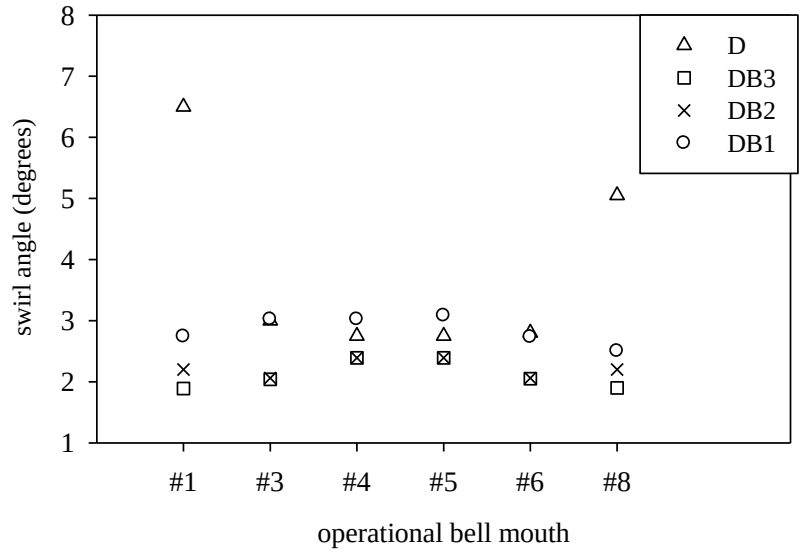

Figure 7.21 Swirl angles in working bays for run D, DB3, DB2 and DB1

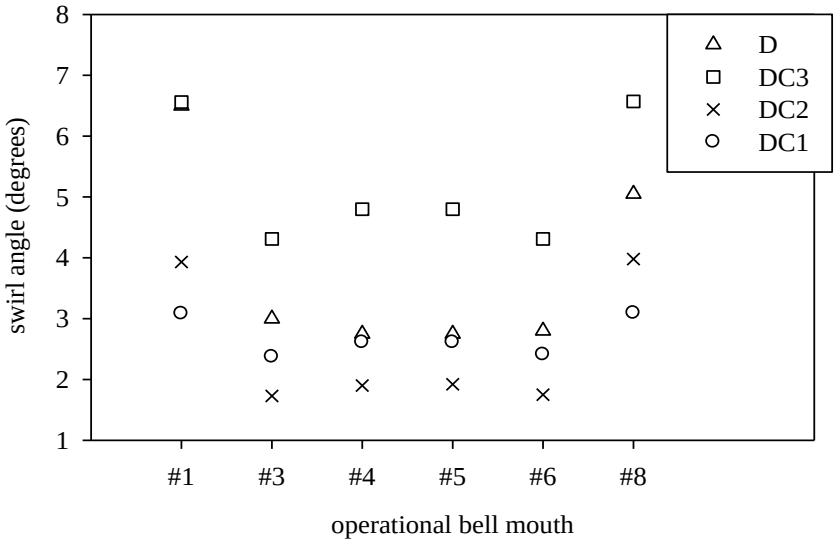

Figure 7.22 Swirl angles in working bays for run D, DC3, DC2 and DC1

7.3.2 Effect of AVDs on subsurface vortices

Figures 7.23 to 7.32 show the comparison of streamline pattern and out planes vorticity (non-dimensionalized ω_z) contour plots in horizontal plane (z = 0.01D) around the pump intake structure with and without the AVDs. The velocity streamlines and out-plane vorticity contour plots were constructed from the calculated in-plane velocity fields. When plotted in this way, the results reveal vortices and swirling motions. In each case, the streamlines and the component of vorticity normal to that plane were calculated from the in-plane velocity components using CFDPOST. The figures show only a few streamlines overlaid on the contours of the ω_z for better understanding. From figures the location of subsurface vortices can be visualised and it is observed that the location and strength of vortices show the variation with respect to the without AVD conditions.

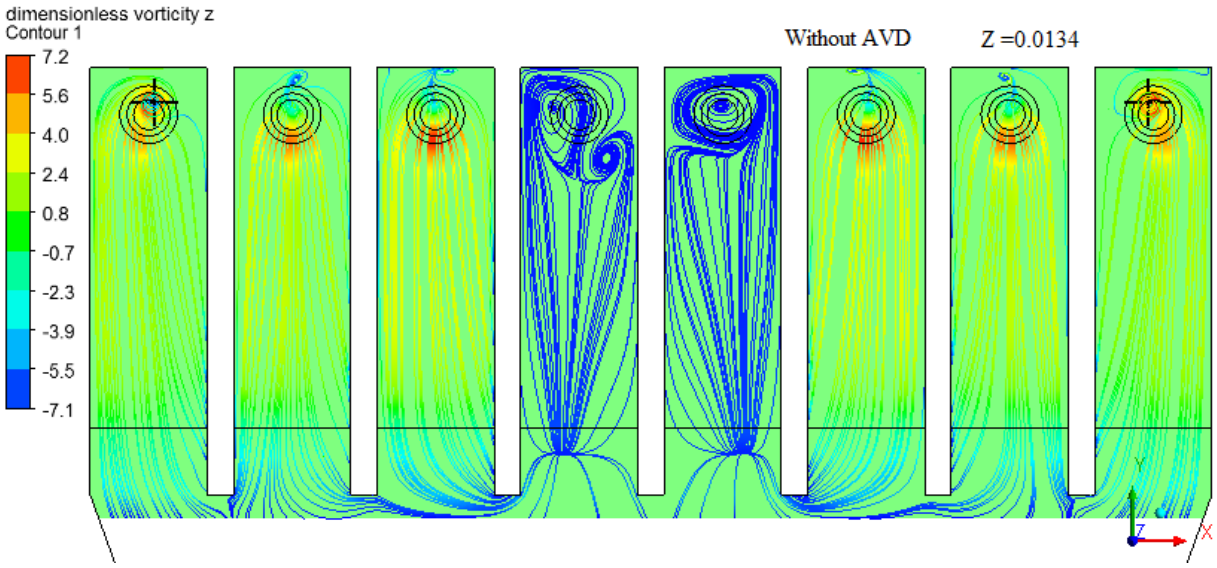

Figure 7.23 Streamline and out-plane vorticity plot in z = 0.01D for run A

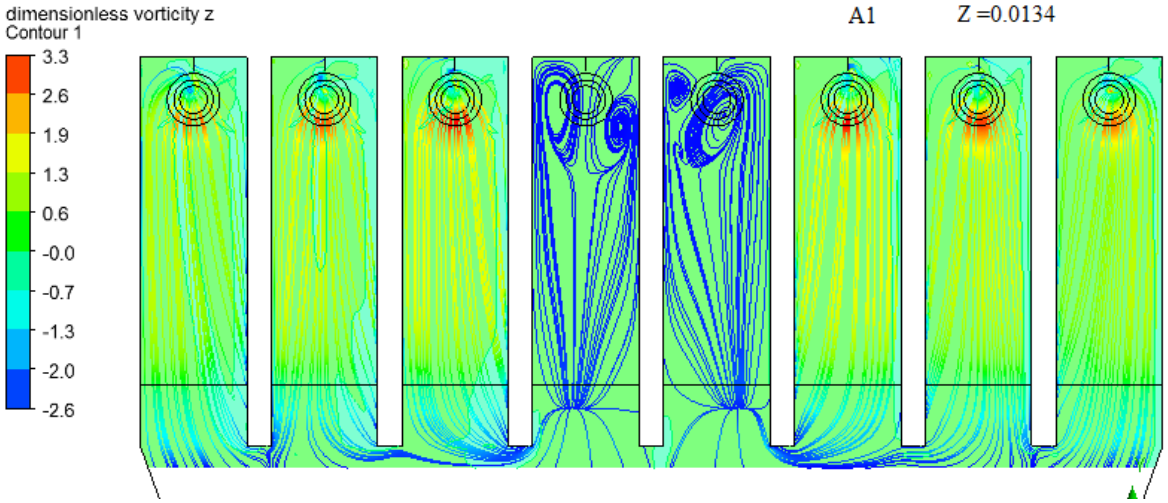

Figure 7.24 Streamline and out-plane vorticity plot in z = 0.01D for run AA1

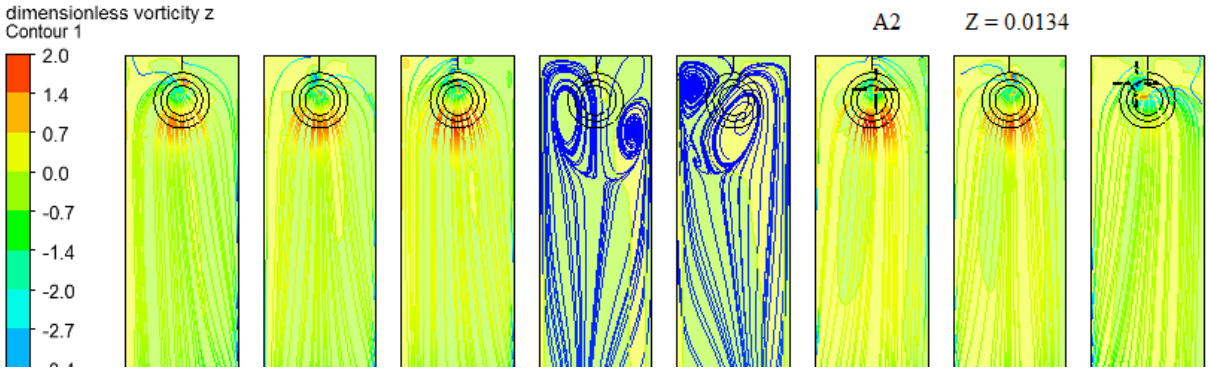

Figure 7.25 Streamline and out plane vorticity plot in $z = 0.01D$ for run AA2

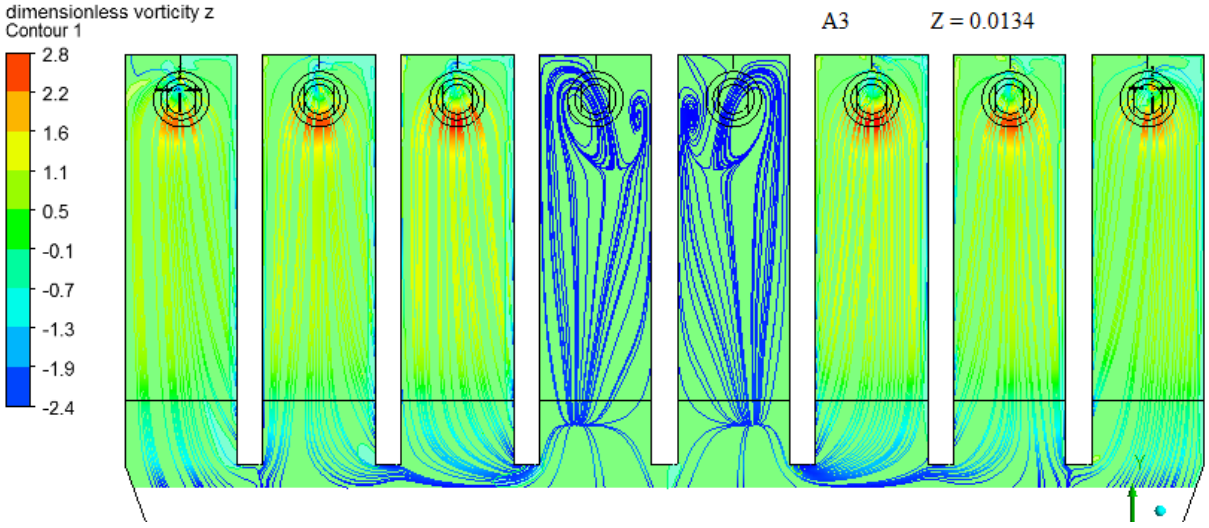

Figure 7.26 Streamline and out-plane vorticity plot in $z = 0.01D$ for run AA3

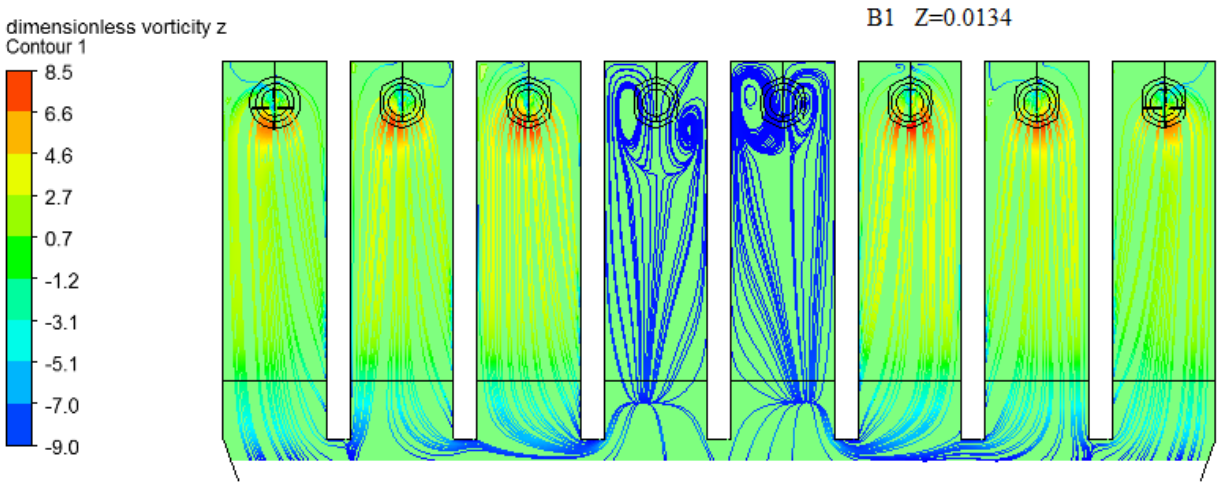

Figure 7.27 Streamline and out-plane vorticity plot in $z = 0.01D$ for run AB1

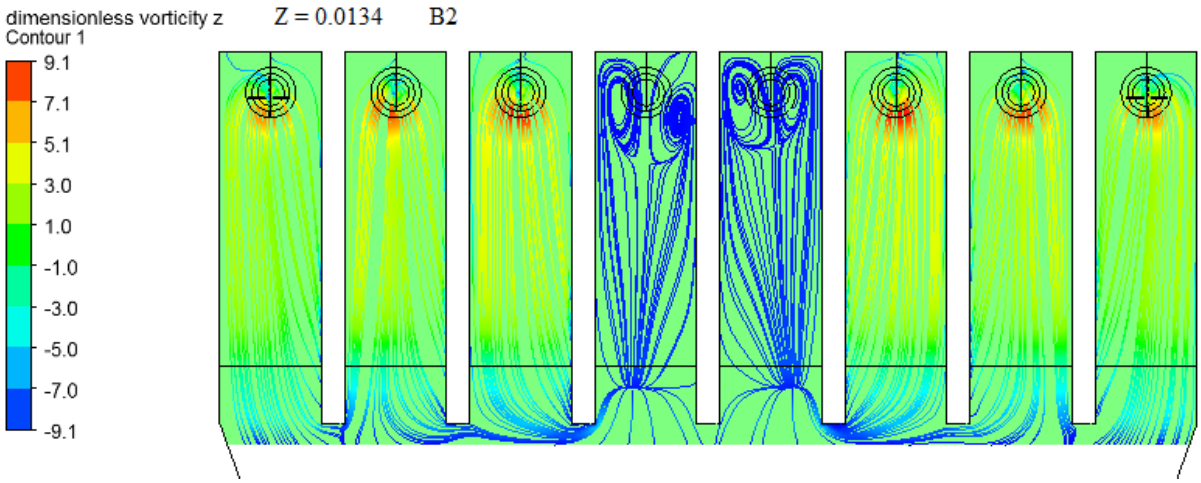

Figure 7.28 Streamline and out-plane vorticity plot in $z = 0.01D$ for run AB2

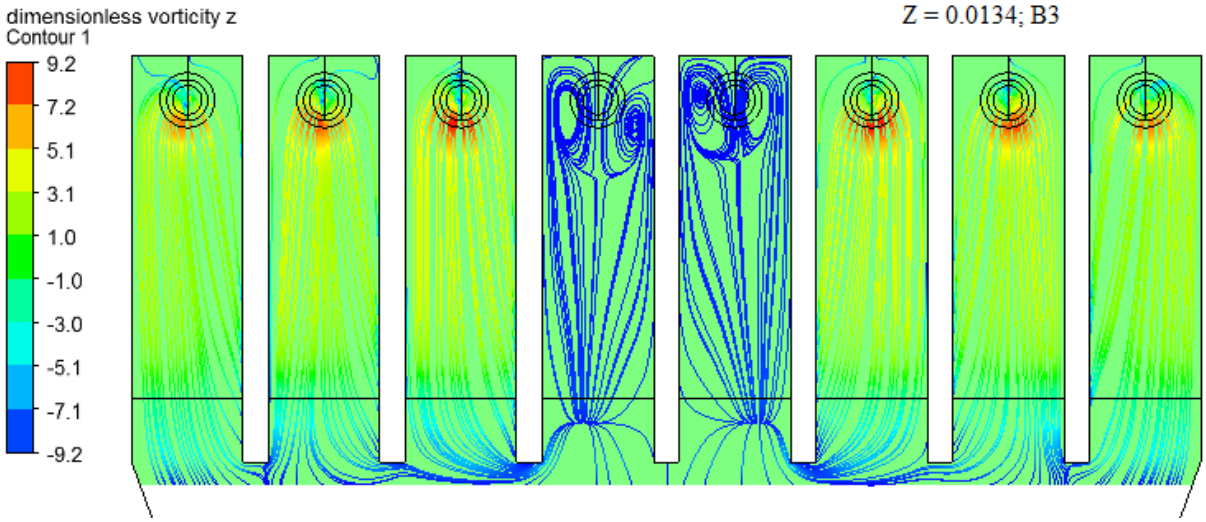

Figure 7.29 Streamline and out plane vorticity plot in $z = 0.01D$ for run AB3

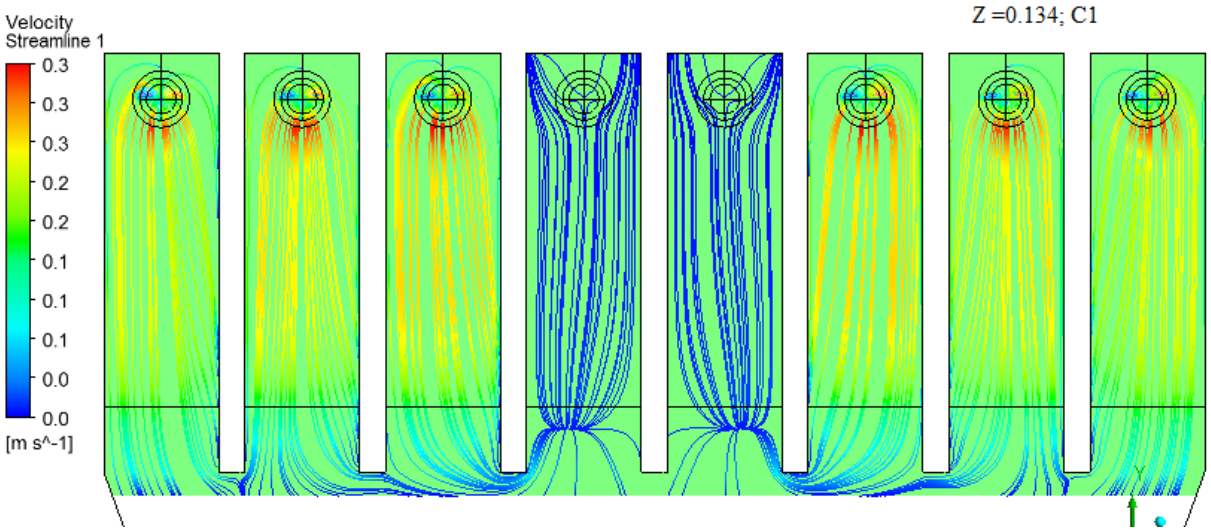

Figure 7.30 Streamline and out plane vorticity plot in z = 0.01D for run AC1

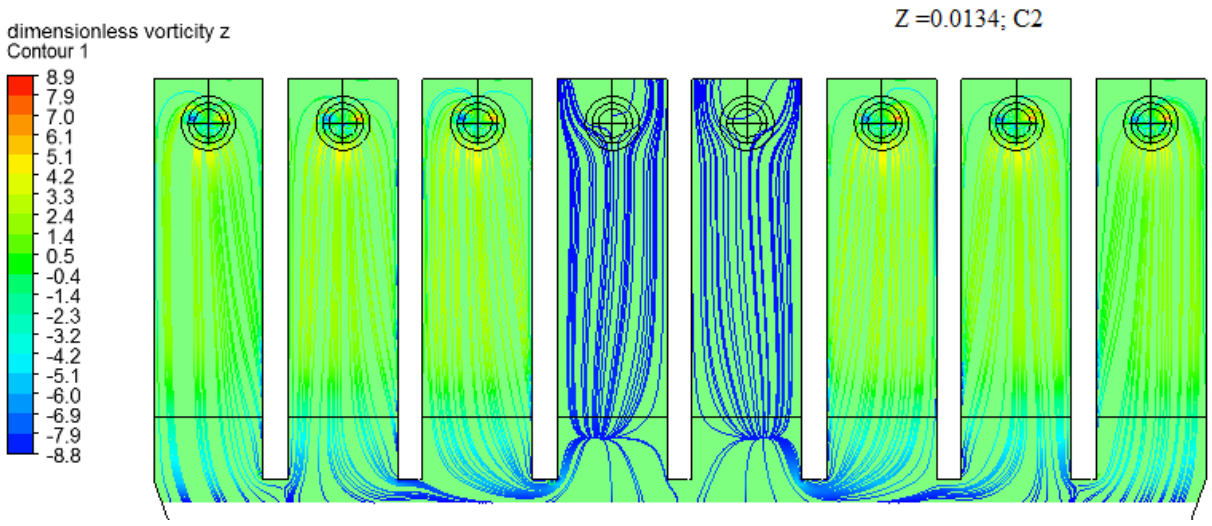

Figure 7.31 Streamline and out plane vorticity plot in $z = 0.01D$ for run AC2

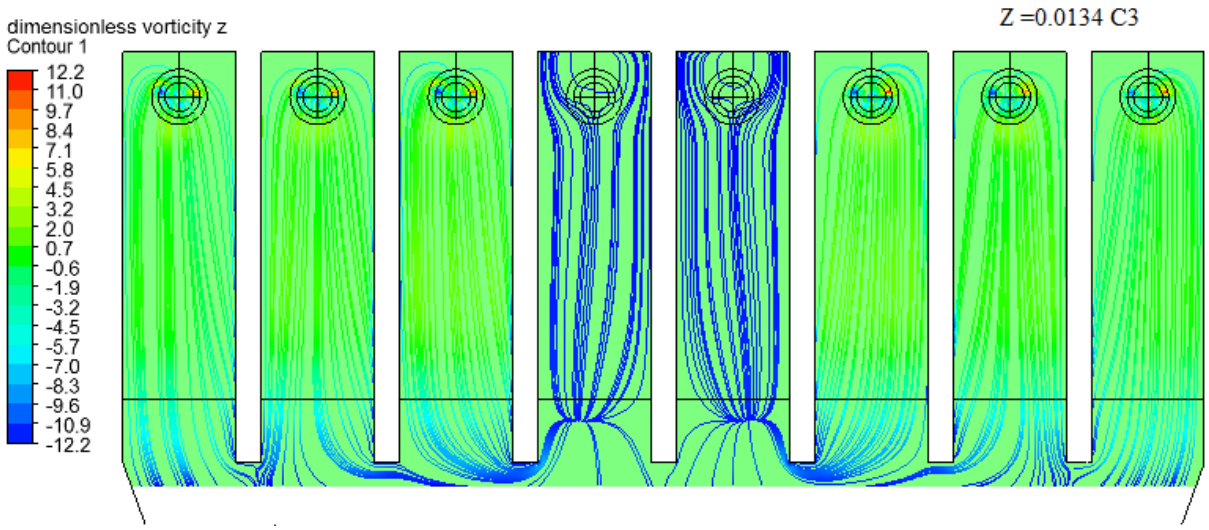

Figure 7.32 Streamline and out plane vorticity plot in $z = 0.01D$ for run AC3

7.3.3 Effect of AVDs on decay of swirl

To see the effect of shape and size of AVDs on decay of swirl in one suction column of bay 1, the swirl along the distance from floor (z coordinate) was analysed and the results were shown graphically in Figure 7.33, in suction pipe of bay 1 for all CFD simulation runs for bell mouth combination A (namely A, AC1, AC2, AC3, AA1, AA2, AA3, AB1, AB2, AB3 of Table 7.3). In this figure, it is clear that maximum and minimum swirl at any point is observed in run A and AC1 respectively. The AVDs A1, A2, A3, B1, B2, B3 and C3 show almost similar values at all the points. It is observed that the most suitable AVD is C1 as it shows rapid decay in swirl and the same has been observed in summary Table 7.8. The suitability of the AVD C1 is 27 in Run A, i.e. maximum among all other AVDs.

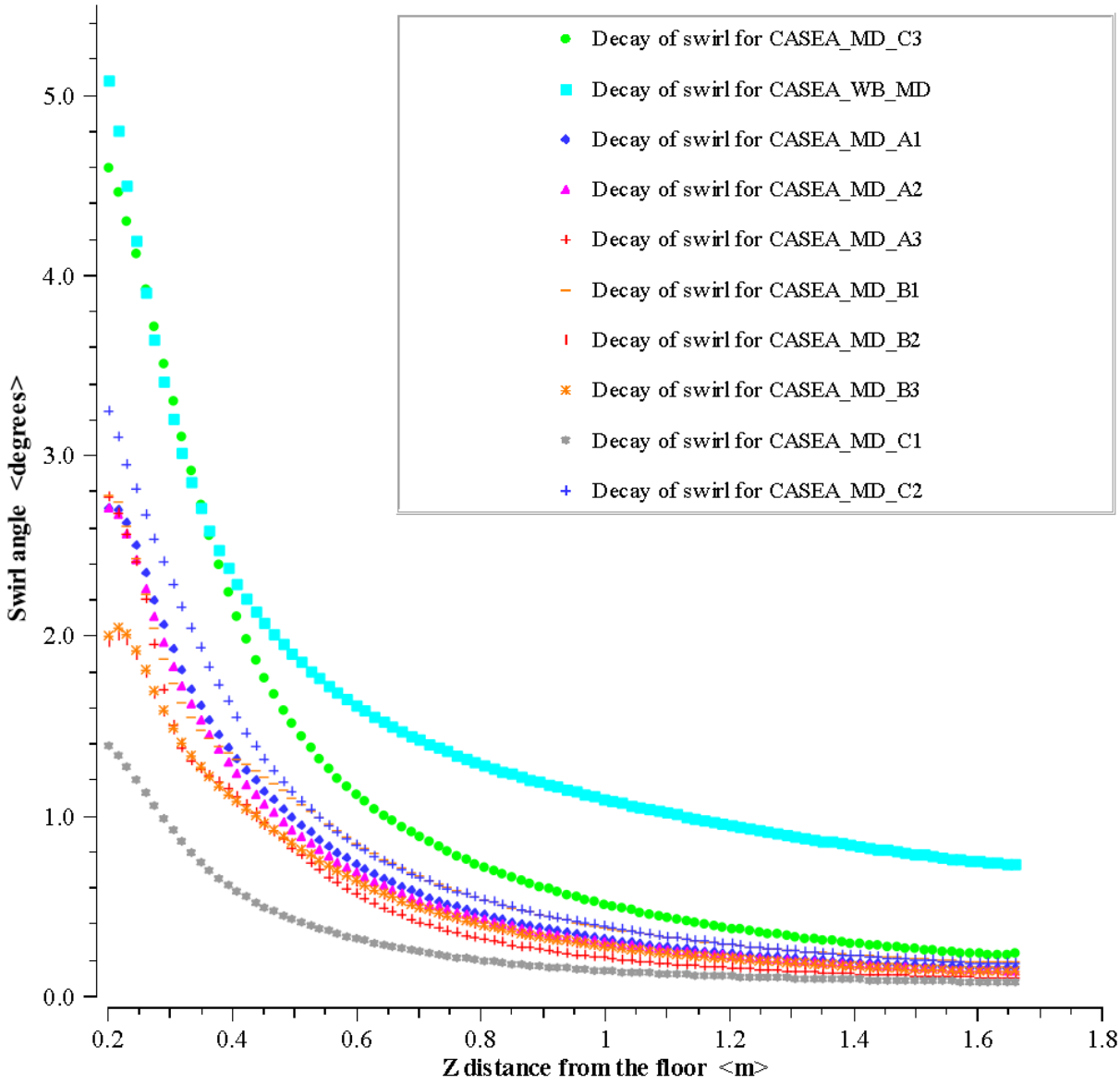

Figure 7.33 Decay of swirl in suction column along the distance for case A (Q_s = 13.69L/s)

7.4 OPTIMIZED SHAPE AND SIZE OF VORTEX BREAKER

From the swirl angles computed for the pump sump intake model without any modifications, it is observed that the most of the pumps showed swirl angles greater than 3° except for few pumps. In case A, #1 and #8 were showing swirl greater than 6.5 degrees. Therefore, it is necessary (as discussed in Chapter 2) to control the swirl in such combinations. To control swirl, a parametric study has been carried out to find the suitable shape and size of the anti-vortex device. Three different shapes (namely Type A, Type B and Type C) and three different sizes as shown in Figure 7.1 were tested. First, the direct effect of different shapes and sizes on computed swirl using CFD model has been discussed in Section 7.3.1. Further in

Section 7.3.2, the flow characteristic analysis of the CFD results has been presented using stream lines and out plane vorticity contours for different pump combinations.

7.5 CONCLUDING REMARKS

Three different sizes of cross type anti-vortex devices are used in the physical model below the bell mouth intake for the control of swirling flow in the suction lines. Out of the three sizes of AVD, the middle size is found more effective in controlling the swirling flow. Nevertheless the higher size of the AVD breaks the swirling nature of the incoming flow, however, due to blockage effect it induces additional swirl which results in higher swirl compared to medium size of the AVD.

CFD modelling has been carried out to investigate the effectiveness of three shapes of the AVD i.e. vertical backwall splitter, L shape splitter and cross type. For each shape, three sizes of the AVD have been investigated. For each AVD, swirl angle in the suction line, flow pattern near the bell mouth, subsurface vortices have been investigated. It is found that L shape AVD of medium size is more effective in having favourable flow conditions in the suction lines.

CHAPTER 8 CONCLUSIONS AND RECOMMONDATIONS

8.1 INTRODUCTION

The present study was aimed at to investigate flow patterns and swirl in suction lines for different pumps combination and their operating conditions and control of swirl from experimental and CFD modelling.

A 1:12 scaled model of eight bays pump sump intakes was constructed in the Hydraulics laboratory of Department of Civil Engineering, IIT Roorkee and tested for different flow conditions to achieve the objectives of the present study. Froudian similitude law was followed in the physical modelling to generate the flow conditions of the prototype. The experimental runs have been carried out to investigate the stringent pump combinations and flow conditions. Also the effect of Froude number on swirl has been investigated. Experimental data for the validation of the CFD model has been collected. A cross type AVD has been tested to investigate the effect of height of the AVD on swirl.

A CFD model of the pump sump intake model has been developed. The standard k-ε model is used to model the turbulence. The 3-Dimensional model geometry in ICEMCFD has been created and a multiblock hexahedral mesh of the pump sump model has been created. The meshed geometry further used to simulate the flow using Fluent solver. The simulated results were further processed for the presentation of the results using CFD POST.

The CFD model is verified by grid dependency tests. In grid dependency test the swirl angles on three different grids were compared. The decay of swirl, circulation and tangential velocity distributions in subsurface vortices has been also compared for the three different grids. After verification the CFD model results were compared with experimental values to validate the CFD model. For the validation the swirl angles and velocity distributions in bays are used.

The developed CFD model has been used to investigate the effect of Froude number on swirl. From the computed results the decay of swirl in a suction line has been analysed.

Also the CFD modelling has been used to investigate the effect of AVDs of different shape and sizes on swirl. Among the different AVDs most suitable AVD has been suggested using suitability index (SI) analysis.

8.2 CONCLUSIONS

The following conclusions have been derived from the present study:

1. From the convergence history of residuals and swirl angles study it is observed that the developed CFD model is showing better convergence properties and giving stable solution. Also, the convergence for momentum and turbulence properties shows better convergence than the continuity equation.
2. Examination of flow patterns, location of vortices, distribution of effective tangential velocity and circulation in vortices for the three different grid sizes concludes that the adopted grid size of 16 mm is fine enough to get the grid independent solutions.
3. From the comparison of physical and CFD model results of swirl angle in suction columns for different flow conditions (12 runs), it is concluded that CFD model predicts the swirl angle with good accuracy. It is observed that the CFD slightly under predicts the swirl in suction pipes that can be attributed to unsteady nature in the flow near the bell mouth.
4. The comparison of the CFD and physical model results also confirm the assumptions associated with the boundary conditions and turbulence model.
5. The comparison of CFD and experimental results of velocity distribution in bays indicates that the CFD model can be used to predict the velocity distribution in bays. The standard k-ε model is found suitable for the computation of swirl in the pump sump model.
6. Through experimentation and CFD modelling, it is found that swirl angle in suction pipe of the pump increases with increase in Froude number in the pipe. Such increase is not severe and that may be due to increase in turbulence level at higher Froude number. The minor increase in the swirl angle at higher discharges, i.e. at higher Froude number and velocity, is mainly attributed to high turbulence rather than the presence of swirl in the flow.
7. Three different sizes of cross type anti-vortex devices are used in the physical model below the bell mouth intake for the control of swirling flow in the suction lines. Out of the three sizes of AVD, the middle size is found more effective in controlling the swirling flow. Nevertheless the higher size of the AVD breaks the swirling nature of the incoming flow, however, due to blockage effect it induces additional swirl which results in higher swirl compared to medium size of the AVD.
8. CFD modelling has been carried out to investigate the effectiveness of three shapes of the AVD i.e. vertical backwall splitter, L shape splitter and cross type. For each shape,

three sizes of the AVD have been investigated. For each AVD, swirl angle in the suction line, flow pattern near the bell mouth, subsurface vortices have been investigated. It is found that L shape AVD of medium size is more effective in having favourable flow conditions in the suction lines.

9. Decay of swirl along the suction pipe has also been studied using CFD and it is found that swirl angle decreases exponential along the length of suction pipe.
10. A new equation has been proposed for the computation of decay in swirl angle along the length of the suction pipe. The computed decay of swirl from the proposed equation is matching with the computed swirl decay from CFD results.

REFERENCES

Ahmad, Z., Jain, B., Kumar, S., and Mittal, M. K. (2011). 'Rational design of a pump-sump and its model testing.' *Journal of Pipeline Systems Engineering and Practice*, 2(2), 53–63.

American National Standards Institute (ANSI). (1998). *Pump Intake Design*. Hydraulic Institute, ANSI/HI 9.8, 9 Sylvan Way, Parsippany, New Jersey.

Ansar, M., and Nakato, T. (2001). 'Experimental study of 3D pump intake flows with and without cross flow.' *Journal of Hydraulic Engineering*, 127(10), 825–834.

Ansar, M., Nakato, T., and Constantinescu, G. S. (2002). 'Numerical simulations of inviscid three-dimensional flows at single and dual-pump intakes.' *Journal of Hydraulic Research*, 40(4), 461–470.

Anwar, H. O. (1965). 'Flow in a free vortex.' *Water Power*, 4, 153–161.

Anwar, H. O. (1966). 'Formation of a weak vortex.' *Journal of Hydraulic Research*, 4(1), 1–16.

Anwar, H. O. (1967). 'Vortices at low-head intakes.' *Water Power*, 19(11), 455.

Anwar, H. O. (1968). 'Prevention of vortices at intakes.' *Water Power*, 20(10), 393–401.

Anwar, H. O., and Amphlett, M. B. (1980). 'Vortices At Vertically Inverted Intake.' *Journal of Hydraulic Research*, 18(2), 123–134.

Anwar, H. O., Weller, J. A., and Amphlett, M. B. (1978). 'Similarity of free-vortex at horizontal intake.' *Journal of Hydraulic Research*, 16(2), 95–105.

Arboleda, G., and El-Fadel, M. (1996). 'Effects of approach flow conditions on pump sump design.' *Journal of Hydraulic Engineering*, 122(9), 489–494.

Baker, D. W., and Sayre, C. L. (1974). 'Decay of swirling turbulent flow of incompressible fluids in long pipes.' *Proc. Symp. Flow - Its Measurements and Control in science and Industry*, 301–312.

Bauer, D. I., and Nakato, T. (1997). *Subsurface vortex supression in water intakes with multiple pump sumps*. IIHR Rep. 387, Iowa Institute of Hydraulic Research, Univ. of Iowa, Iowa City, IA.

Bayeul-Laine, A. C., Bois, G., and Issa, A. (2010a). 'Numerical simulation of flow field in water pump sump and inlet suction pipe.' *25th IAHR Symposium on hydraulic machinery and systems*, IAHR, Timisoara, Romania, 1–8.

Bayeul-Laine, A. C., Bois, G., and Issa, A. (2010b). 'Numerical simulation of flow field in water-pump sump and inlet suction pipe.' *IOP Conference Series: Earth and Environmental Science*, 012083.

Bureau of Indian Standards (BIS). (2003). *Hydraulic design of pump sump and intakes-Guidelines*. IS:15310, New Delhi, India.

Chang, E. (1977). *Review of literature on the formation and modelling of vortices in rectangular pump sumps*. British Hydromechanics Research Association.

Chen, H. C., and Patel, V. C. (1988). 'Near-wall turbulence models for complex flows including separation.' *AIAA journal*, 26(6), 641–648.

Chen, H., and Guo, J. (2007). 'Numerical simulation of 3-D turbulent flow in the multi-intakes sump of the pump station.' *Journal of Hydrodynamics*, 19(1), 42–47.

Choi, J. W., Choi, Y. Do, Kim, C. G., and Lee, Y. H. (2010). 'Flow uniformity in a multi-intake pump sump model.' *Journal of Mechanical Science and Technology*, 24(7), 1389–1400.

Chuang, W.-L., Hsiao, S.-C., and Hwang, K.-S. (2014). 'Numerical and experimental study of pump sump flows.' *Mathematical Problems in Engineering*, 2014, 1–20.

Constantinescu, G. S., and Patel, V. C. (1998). 'Numerical Model for Simulation of Pump Intake Flow and Vortices.' *Journal of Hydraulic Engineering*, 124(2), 123–134.

Constantinescu, G. S., and Patel, V. C. (2000). 'Role of turbulence model in prediction of pump-bay vortices.' *Journal of Hydraulic Engineering*, 126(May), 387–391.

Daggett, L. L., and Keulegan, G. H. (1974). ‘Similitude conditions in free surface vortex formations.’ *Jounal of Hydraulic Divisionivision*, 100(11).

Denny, D. F. (1956). ‘An experimental study of air-entraining vortices in pump sumps.’ *Proceedings of the Institution of Mechanical Engineers*, 170(1), 106–125.

Denny, D. F., and Young, G. A. J. (1957). ‘The prevention of vortices and swirl at intakes.’ *IAHR 7th Congress*, Lisbon, C1, 1–18.

Desmukh, T. S., and Gahlot, V. K. (2010). ‘Simulation of flow through a pump sump and its validation.’ *IJRRAS*, 4(1), 7–17.

Desmukh, T. S., and Gahlot, V. K. (2011). ‘Numerical study of flow behavior in a multiple intake pump sump.’ *International Journal of Advanced Engineering Technology*, 2(2), 118–128.

Dhillon, G. S. (1980). *Vortex Formation at Pipe Intakes and its Prediction: a Status Report. Irrigation and Power Research Institute, Punjab, Report No. 6.*

Dimas, A. A., and Vouros, A. P. (2012). ‘Effect of cross-flow velocity at forebay on swirl in pump suction pipe : hydraulic model of seawater intake at Aliveri power plant in Greece.’ *Journal of Hydraulic Engineering*, 138(9), 812–816.

Durgin, W. W., and Hecker, G. E. (1978). ‘The modeling of vortices at intake structures.’ *Proceedings of the ASCE, IAHR, and ASME Joint Symposium on Design and Operation of Fluid Machinery*, 381.

Eldho, T. I. (2010). *Hydraulic sump model study of Jhajjar*. Technical report, department of civil engineering, IIT bombay, Bombay,India.

Farell, C. (1976). *Model study of the inlet and sump of the Clinton First Avenue pump station*. IIHR Report 196, Iowa Institute of Hydraulic Research, University of Iowa, Iowa.

Fletcher, B. P. (1979). *Pumping stations-field performance investigation*. Report no. HL-79-7, Hydraulics laboratory, U S army Engineer waterways experiment station.

Frizell, K. W. (1994). *Hydraulic model tests: twin peaks pumping plant*. R-94-05, U.S. Department of the Interior, Bureau of Reclamation Denver Office, Research and Laboratory Services Division Hydraulics Branch.

Gordon, J. L. (1970). 'Vortices at Intakes.' *Water power*, (4), 137–138.

Haindl, K. (1959). 'Contribution to air entrainment by a vortex.' *International Association for Hydraulic Research, Montreal*, 16D.

Haradasa, D. K. C., and Cox, R. J. (1980). 'Flow improvement at pump intakes by the use of baffles.' *7th Australian Hydraulics and Fluid Mechanics Conference*, Brisbane, 561–564.

Hecker, G. E. (1981). 'Model-Prototype Comparision of Free Surface Vortices.' *Journal of the Hydraulics Division*, ASCE, 107(10), 1243–1259.

Issa, A., Bayeul-Laine, A. C., and Bois, G. (2008). 'Numerical simulation of flow field formed in water pump-Sump.' *24th Symposium on hydraulic Machinery and Systems*, IAHR, Argentina.

Issa, A., and Bois, G. (2009). 'Numerical study of the influence of geometrical parameters on flow in water pump-sump.' *Conference on Modelling Fluid Flow (CMFF'09) The 14th International Conference on Fluid Flow Technologies*, Budapest, Hungary.

Jain, A. K., Garde, R. J., and Ranga Raju, K. G. (1978). 'Vortex formation at vertical pipe intakes.' *Journal of the Hydraulics Division*, ASCE, 104(10), 1429–1445.

Jermy, M., and Ho, W. H. (2008). 'Location of the vortex formation threshold at suction inlets near ground planes by computational fluid dynamics simulation.' *Proceedings of the Institution of Mechanical Engineers, Part G: Journal of Aerospace Engineering*, 222(3), 393–402.

Kang, W. T., Shin, B. R., and Doh, D. H. (2014). 'An effective shape of floor splitter for reducing sub-surface vortices in pump sump.' *Journal of Mechanical Science and Technology*, 28(1), 175–182.

Kang, W. T., Yu, K. H., and Shin, B. R. (2011). ‘An investigation of surface vortices behavior in pump sump.’ *11th Asian International Conference on fluid machinery and 3rd fluid power Technology exihibition*, IIT Madras, Chennai, India, 1–6.

Kawakita, K., Matsui, J., and Isoda, H. (2012). ‘Experimental study on the similarity of flow in pump sump models.’ *26th IAHR Symposium on Hydraulic Machinery and Systems*, IAHR, 1–9.

Kim, C. G., Choi, Y.-D., Choi, J.-W., and Lee, Y.-H. (2012). ‘A study on the effectiveness of an anti vortex device in the sump model by experiment and CFD.’ *IOP Conference Series: Earth and Environmental Science*, 15(7), 072004.

Kim, C. G., Kim, B. H., Bang, B. H., and Lee, Y.-H. (2015). ‘Experimental and CFD analysis for prediction of vortex and swirl angle in the pump sump station model.’ *IOP Conference Series: Materials Science and Engineering*, 72(4), 1–7.

Knauss, J. (Ed.). (1987). *Swirling flow problems at intakes*. IAHR Hydraulic structures design manual, Taylor and Farncis, London.

Lai, Y. G., Weber, L. J., and Patel, V. C. (2003). ‘Nonhydrostatic three-dimensional model for hydraulic flow simulation. I: formulation and verification.’ *Journal of Hydraulic Engineering*, 129(3), 196–205.

Launder, B. E., and Spalding, D. B. (1972). ‘Lectures in mathematical models of turbulence.’ Academic press.

Lewellen, W. S. (1962). ‘A solution for three-dimensional vortex flows with strong circulation.’ *Journal of Fluid Mechanics*, Cambridge Univ Press, 14(03), 420–432.

Li, S., Lai, Y. G., Silva, M. S., and Patel, V. C. (2001). ‘CFD Model of Three-Dimensional Flow in Practical Water-Pump Intakes.’ *IIHR Technical Rep*, 419.

Li, S., Lai, Y., Weber, L., Silva, J. M., and Patel, V. C. (2004). ‘Validation of a three-dimensional numerical model for water-pump intakes.’ *Journal of Hydraulic Research*, 42(3), 282–292.

Li, S., Silva, J. M., Lai, Y., Weber, L. J., and Patel, V. C. (2006). 'Three-dimensional simulation of flows in practical water-pump intakes.' *Journal of Hydroinformatics*, 8, 111–124.

Long, N. I., Shin, B. R., and Doh, D. H. (2012). 'Study on surface vortices in pump sump.' *Journal of Fluid Machinery*, 15(5), 60–66.

Lucino, C., and Duro, S. L. y G. (2010). 'Vortex detection in pump sumps by means of CFD.' *XXIV Latin American Congress on Hydraulics P*, IAHR, Punta Del Este, Uruguay, 21–25.

Meena, V., Bhatt, A., and Eldho, T. I. (2013). 'Numerical simulation of pump sump flow characteristics.' *Research and Reviews:Journal of Engineering and Technology*, 2(3), 49–57.

Melville, B. W., Ettema, R., and Nakato, T. (1994). *Review of flow problems at water intake pump sump*. EPRI TR-103474, Proj.3456-01, Iowa Institute of Hydraulic Research, Univ. of Iowa, Iowa City, IA.

Murakami, M., Suehiro, H., Isaji, T., and Kajita, J. (1969). 'Flow of Entrained Air in Centrifugal Pumps.' *Proceedings of the 13th Congress IAHR*, Kioto, 71.

Nakato, T., and Jong, D. De. (1999). *Hydraulic Model Study Of water-Intake Structures For Meizhou Wan Power Station,Putian City,Fujian province,The People's Republic Of China*. IIHR Rep. 402, Iowa Institute of Hydraulic Research, Univ. of Iowa, Iowa City, IA.

Nakato, T., and Kennedy, J. F. (1977). *Detailed model study of pump approach flows for the Lake Chicot pumping plant*. Iowa.

Nathan, G. K. (1981). 'Flow investigations in two pumping pits.' *Journal of the Hydraulics Division*, ASCE, 107(1), 127–132.

Odgaard, A. J., and Dlubac, J. J. (1983). 'Hydraulic model study of pump sump design.' *Journal of Hydraulic Engineering*, 110(9), 1267–1272.

Okamura, T., Kamemoto, K., and Matsui, J. (2007). 'CFD prediction and model experiment on suction vortices in pump sump.' *The 9th Asian International Conference on Fluid Machinery*, Jeju, Korea, 1–10.

Padmanabhan, M. (1984). 'Air ingestion due to free-surface vortices.' *Journal of Hydraulic Engineering*, 110(12), 1855–1859.

Padmanabhan, M., and Hecker, G. E. (1982). *Assessment of scale effects on vortexing, swirl, and inlet losses in large scale sump models*. Alden research laboratory, Holden.

Padmanabhan, M., and Hecker, G. E. (1984). 'Scale effects in pump sump models.' *Journal of Hydraulic engineering*, 110(11), 1540–1556.

Padmanabhan, M., and Janek, C. R. (1980). 'Swirling flow and its effect on wall pressure drop within pipes.' *Vortex Flows: ASME Winter Annual Meeting*, 1980.

Park, Y. K., Li, K. M., Chi, Y. H., and Lee, Y. W. (2011a). 'A Study on the Generation of Vortices around a Sump Intake with Multiphase Flow.' *11th asian International Conference on fluid machinery and 3rd fluid power Technology exihibition*, IIT Madras, Chennai, India, 1–7.

Park, Y. K., Li, K. M., Choi, Y. H., and Lee, Y. W. (2011b). 'Visualization of air absorption induced by free surface vortex in the pump sump using multi-phase flow Simulation.' *Journal of the Korean Society of*, 9(3), 59–64.

Patel, A. K., Rao, A. R. K., and Pawar, V. (2013). 'Computational and experimental modelling of pump sump.' *Hydro 2013 International*, Indian Institute of Technology, Madras, Chennai, 299–307.

Patel, P. L. (2012). *Conducting CFD simulations of river pocket in front of Tail Race tunnels (TR1and TR2) of Tehri HPP*. Tehri Hydro Development India Corporation Limited (THDICL) -Rishikesh Uttarakhand.

Patel, P. L. (2013). *CFD analysis of Maneri Bhali Stage II (Part I&II)*. Uttaranchal Jal Vidyut Nigam Limited- Dehradun.

Patel, P. L. (2014). *CFD simulations of hydro turbines including tail race of Koteshwar hydro power project*.

Peijian, Z., Fujun, W., and Zhimin, Z. (2013). ‘Effect of guide cone configuration on hydraulic performance of low head pumping station.’ *Drainage and Irrigation machinery Engineering*, 31(9), 768–773.

Pradeep, S., Sayantan, G., Prasad, P. G., and Mohan Kumar, M. S. (2012). ‘CFD simulation and experimental validation of a horizontal pump intake system.’ *ISH Journal of Hydraulic Engineering*, 18(3), 173–185.

Pratap, M. K., and Chavan, D. S. (2013). ‘CFD analysis of flow in pump sump to check suitability for better performance of pump.’ *International Journal on Mechanical Engineering and Robotics (IJMER) pump*, 1(2), 59–65.

Prosser, M. J. (1977). *The hydraulic design of pump sumps and intakes*. British Hydromechanics Research Association.

Rahiman, P. M. A., Chavan, A. R., Bhambure, S. R., and James, A. S. (2003). ‘Discussion of “‘Experimental Study of 3D Pump-Intake Flows with and without Cross Flow’” by Matahel Ansar and Tatsuaki Nakato’. *Journal of Hydraulic Engineering*, 127(11), 414–416.

Rajendran, V. P., Constantinescu, G. S., and Patel, V. C. (1999). ‘Experimental validation of numerical model pump intake bays.’ *Journal of Hydraulic Engineering*, 125(11), 1119–1125.

Rajendran, V. P., and Patel, V. C. (2000). ‘Measurement of vortices in model pump-intake bay by PIV.’ *Journal of Hydraulic Engineering*, 126(5).

Rozainy, M. R., Abustan, I., Zulfiquar, A. M., and Ismail, M. A. M. (2008). ‘Application of computational fluid dynamics (CFD) in physical model of pump sump to predict the flow characteristics.’ *International Conference On Construction and Building Technology*, 79–90.

Samir A S Ibrahim. (2011). ‘Evaluation of the flow characteristics in the intake structure and pump sumps using physical model.’ *Nile Basin Water Science & Engineering Journal*, 4(1), 36–48.

Shabayek, S. A. (2010). ‘Improving approach flow hydraulics at pump intakes.’ *International Journal of Civil & Environmental Engineering*, 10(6), 23–31.

Shibata, T., Iwano, R., Nagahara, T., and Okamura, T. (2000). 'A numerical method for predicting the cavitation inception of a submerged vortex in a pump sump.' *Hydraulic Machinery and Systems 20th IAHR Symposium*, Charlotte (NC), USA.

Shukla, S. N., and Kshirsagar, J. T. (2008a). 'Numerical Simulation of Drawdown in Pump Sumps.' *The 4th International Symposium on Fluid Machinery and Fluid Engineering*, Beijing, China, 352–356.

Shukla, S. N., and Kshirsagar, J. T. (2008b). 'Numerical prediction of air entrainment in pump intakes.' *30 Proceedings of Thetwenty-Fourth International Pump Users Symposium*, 29–33.

Skerlavaj, A., Skerget, L., Ravnik, J., and Lipej, A. (2011). 'Choice of a turbulence model for pump intakes.' *Proceedings of the Institution of Mechanical Engineers, Part A: Journal of Power and Energy*, 225(6), 764–778.

Sontek. (1997). *Acoustic Doppler velocimeter technical documentation*. San Diego.

Stern, F., Wilson, R. V, Coleman, H. W., and Paterson, E. G. (1999). *Verification and validation of CFD simulations*. IIHR Rep. 407, Iowa Institute of Hydraulic Research, Univ. of Iowa, Iowa City, IA.

Swainston, M. J. C. (1977). 'Experimental and theoretical identification of air ingestion regimes in pump sumps.' *Proc Inst Mech. Engrs*, 190(59), 671–678.

Sweeney, C. E., Elder, R. A., and Hay, D. (1982). 'Pump sump design experience.' *Journal of Hydraulics Division*, 108(3), 361–377.

Tang, X. lin, Wang, W., Wang, F. J., Yu, X., Chen, Z., and Shi, X. (2010). 'Application of LBM-SGS model to flows in a pumping-station forebay.' *Journal of Hydrodynamics, Ser. B*, 22(2), 196–206.

Tang, X., Wang, F. J., Li, Y. J., Cong, G. H., Shi, X. Y., Wu, Y. L., and Qi, L. Y. (2011). 'Numerical investigations of vortex flows and vortex suppression schemes in a large pumping-station sump.' *Part C:Journal of Mechanical Engineering Science*, 225(6), 1459–1480.

Thomas, T. G., Leslie, D. C., and Williams, J. J. R. (1995). ‘Free surface simulations using a conservative 3D code.’ *Journal of Computational Physics*, Elsevier, 116(1), 52–68.

Thomas, T. G., and Williams, J. J. R. (1992). ‘Development of a conservative 3D free surface code.’ *Journal of Hydraulic Research*, 30(1), 107–115.

Thomas, T. G., and Williams, J. J. R. (1994). ‘The numerical simulation of laminar free-surface flows.’ *Journal of Hydraulic Research*, Taylor & Francis, 32(4), 599–613.

Thomas, T. G., and Williams, J. J. R. (1995). ‘Turbulent simulation of open channel flow at low Reynolds number.’ *International journal of heat and mass transfer*, Elsevier, 38(2), 259–266.

Tokyay, T. E., and Constantinescu, G. S. (2006). ‘Validation of a large-eddy simulation model to simulate flow in pump intakes of realistic geometry.’ *Jounal of Hydraulic Engineering*, 132(12), 1303–1315.

Tullis, J. P. (1979). ‘Modeling in design of pumping pits.’ *Journal of the Hydraulics Division*, ASCE, 105(9), 1053–1063.

Versteeg, H. K., and Malalasekera, W. (2007). *An introduction to computational fluid dynamics: the finite volume method*. Pearson Education.

Wicklein, E., Sweeney, C., Senon, C., Hattersley, D., Schultz, B., and Naef, R. (2006). ‘Computation Fluid Dynamic Modeling of a Proposed Influent Pump Station.’ *WEFTEC 06*, 7094–7114.

Yulin, W., Yong, L., and Xiaoming, L. (2000). *PIV experiments on flow in a model pump suction sump*. Research Rep, Thermal engineering department, Tsinghua Univ., Tsinghu, China.

Zhao, Y. X., Kim, C.-G., and Lee, Y.-H. (2013). ‘CFD study on flow characteristics of pump sump and performance analysis of the mixed flow pump.’ *6th International Conference on Pumps and Fans with Compressors and Wind Turbines*, Beijing, China.

Zhou, L., Li, X., Song, Y., and Longcai, Z. (2009). ‘Numerical simulation of turbulent flow in recycled water pump intake sump of thermal power plant.’ *Asia-Pacific Power and Energy Engineering Conference*, IEEE, 1–4.